THE COWPEA CHLOROTIC MOTTLE VIRUS AS A BUILDING BLOCK IN NANOTECHNOLOGY

MARTA COMELLAS ARAGONÈS

The cowpea chlorotic mottle virus
as a building block in nanotechnology

Een wetenschappelijke proeve op het gebied van de
Natuurwetenschappen, Wiskunde en Informatica

Proefschrift

ter verkrijging van de graad van doctor
aan de Radboud Universiteit Nijmegen
op gezag van de rector magnificus prof. mr. S.C.J.J. Kortmann,
volgens besluit van het college van decanen
in het openbaar te verdedigen op dinsdag 5 januari 2010
om 13.30 uur precies

door

Marta Comellas Aragonès
geboren op 7 februari 1978
te Barcelona

Promotores:

Prof. dr. Roeland J.M. Nolte

Prof. dr. Jeroen J.L.M. Cornelissen (Universiteit Twente)

Manuscriptcommissie:

Prof. dr. ir. Jan C.M. van Hest

Prof. dr. Gijs J.L. Wuite (Vrije Universiteit Amsterdam)

Dr. ir. Benedictus (Dick) J.M. Verduin (Wageningen Universiteit)

Paranimfen:

Henar Tejedor Vinent

Joost Clerx

The cowpea chlorotic mottle virus
as a building block in nanotechnology

An academic essay in
Science

Doctoral Thesis

To obtain the degree of doctor
from Radboud University Nijmegen
on the authority of the Rector Magnificus, prof. dr. S.C.J.J. Kortmann,
according to the decision of the Council of Deans
to be defended in public on Tuesday January 5, 2010
at 13.30 hours

by

Marta Comellas Aragonès
Born on 7 February 1978
in Barcelona

Supervisors:

Prof. dr. Roeland J.M. Nolte

Prof. dr. Jeroen J.L.M. Cornelissen (University of Twente)

Doctoral Thesis Committee:

Prof. dr. ir. Jan C.M. van Hest

Prof. dr. Gijs J.L. Wuite (VU University Amsterdam)

Dr. ir. Benedictus (Dick) J.M. Verduin (Wageningen University)

Defence Assistants:

Henar Tejedor Vinent

Joost Clerx

Table of Contents

CHAPTER 1

Aim and Outline of the Thesis

1.1 Introduction

What is a virus?

Viruses are infectious agents that replicate only within living cells. Viruses are not "alive" because they need resources from a host cell to be able to reproduce. They can be classified depending on the host that they infect, which can be plants, bacteria (the virus is then called a bacteriophage), fungi, or animals. After entering the host cells, viruses are able to control the transcription/translation machinery of the cell, which is then employed for the production of the virus constituents that assemble again to form new virus particles (Figure 1.1).
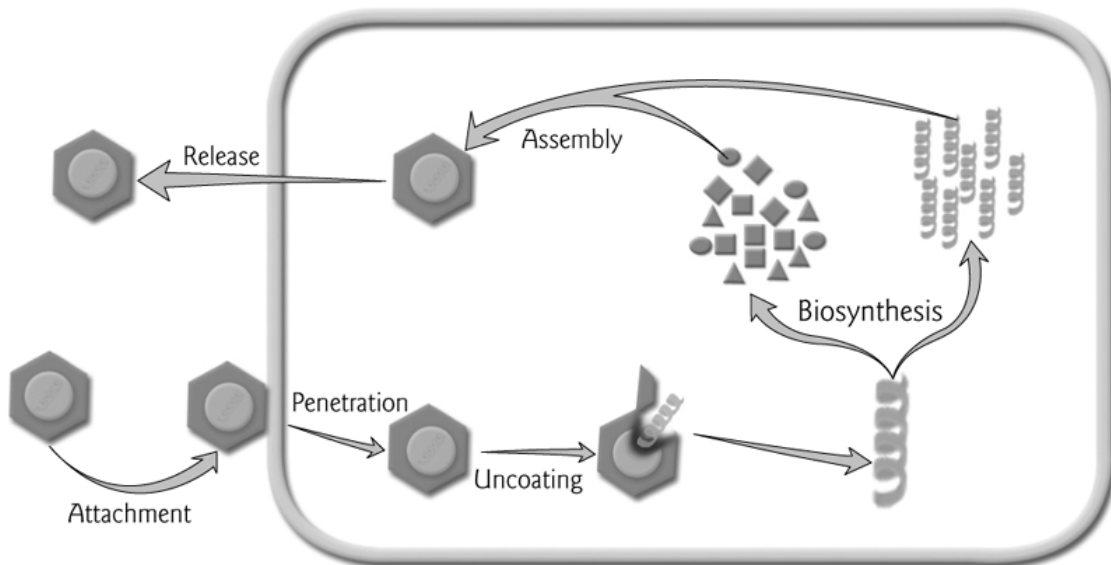
Figure 1.1 *A diagrammatic representation of the six phases common to all virus multiplication cycles.*

A complete virus particle, also known as virion, consist of two or three parts: the genetic material, which can be DNA or RNA; the protein capsid that protects this genetic material by assembling around it; and some viruses (termed "enveloped" viruses) additionally have a lipidic membrane that surrounds the protein capsid (Figure 1.2). Although we used to relate viruses with disease-causing agents, since the pioneering work of Douglas and Young,[1] viruses are seen as new biomaterials that are

attractive for different fields, such as materials science and nanotechnology. Most of such studies involve viruses without enveloping membranes.
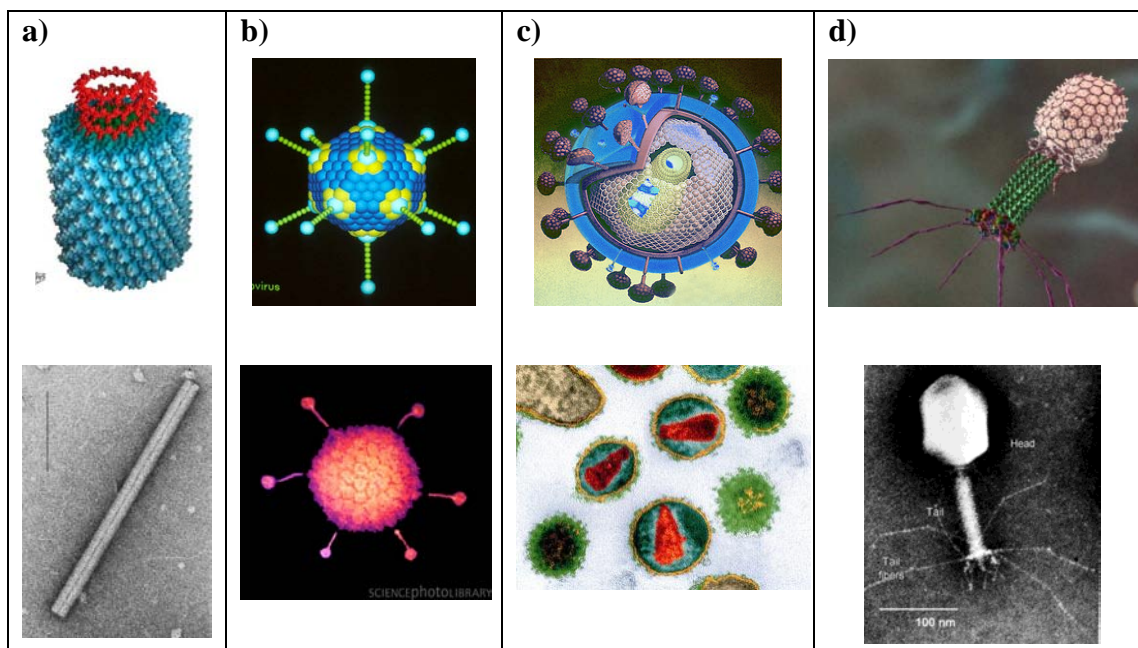
Figure 1.2 Image reconstructions or models, and cryo–electron micrographs of different kind of viruses. a) The rod-shaped virus tobacco mosaic virus. b) An example of an adenovirus. c) The human immunodeficiency virus (HIV). d) The T4 bacteriophage.

Bionanotechnology

At the interfaces of chemistry, biology, physics, medicine, engineering, and materials science exists the field of bionanoscience. This multidisciplinary field involves the exploitation of biomaterials, devices, or methodologies on the nanoscale. There is an increasing interest in the production of nanosized materials for different fields and applications. For example, in the field of electronics there are strong commercial incentives to produce increasingly miniaturized microelectronic devices and in the field of medicine there is great interest in the development of new nanoscale systems for drug delivery and imaging.

There are two different approaches for the production of these nanosystems: top-down and bottom-up. The top-down approach involves the construction of increasingly smaller structures down to the nanoscale often by using masks and light or the embedding of nano-features into macroscopic materials, whereas the bottom-up approach uses the techniques of component assembly and/or supramolecular chemistry to make small molecules bigger. A number of groups are rapidly expanding the repertoire of biological scaffolds for nanochemistry and several investigations have

recognized virus capsids as versatile building blocks for the production of nanomaterials by using the bottom-up approach.

In recent years an increasing number of reviews have appeared describing new approaches that use biological molecules as building blocks in nanoscience. Many detailed reviews[2-7] of using protein cages and viruses in nanotechnology have followed the initial ones from Niemeyer,[8] Douglas and Young,[9] Belcher *et al.*,[10] and Vriezema *et al.*[11] An essential feature of all viruses is their ability to infect a host cell, replicate, package the nucleic acid, and exit the cell. During this process, viruses have evolved to move through a broad range of chemical environments. The intrinsic properties obtained during evolution, together with the properties that can nowadays be realized with the help of modern genetic and/or chemical techniques, can impart new functions to protein cage architectures, which is important for the development of multifunctional nanoplatforms.[4,7]

 Why viruses?

Viruses are interesting particles for use in nanotechnology for the following reasons:[6,12]

(i) Viruses can be found in a variety of distinct shapes (most commonly icosahedrons, spheres, tubes, and helices) and their sizes range from approximately 10 to 500 nm for icosahedral structures to more than a micron for filamentous or rod-shaped viruses (Figure 1.3).
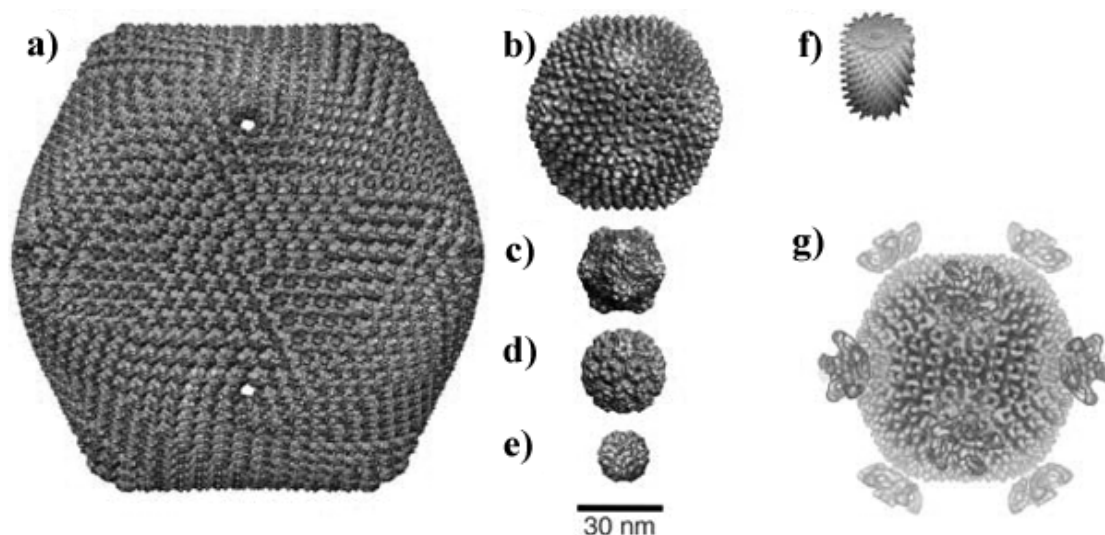
Figure 1.3 Cryo–electron micrograph and image reconstructions of a library of viral capsids, including both icosahedral and helical viruses. a) Paramecium bursaria Chlorella virus type 1, 170 nm in diameter. b) Murine polyoma virus, 51 nm in diameter. c) Cowpea mosaic virus, 31 nm in diameter. d) Cowpea chlorotic mottle virus, 28 nm in diameter. e) Satellite tobacco necrosis virus, 18 nm in diameter. f) A small section of the rod-shaped tobacco mosaic virus, which measures 18 by 300 nm.

g) Sulfolobus turreted icosahedral virus isolated from a boiling, acid environment in Yellowstone National Park.[4]

(ii) Viral capsids are typically assembled from repeating protein subunits to form highly symmetrical and polyvalent architectures. The coat proteins of several viruses have been characterized at atomic resolution,[13,14] providing essential knowledge required for making modifications to the capsid to impart new synthetic functions by design.

(iii) Unlike other materials in this size range, viruses are often perfectly monodisperse in size and composition. Only in rare cases does a particular virus exist in more than one size or shape. On the other hand, species such as colloids, dendrimers, and polymers of comparable dimensions (200–800 Å in diameter), which are made in the laboratory, are all polymorphous.

(iv) Viruses offer three different interfaces that can be exploited: the exterior, the interior, and the interface between the protein subunits (see next section).

(v) The protein subunits that comprise the building blocks of the virus structures can be modified both chemically and genetically to introduce designed functionality to different surfaces of the cage. It should be noted, however, that these changes can affect the assembly of the particle; therefore, it is important to leave those regions of the protein surface that are responsible for the intermolecular interactions, which guide and stabilize assembly, undisturbed.

(vi) Many viruses can be obtained in large quantities. They can be isolated from their natural host cell masses in a few hours and substantial yields (often in the range of 0.1–1% by weight).

(vii) Viruses are more stable toward variations in pH, temperature, and solvent than standard proteins, thereby providing a wider range of conditions for their isolation, storage, and use. This stability can be in some cases enhanced by chemical or genetic modification of the viral capsid.

Virus exploitable surfaces

As mentioned at point (iv) above, when we look at viruses as molecular containers there are three important interfaces that can be exploited (Figure 1.4).[4] All viruses encode, package, and transport viral nucleic acid. However, many will assemble *in vitro* (either naturally or through genetic manipulation) into noninfectious containers, called capsids or virus-like particles (VLPs), devoid of genetic material. These protein capsids have an inner cavity accessible to small molecules and impermeable to big ones, which allows one to use the interior space of viral capsids as nanotemplates and nanoreactors.

Furthermore, the viral container interacts with its environment through its external surface which can be genetically or chemically modified in order to obtain specific interactions with biological or nonbiological surfaces. The exterior surface of many

viruses has emerged as a robust platform for chemical and genetic modification, allowing multivalent ligand display.

The subunit interface in the viral architecture is crucial for assembly and provides a tool for the manipulation of the cage architecture and stability. Many viral capsids exhibit pleomorphism, which is the ability to assemble into a range of different architectures, either naturally or through genetic and chemical manipulation. In this way it is possible to have control over the kind of assembly and the stability of the structure.[3,4]
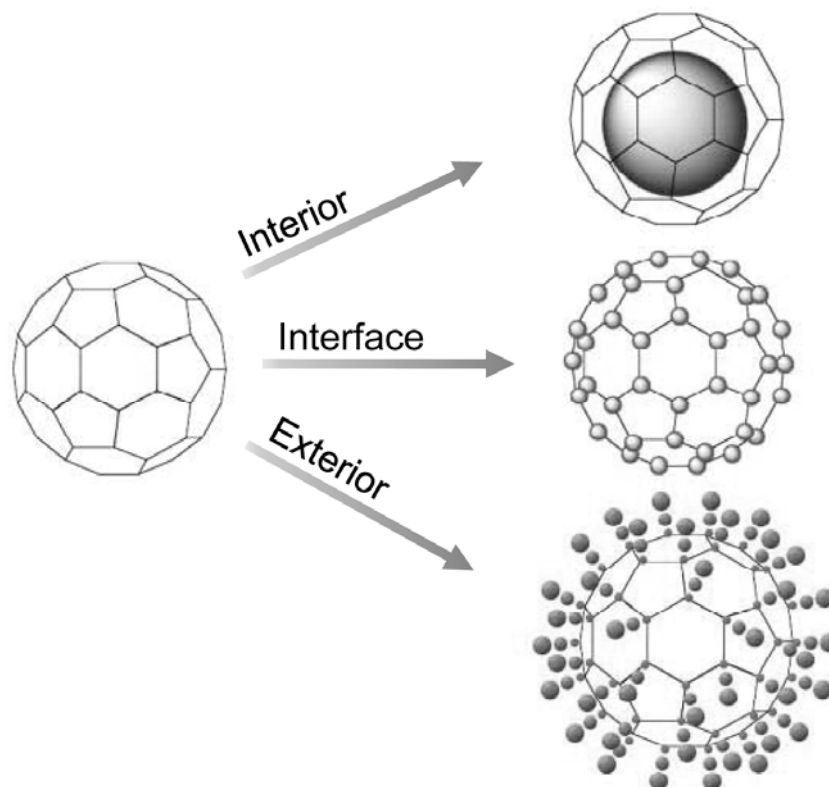
Figure 1.4 *Scheme of the three important interfaces available for chemical and genetic manipulation in an assembled viral protein cage architecture.[4] The interior surface, the exterior surface, and the interface between the subunits have all been used for the construction of multivalent or multifunctional viral-cage-based materials.*

1.2 Aim and outline of this thesis

The research described in this thesis aims to construct a virus nanoreactor by the encapsulation of enzymes within the cowpea chlorotic mottle virus (CCMV) protein capsid. In the Nolte group there has been much interest in the construction of supramolecular assemblies using both synthetic and biological building blocks. Many of these assemblies were prepared starting from catalytically active building blocks, the goal being to mimic the efficiency of enzymes, mainly based on molecular recognition

processes.[11] Furthermore, these assemblies were also designed to resemble the constrained environment of a cell, in which multienzymatic processes occur with high efficiencies. Enzyme assemblies obtained through the synthesis of giant amphiphiles[15-17] or the formation of enzyme-encapsulating polymersomes[18,19] are examples of supramolecular assemblies designed for this purpose (Figure 1.5).
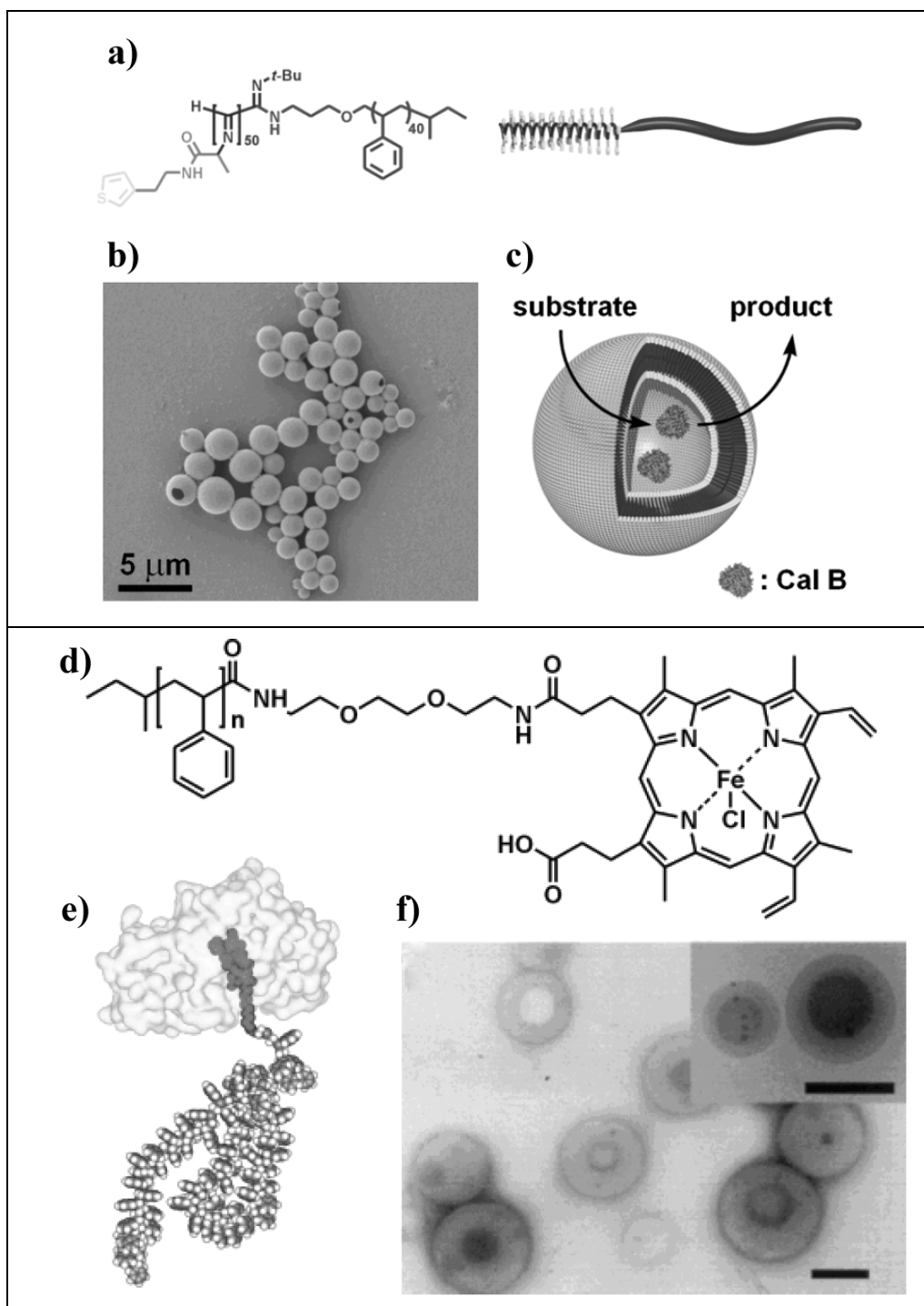
Figure 1.5 Top: Nanoreactors based on polymersomes of polystyrene–
polyisocyanopeptide with pendant thiophenes (PS-PIAT), encapsulating CAL B lipase

enzymes. a) Structural formula and schematic representation of PS-PIAT. b) Scanning electron micrograph of PS-PIAT polymersomes. c) Schematic representation of the nanoreactor.[18] Bottom: Vesicles formed in water by a horseradish peroxidase (HRP)– polystyrene biohybrid amphiphile. d) Structural formula of the modified heme cofactor. e) Computer-generated model of the HRP–polystyrene biohybrid. f) Transmission electron micrograph of the formed polymersomes (scale bars represent 200 nm).

The studies reported in this thesis describe the first fundamental steps in the construction of a nanoreactor by encapsulating enzymes in the viral protein capsid. We have chosen CCMV for this goal because of its remarkable assembly properties. This thesis not only describes the investigations, in which CCMV is used as a platform for nanotechnology, but also reports in detail the procedures to purify the virus and basic studies of its properties, which are needed to carry out such investigations.

Chapter 2 of this thesis is a literature survey discussing a selection of the work that has been carried out with viruses in the field of nanotechnology and materials science. Studies with the protein cage ferritin, similar protein cages, and the tobacco and cowpea mosaic viruses are described. Since the number of studies reported in the literature regarding this topic is rather large, only three of the most used particles are described in detail to exemplify the approaches that are being followed with different kinds of protein cages and viruses. The last section of the chapter focuses on the virus used in this thesis, namely CCMV.

In order to be able to work with CCMV it was first necessary to obtain the virus in sufficient quantities and to establish the optimal purification. In **Chapter 3** a detailed protocol for the purification of CCMV is described, following the procedure of Verduin,[20,21] based on the first reports from Bancroft et al.[22] Once purified the self-assembly properties of the virus were investigated to find the optimum conditions to exploit the virus as a nanoreactor. **Chapter 4** describes how, based on established methods, the RNA could be removed from the virus and how the different forms of assembly of the isolated coat protein were characterized. The chapter aims to guide the reader through the different techniques that are available for the characterization of the CCMV assemblies, which is thought to be useful for the proper understanding and evaluation of the studies described in subsequent chapters.

Chapter 5 reports on investigations that provide additional information about the CCMV assembly properties in solution and about the structure of the viral capsid when it is used as a host for the inclusion of an ionic organic polymer. Small-angle neutron scattering (SANS), performed at the ISIS facility in the UK, and dynamic light scattering (DLS) are the two non-destructive techniques used for this study.

After the assembly properties of the virus and the capsid structure had been defined, attention was focused on studies in which CCMV was used as a host for proteins. The

encapsulation of three different model proteins, namely myoglobin, dronpa, and streptavidin, is described in **Chapter 6**. The results show that the CCMV capsid indeed is a suitable system for the encapsulation of proteins. **Chapter 7** is a follow-up of Chapter 6. In this chapter the encapsulation of an enzyme, that is HRP, in the CCMV capsid is described. After encapsulation, single-molecule fluorescence spectroscopy experiments were performed to study the catalytic activity of the enzyme at the single-capsid level.

As outlined in Section 1.1, the outer surfaces of viruses are ideal platforms for chemical modifications. **Chapter 8** reports on studies in which the outer surface of CCMV is modified with polyethylene glycol (PEG) tails. By combining the PEG-functionalized viral coat protein with the assembly properties of a polystyrene sulfonate polymer described by Sikkema et al.,[23] the controlled integration of two different synthetic polymers into a viral capsid was obtained for the first time.

1.3 References

[1]   T. Douglas, M. Young, *Nature* **1998**, *393*, 152.

[2]   A. de la Escosura, R. J. M. Nolte, J. J. L. M. Cornelissen, *J. Mater. Chem.* **2009**, *19*, 2274.

[3]   M. Uchida, M. T. Klem, M. Allen, P. Suci, M. Flenniken, E. Gillitzer, Z. Varpness, L. O. Liepold, M. Young, T. Douglas, *Adv. Mater.* **2007**, *19*, 1025.

[4]   T. Douglas, M. Young, *Science* **2006**, *312*, 873.

[5]   M. Fischlechner, E. Donath, *Angew. Chem. Int. Ed.* **2007**, *46*, 3184.

[6]   M. Manchester, N. F. Steinmetz, *Viruses and Nanotechnology*, Springer, Heidelberg (Germany), **2009**.

[7]   M. Young, D. Willits, M. Uchida, T. Douglas, *Annu. Rev. Phytopathol.* **2008**, *46*, 361.

[8]   C. M. Niemeyer, *Angew. Chem. Int. Ed.* **2001**, *40*, 4128.

[9]   T. Douglas, M. Young, *Adv. Mater.* **1999**, *11*, 679.

[10]   C. E. Flynn, S.-W. Lee, B. R. Peelle, A. M. Belcher, *Acta Mater.* **2003**, *51*, 5867.

[11]   D. M. Vriezema, M. Comellas Aragones, J. A. A. W. Elemans, J. J. L. M. Cornelissen, A. E. Rowan, R. J. M. Nolte, *Chem. Rev.* **2005**, *105*, 1445.

[12]   E. Strable, M. G. Finn, *Curr. Top. Microbiol. Immunol.* **2009**, *327*, 1.

[13]   M. Carrillo-Tripp, C. M. Shepherd, I. A. Borelli, S. Venkataraman, G. Lander, P. Natarajan, J. E. Johnson, C. L. Brooks III, V. S. Reddy, *Nucleic Acids Res.* **2009**, *37*, D436.

[14]   P. Natarajan, G. C. Lander, C. M. Shepherd, V. S. Reddy, C. L. Brooks III, J. E. Johnson, *Nat. Rev. Microbiol.* **2005**, *3*, 809.

[15]   K. Velonia, A. E. Rowan, R. J. M. Nolte, *J. Am. Chem. Soc.* **2002**, *124*, 4224.

[16]   J. M. Hannink, J. J. L. M. Cornelissen, J. A. Farrera, P. Foubert, F. C. De Schryver, N. A. Sommerdijk, R. J. M. Nolte, *Angew. Chem. Int. Ed.* **2001**, *40*, 4732.

[17]   M. J. Boerakker, J. M. Hannink, P. H. Bomans, P. M. Frederik, R. J. M. Nolte, E. M. Meijer, N. A. Sommerdijk, *Angew. Chem. Int. Ed.* **2002**, *41*, 4239.

[18]   D. M. Vriezema, J. Hoogboom, K. Velonia, K. Takazawa, P. C. M. Christianen, J. C. Maan, A. E. Rowan, R. J. M. Nolte, *Angew. Chem. Int. Ed.* **2003**, *42*, 772.

[19]   D. M. Vriezema, P. M. Garcia, N. Sancho Oltra, N. S. Hatzakis, S. M. Kuiper, R. J. M. Nolte, A. E. Rowan, J. C. van Hest, *Angew. Chem. Int. Ed.* **2007**, *46*, 7378.

[20]   B. J. M. Verduin, *FEBS Lett.* **1974**, *45*, 50.

[21]   B. J. M. Verduin, *J. Gen. Virol.* **1978**, *39*, 131.

[22]   J. B. Bancroft, G. J. Hills, R. Markham, *Virology* **1967**, *31*, 354.

[23]   F. D. Sikkema, M. Comellas-Aragones, R. G. Fokkink, B. J. Verduin, J. J. L. M. Cornelissen, R. J. M. Nolte, *Org. Biomol. Chem.* **2007**, *5*, 54.

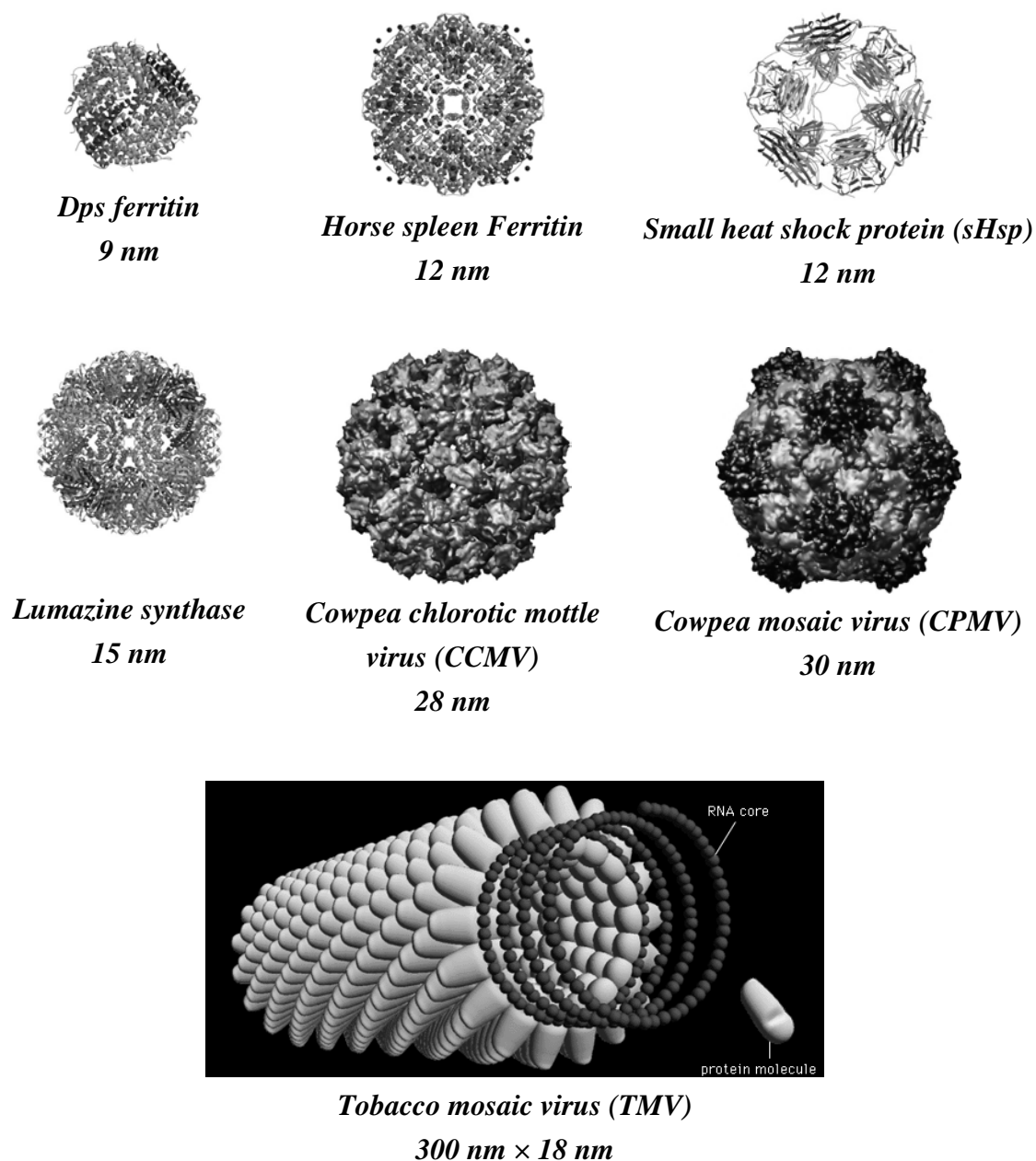# CHAPTER 2

Protein Cages as Multifunctional Nanoplatforms

2.1 Introduction

This chapter is a short literature survey of the research carried out over the last two decades in which viruses have served as building blocks in nanoscience and nanotechnology. In recent years an increasing number of reviews have appeared in this topic[1-10] and the current interest stems from the fact that viruses display a high degree of organization, are often easy to modify, and occur in well-defined self-assembly motifs.[11]

Research on what may be called 'chemical virology' has expanded enormously over the last 10 years, with an increasing number of publications in different fields, such as medicine, materials science, and nanotechnology. This chapter does not review all work reported about viruses, instead only a few examples that are relevant for this thesis to demonstrate the vast potential virus particles offer as platforms in nanotechnology are chosen. The use of viruses as building blocks was inspired by protein cages, such as ferritin. The first section of this chapter is therefore focused on the protein cages Dps (DNA-binding protein from starved cells) ferritin, horse spleen ferritin, small heat shock protein, and lumazine synthase (Figure 2.1). In the next section relevant studies on tobacco mosaic virus (TMV) and cowpea mosaic virus (CPMV) are highlighted. These two viruses have a very different shape (rod-shaped vs. icosahedral, Figure 2.1) and are much used in bio-nanotechnology research nowadays. The last section gives a detailed overview of CCMV because it is the virus that we have used for the studies presented in this thesis (Figure 2.1). It is important to note that throughout this chapter the terms "protein cage", "capsid", and "virus-like particle" (VLP) are often used interchangeably; they refer to the protein shell derived from the dissociated protein subunits or virus.

Dps ferritin
9 nm

Horse spleen Ferritin
12 nm

Small heat shock protein (sHsp)
12 nm

Lumazine synthase
15 nm

Cowpea chlorotic mottle virus (CCMV)
28 nm

Cowpea mosaic virus (CPMV)
30 nm

Tobacco mosaic virus (TMV)
300 nm × 18 nm

Figure 2.1 *Protein cages and viruses mentioned in this chapter, ordered by average diameter. The images are colored to distinguish the symmetry-related subunits and are taken from the VIPER database (http://viperdb.scripps.edu)[12,13] and the Protein Data Bank (www.rcsb.org/pdb/).*

2.2 Protein Cages

Nature has developed a variety of proteins that function as carriers or storage devices for metal ions and minerals. The iron storage protein ferritin is probably the most intensively studied and best understood example. In this protein the mineral is sequestered within one single compartment, which has a shell of well-defined size and form. Since the early 1990s the use of ferritin and other storage proteins as nanometer-sized reaction vessels has been explored.[7] The use of protein cages in nanotechnology has been reviewed in several recent publications.[2,14,15]

Ferritin

Ferritins are found throughout the animal, plant, and microbial kingdoms.[16] They consist of a central core of hydrated iron(III) oxide encapsulated within a multi-subunit protein shell. Ferritins are robust proteins that can withstand high temperatures (85 °C) and high pH (8.5−9) for an appreciable period of time without significant disruption of their quaternary structure. Iron-free ferritin molecules (apoferritin) are composed of 24 polypeptide subunits that assemble into a hollow sphere of approximately 500 KDa. The outer diameter of the protein is 12 nm, while the inner diameter is 8 nm (Figure 2.1). The ferritin protein shell has several functions: it acquires iron(II), catalyzes its oxidation, and induces mineralization within the cavity. Up to 4500 iron atoms can be housed within the protein cavity. Such a high iron-to-protein ratio is made possible by sequestering the iron as a compact mineral, which has a structure similar to that of the mineral ferrihydrite ($5Fe_2O_3 \cdot 9H_2O$). Hydrophilic and hydrophobic channels are incorporated into the shell, and as a result, iron atoms can be removed from the cage by reductive dissolution. *In vitro* reconstitution of iron(III) oxide cores can be readily achieved by room-temperature incubation of intact empty protein (apoferritin) with Fe^{II} solutions at moderate pH.[17]

In 1991, Mann and co-workers began to explore the use of ferritin as a nanometer-sized bioreactor for producing monodisperse metal particles from metal ions other than the natural hydrated iron(III) oxide.[17] They showed, for the first time, that supramolecular protein cages have the potential to act as constrained reaction environments in the synthesis of inorganic materials of nanometer dimensions. Horse spleen apoferritin (HSFn) was used as a nanocontainer to generate iron sulfide particles, manganese oxide, and uranyl oxohydroxide crystals.[17-19] In Figure 2.2 the three different approaches followed by Mann and co-workers are schematically depicted. For example, incubation of the empty protein cages with $MnCl_2$ at pH 9 resulted in specific manganese ion uptake, oxidation, and precipitation. Depending on the original concentrations of protein and Mn^{II}, discrete manganese oxide cores up to 7 nm in diameter were formed, as shown by transmission electron microscopy (TEM) and electron dispersive X-ray

analysis (EDXA) spectroscopy. Other inorganic nanoparticles have been synthesized within apoferritin by using similar biomimetic strategies. Thus, iron sulfide,[20] manganese oxide, manganese oxyhydroxide,[21,22] cobalt oxide,[23] cobalt oxyhydroxide,[24] chromium hydroxide, nickel hydroxide,[25] indium oxide,[26] cadmium sulfide,[27] cadmium selenide,[28] and zinc selenide[29] have been prepared within the nanosized cavity of horse spleen ferritin. Oxyhydroxide nanoparticles of high-oxidation-state transition metals (Eu and Ti) have also been synthesized in the iron storage protein ferritin by using a new synthetic approach consisting of photoinduced mineralization.[30]
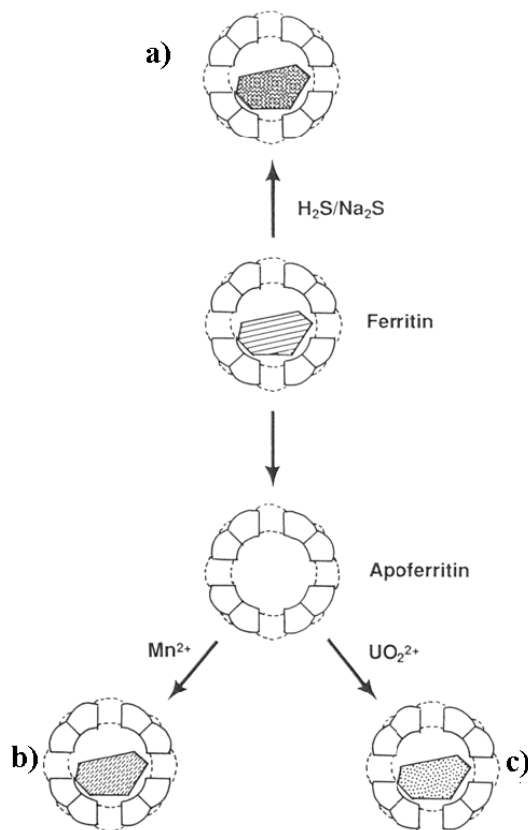
Figure 2.2 *Schematic representation of the use of ferritin in the synthesis of nanophase materials. a) Iron sulfide formation by in situ reaction of native iron oxide cores.*
b) Manganese oxide reconstitution by redox-driven reactions within apoferritin.
c) Uranyl oxyhydroxide deposition by ion binding and hydrolytic polymerization.[18]

Other work consisted of synthesizing the ferromagnetic nanocrystals of magnetite (Fe_2O_4),[31,32] and magnetite/maghemite $(Fe_3O_4/\gamma\text{-}Fe_2O_3)$,[33] within the ferritin cavity to construct a magnetic protein, "magnetoferritin"; this could be performed under conditions of elevated temperatures and pH. As a result of the restricted space within the nanoreactors, crystalline inorganic particles with diameters of approximately 6−7 nm were formed, as determined by TEM. The magnetite/maghemite particles were generated by trimethylamino-*N*-oxide oxidation of apoferritin, which was loaded with various amounts of iron(II) ions. The temperature-dependent magnetic properties of

magnetoferritins with different iron loadings were investigated. Recently, the preparation of mixed Co/Fe oxide materials in the inner cavity of ferritin was reported. A two- to fourfold increase in the ferromagnetic blocking temperature, with respect to undoped magnetoferritin, was observed by controlled addition of Co to the reaction mixture.[34]

A new approach in the use of ferritin was introduced by Douglas et al., who studied the protein-constrained iron oxide core of ferritin as a catalyst for photoreduction reactions.[35] They demonstrated that the iron oxide nanoparticle encapsulated within the protein cage of ferritin could act as a semiconductor photocatalyst for the reduction of Cr^{VI} to Cr^{III}. Furthermore, the same system was shown to be capable of photoreducing Cu^{II} to form a colloidal dispersion of Cu^0 with a fairly narrow size distribution.[36] Examination of the photolysis products by TEM revealed electron-dense spheroid particles. It was found that the molar ratio of Cu^{II}/ferritin was the major factor in determining the particle size. A similar approach was followed by Ueno and co-workers when they constructed a size-selective hydrogenation biocatalyst.[37] They encapsulated a Pd nanocluster in the apoferritin cavity by in situ chemical reduction of Pd^{II} ions. Subsequently, the catalytic hydrogenation of olefins by the Pd−apoferritin hybrid was evaluated in aqueous media. It was shown that the catalytic system discriminates with respect to size of the substrates through the threefold channels that cross the protein cage (Figure 2.3). Similarly, Ag nanoparticles were synthesized by combining the protein-cage encapsulation approach and selective nucleation by specific phage-display peptides.[38] Furthermore, the formation of a ferritin encapsulating up to ten Gd complexes resulted in a complex that exhibited high relaxivity of water protons with potential applications in magnetic resonance imaging (MRI).[39] A recombinant human ferritin (rHFn)–iron oxide nanocomposite has also been investigated as an MRI contrast agent for the imaging of macrophages that play an important role in inflammatory diseases.[40]
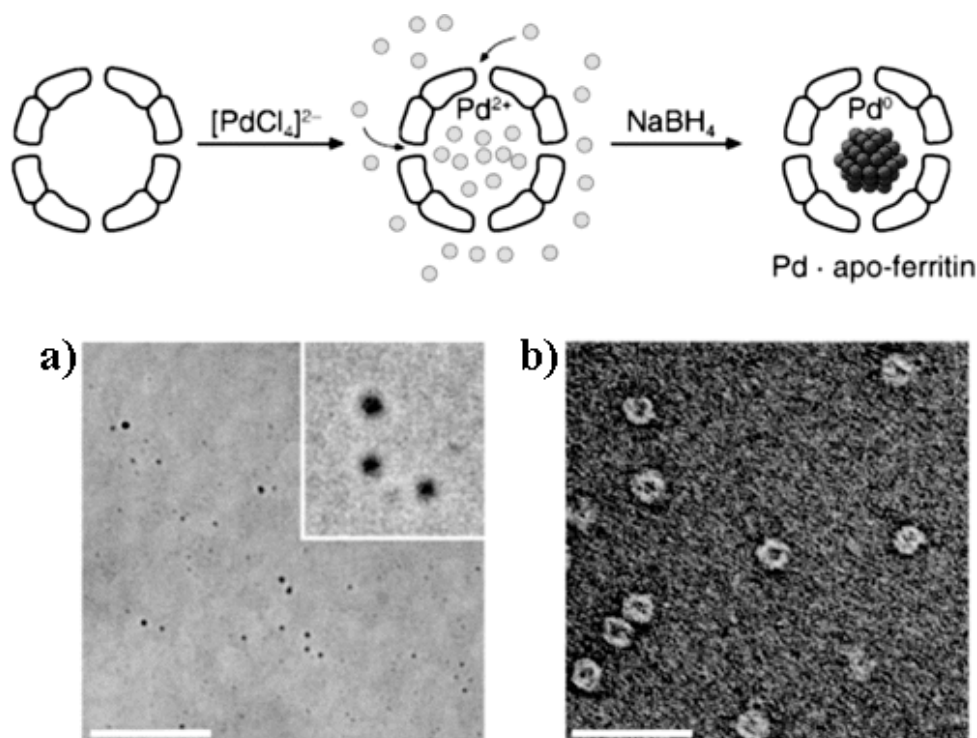
Figure 2.3 Top: Scheme showing the preparation of Pd–apoferritin. Bottom: TEM images of the Pd–apoferritin: a) an ice-embedded unstained sample (inset: magnification 4×), b) a sample negatively stained with uranyl acetate. Scale bars represent 50 nm.[37]

Modification of the outer surface of ferritin has been investigated by Mann and co-workers.[33,41] Alkylated derivatives of ferritin were prepared by carbodiimide-activated coupling of long-chain primary amines to carboxylic acid residues on the protein surface. As a consequence of this surface modification, the proteins become soluble in several organic solvents as intact, nonaggregated biomolecules. The long-term goal of this approach is to exploit alkylated ferritins as nanoreactors for condensation reactions involving metal alkoxides and related organometallic compounds, which is only possible in nonaqueous systems. Another surface modification involved the preparation of biotinylated ferritin.[42] In this case, the outer protein surface was derivatized with approximately 70 biotinylated ligands, which were available to interact with streptavidin to form a cross-linked network of biomacromolecules. Such ferritin-based arrays could have important applications in magnetic storage and nanoelectronic devices. In another example, titanium-binding peptides were introduced to the N-terminus of the ferritin subunit, so that the resultant modified ferritin displayed specific affinity for titanium metals. The N-terminal extension was genetically engineered so that it was uniquely present on the exterior surface of the ferritin cage.[43,44] Following a similar approach, a tumor-binding peptide was genetically introduced onto the exterior surface of a magnetite-containing ferritin as an N-terminal fusion.[45] The complex

bound to melanoma cells *in vitro* due to the specific interaction of the peptide. These results demonstrate the capability of a genetically modified protein-cage architecture to serve as a multifunctional nanoscale container for simultaneous iron oxide loading and cell-specific targeting.

Dps ferritin

Dps ferritin is a protein-cage member from the ferritin family. The Dps ferritin from the bacterium *Listeria inocua* prevents oxidative damage of DNA by accumulating iron atoms within the central cavity to produce an iron oxide core similar to that of ferritins.[46,47] This protein cage was also utilized as a size- and shape-constrained reaction environment, as previously described for ferritin. Dps ferritin differs from other known ferritins in that the protein shell is assembled from 12 instead of 24 identical subunits; it can accumulate only 500 iron atoms within its 5 nm diameter central cavity (Figure 2.1).[48] Ferrimagnetic iron oxide,[49] cobalt oxide,[50] cadmium sulfide,[51] and platinum[52] nanoparticles were synthesized within the Dps protein cage. The formation of these particles has been recently monitored for the first time by using mass spectrometry.[52,53] The combination of electrospray ionization (ESI) and time-of-flight (TOF) mass analysis makes it possible to measure the mass of intact noncovalently associated macromolecular complexes without disturbing the structures, as well as the masses of individual protein components.[54] This has allowed one to precisely follow the transition from metal binding to nucleation and subsequently to nanocluster formation within a protein cage at the molecular level. Moreover, Dps protein cages have been synthesized with a hydrophobic interior surface to enhance the formation of metal nanoparticles.[55]

Other protein cages

The investigations on ferritin as a size- and shape-constrained reaction vessel have paved the way for other groups to use different biomolecular systems for the same purpose leading to the development of a general class of self-assembled bioinorganic hybrid materials with designed functionality and biocompatibility. Aside from ferritin, the following proteins have been used as bionanoreactors.

Lumazine synthase

Lumazine synthase is a hollow icosahedral bacterial enzyme with a molecular weight of 1 MDa, which is formed by the self-assembly of 60 subunits (Figure 2.1).[56] The self-assembled structure of this protein is very similar to the structures of the protein cages described above. Following the same concept as published for the protein ferritin, lumazine synthase was shown to be a suitable mineralization template for the fabrication of nanocrystalline iron oxide.[57]

The small heat shock protein

The small heat shock protein (sHsp) cage from *Methanococcus jannaschii* consists of 24 subunits that self-assemble into a cage with octahedral symmetry (Figure 2.1).[58,59] The main difference between sHsp and ferritin are the large pores (3 nm in diameter) that the former compound presents on its surface, which allow easy access from the interior to the exterior environments of the cage.[60] The protein has an exterior diameter of 12 nm, is stable in the pH range 5−11, and can withstand temperatures up to 70 °C. The possibility to functionalize this template with organic and inorganic groups was first studied by Douglas and co-workers.[61] Thiol groups, which were engineered by genetic manipulation of the protein, and endogenous amine groups on both the exterior and the interior surfaces were used for the attachment of different molecules and the templation of reactions. By analogy to ferritin, sHsp was studied for its ability to act as a size-constrained reaction environment for mineralization.[61,62] A novel route for nanoparticle synthesis with an engineered crystal phase was developed by genetically engineering peptide sequences (specific for particular inorganic materials) in the sHsp inner cavity.[63,64] This allowed for the selective design of the properties of the material and helped nanoparticle synthesis to be performed under milder conditions.

The thiol groups engineered in the sHsp cage were also used for the chemical attachment of an organic drug molecule, namely doxorubicin, a chemotherapeutic agent.[65] The drug could be released under acidic conditions, such as those found in an endosome. The outer surface of sHsp has been decorated, by chemical and genetic manipulation, with fluorescent probes and cell-specific targeting antibodies and peptides, highlighting the potential of this cage as a (targeted) imaging agent and drug-delivery vehicle.[61,65,66]

Recently, the first example of the synthesis of a cross-linked, branched polymer network inside a protein cage has been reported (Figure 2.4).[67] This polymer material was generated by the sequential coupling of multifunctional monomers using click chemistry. The encapsulated polymer was found to dramatically increase the stability of the protein cage.
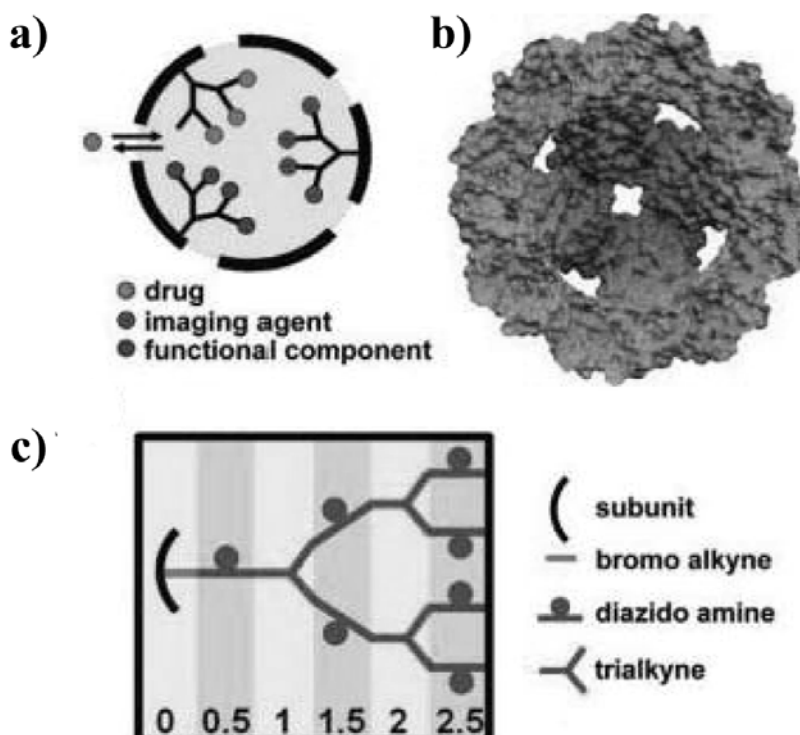
Figure 2.4 *Rationale and strategy for the fabrication of a hybrid protein dendritic cage structure. a) Scheme of a protein cage filled with a branched polymer; addressable sites on the polymer can be used to load drugs, imaging agents, or functional components of a solid-state device. b) A cutaway view of the HspG41C genetic construct. c) Scheme for sequential synthesis of the dendritic structure. Generation numbers are indicated at the bottom.*[67]

2.3 Viruses

Virus particles typically consist of several hundred to thousands of protein molecules, which self-assemble to form a hollow scaffold that holds the viral nucleic acid. In the past decade there has been growing interest in the use of virus particles as templates for nanosized materials. Viral capsids (the self-assembled protein-cage structures) offer robust and monodisperse structures and exist in a large variety of sizes and shapes. Moreover, the protein surface can be used as a synthetic platform for chemical modification. Because certain types of viruses can be obtained in large quantities and manipulated at the genetic level, they afford a unique opportunity for chemists to expand the repertoire of natural starting materials for synthetic and catalytic applications.

Rod-shaped virus: tobacco mosaic virus (TMV)

The tobacco mosaic virus (TMV) is the most comprehensively understood system of biological self-assembly to date.[68,69] TMV is a stable virion that can withstand temperatures of up to 90 °C, pH values as low as 2 and as high as 10, and solvents such as ethanol and DMSO. TMV can be obtained in large quantities from infected plants and it is made up of 2130 identical protein building blocks (of molecular weight 17.5 kDa) arranged in a helical motif around the viral RNA to form a hollow tube 300×18 nm in size with a central channel that has a diameter of 4 nm (Figure 2.1).[6,7] The TMV assembly process results in a template that has an inherent asymmetry and chirality, which is distinct from that of the spherical viral capsids. This allows for chemical and genetic modifications at one end or the other of the helical rod. TMV can form three different kind of assemblies, depending on the solution conditions, as depicted in Figure 2.5.[70] Furthermore, mutations in which aspartic acid or glutamic acid are transformed into asparagine or glutamine, respectively, showed that assembly of the virion is possible without RNA.[71]
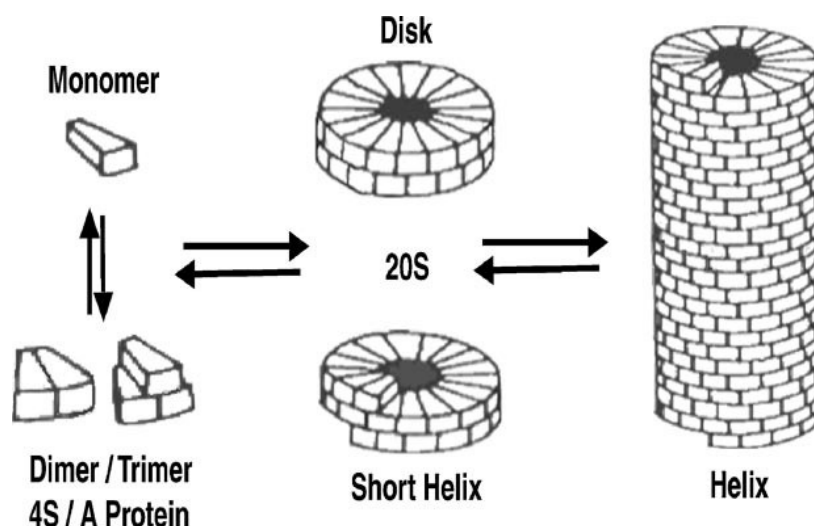
Figure 2.5 *The three possible assembly forms of the TMV coat protein. 1) The 4S/A-protein dimers and trimers, 2) the 20S disks and short helices, and 3) the extended helical rod.[70]*

Template mineralization of TMV: formation of nanotubes and nanowires

The internal and external surfaces of the TMV protein capsid consist of repeat patterns of charged amino acid residues, such as glutamate, aspartate, arginine, and lysine. These functionalities were first used by Mann and co-workers as nucleation sites for surface-controlled biomineralization.[72] Taking advantage of the surface chemistry of TMV, and the high stability of the protein assembly, they could mineralize a variety of inorganic solids on the virus outer surface with the concomitant formation of nanotubes (Figure 2.6a).

The electrochemical modification of the TMV inner and outer surface was performed by Knez et al., by electroless deposition of different metals such as nickel and silver.[73,74] Depending on the metallization conditions, they could selectively target the outer or inner surface of the tubelike TMV, as shown by TEM (Figure 2.6b). Furthermore, the same group used TMV for the synthesis of metal nanowires.[75] The central channel of the virus was used as a template to synthesize nickel and cobalt wires only a few atoms in diameter and lengths up to the micrometer range. More recently, bimetallic alloys of $CoPt$, $CoPt_3$, and $FePt_3$ nanowires have been synthesized in the TMV capsid channel.[76] Dujardin et al. also investigated the use of cylindrical particles of TMV as templates for the in situ formation of anisotropic assemblies of spherical Pt, Au, or Ag nanoparticles.[77]

a)

b)
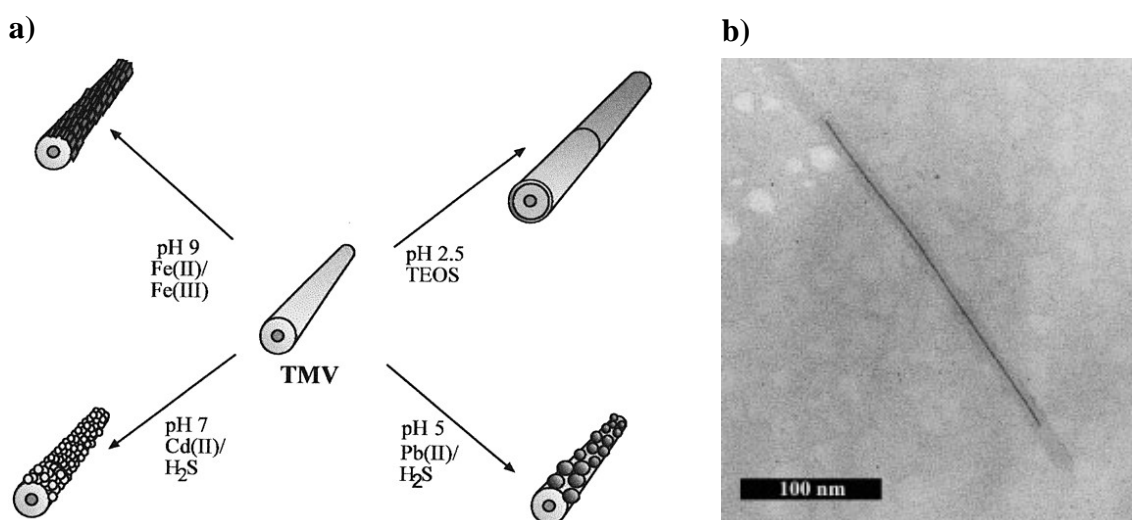
Figure 2.6 a) Routes for the synthesis of nanotube composites by using TMV templates. Clockwise from top right: sol−gel condensation (silica); coprecipitation (PbS and CdS nanocrystals); oxidative hydrolysis (iron oxide).[72] b) TEM image of a TMV virion containing a nickel wire inside the central channel of the capsid.[74]

More recently other examples of TMV surface modification have been described. Royston et al., for example, have attached TMV1cys-based nanotemplates onto a solid surface to produce functional high-surface-area nanomaterials (Figure 2.7).[78] First, TMV templates were engineered to encode unique cysteine residues (TMV1cys). In a second step these templates were assembled onto a gold patterned surface. Because the engineered cysteine residues at the 3' terminus are more exposed than those embedded in the helix, the particles assembled in a vertically oriented fashion. Subsequently, electroless deposition of ionic metals onto the surface-assembled virus templates was performed, producing uniform metal coatings up to 40 nm thick. Organic molecules such as poly(ethylene glycol)[79] and carbon nanotubes[80] were also attached to the exterior surface of TMV.
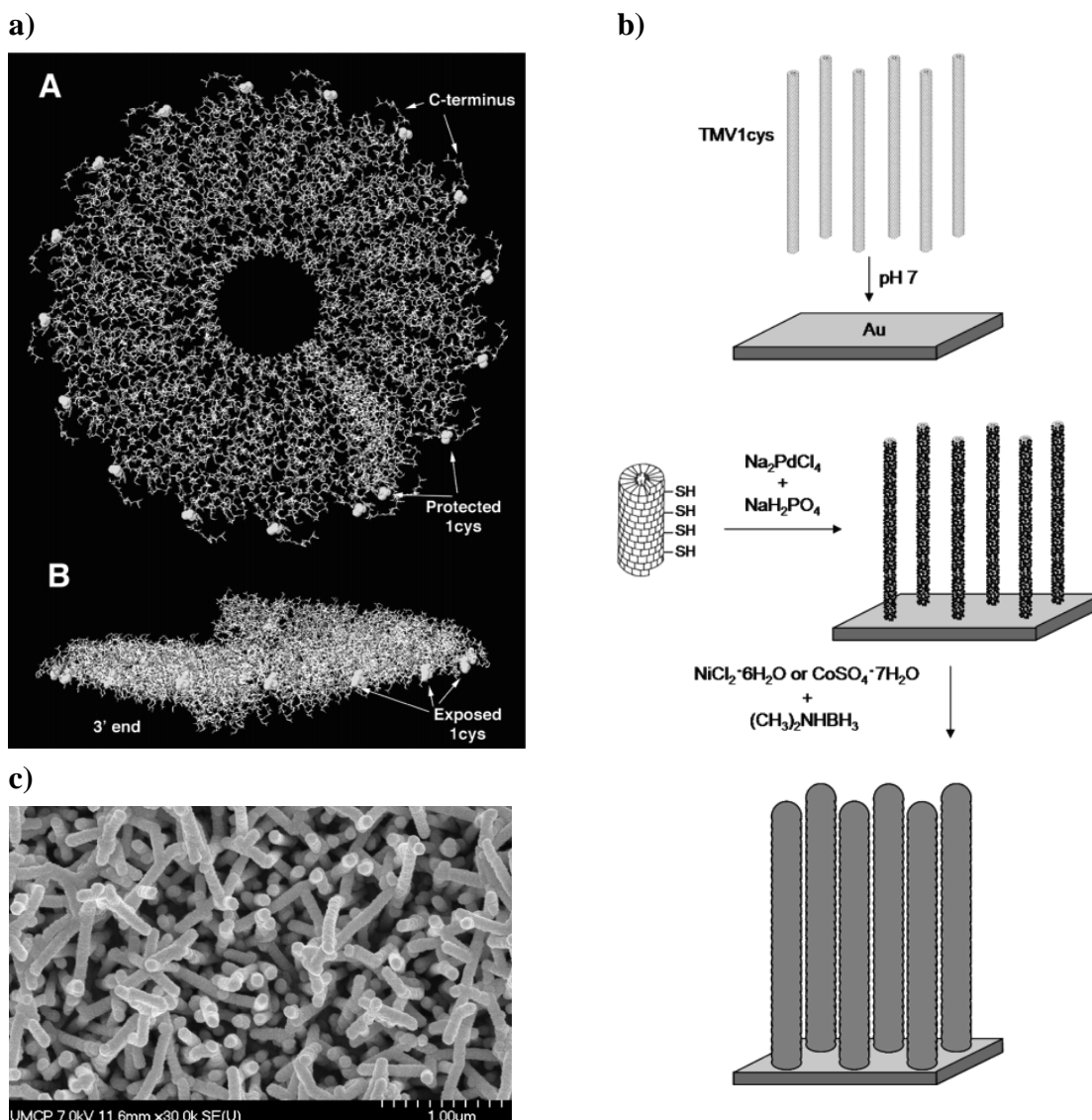
Figure 2.7 *a) Computer-generated model depicting the position of the 1cys mutations on the outer rod surface (above) and at the 3' end of TMV (below). b) Diagram showing the construction of nickel- and cobalt-coated TMV1cys molecules onto a gold surface. c) Field emission electron microscopy (FESEM) images showing a nickel-coated gold surface with 1 mg mL^{-1} TMV1cys particles.*[78]

TMV as a self-assembling, multichromophoric system

The development of synthetic self-assembling, multichromophoric systems to create tunable light-harvesting architectures is an important goal in the fields of materials science and nanotechnology. The Francis group has used the *in vitro* assembly of TMV capsids to create such systems.[81] Three different fluorescent chromophores were separately attached to genetically introduced cysteine residues on the surface of the TMV coat protein. When placed under the appropriate assembly conditions, these conjugates could be assembled into stacks of disks or extended rods that reached

hundreds of nanometers in length (Figure 2.8). Photophysical studies demonstrated that efficient energy transfer is possible in these rods through direct donor–acceptor interactions. In a similar approach, Endo et al. showed that TMV coat-protein subunits could be chemically modified with either Zn-coordinated porphyrin or free-base porphyrin.[82] When assembled *in vitro*, these materials also displayed energy-transfer and light-harvesting properties.
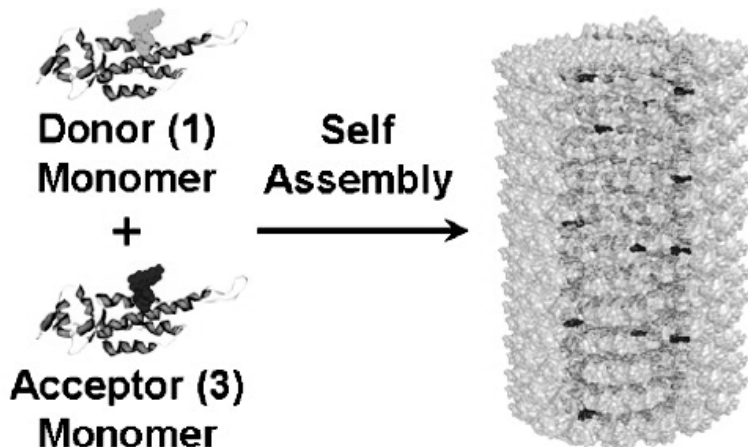
Figure 2.8 Synthetic of light-harvesting structures. Mixtures of modified TMV coat protein monomers labeled with dye 1 and dye 3 were assembled into rods,[81]that display energy transfer and light-harvesting properties.

 Patterning and arrays

The formation of ordered aggregates of TMV in the presence of divalent metal ions has been studied in concentrated solutions of the virus.[83] Some divalent metal ions were found to promote the precipitation of TMV and it was shown that the precipitates possessed nematic liquid-crystalline behavior. Nematic liquid crystals of TMV have also been used to prepare silica nano- and mesostructures with parallel or radial arrays of linear channels.[84] Tubular structures based on TMV as a template have been obtained by Fujikawa and Kunitake.[85] They assembled TMV on a surface and then covered it with ultrathin titania films in a sol−gel process. Another example is the work of Yi et al., who assembled TMV onto glass substrates patterned with specifically captured DNAs.[86,87] This approach provides a reliable, selective, and controllable approach to assemble multiple TMV molecules. Furthermore, a paper has been published in which the adsorption and surface behavior of TMV on different surfaces was studied by noncontact atomic force microscopy (AFM).[88]

Cage-structured virus: cowpea mosaic virus (CPMV)

The cowpea mosaic virus (CPMV) is a plant virus that belongs to the family of *Comoviridae*. It infects black-eyed pea plants (*Vigna unguiculata*) and it can be obtained in good yields; gram quantities of virus particles can be isolated from a kilogram of infected leaf tissue.[89]

The virus possesses a structure that is known at atomic resolution[90] and it is remarkably stable; its particles maintain their integrity at 60 °C (pH 7) for at least 1 h and at room temperature and pH values from 3.5 to 9 for almost indefinite periods of time.[91,92] The virus, therefore, is of potential use as a building block in bio-nanotechnology. The CPMV capsid is formed by 60 copies of an asymmetric unit that is composed of two protein subunits: a small one, the A domain, and a large one, the B+C domain (Figure 2.9a). These 60 asymmetric units self-assemble around a single-stranded RNA genome to form the virus particle. The virus displays icosahedral symmetry, the outer diameter of which is approximately 30 nm (Figure 2.1). In addition to the small percentage of capsids devoid of RNA which are produced during infection,[93] it is possible to generate empty CPMV capsids by hydrolyzing the RNA.[94] Infectious clones of the virus RNAs are available and allow site-directed mutations or peptide insertions in the capsid proteins.[95] When plants are infected with the mutated RNAs, the sequence is genetically stable through multiple rounds of infection, harvesting, and reinoculation.[96,97]

a)

b)   c)   d)

βB-βC loop (small subunit)

	18	19	20	21	22	23	24	25	26
wild type	S	T	P	P	A	P	F	S	D

virus 1 ····S—T—P—P—A   R—F—S—D····
                    18 19 20 21 22   23 24 25 26
                         G   G
                          G—C—G

virus 2 ····S—T—P—P—A—P—F—C—D····
        18 19 20 21 22 23 24 25 26

βE-βF loop (large subunit)

	94	95	96	97	98	99	100	101
wild type	S	G	V	R	G	K	Y	S

virus 3 ····S—G—V—R—G   K—Y—S····
        94 95 96 97 98   99 100 101
                 G   G
                  G—C—G

virus 4 ····S—G—V—R—G   K—Y—S····
        94 95 96 97 98   99 100 101
                 C—A
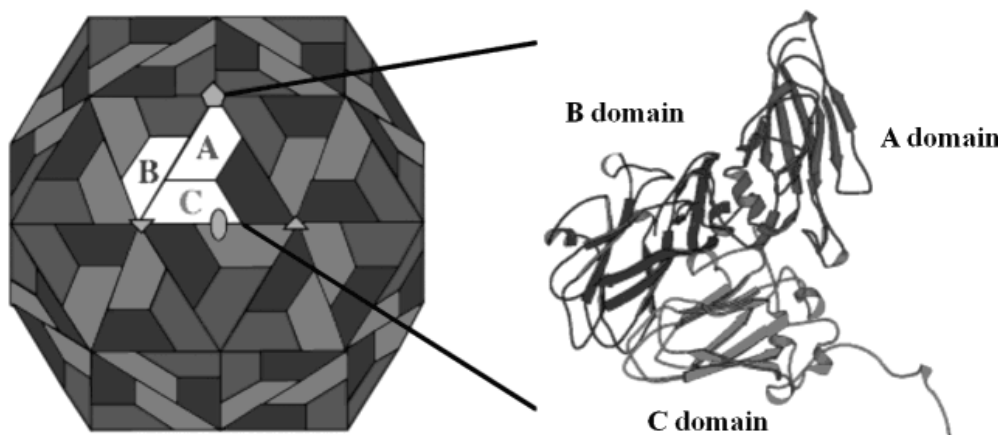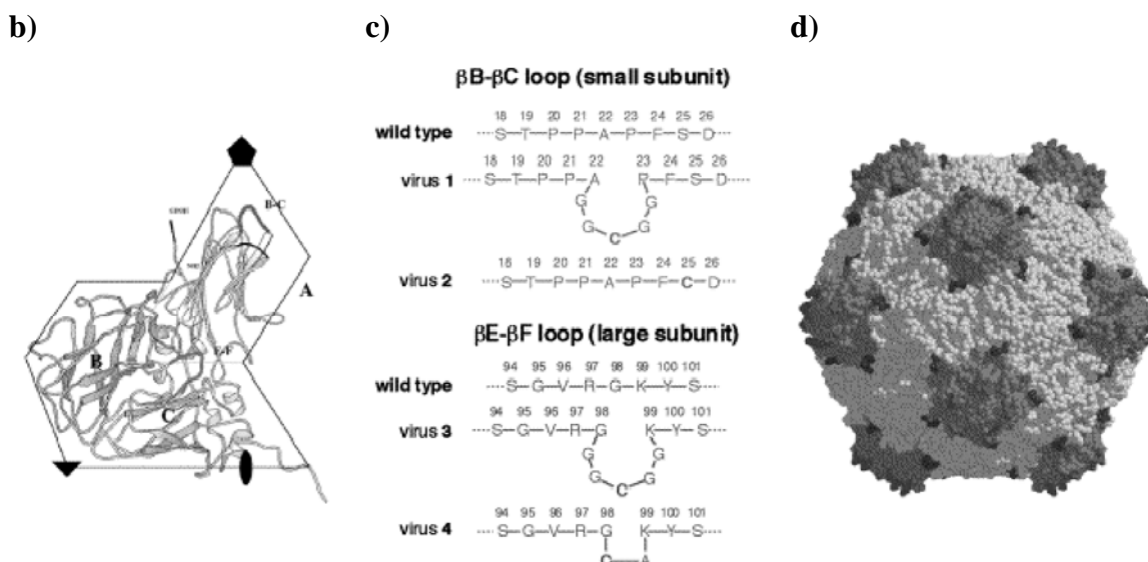
Figure 2.9 *Structure of CPMV and cysteine-added mutant of CPMV. a) Left: schematic representation of CPMV, showing the distribution of the protein subunits that comprise the asymmetric unit. Right: the folds of the two subunits, A and B+C.[91] b) The atomic structure of the CPMV coat protein, with the sites of mutational insertion βB-βC loop and βE-βF loop. c) Amino acid sequences corresponding to native and mutant CPMVs 1–4. d) A model of the entire particle showing the addition of a five amino acid residue insert (GGCGG) at the two positions of interest in the wild-type CPMV structure. The resulting mutant viruses correspond to 1 and 3. The BC loop resides further "up" on the protruding cap than the EF loop at each fivefold axis of the icosahedral structure.[98]*

Traditional bioconjugation strategies

Both wild-type (wt) and genetic variants of CPMV have been used as scaffolds for chemical derivatization. Early investigations of the chemical reactivity of wt CPMV,[99] and mutant CPMV,[98] which aimed at lysine- and cysteine-selective derivatives, revealed that CPMV can be easily modified. Finn and co-workers showed that activated fluorophores in the form of N-hydroxysuccinimide (NHS) esters can react with endogenous lysines (K) and be linked to the virus surface.[99] Unique reactivity was achieved through the introduction of cysteine residues on the virus outer surface, which could be modified with either maleimide-functionalized fluorophores or gold nanoparticles (see below), by means of genetic manipulation (Figure 2.9b–d).[91,98] The functionalization of cysteine and lysine residues with biotin derivatives resulted in virions decorated with biotin molecules, which were shown to assemble by cross-linking with avidin or streptavidin (Figure 2.10).[98-100] These types of experiments provide information as to whether the reactive thiol and amine groups are situated on the inner or outer surface of the virus particle.

a)   b)
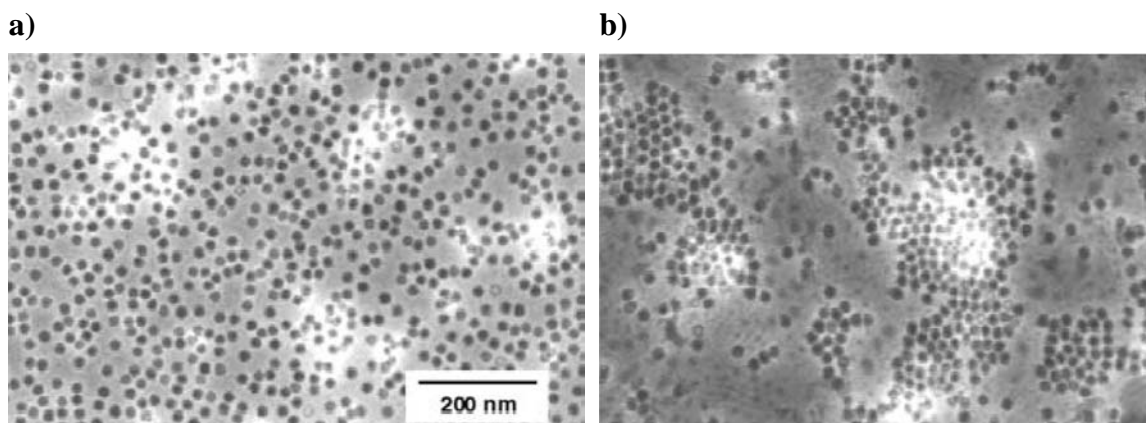
Figure 2.10 *Electron microscopy images of virus–biotin–avidin aggregates. a) CPMV–(biotin)$_{20}$ (0.1 mg mL^{-1}). b) CPMV–(biotin)$_{20}$ (1.5 mg mL^{-1}) plus avidin (0.5 mg mL^{-1}); the mixture was diluted by a factor of 10 before observation by means of TEM.*

Once the reactivity of the different endogenous and engineered functional groups on the inner and outer surface of the CPMV had been determined, different types of modifications of the virus could be performed, for example, the construction of hybrid CPMV virus−polymer particles by derivatizing the outer surface of the virus with poly(ethylene glycol) (PEG).[101-103] The resulting hybrids had physical and immunogenic properties that were markedly different from those of the native virus, which opens possibilities for biomedical applications. In addition to PEG, other compounds have been covalently attached to surface-exposed amino acids, for example redox-active compounds,[104,105] antibodies,[106] small proteins,[107] oligonucleotides,[108] quantum dots (QD),[109-111] and carbohydrates.[112,113] Furthermore, different mutants of CPMV have been used as scaffolds to bind gold nanoparticles through gold−sulfur bond formation.[114,115] Unstained TEM images showed patterns that were in line with the locations of the cysteine functions on the capsid (Figure 2.11). Such experiments in which the CPMV capsid acts as a template, to create complex 3D assemblies, have great potential for the design of nanodevices such as sensors or electronic circuits.[114,116]
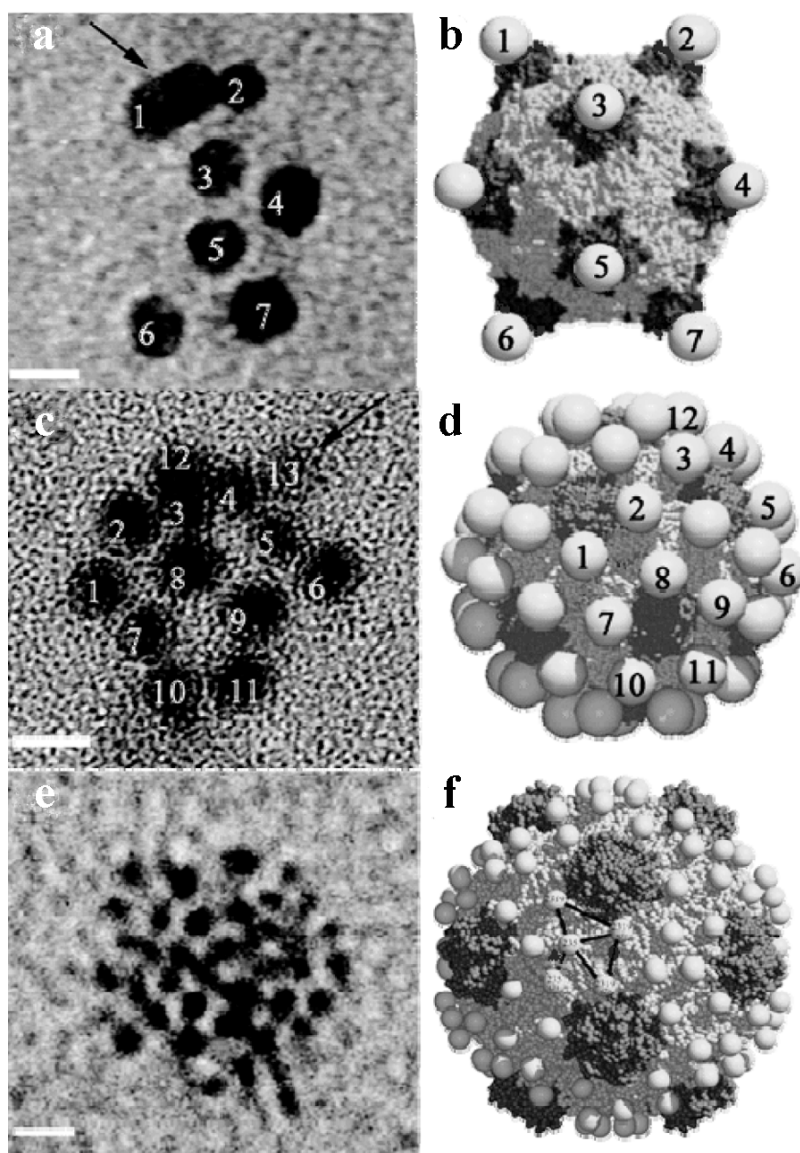
Figure 2.11 TEM images and models of three different CPMV mutants with gold nanoparticles on the outside surface (scale bars are 5 nm long). a) Unstained TEM image of eight gold nanoparticles bound to an isolated CPMV virus mutant. The arrow marks a fivefold axis with two particles bound to two different cysteine residues around the axis. b) Model of the CPMV mutant in (a) showing the location of the eight gold particles (one gold particle per fivefold axis). c) Unstained TEM image of 13 gold nanoparticles bound to an isolated CPMV virus mutant. The arrow marks a nanoparticle on the other side of the virus that is out of focus. d) Model of the mutant in (c) showing the 13 gold particles. e) Unstained TEM image of an isolated CPMV mutant with 42 gold particles bound to it. The spherical shape of the virus is clearly visible due to the large number of gold particles that are bound to the virus. f) Model of the CPMV mutant shown in e).[114]

Bioconjugation via the copper(I)-catalyzed azide–alkyne cycloaddition reaction

The exterior surface of the protein cage of CPMV has also been decorated with azide and alkyne groups, which were treated with derivatives containing the complementary groups (alkyne or azide) for a copper(I)-catalyzed azide–alkyne [3+2] cycloaddition reaction (so-called "click" reaction).[117] The improved efficiency and selectivity of this bioconjugation approach has expanded the array of compounds that can be attached to virus scaffolds. CPMV has been modified in this way with small compounds, such as fluorescent dyes,[117-119] gadolinium complexes,[120] and sugars, but also with large compounds as polymers,[121] and even the 80 kDa protein transferrin.[119] Many of these constructs have important applications in biomedicine, for example, CPMV coupled to gadolinium-tetraazacyclododecanetetraacetic acid (Gd(DOTA)) analogues by "click chemistry" has been used as contrast-enhancing agent for medical diagnostics (Figure 2.12).[120]
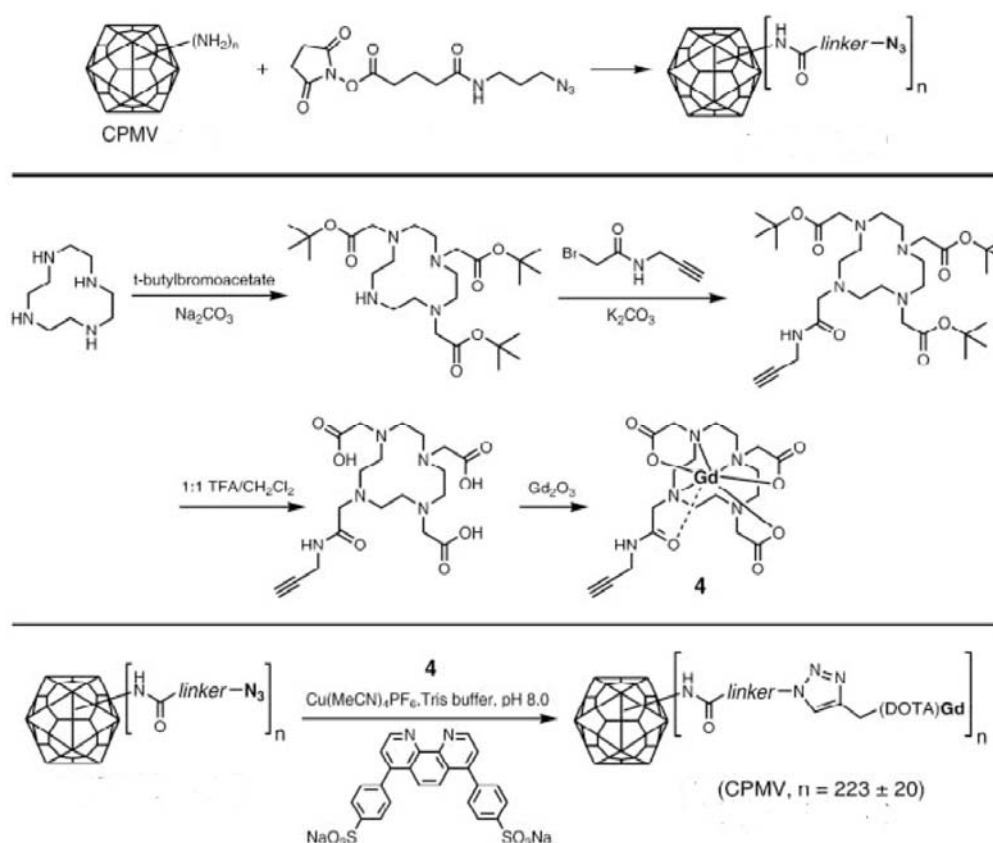
Figure 2.12 *Synthesis of Gd(DOTA)-derivatized CPMV.[120]*

Fabrication of CPMV arrays

The presence of two different subunits (A and B) in CPMV offers the possibility to specifically modify the viral protein capsid at different locations by genetic methods or chemical reactions. This allows breaking of the symmetry of CPMV and the ordering of
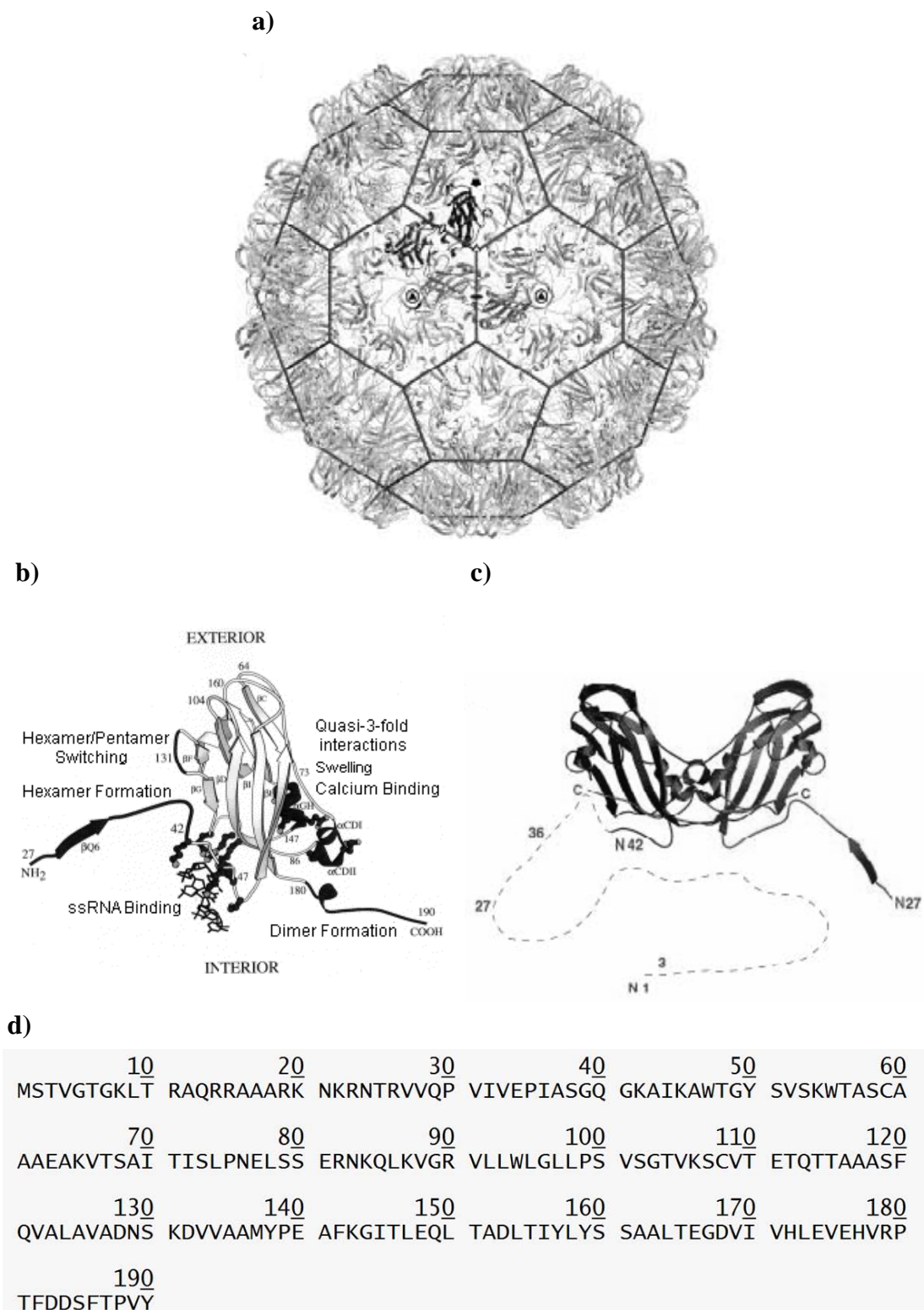
the virus into 2D and 3D structures. Different approaches have been followed to assemble modified CPMV particles into hierarchically ordered structures.[108,109,122,123] For example, complex patterns could be made by allowing droplets of concentrated solutions of modified CPMV to dry on mica surfaces. The resulting patterns were studied by AFM.[124] Furthermore, dip pen nanolithography (DPN) has been combined with chemoselective protein-to-surface linkers to create nanometric chemical templates for the fabrication of arrays of virus particles.[125,126] To this end, DPN was used to pattern a gold substrate with a thiol-selective linker to which a genetically modified Cys-CPMV was immobilized. Layer-by-layer assembly using solutions containing the streptavidin–biotin pair has been applied to make arrays of CPMV on a solid support.[100,127] All these examples highlight that CPMV offers great opportunities for new science in the fields of biomaterials and nanotechnology.[128]

2.4 The Cowpea Chlorotic Mottle Virus (CCMV)

In this section a detailed description of the cowpea chlorothic mottle virus (CCMV) is given because CCMV is the virus used for the studies described in this thesis. First the structure and properties of the virus will be discussed as well as its assembly pathways. Subsequently, the potential use of CCMV as a reaction vessel, as a scaffold for chemical derivatization, and as a building block in hierarchical assemblies will be highlighted.

Structure

CCMV is a member of the bromovirus group of the *Bromoviridae* family of plant viruses.[129] It is formed by the assembly of 180 identical coat protein subunits around the genetic material, which is RNA. The CCMV genome consists of four single-stranded, positive-sense RNA molecules, which are encapsidated into three structurally similar virions.[130,131] The protein subunits are arranged as 20 hexamers and 12 pentamers altogether forming an icosahedral shell 28 nm in diameter with T = 3 quasi-symmetry (see Appendix, Figure 2.13). Every coat protein contains 190 amino acids with the N terminus located on the inside of the virus capsid (Figure 2.13a and b). The residues on the N terminus (amino acids 1–25) are predominantly basic and are responsible for interaction with the negatively charged RNA. The residues are not ordered according to icosahedral symmetry and therefore not seen in the crystal structure of the virus (Figure 2.13c). The C terminus, namely, amino acids 186–190 (for the complete amino acid sequence see Figure 2.13d), of a subunit reciprocally deeply invades an adjacent subunit and results in the formation of a noncovalent coat-protein dimer (Figure 2.13c). This explains the existence of subunit dimers in solution when the virus is completely disassembled.[129,132]

a)

b)   **c)**

Hexamer/Pentame
Switching

Hexamer Formatio

27   βQ6
NH₂

ssRNA Bind

d)

```
          10          20          30          40          50          60
MSTVGTGKLT  RAQRRAAARK  NKRNTRVVQP  VIVEPIASGQ  GKAIKAWTGY  SVSKWTASCA

          70          80          90         100         110         120
AAEAKVTSAI  TISLPNELSS  ERNKQLKVGR  VLLWLGLLPS  VSGTVKSCVT  ETQTTAAASF

         130         140         150         160         170         180
QVALAVADNS  KDVVAAMYPE  AFKGITLEQL  TADLTIYLYS  SAALTEGDVI  VHLEVEHVRP

         190
TFDDSFTPVY
```

***Figure 2.13*** *The CCMV particle. a) The crystal structure of the T = 3 CCMV capsid with the pentameric and hexameric faces drawn on the cage structure. The symmetry axes are highlighted with two-, three-, five-, and sixfold symbols, open symbols indicate quasi-symmetry and filled symbols icosahedral symmetry. Each asymmetric unit contains three subunits, A in blue, B in red, and C in green (for colors see Figure 2.16*

and the Schematic Overview on page 187). There are two types of dimers in the capsid: the A–B dimer and the C–C dimer. b) Ribbon diagram showing the tertiary structure of the protein subunit of CCMV. Selected residues and secondary structure elements are labeled together with the functions of the highlighted regions. c) A close-up view of the A–B dimer interaction showing the interdigitated C-terminal peptides that produce a strong dimer. The crystal structure of the A subunit (blue) starts at amino acid residue 42, whereas the B subunit (red) has a more ordered N-terminus and starts at residue 27.[129,132,133] *d) Amino acid sequence of the CCMV coat protein.*

Properties

Dynamic structural transitions occur in many viruses, often induced by specific chemical signals. One interesting feature of CCMV is its sensitivity to pH and ionic strength.[132] CCMV undergoes a reversible pH-dependent swelling, which results in a 10% increase in virus dimension. Structural analysis has revealed that CCMV swelling leads to the formation of 60 separate openings (2 nm in diameter) at the quasi-threefold axes (Figure 2.14).[129] Furthermore, depending on the pH and ionic strength, CCMV particles can be rapidly disassembled *in vitro* into dimers and RNA, and then reassembled again. Empty capsids (capsids devoid of viral RNA) are not found in natural infections. In contrast, *in vitro* assembly using purified coat protein or expression of the CCMV coat protein in heterologous expression systems (*e.g.*, bacteria) can result in capsids devoid of viral RNA.[131,134-136] The cavity is 18 nm in diameter; approximately twice the diameter of the iron storage protein ferritin. In the assembled empty capsid, the interior surface carries a high positive-charge density due to the presence of nine basic residues (arginine and lysine) in the amino-terminal region that project inward into the capsid interior. This interior surface, in the absence of RNA, can be used for directing the nucleation of mineralization to produce spatially constrained nanoparticles in the preformed capsid, as shown below.

a)   b)
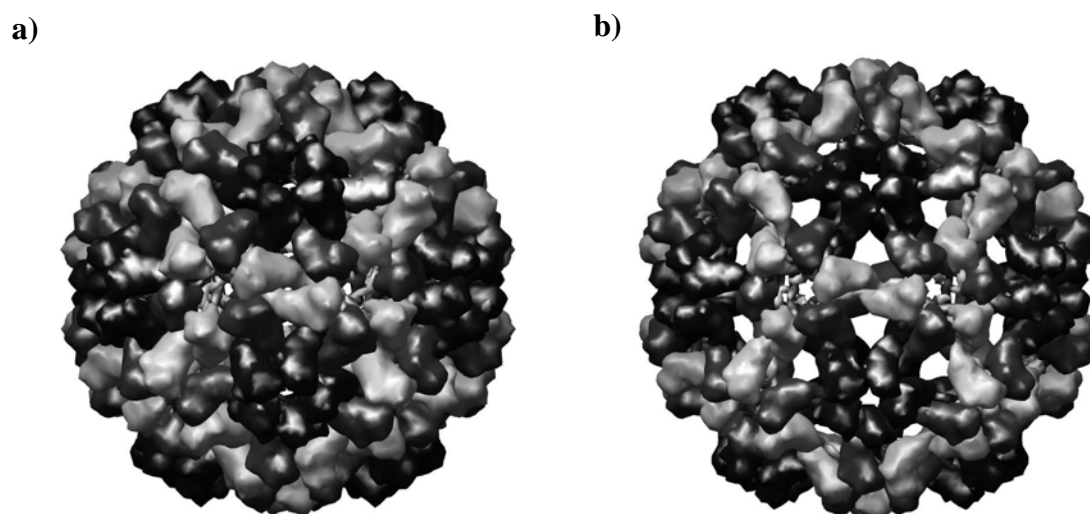
Figure 2.14 *Model of the a) unswollen and b) swollen CCMV.*

CCMV assembly

In the 1960s, Bancroft et al. performed the first steps towards the mechanistic elucidation of CCMV virus and capsid assembly *in vivo* and *in vitro* under different solution conditions (*e.g.*, pH) and in the presence of different polyelectrolytes.[134,137-140] They observed that the virus assembly is dynamic and that different types of architectures (*e.g.*, tubes, sheets, and multiple shells) can be formed by varying the assembly conditions. An increased understanding of the system has been obtained by a combination of genetic modifications of the subunits and controlling the *in vitro* assembly conditions. Based on the X-ray structure of CCMV, it was postulated in 1995 that hexamers of dimers nucleate the assembly process.[132] This hypothesis was weakened when Zlotnick et al., using full-length CCMV subunits in the absence of RNA, demonstrated *in vitro* that pentamers of dimers (PODs) nucleate protein capsid assembly and that propagation of this process proceeds via the addition of subunit dimers and PODs.[141] Willits et al. corroborated this hypothesis by proving that hexamers with their associated β-barrel structure were not critical for proper assembly.[142] Johnson et al. proposed a mechanism for CCMV assembly in which the first step consists in the formation of a coat protein–RNA complex followed by folding and growth (Figure 2.15).[143,144]
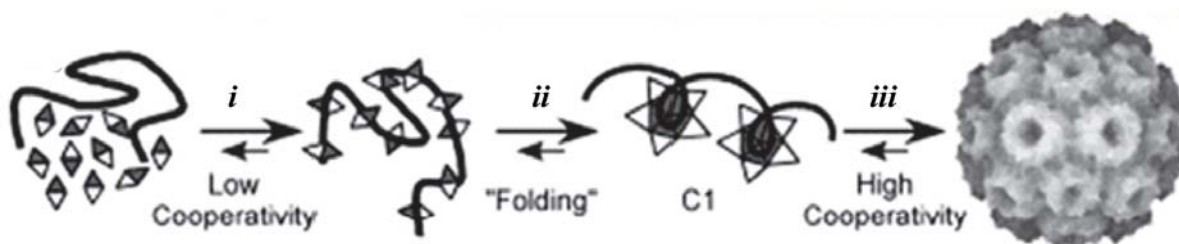
Figure 2.15 *Proposed assembly path for CCMV. i) CP initially binds excess RNA with low cooperativity. ii) CP and RNA slowly fold to form the C1 nucleoprotein complex. This step is not required for RNA packaging. It is found that about ten CP per RNA are required for folding; the actual stoichiometry and structure of the C1 complex however is not known. iii) Addition of CP to C1 is highly cooperative and yields the complete virus particle.*

Other *in vitro* studies on the assembly of the CCMV coat protein have shown that a mutant CCMV coat protein lacking most of the N-terminal domain (3–36) or naturally degraded subunits (which usually lack the same N-terminal domain), assemble *in vitro* into products with high heterogeneity (polymorphism).[133] This observed behavior is believed to be the result of a change in the interaction between two dimers, which in turn depends on the increased flexibility of the structure defining the dihedral angle between the two protein subunits present in the dimers. Not only the expected native-like T = 3 capsids of 90 dimers are formed, but also smaller capsids, namely, "T = 2"

capsids of 60 dimers and T = 1 capsids of 30 dimers (see Appendix). The results are consistent with the POD nucleating assembly theory, and assembly pathways were proposed for each of the particles (Figure 2.16). However, the outcome also shows that the capsid geometry is flexible and may readily adapt to new requirements as the virus evolves. Recently, these same mutant coat proteins have been assembled around solid nongenomic cores, resulting into structures that can be tuned by varying the nongenomic core size.[145]
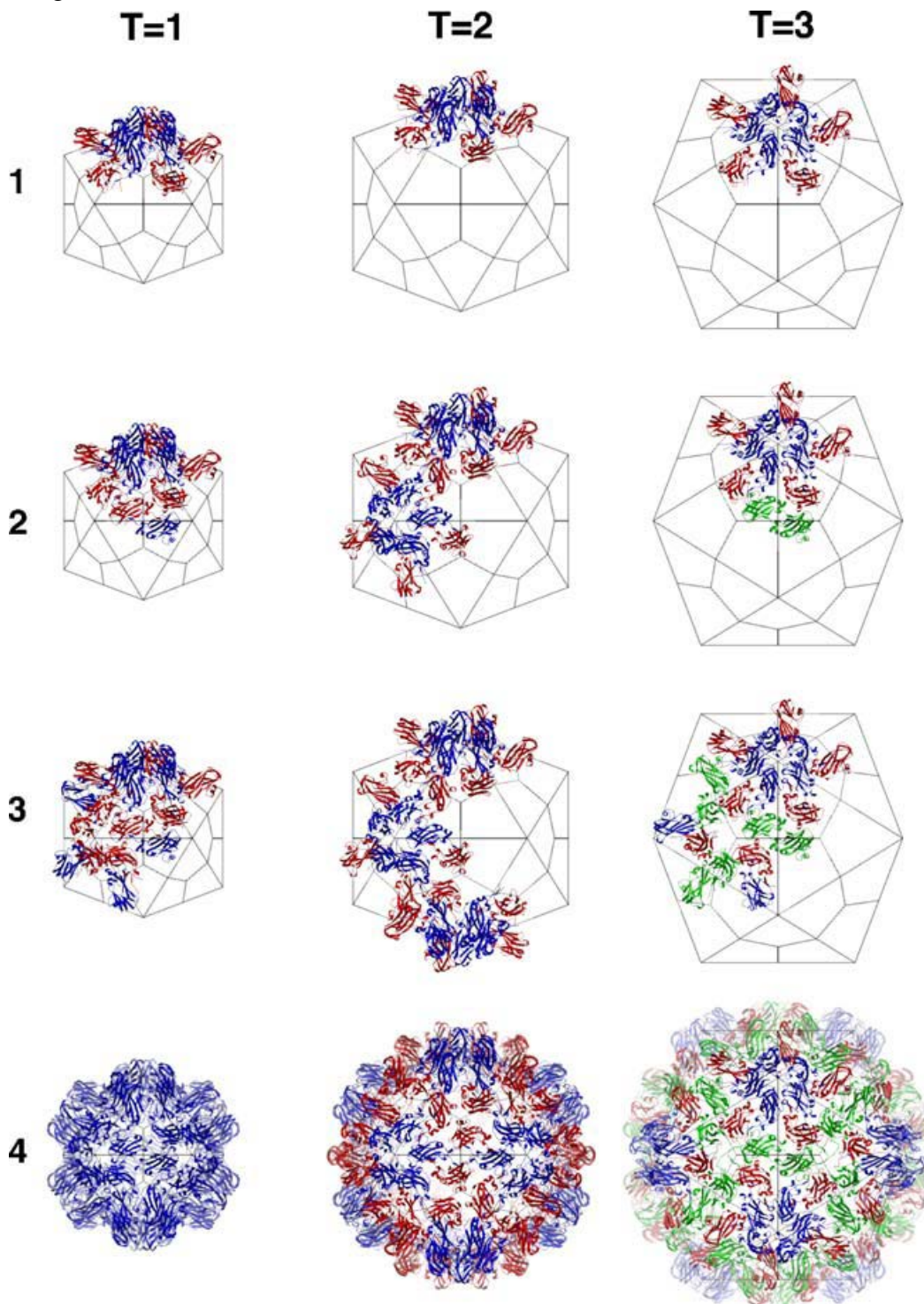
Figure 2.16 Proposed assembly pathways for the different particle types. The assembly proceeds from top to bottom. 1) The assembly of each particle type starts with a POD for nucleation. 2) Addition of a dimer to the starting POD can direct assembly toward T = 1 or T = 3 particles, depending on the trajectory established by the dihedral angle in the dimer. The "T = 2" is formed by the addition of preformed PODs. In the case of T = 1 only A–B dimers are added (blue/red), while T = 3 particles can add either A–B or C–C (green/green) dimers. 3) More dimers have been added to T = 1 and T = 3 particles, while "T = 2" receive more PODs. 4) The finished T = 1 particle has all subunits in the same conformation, depicted in blue. The "T = 2" particle contains two kinds of subunits (blue/red) and the T = 3 particle has three structurally unique subunits in its asymmetric unit (blue, red, and green).

As shown above, the manipulation of the interactions between coat-protein subunits allows some degree of control over the final capsid shape. This has important consequences for applications in nanotechnology. The way the capsid architecture is directed by the nucleic acid has been mimicked, for example, by using carboxyl acid terminated PEGs to which Au nanoparticles were attached,[146] sulfonated polymers,[147-149] TMV polynucleotides,[150] and DNA.[151]

CCMV as reaction vessel

Inspired by ferritin, the well-defined cavity of CCMV has been used as a nanoreaction vessel for the reversibly gated entrapment of organic and inorganic compounds.[1,2,6,8,15,148] The assembly properties of CCMV provides a unique pH-dependent gating mechanism to control the entrapment and release of different guest compounds. There are two different approaches for the encapsulation of material within the capsid interior. The guest molecules can be entrapped during the capsid assembly process or they can diffuse into the preassembled capsid architectures through the capsid pores. The host−guest relationship between the viral cage and the encapsulated material is primarily based on a complementary electrostatic interaction. In the native viral protein cage, the cationic interior of the virus interacts with the polyanionic RNA. This electrostatic host−guest interaction has also been used to bind other polyanions.[138,147,148,151]

Douglas and Young were the first to report the encapsulation of polyoxometalate species (paratungstate and decavanadate) inside the CCMV cage, controlled by the pH-dependent gating of the virion's pores.[148] To this end, empty virions were incubated with inorganic tungstate (WO_4^{2-}) at pH 6.5, after which the solution was concentrated, and washed at pH 5, at which point the pores in the protein shell closed and the tungstate ions oligomerized to form the polyoxytungstate. The final process was a crystallization that yielded uniform nanocrystals with a diameter of 6.7 nm, which were

characterized by TEM. In a similar way, our group recently reported a fast and efficient route to prepare, under mild conditions, monodisperse Prussian blue (PB) nanoparticles (schematically depicted in Figure 2.17a) inside CCMV capsid.[152] In this case, after the PB precursors had diffused through the pores into the capsid, the reaction was initiated by UV irradiation using a 405 nm laser beam. Fast protein liquid chromatography (FPLC), UV/Vis spectroscopy, and TEM confirmed the formation of the PB nanoparticles. In Figure 2.17b, TEM micrographs of the PB-containing capsids which were taken with and without uranyl acetate staining are shown. The particle size distribution of the PB particles was 18±1.7 nm, which accurately corresponds to the dimensions of the inner cavity of the CCMV capsid.

a)
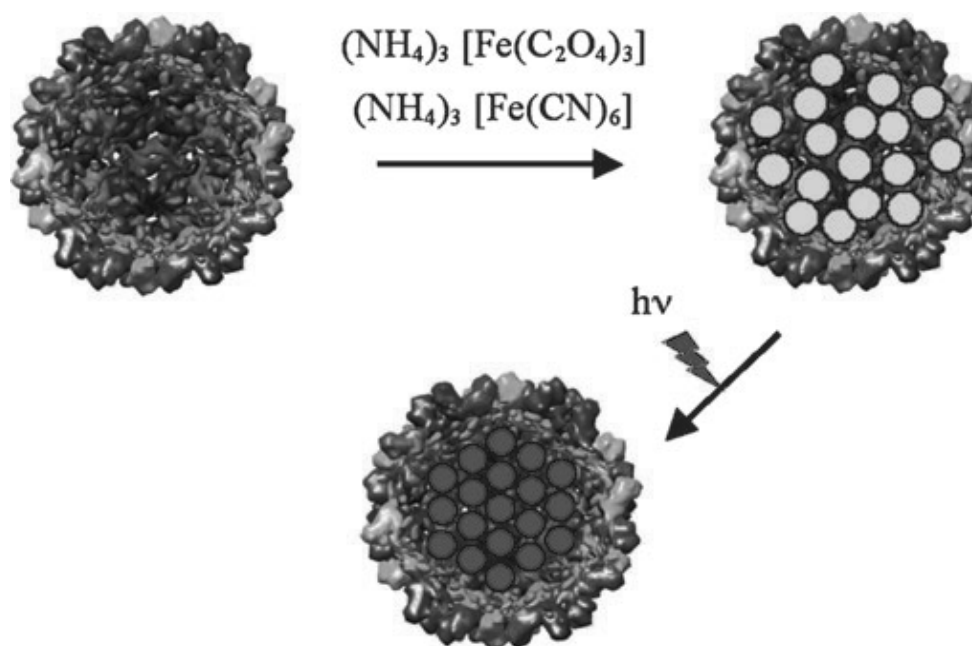
b)
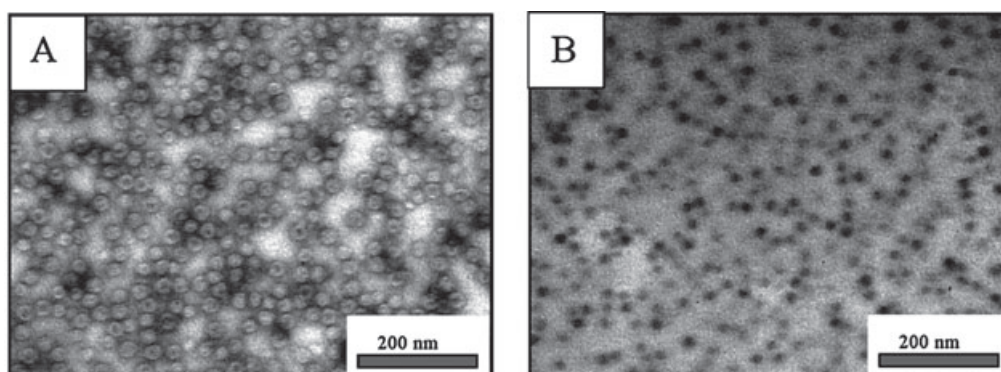
Figure 2.17 *a) Schematic representation of the approach employed to prepare PB nanoparticles within the CCMV virus particle. b) TEM micrographs of the PB–CCMV nanoparticles. A) grid stained with uranyl acetate showing the complete PB–CCMV particles. B) unstained grid, which only shows the PB particles inside the CCMV capsid.[152]*

The electrostatic properties of the interior surface of the CCMV protein cage have been altered by replacing nine basic residues at the N-terminus of every protein subunit with glutamic acid residues.[153] Also this mutant CCMV was found to assemble readily into a cage-like architecture similar to that of the wild-type virus. The modified CCMV cages were treated with Fe^{II} salts at pH 6.5, after which the particles were allowed to oxidize in air, yielding iron oxide cores as was shown by electron microscopy. The synthesis proceeded through cationic precursors that are likely to be stabilized at the interior surface of the engineered cage by complementary electrostatic interactions.

Functionalization of CCMV on the outer surface

In 2002, Douglas and Young performed the first studies on the derivatization of the external surface of CCMV by using both endogenous functional groups and engineered site-specific functional groups.[154] To these groups fluorophores could be attached without disrupting the overall cage architecture. Coupling was achieved to surface-exposed amines, carboxylic acids, and engineered thiol groups, and the degree of surface modification (and hence the number of available reactive sites) was varied (Table 2.1).[154]

Table 2.1 *Labeling of CCMV with fluorophores that react with different functional groups (between brackets) at the outside of the virus.*[154]

Fluorophore	Mol excess	Average number of attached fluorophores
FAM (lysines)	100	180/cage
	300	380/cage
	1000	540/cage
F5M (sulfhydryls)	100	30/cage
	500	60/cage
	1000	100/cage
Cadaverine (carboxylic acids)	100	500/cage
	500	520/cage
	1000	560/cage
SAMSA (bifunctional linker to lysines)	250	45/cage
	500	95/cage
	1000	150/cage

More recently, a large variety of ligands, including fluorescent dyes,[154,155] organometallic photosensitizer,[156] biotin,[155,156] small peptides,[154] and even intact IgG antibodies,[155,156] have been effectively linked to the exterior surface of CCMV by the Douglas and Young groups. Furthermore, paramagnetic gadolinium atoms (Gd^{3+}), commonly used as MRI contrast agents in humans, have been bound to the CCMV coat protein subunits.[6,155,157,158] They are located at the interface between the subunits in the assembled CCMV capsid, namely, at the quasi-threefold axes (Figure 2.18).[159]
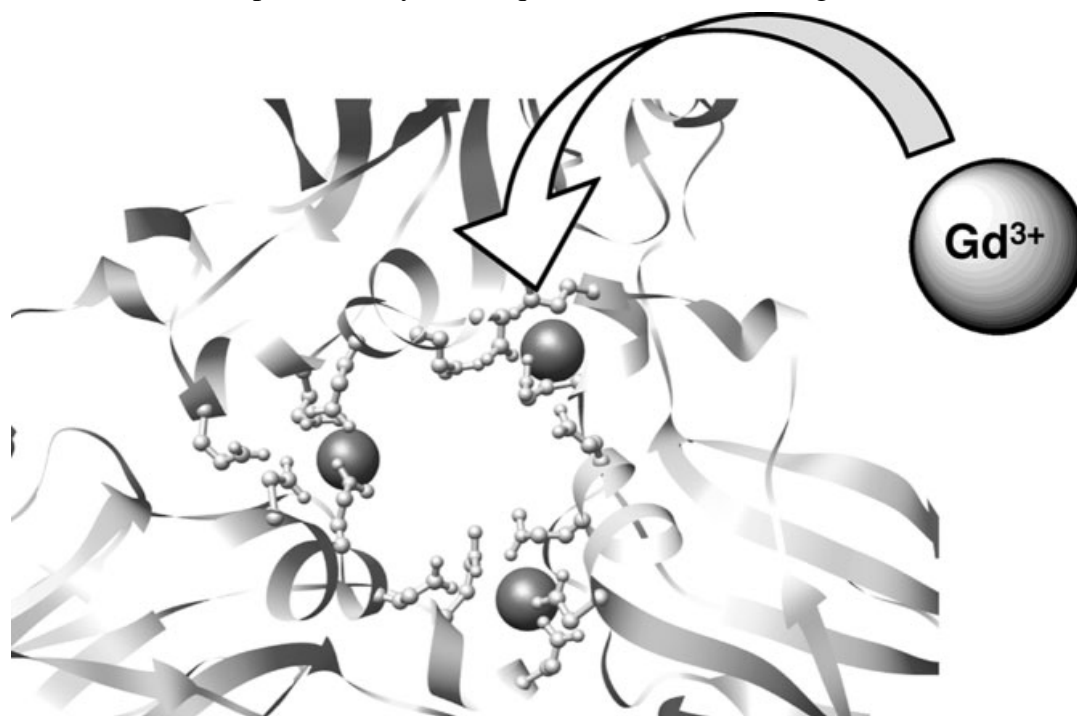
Figure 2.18 Ball and stick model of amino acids (E81, Q81, E148, Q149, D153) that make up the binding site for gadolinium ions, at the quasi-threefold axis of the CCMV.[2]

The above results demonstrate the robust nature of CCMV offering the possibility to impart multiple functionalities to the same capsid by using both the endogenous groups and the groups that can be introduced by genetic and chemical modification. The combination of surface modification and the possibility to locate molecules at the interface and in the inner cavity of the CCMV protein cage makes this virus a very interesting nanoplatform for medical and biotechnological applications (Figure 2.19).[6,155,156,160] This conclusion is supported by *in vivo* studies. When tested in mice, CCMV showed a rapid and broad distribution throughout most tissues and organs. Furthermore, it was rapidly excreted, displaying no overt toxicity after a single injection.[161]
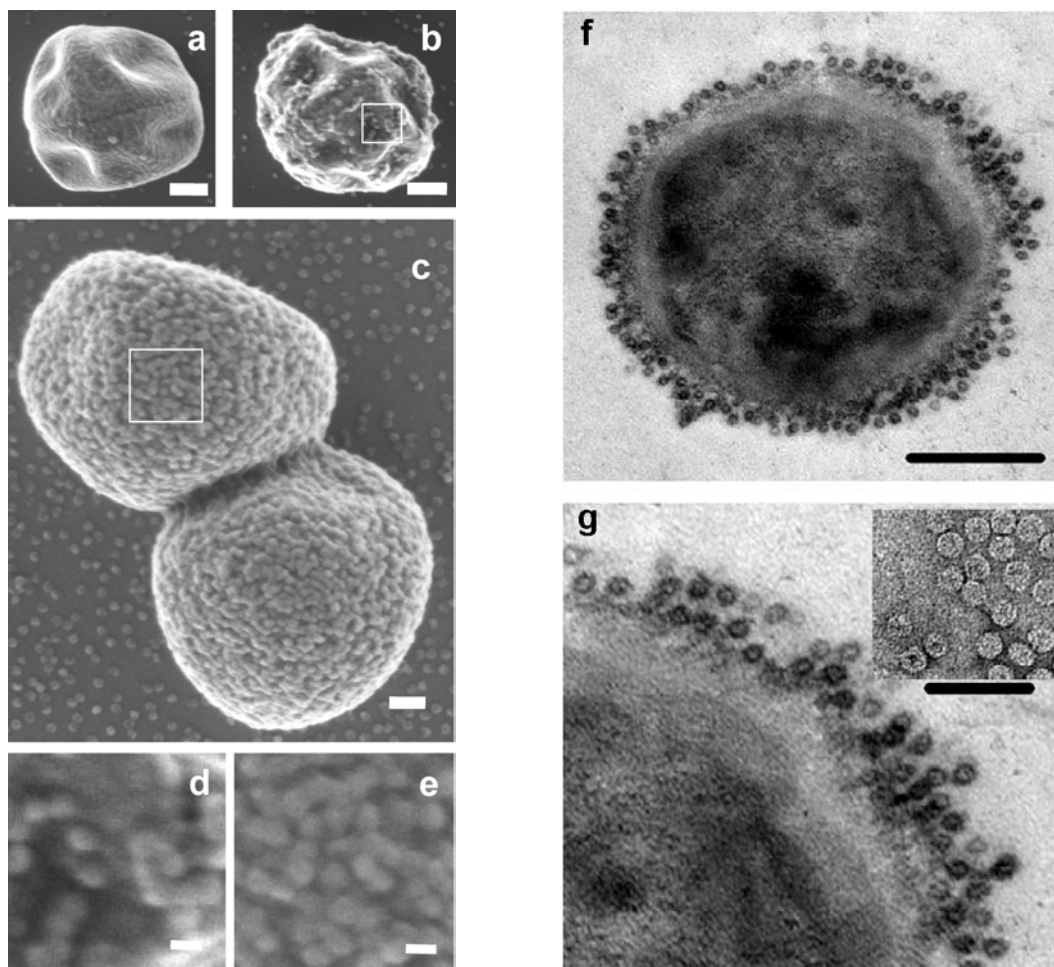
Figure 2.19 *a–e) Scanning electron microscopy (SEM) images showing the arrangement of targeted CCMV particles containing a conjugated photosensitizer (PS) on a pathogenic bacterium wall.: a) cell exposed to a CCMV mutant (S102C/K42R) with no targeting groups; b) cell targeted with a CCMV mutant (S102C/K42R-PS). Binding of the virus occurs through electrostatic interactions; c) cells targeted with a CCMV mutant (S130C/K42R-PS). Binding occurs via complementary biological interactions; d) magnification of the region indicated in (b); e) magnification of the region indicated in (c). The scale bars are: a,b) 200 nm; c) 100 nm; d,e) 28 nm (the diameter of CCMV).[156] f) TEM images of a thin section showing a high-density coverage of CCMV on* S. aureus *cells. Binding occurs through specific protein–ligand interactions. g) Magnification presented in (f). Insert shows a TEM image at the same scale as the thin slice of CCMV particles adsorbed on Formvar. The scale bars in (f) and (g) are 200 and 100 nm, respectively.[155]*

Assembly of CCMV capsids into higher-order structures

The higher order assembly of viruses into well defined 2D and 3D architectures, all the way from the nanoscale to the macroscopic scale, is one of the major challenges in the

field of bionanotechnology.[2,6,128] The construction of such high-order assemblies will need asymmetric building blocks and hence will be difficult with a particle like CCMV, which is symmetrical. Two different approaches have been reported to break the symmetry of CCMV by using either the exterior surface[162] of the virus or by manipulating its *in vitro* assembly pathway (Figure 2.20).[163] The first approach involved the synthesis of a CCMV capsid with a reactive thiol group present on only one single face, which was used to direct a 2D monolayer of capsids onto a gold surface (Figure 2.20b).[162] The second approach consisted of mixing two populations of coat proteins, each labeled with a different ligand, which resulted in capsids with a controlled stoichiometry of ligand display (Figure 2.20a).[163] Suci et al. have investigated the higher order 2D and 3D assembly of CCMV capsids by making use of electrostatic interactions. Different surfaces were tested and the assemblies were studied with AFM and Fourier transform infrared spectroscopy (FT-IR).[164] In another report three different approaches were employed to form higher order 3D architectures via the layer-by-layer (LbL) technique. In this case capsids were incorporated into multilayer films.[165]
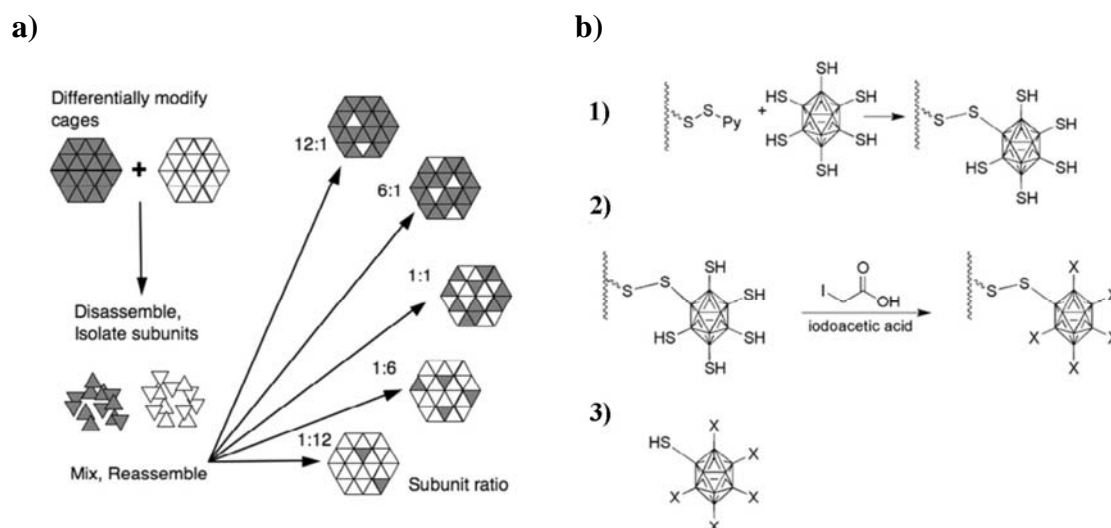
Figure 2.20 *Two different strategies to break the symmetry of the CCMV particle.*
a) Disassembly of differently modified CCMV followed by mixing and reassembly of the subunits.[163] b) Symmetry breaking by synthesizing a CCMV mutant whose alanine was replaced by a cysteine residue at position 163 on one of the subunits (A163C): 1) The viral cage is bound to resin containing activated thiol groups; 2) passivation of the remaining cysteine residues of the virus with iodoacetic acid; 3) removal of the virus by reduction, which leads to a unique SH group on the virus surface.[162]

2.5 Conclusion

The use of protein cages and viruses as multifunctional nanoplatforms and as building blocks for nanotechnology provides unique advantages. Protein cages are biological in origin and, as such, highly monodisperse and amenable to genetic manipulation and large-scale production. As exemplified in this chapter, nature has provided a wide variety of protein capsids that vary in size, stability, and functionality. These capsids can be modified by using either chemical or genetic approaches to impart specific designed functionalities. The ability to utilize the interior and exterior surfaces of the viral capsids, as well as the interface between the subunits, allows for a degree of control that spans the full range of possibilities offered by these particles. All these features will allow many of the capsid systems described in this chapter to be engineered for specific applications in materials science. This research is ongoing and can be expected to have an increasing impact on the field in the future.

2.6 References

[1]   A. de la Escosura, R. J. M. Nolte, J. J. L. M. Cornelissen, *J. Mater. Chem.* **2009**, *19*, 2274.

[2]   M. Uchida, M. T. Klem, M. Allen, P. Suci, M. Flenniken, E. Gillitzer, Z. Varpness, L. O. Liepold, M. Young, T. Douglas, *Adv. Mater.* **2007**, *19*, 1025.

[3]   T. Douglas, M. Young, *Science* **2006**, *312*, 873.

[4]   M. Fischlechner, E. Donath, *Angew. Chem. Int. Ed.* **2007**, *46*, 3184.

[5]   M. Manchester, N. F. Steinmetz, *Viruses and Nanotechnology*, Springer, Heidelberg (Germany), **2009**.

[6]   M. Young, D. Willits, M. Uchida, T. Douglas, *Annu. Rev. Phytopathol.* **2008**, *46*, 361.

[7]   C. M. Niemeyer, *Angew. Chem. Int. Ed.* **2001**, *40*, 4128.

[8]   T. Douglas, M. Young, *Adv. Mater.* **1999**, *11*, 679.

[9]   C. E. Flynn, S.-W. Lee, B. R. Peelle, A. M. Belcher, *Acta Mater.* **2003**, *51*, 5867.

[10]   P. S. Arora, K. Kirshenbaum, *Chem. Biol.* **2004**, *11*, 418.

[11]   C. B. Mao, D. J. Solis, B. D. Reiss, S. T. Kottmann, R. Y. Sweeney, A. Hayhurst, G. Georgiou, B. Iverson, A. M. Belcher, *Science* **2004**, *303*, 213.

[12]   P. Natarajan, G. C. Lander, C. M. Shepherd, V. S. Reddy, C. L. Brooks III, J. E. Johnson, *Nat. Rev. Microbiol.* **2005**, *3*, 809.

[13]   M. Carrillo-Tripp, C. M. Shepherd, I. A. Borelli, S. Venkataraman, G. Lander, P. Natarajan, J. E. Johnson, C. L. Brooks III, V. S. Reddy, *Nucleic Acids Res.* **2009**, *37*, D436.

[14]   I. Yamashita, *J. Mater. Chem.* **2008**, *18*, 3813.

[15]   D. M. Vriezema, M. Comellas Aragones, J. A. A. W. Elemans, J. J. L. M. Cornelissen, A. E. Rowan, R. J. M. Nolte, *Chem. Rev.* **2005**, *105*, 1445.

[16]   N. D. Chasteen, P. M. Harrison, *J. Struct. Biol.* **1999**, *126*, 182.

[17]   F. C. Meldrum, V. J. Wade, D. L. Nimmo, B. R. Heywood, S. Mann, *Nature* **1991**, *349*, 684.

[18]   S. Mann, F. C. Meldrum, *Adv. Mater.* **1991**, *3*, 316.

[19]   S. Mann, D. D. Archibald, J. M. Didymus, T. Douglas, B. R. Heywood, F. C. Meldrum, N. J. Reeves, *Science* **1993**, *261*, 1286.

[20]   T. Douglas, D. P. E. Dickson, S. Betteridge, J. Charnock, C. D. Garner, S. Mann, *Science* **1995**, *269*, 54.

[21]   F. C. Meldrum, T. Douglas, S. Levi, P. Arosio, S. Mann, *J. Inorg. Biochem.* **1995**, *58*, 59.

[22]   P. Mackle, J. M. Charnock, C. D. Garner, F. C. Meldrum, S. Mann, *J. Am. Chem. Soc.* **1993**, *115*, 8471.

[23]   R. Tsukamoto, K. Iwahor, M. Muraoka, I. Yamashita, *Bull. Chem. Soc. Jpn.* **2005**, *78*, 2075.

[24]   T. Douglas, V. T. Stark, *Inorg. Chem.* **2000**, *39*, 1828.

[25]   M. Okuda, K. Iwahori, I. Yamashita, H. Yoshimura, *Biotechnol. Bioeng.* **2003**, *84*, 187.

[26]   M. Okuda, Y. Kobayashi, K. Suzuki, K. Sonoda, T. Kondoh, A. Wagawa, A. Kondo, H. Yoshimura, *Nano Lett.* **2005**, *5*, 991.

[27]   K. K. W. Wong, S. Mann, *Adv. Mat.* **1996**, *8*, 928.

[28]   I. Yamashita, J. Hayashi, M. Hara, *Chem. Lett.* **2004**, *33*, 1158.

[29]   K. Iwahori, K. Yoshizawa, M. Muraoka, I. Yamashita, *Inorg. Chem.* **2005**, *44*, 6393.

[30]   M. T. Klem, J. Mosolf, M. Young, T. Douglas, *Inorg. Chem.* **2008**, *47*, 2237.

[31]   F. C. Meldrum, B. R. Heywood, S. Mann, *Science* **1992**, *257*, 522.

[32]   J. W. Bulte, T. Douglas, S. Mann, R. B. Frankel, B. M. Moskowitz, R. A. Brooks, C. D. Baumgarner, J. Vymazal, M. P. Strub, J. A. Frank, *J. Magn. Reson. Imaging* **1994**, *4*, 497.

[33]   K. K. W. Wong, T. Douglas, S. Gider, D. D. Awschalom, S. Mann, *Chem. Mater.* **1998**, *10*, 279.

[34]   M. T. Klem, D. A. Resnick, K. Gilmore, M. Young, Y. U. Idzerda, T. Douglas, *J. Am. Chem. Soc.* **2007**, *129*, 197.

[35]   I. Kim, H. A. Hosein, D. R. Strongin, T. Douglas, *Chem. Mater.* **2002**, *14*, 4874.

[36]   D. Ensign, M. Young, T. Douglas, *Inorg. Chem.* **2004**, *43*, 3441.

[37]   T. Ueno, M. Suzuki, T. Goto, T. Matsumoto, K. Nagayama, Y. Watanabe, *Angew. Chem. Int. Ed.* **2004**, *43*, 2527.

[38]   R. M. Kramer, C. Li, D. C. Carter, M. O. Stone, R. R. Naik, *J. Am. Chem. Soc.* **2004**, *126*, 13282.

[39]   S. Aime, L. Frullano, S. Geninatti Crich, *Angew. Chem. Int. Ed.* **2002**, *41*, 1017.

[40]   M. Uchida, M. Terashima, C. H. Cunningham, Y. Suzuki, D. A. Willits, A. F. Willis, P. C. Yang, P. S. Tsao, M. V. McConnell, M. J. Young, T. Douglas, *Magn. Reson. Med.* **2008**, *60*, 1073.

[41] K. K. W. Wong, H. Colfen, N. T. Whilton, T. Douglas, S. Mann, *J. Inorg. Biochem.* **1999**, *76*, 187.

[42] M. Li, K. K. W. Wong, S. Mann, *Chem. Mater.* **1999**, *11*, 23.

[43] K. Sano, K. Ajima, K. Iwahori, M. Yudasaka, S. Iijima, I. Yamashita, K. Shiba, *Small* **2005**, *1*, 826.

[44] T. Hayashi, K. Sano, K. Shiba, Y. Kumashiro, K. Iwahori, I. Yamashita, M. Hara, *Nano Lett.* **2006**, *6*, 515.

[45] M. Uchida, M. L. Flenniken, M. Allen, D. A. Willits, B. E. Crowley, S. Brumfield, A. F. Willis, L. Jackiw, M. Jutila, M. J. Young, T. Douglas, *J. Am. Chem. Soc.* **2006**, *128*, 16626.

[46] X. Yang, E. Chiancone, S. Stefanini, A. Ilari, N. D. Chasteen, *Biochem J.* **2000**, *349 Pt 3*, 783.

[47] B. Wiedenheft, J. Mosolf, D. Willits, M. Yeager, K. A. Dryden, M. Young, T. Douglas, *Proc. Natl. Acad. Sci. U. S. A.* **2005**, *102*, 10551.

[48] R. A. Grant, D. J. Filman, S. E. Finkel, R. Kolter, J. M. Hogle, *Nat. Struct. Biol.* **1998**, *5*, 294.

[49] M. Allen, D. Willits, J. Mosolf, M. Young, T. Douglas, *Adv. Mat.* **2002**, *14*, 1562.

[50] M. Allen, D. Willits, M. Young, T. Douglas, *Inorg. Chem.* **2003**, *42*, 6300.

[51] K. Iwahori, T. Enomoto, H. Furusho, A. Miura, K. Nishio, Y. Mishima, I. Yamashita, *Chem. Mat.* **2007**, *19*, 3105.

[52] S. Kang, J. Lucon, Z. B. Varpness, L. Liepold, M. Uchida, D. Willits, M. Young, T. Douglas, *Angew. Chem. Int. Ed.* **2008**, *47*, 7845.

[53] S. Kang, C. C. Jolley, L. O. Liepold, M. Young, T. Douglas, *Angew. Chem. Int. Ed.* **2009**.

[54] R. H. van den Heuvel, A. J. Heck, *Curr. Opin. Chem. Biol.* **2004**, *8*, 519.

[55] J. Swift, W. A. Wehbi, B. D. Kelly, X. F. Stowell, J. G. Saven, I. J. Dmochowski, *J. Am. Chem. Soc.* **2006**, *128*, 6611.

[56] K. Schott, R. Ladenstein, A. Konig, A. Bacher, *J. Biol. Chem.* **1990**, *265*, 12686.

[57] W. Shenton, S. Mann, H. Cölfen, A. Bacher, M. Fischer, *Angew. Chem. Int. Ed.* **2001**, *40*, 442.

[58] K. K. Kim, R. Kim, S. H. Kim, *Nature* **1998**, *394*, 595.

[59] R. Kim, K. K. Kim, H. Yokota, S. H. Kim, *Proc. Natl. Acad. Sci. U. S. A.* **1998**, *95*, 9129.

[60] L. O. Liepold, J. Revis, M. Allen, L. Oltrogge, M. Young, T. Douglas, *Phys. Biol.* **2005**, *2*, S166.

[61] M. L. Flenniken, D. A. Willits, S. Brumfield, M. J. Young, T. Douglas, *Nano Lett.* **2003**, *3*, 1573.

[62] Z. Varpness, J. W. Peters, M. Young, T. Douglas, *Nano Lett.* **2005**, *5*, 2306.

[63] B. D. Reiss, C. Mao, D. J. Solis, K. S. Ryan, T. Thomson, A. M. Belcher, *Nano Lett.* **2004**, *4*, 1127.

[64] M. T. Klem, D. Willits, D. J. Solis, A. M. Belcher, M. Young, T. Douglas, *Advanced Funct. Mat.* **2005**, *15*, 1489.

[65] M. L. Flenniken, L. O. Liepold, B. E. Crowley, D. A. Willits, M. J. Young, T. Douglas, *Chem. Commun.* **2005**, 447.

[66] M. L. Flenniken, D. A. Willits, A. L. Harmsen, L. O. Liepold, A. G. Harmsen, M. J. Young, T. Douglas, *Chem. Biol.* **2006**, *13*, 161.

[67] M. J. Abedin, L. Liepold, P. Suci, M. Young, T. Douglas, *J. Am. Chem. Soc.* **2009**, *131*, 4346.

[68] H. Fraenkel-Conrat, R. C. Williams, *Proc. Natl. Acad. Sci. U.S.A.* **1955**, *41*, 690.

[69] G. Stubbs, *Philos. Trans. R. Soc. Lond. B Biol. Sci.* **1999**, *354*, 551.

[70] A. C. Durham, J. T. Finch, A. Klug, *Nat. New Biol.* **1971**, *229*, 37.

[71] J. N. Culver, W. O. Dawson, K. Plonk, G. Stubbs, *Virology* **1995**, *206*, 724.

[72] W. Shenton, T. Douglas, M. Young, G. Stubbs, S. Mann, *Adv. Mater.* **1999**, *11*, 253.

[73] M. Knez, M. Sumser, A. M. Bittner, C. Wege, H. Jeske, S. Kooi, M. Burghard, K. Kern, *J. Electroanal. Chem.* **2002**, *522*, 70.

[74] M. Knez, M. Sumser, A. M. Bittner, C. Wege, H. Jeske, T. P. Martin, K. Kern, *Adv. Funct. Mat.* **2004**, *14*, 116.

[75] M. Knez, A. M. Bittner, F. Boes, C. Wege, H. Jeske, E. Maiβ, K. Kern, *Nano Lett.* **2003**, *3*, 1079.

[76] R. Tsukamoto, M. Muraoka, M. Seki, H. Tabata, I. Yamashita, *Chem. Mat.* **2007**, *19*, 2389.

[77] E. Dujardin, C. Peet, G. Stubbs, J. N. Culver, S. Mann, *Nano Lett.* **2003**, *3*, 413.

[78] E. Royston, A. Ghosh, P. Kofinas, M. T. Harris, J. N. Culver, *Langmuir* **2008**, *24*, 906.

[79] T. L. Schlick, Z. Ding, E. W. Kovacs, M. B. Francis, *J. Am. Chem. Soc.* **2005**, *127*, 3718.

[80] P. G. Holder, M. B. Francis, *Angew. Chem. Int. Ed.* **2007**, *46*, 4370.

[81] R. A. Miller, A. D. Presley, M. B. Francis, *J. Am. Chem. Soc.* **2007**, *129*, 3104.

[82] M. Endo, M. Fujitsuka, T. Majima, *Chem. Eur. J.* **2007**, *13*, 8660.

[83] A. Nedoluzhko, T. Douglas, *J. Inorg. Biochem.* **2001**, *84*, 233.

[84] C. E. Fowler, W. Shenton, G. Stubbs, S. Mann, *Adv. Mat.* **2001**, *13*, 1266.

[85] S. Fujikawa, T. Kunitake, *Langmuir* **2003**, *19*, 6545.

[86] H. Yi, S. Nisar, S. Y. Lee, M. A. Powers, W. E. Bentley, G. F. Payne, R. Ghodssi, G. W. Rubloff, M. T. Harris, J. N. Culver, *Nano Lett.* **2005**, *5*, 1931.

[87] H. Yi, G. W. Rubloff, J. N. Culver, *Langmuir* **2007**, *23*, 2663.

[88] M. Knez, M. P. Sumser, A. M. Bittner, C. Wege, H. Jeske, D. M. P. Hoffmann, K. Kuhnke, K. Kern, *Langmuir* **2004**, *20*, 441.

[89] J. Wellink, *Methods Mol. Biol.* **1998**, *81*, 205.

[90] T. Lin, Z. Chen, R. Usha, C. V. Stauffacher, J. B. Dai, T. Schmidt, J. E. Johnson, *Virology* **1999**, *265*, 20.

[91] Q. Wang, T. Lin, L. Tang, J. E. Johnson, M. G. Finn, *Angew. Chem. Int. Ed.* **2002**, *41*, 459.

[92] T. Lin, J. E. Johnson, *Adv. Virus. Res.* **2003**, *62*, 167.

[93] G. P. Lomonossoff, J. E. Johnson, *Progress in Biophysics & Molecular Biology* **1991**, *55*, 107.

[94]   W. F. Ochoa, A. Chatterji, T. Lin, J. E. Johnson, *Chem. Biol.* **2006**, *13*, 771.

[95]   J. T. Dessens, G. P. Lomonossoff, *J. Gen. Virol.* **1993**, *74 (Pt 5)*, 889.

[96]   E. Strable, M. G. Finn, *Curr. Top. Microbiol. Immunol.* **2009**, *327*, 1.

[97]   N. F. Steinmetz, T. Lin, G. P. Lomonossoff, J. E. Johnson, *Curr. Top. Microbiol. Immunol.* **2009**, *327*, 23.

[98]   Q. Wang, T. Lin, J. E. Johnson, M. G. Finn, *Chem. Biol.* **2002**, *9*, 813.

[99]   Q. Wang, E. Kaltgrad, T. Lin, J. E. Johnson, M. G. Finn, *Chem. Biol.* **2002**, *9*, 805.

[100]   N. F. Steinmetz, G. Calder, G. P. Lomonossoff, D. J. Evans, *Langmuir* **2006**, *22*, 10032.

[101]   K. S. Raja, Q. Wang, M. J. Gonzalez, M. Manchester, J. E. Johnson, M. G. Finn, *Biomacromolecules* **2003**, *4*, 472.

[102]   Q. Wang, K. S. Raja, K. D. Janda, T. Lin, M. G. Finn, *Bioconjugate Chem.* **2003**, *14*, 38.

[103]   N. F. Steinmetz, M. Manchester, *Biomacromolecules* **2009**, *10*, 784.

[104]   N. F. Steinmetz, G. P. Lomonossoff, D. J. Evans, *Langmuir* **2006**, *22*, 3488.

[105]   N. F. Steinmetz, G. P. Lomonossoff, D. J. Evans, *Small* **2006**, *2*, 530.

[106]   K. E. Sapsford, C. M. Soto, A. S. Blum, A. Chatterji, T. Lin, J. E. Johnson, F. S. Ligler, B. R. Ratna, *Biosens. Bioelectron.* **2006**, *21*, 1668.

[107]   A. Chatterji, W. Ochoa, L. Shamieh, S. P. Salakian, S. M. Wong, G. Clinton, P. Ghosh, T. W. Lin, J. E. Johnson, *Bioconjugate Chemistry* **2004**, *15*, 807.

[108]   E. Strable, J. E. Johnson, M. G. Finn, *Nano Lett.* **2004**, *4*, 1385.

[109]   I. L. Medintz, K. E. Sapsford, J. H. Konnert, A. Chatterji, T. W. Lin, J. E. Johnson, H. Mattoussi, *Langmuir* **2005**, *21*, 5501.

[110]   N. G. Portney, K. Singh, S. Chaudhary, G. Destito, A. Schneemann, M. Manchester, M. Ozkan, *Langmuir* **2005**, *21*, 2098.

[111]   N. G. Portney, R. J. Tseng, G. Destito, E. Strable, Y. Yang, M. Manchester, M. G. Finn, M. Ozkan, *Appl. Phys. Lett.* **2007**, *90*.

[112]   K. S. Raja, Q. Wang, M. G. Finn, *ChemBioChem* **2003**, *4*, 1348.

[113]   A. Miermont, H. Barnhill, E. Strable, X. Lu, K. A. Wall, Q. Wang, M. G. Finn, X. Huang, *Chem. Eur. J.* **2008**, *14*, 4939.

[114]   A. S. Blum, C. M. Soto, C. D. Wilson, J. D. Cole, M. Kim, B. Gnade, A. Chatterji, W. F. Ochoa, T. W. Lin, J. E. Johnson, B. R. Ratna, *Nano Lett.* **2004**, *4*, 867.

[115]   C. M. Soto, A. S. Blum, C. D. Wilson, J. Lazorcik, M. Kim, B. Gnade, B. R. Ratna, *Electrophoresis* **2004**, *25*, 2901.

[116]   A. S. Blum, C. M. Soto, C. D. Wilson, T. L. Brower, S. K. Pollack, T. L. Schull, A. Chatterji, T. W. Lin, J. E. Johnson, C. Amsinck, P. Franzon, R. Shashidhar, B. R. Ratna, *Small* **2005**, *1*, 702.

[117]   Q. Wang, T. R. Chan, R. Hilgraf, V. V. Fokin, K. B. Sharpless, M. G. Finn, *J. Am. Chem. Soc.* **2003**, *125*, 3192.

[118]   S. Meunier, E. Strable, M. G. Finn, *Chem. Biol.* **2004**, *11*, 319.

[119]   S. Sen Gupta, J. Kuzelka, P. Singh, W. G. Lewis, M. Manchester, M. G. Finn, *Bioconjugate Chem.* **2005**, *16*, 1572.

[120] D. E. Prasuhn, Jr., R. M. Yeh, A. Obenaus, M. Manchester, M. G. Finn, *Chem. Commun.* **2007**, 1269.

[121] S. Sen Gupta, K. S. Raja, E. Kaltgrad, E. Strable, M. G. Finn, *Chem. Commun.* **2005**, 4315.

[122] J. T. Russell, Y. Lin, A. Boker, L. Su, P. Carl, H. Zettl, J. He, K. Sill, R. Tangirala, T. Emrick, K. Littrell, P. Thiyagarajan, D. Cookson, A. Fery, Q. Wang, T. P. Russell, *Angew. Chem. Int. Ed.* **2005**, *44*, 2420.

[123] J. C. Falkner, M. E. Turner, J. K. Bosworth, T. J. Trentler, J. E. Johnson, T. Lin, V. L. Colvin, *J. Am. Chem. Soc.* **2005**, *127*, 5274.

[124] J. Y. Fang, C. M. Soto, T. W. Lin, J. E. Johnson, B. Ratna, *Langmuir* **2002**, *18*, 308.

[125] C. L. Cheung, J. A. Camarero, B. W. Woods, T. Lin, J. E. Johnson, J. J. De Yoreo, *J. Am. Chem. Soc.* **2003**, *125*, 6848.

[126] J. C. Smith, K. B. Lee, Q. Wang, M. G. Finn, J. E. Johnson, M. Mrksich, C. A. Mirkin, *Nano Lett.* **2003**, *3*, 883.

[127] N. F. Steinmetz, E. Bock, R. P. Richter, J. P. Spatz, G. P. Lomonossoff, D. J. Evans, *Biomacromolecules* **2008**, *9*, 456.

[128] D. J. Evans, *J. Mat. Chem.* **2008**, *18*, 3746.

[129] J. A. Speir, S. Munshi, G. J. Wang, T. S. Baker, J. E. Johnson, *Structure* **1995**, *3*, 63.

[130] P. Ahlquist, *Curr. Opin. Genet. Dev.* **1992**, *2*, 71.

[131] J. M. Fox, G. Wang, J. A. Speir, N. H. Olson, J. E. Johnson, T. S. Baker, M. J. Young, *Virology* **1998**, *244*, 212.

[132] J. E. Johnson, J. A. Speir, *J. Mol. Biol.* **1997**, *269*, 665.

[133] J. Tang, J. M. Johnson, K. A. Dryden, M. J. Young, A. Zlotnick, J. E. Johnson, *J. Struct. Biol.* **2006**, *154*, 59.

[134] J. B. Bancroft, G. W. Wagner, C. E. Bracker, *Virology* **1968**, *36*, 146.

[135] S. Brumfield, D. Willits, L. Tang, J. E. Johnson, T. Douglas, M. Young, *J. Gen. Virol.* **2004**, *85*, 1049.

[136] X. Zhao, J. M. Fox, N. H. Olson, T. S. Baker, M. J. Young, *Virology* **1995**, *207*, 486.

[137] J. B. Bancroft, C. E. Bracker, G. W. Wagner, *Virology* **1969**, *38*, 324.

[138] J. B. Bancroft, E. Hiebert, C. E. Bracker, *Virology* **1969**, *39*, 924.

[139] E. Hiebert, J. B. Bancroft, *Virology* **1969**, *39*, 296.

[140] J. B. Bancroft, J. G. Mcdonald, M. W. Rees, *Virology* **1976**, *75*, 293.

[141] A. Zlotnick, R. Aldrich, J. M. Johnson, P. Ceres, M. J. Young, *Virology* **2000**, *277*, 450.

[142] D. Willits, X. Zhao, N. Olson, T. S. Baker, A. Zlotnick, J. E. Johnson, T. Douglas, M. J. Young, *Virology* **2003**, *306*, 280.

[143] J. M. Johnson, D. A. Willits, M. J. Young, A. Zlotnick, *J. Mol. Biol.* **2004**, *335*, 455.

[144] S. E. Aniagyei, C. DuFort, C. C. Kao, B. Dragnea, *J. Mater. Chem.* **2008**, *18*, 3763.

[145] S. E. Aniagyei, C. J. Kennedy, B. Stein, D. A. Willits, T. Douglas, M. J. Young, M. De, V. M. Rotello, D. Srisathiyanarayanan, C. C. Kao, B. Dragnea, *Nano Lett.* **2009**, *9*, 393.

[146] C. Chen, E. S. Kwak, B. Stein, C. C. Kao, B. Dragnea, *J. Nanosci. Nanotechnol.* **2005**, *5*, 2029.

[147] F. D. Sikkema, M. Comellas-Aragones, R. G. Fokkink, B. J. Verduin, J. J. L. M. Cornelissen, R. J. M. Nolte, *Org. Biomol. Chem.* **2007**, *5*, 54.

[148] T. Douglas, M. Young, *Nature* **1998**, *393*, 152.

[149] Y. F. Hu, R. Zandi, A. Anavitarte, C. M. Knobler, W. M. Gelbart, *Biophys. J.* **2008**, *94*, 1428.

[150] B. J. Verduin, J. B. Bancroft, *Virology* **1969**, *37*, 501.

[151] S. Mukherjee, C. M. Pfeifer, J. M. Johnson, J. Liu, A. Zlotnick, *J. Am. Chem. Soc.* **2006**, *128*, 2538.

[152] A. de la Escosura, M. Verwegen, F. D. Sikkema, M. Comellas-Aragones, A. Kirilyuk, T. Rasing, R. J. M. Nolte, J. J. L. M. Cornelissen, *Chem. Commun.* **2008**, 1542.

[153] T. Douglas, E. Strable, D. Willits, A. Aitouchen, M. Libera, M. Young, *Adv. Mater.* **2002**, *14*, 415.

[154] E. Gillitzer, D. Willits, M. Young, T. Douglas, *Chem. Commun.* **2002**, 2390.

[155] P. A. Suci, D. L. Berglund, L. Liepold, S. Brumfield, B. Pitts, W. Davison, L. Oltrogge, K. O. Hoyt, S. Codd, P. S. Stewart, M. Young, T. Douglas, *Chem. Biol.* **2007**, *14*, 387.

[156] P. A. Suci, Z. Varpness, E. Gillitzer, T. Douglas, M. Young, *Langmuir* **2007**, *23*, 12280.

[157] M. Allen, J. W. Bulte, L. Liepold, G. Basu, H. A. Zywicke, J. A. Frank, M. Young, T. Douglas, *Magn. Reson. Med.* **2005**, *54*, 807.

[158] L. Liepold, S. Anderson, D. Willits, L. Oltrogge, J. A. Frank, T. Douglas, M. Young, *Magn. Reson. Med.* **2007**, *58*, 871.

[159] G. Basu, M. Allen, D. Willits, M. Young, T. Douglas, *J. Biol. Inorg. Chem.* **2003**, *8*, 721.

[160] M. L. Flenniken, M. Uchida, L. O. Liepold, S. Kang, M. J. Young, T. Douglas, *Curr Top. Microbiol. Immunol.* **2009**, *327*, 71.

[161] C. R. Kaiser, M. L. Flenniken, E. Gillitzer, A. L. Harmsen, A. G. Harmsen, M. A. Jutila, T. Douglas, M. J. Young, *Int. J. Nanomedicine* **2007**, *2*, 715.

[162] M. T. Klem, D. Willits, M. Young, T. Douglas, *J. Am. Chem. Soc.* **2003**, *125*, 10806.

[163] E. Gillitzer, P. Suci, M. Young, T. Douglas, *Small* **2006**, *2*, 962.

[164] P. A. Suci, M. T. Klem, T. Douglas, M. Young, *Langmuir* **2005**, *21*, 8686.

[165] P. A. Suci, M. T. Klem, F. T. Arce, T. Douglas, M. Young, *Langmuir* **2006**, *22*, 8891.

CHAPTER 3

CCMV Isolation and Purification

3.1 Introduction

Plant virus purification

Purified virus samples are essential to obtain information about chemical, physical, biochemical, and biological properties of viruses.[1] Purification, with its usual aims of high quality and quantity, is often a major stumbling block in such studies.[2] The tobacco mosaic virus (TMV) was the first plant virus to be purified, which resulted in Stanley being awarded the Nobel Prize for Chemistry in 1946.[3-5] In 1936, he published the successful isolation of TMV in apparently a pure crystalline state and he also reported the protein nature of the virus. The virus was isolated after several extractions and precipitation steps. One year later Bawden and Pirie discovered the RNA content of TMV particles.[6] TMV was also the first virus that was reassembled from its constituents (RNA and capsid protein), which will be further discussed in the next chapter.[7]

Following the purification of TMV, other plant viruses, including spherical ones, were also purified as well with essentially the same extraction and precipitation technology, for example, potato virus X (PVX) and tomato bushy stunt virus (TBSV). The choice of extraction buffer and additives can greatly influence the outcome of purification attempts and it is based on the physical and chemical properties of the virus. Acidic buffers of about pH 5 are useful for the extraction of some icosahedral viruses because their host proteins are precipitated at low pH. For cases in which pH-induced purification may result in low virus yields, the use of organic solvents or detergents may be required to remove the contaminating plant material.[2] A more recent method for further purification is the specific precipitation of the virus, for example, by the so-called polyethylene glycol (PEG) precipitation.[8] Since the late 1940s, isolation and purification were facilitated by the fact that preparative ultracentrifugation became available. This technique separates viruses on the basis of size, shape, and density of a virus.[9] In 1951, Brakke developed the density gradient centrifugation to purify viruses.[10] The final purification of viruses that are contaminated by host materials, is often carried out by centrifugation in density gradients, either by so-called rate-zonal centrifugation in sucrose (separation based on size, shape, and density) or by so-called

isopycnic sedimentation in gradients of sucrose or cesium salts (separation based on density only).[2]

Purification and characterization of CCMV

The purification of CCMV was described for the first time by Kuhn.[11] Leaves of cowpea plants were mechanically inoculated with virus particles and after further growth of the plant and harvesting of the leaves, isolation was carried out by extraction with chloroform and *n*-butanol. The resulting material was characterized by electron microscopy and UV/Vis spectroscopy. The nucleic acid content of the isolated virus was determined by phosphorous analysis and amounted to approximately 22% (w/w).

Bancroft *et al.* in their studies on the assembly properties of CCMV (see Chapter 4) used a modified procedure to isolate and purify the virus particles. The virus was grown in cowpea plants (*Vigna unguiculata*), which were harvested about 10–15 days after inoculation.[12] The leaves were blended in sodium acetate buffer of pH 5 and the sap was expressed through cheesecloth and stored overnight at $T = 4\ °C$. The virus was subsequently subjected to differential ultracentrifugation. The resulting solution, when analyzed by TEM, contained spherical particles approximately 28 nm in diameter (Figure 3.1). The yield varied between 20 and 40 mg of virus per 100 g of leaf tissue, depending on the growing conditions.

a)   b)
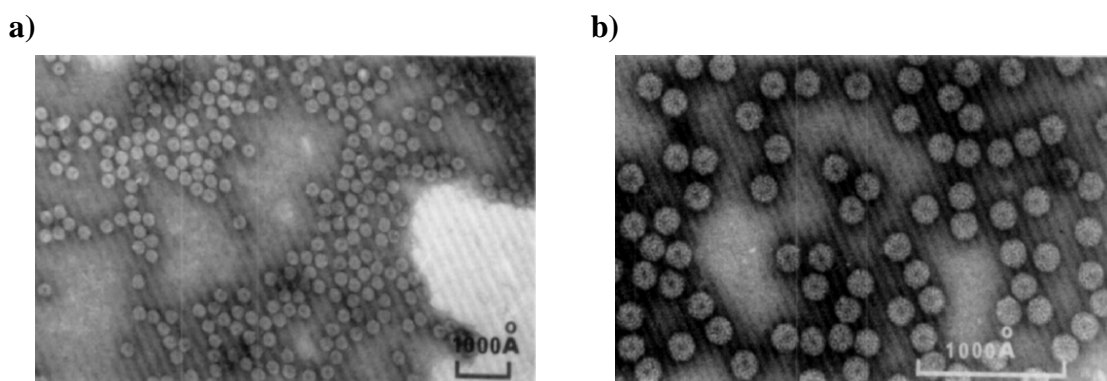
***Figure 3.1** Electron micrographs of CCMV stained with uranyl acetate.[12] a) Typical view. b) A magnification showing stain accumulation in the center in the particle.*

The purification of CCMV was further optimized by other groups,[8,13-16] for example Verduin,[17,18] and the virus was structurally studied by a variety of techniques. The quaternary structure of CCMV was described in 1993 by Speir *et al.* as determined from X-ray studies on crystalline virus (Figure 3.2).[19,20] An improved purification strategy was needed to provide crystalline material suitable for the high-resolution (3.1 Å) X-ray structure determination.

a)   b)
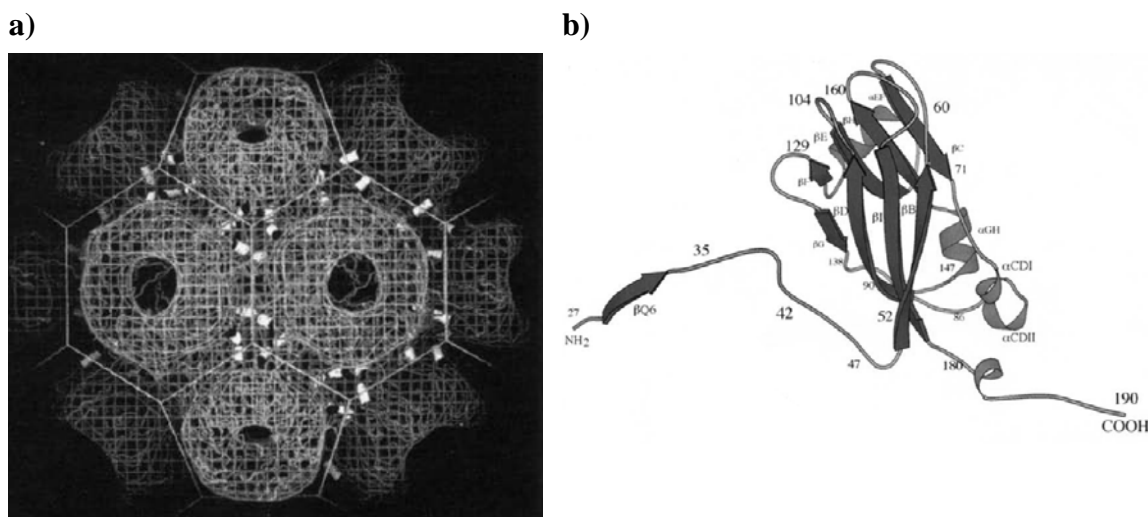
Figure 3.2 *CCMV models obtained from X-ray electron density data* [20] *a) View of the CCMV capsid at pH 4.5. b) Ribbon diagram showing the tertiary structure of the CCMV protein subunit.*

A small scale (1 g tissue) purification method for brome mosaic virus (BMV) and CCMV without the application of density gradient centrifugation was reported by Bujarski which however required a much longer procedure.[21] A virus yield of 0.5–5 mg per g of infected leaf tissue was obtained and it was claimed that the virus would preserve its biological activity for years when stored in storage buffer at −70 °C. In 2004, Michel *et al.* described a new technique for the last step of CCMV purification by applying ultrafiltration through polyethersulfone membranes, instead of ultracentrifugation. The purification protocol was thoroughly explained and both the ultrafiltration and ultracentrifugation methods were compared. CCMV purified by ultrafiltration was shown to provide material of similar quality as CCMV purified by CsCl ultracentrifugation.[22] The advantage of their ultrafiltration method was that expensive equipment and materials such as ultracentrifuges and rotors, and toxic CsCl chemical waste could be avoided. Recently, a new procedure was published for the rapid and efficient purification of CCMV, namely, by sucrose-cushion ultracentrifugation. A five-step protocol was developed to allow the purification of CCMV in approximately 4 h.[1] However, the coat protein obtained showed a low molecular weight by SDS-PAGE electrophoresis, probably due to degradation of the protein, which makes the method inconvenient.

Apart from plant extraction, the CCMV virions can also be obtained from bacteria, namely, by using a molecular biology approach. Zhao *et al.* reported on a CCMV *in vitro* assembly system that uses coat protein expression in *Escherichia coli* (*E.coli*) and viral RNAs transcribed from full-length cDNA clones *in vitro*.[23] According to electron microscopy, particles assembled from coat protein expressed in *E. coli* were virtually identical to virus particles purified from infected plants. This approach opened the way

57

to study CCMV assembly by constructing different mutants of this virus by using tools from molecular biology.

CCMV yields (mg of CCMV per gram plant leaf) depend not only on the purification procedure, but also on the strength of the inoculation solution, the type of the light source, the duration of light exposure, the health of the plant, and so forth.[22] Virus purity is routinely determined with the help of denaturating SDS polyacrylamide gel electrophoresis (SDS-PAGE) of the protein and by UV/Vis spectrophotometry (A_{260nm}(1 mg mL^{-1}) = 5.87; A_{260}/A_{280} = 1.5–1.7).[19]

Purification of the CCMV virions is still in the process of being further developed and new technology often leads to an improvement of the established protocols (see above). In the next paragraph the protocol for the purification of CCMV as developed and used in our laboratory will be described. It is based on the approach published by Verduin.[17,18] Furthermore, the different characterization techniques used to identify the virus and determine its purity will be discussed.

3.2 Results and Discussion

Purification protocol[1]

Planting of the Cowpea plants

1) Pots (40 to 60) were filled with soil and the Cowpea seeds (Figure 3.3a) were planted 2 cm deep in the soil (4 seeds per pot).

2) The plants were allowed to grow for ten days in a greenhouse or in a growth room (with two lamps hanging approximately 1.5 m above the plants). The plants were watered every two to three days by adding water to the saucers.

(NOTE: Although the virus can only be mechanically transmitted, plants were brought to a growth room before inoculation, to avoid the infection of other plants in the greenhouse. Danger of infection was also the reason for destroying the waste material once the whole plant growth and infection process was finished. With the later batches, to avoid moving the plants from one place to another, the whole process (planting, growing, and inoculation of the plants) was performed in the growth room, which gave the same results with respect to virus yield and purity)

---

[1] The reagents and equipment required for the purification are given in the Experimental Section (Section 3.4).

Inoculation of the plants

3) At this point primary leaves were present (Figure 3.3b). The leaves were dusted with carborundum (to abrase the leaves when the inoculum was applied) such that it was possible to see some of the powder staying on every leaf.

(NOTE: Plants should not be left much longer than 10 days before inoculation because they tend to develop age resistance against the virus)

4) The inoculation solution (inoculum) was prepared either with a purified virus suspension or with infected cowpea leaves. In both cases a mixture of sap from ground leaves, water (5–10 mL), and purified virus solution (*ca.* 0.5 mg virus) or infected leaves (3–4 leaves) was prepared by using mortle and pestle.

5) The leaves were inoculated by smoothly rubbing them with the forefinger dipped in the inoculum (Figure 3.3c). The leaves were rubbed hard, but without putting too much pressure on the leaf to avoid leaf damage.

6) By using a household sprayer, the plants were immediately sprayed with water after inoculation to prevent leaf dehydration.[21]

7) To keep the plants upright, they were attached to wooden garden stakes with small pieces of wire (Figure 3.3d and e).

(NOTE: Leaves may look bad for a day after inoculation. After a week some yellow spots can appear on some leaves, although not all leaves will show the effects of the virus. Some may present some black spots due to leaf damage, which is a consequence of applying too much pressure on the leafs during the inoculation process)
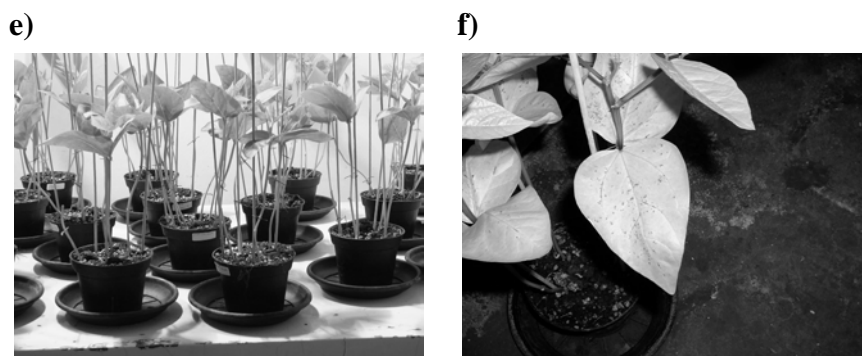
a)   b)

c)   d)

e)   f)

Figure 3.3 *Pictures of the different stages of the process of growing and infecting cowpea plants. a) Bag containing cowpea seeds. b) 10-days-old cowpea plants in the greenhouse, ready for inoculation. c) Inoculation of the plants by hand-rubbing the virus inoculum on every leaf. d) A plant, three days after inoculation. e) Plants in the growth room, one week after inoculation. f) Plant infected with CCMV, just before harvesting.*

Preparation of homogenate

8) Seven to ten days after inoculation (Figure 3.3f), the plants were harvested by cutting the stem at soil level.

9) The plant material (about 500 g) was cut into pieces and blended in portions in cold homogenization buffer (about 1 mL per gram of tissue) for approximately 3 min (Figure 3.4).

(NOTE: The homogenization buffer contains ascorbic acid used as antioxidant (reducing agent) and EDTA to avoid RNA degradation.[18])

10) Two layers of cheesecloth (25×25 cm) were boiled in water containing half a spatula (0.3–0.5 g approximately) of EDTA and rinsed with MilliQ filtered H_2O.

11) The homogenate was pressed through a double layer of cheesecloth to remove the larger plant debris and collected in a 2 L erlenmeyer flask by using a funnel.

12) The homogenate was kept at $T = 4$ °C for an hour to allow the plant proteins to precipitate.[2]

13) The homogenate was subjected to low-speed centrifugation (10 min at 10,000 rpm, $T = 4$ °C) in a Sorvall SLA-1500 rotor to precipitate the leaf tissue.

Precipitation of CCMV with PEG[8]

14) The pellet was discarded and the supernatant was added to 10% (w/v) solid PEG ($MW = 6000$ g/mol) through a funnel containing a small piece of glass wool to filter the remaining plant material.

15) The mixture was stirred for an hour at $T = 4$°C to dissolve the PEG (Figure 3.4b).

16) The precipitate was pelleted by low-speed centrifugation with a Sorvall SLA-1500 rotor (15 min at 10,000 rpm, $T = 4°C$). The supernatant was discarded and the bottles were drip-dried thoroughly to remove the PEG solution (Figure 3.4c).

17) The pellet was resuspended in cold virus buffer (at least 5% of the original homogenization volume, used in Step 9) with the help of a glass stick with a small piece of wet cotton on one of the ends (a so-called policeman).

(NOTE: The virus buffer contains sodium azide to avoid bacterial growth and again EDTA.)

18) The resuspension was cleared of undissolved material by low-speed centrifugation with a Sorvall SS-34 rotor (10 min at 10,000 rpm, $T = 4$ °C).

Purification of CCMV

19) The pellet was discarded and the supernatant was mixed with cesium chloride in such a way that 37.5% of the total weight was cesium chloride and the rest (62.5 weight %) was the supernatant.

20) Once completely dissolved, the mixture was subjected to a density gradient centrifugation (density of CCMV in CsCl is $\rho = 1.36$ g/cm^3) by using the Step Saver 70V6 Sorvall rotor (≥ 16 h at 40,000 rpm, $T = 10°C$).

21) The tubes were carefully removed from the rotor to avoid disturbing the formed brownish band, which contained the pure virus (Figure 3.4d). The cap was removed with a blade and the band was collected with a bent needle.

22) The obtained solution was dialyzed against three volume changes of virus buffer (at least three hours per change) in a cold room at $T = 4$ °C, and then stored at $T = 4$ °C.
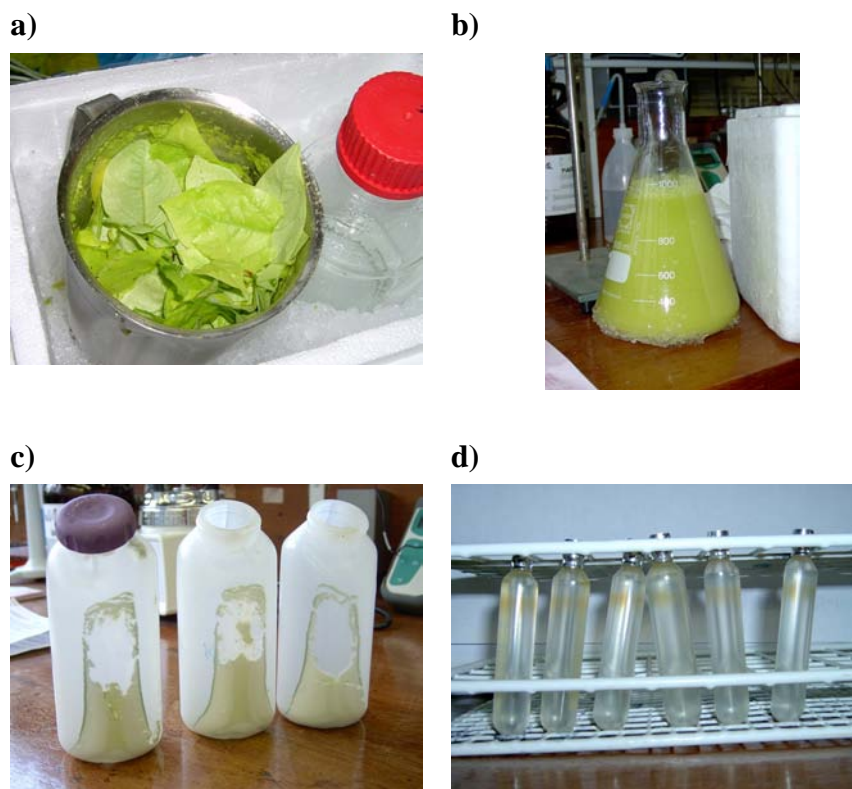
Figure 3.4 *CCMV purification process. a) Leaves in the Waring blender. b) Virus solution mixed with PEG 6000. c) Pellet containing the virus precipitated by the PEG. d) Resulting tubes after CsCl gradient centrifugation. The brownish band contains the CCMV.*

Typical yields of CCMV were 200–300 mg per kg of cowpea tissue. Purification was usually performed starting from 40 to 60 pots, which resulted in 1 kg of plant material, which was purified in two batches to give a final virus solution of approximately 10 mL ($10–15$ mg mL^{-1}) per 500 g of cowpea plants tissue. The virus solution was always kept in the fridge at $T = 4$ °C in virus buffer at pH 5.

During the whole process, the virus solution was kept cold either in an ice bath or in the cold room ($T = 4$ °C). Buffers were used cold and centrifugation was always performed at low temperatures.

Characterization

Many ways have been described in the literature to check the concentration, purity, and degree of degradation of CCMV. We have reproduced many of these analyses following different techniques to obtain experience in CCMV characterization. In-depth analysis of the virus is essential for understanding the properties of future, modified virus particles.
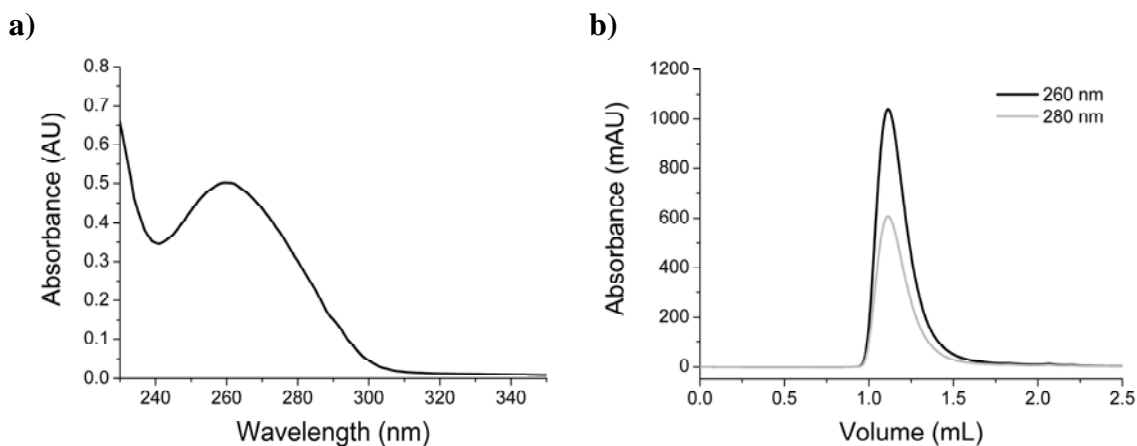
UV/Vis spectroscopy

The first analysis of the virus solution was carried out with the help of UV/Vis spectroscopy, which is a fast and classic way to get information about virus concentration and purity.[19] The CCMV UV/Vis spectrum is typically that of a virus solution, with a maximum absorption occurring at $\lambda = 260$ nm and a minimum at $\lambda = 240$ nm (Figure 3.5a). The $\lambda_{max} = 260$ nm is the wavelength of maximum absorbance of the nucleic acids (RNA and DNA) due to the presence of the aromatic bases in these biomacromolecules, whereas $\lambda_{max} = 280$ nm is the wavelength of characteristic absorption bands in proteins which are due to the presence of the aromatic amino acids phenylalanine, tyrosine, and tryptophane. Tryptophane also has a strong absorbance at $\lambda = 292$ nm, which gives a small peak in the UV/Vis spectrum of CCMV (Figure 3.5a). The extinction coefficients of the RNA (ε_{260}) and the coat protein (ε_{280}) are 27,812,999 $M^{-1}cm^{-1}$ and 24,075 $M^{-1}cm^{-1}$, respectively.[24] Although CCMV contains only approximately 25% of RNA, the contribution of the nucleic acid is 25 times stronger than the contribution of the protein on a weight basis; therefore, the maximum absorbance appears at $\lambda = 260$ nm. The ratio of absorbances at $\lambda = 260$ and 280 nm (A_{260nm}/A_{280nm}) is used to determine the viral purity of the sample, and for CCMV a value of 1.5–1.7 means a sample of good quality.[22]

By using the extinction coefficient of CCMV ($A = 5.85$ at $\lambda = 260$ nm for a concentration of 1 mg mL^{-1} and a light path of $l = 1$ cm), the concentration of the solution was calculated. CCMV purification normally starts from about 500 g of plant material, which, after the whole process is finished provides approximately 10 mL of virus solution of around 10 mg mL^{-1}; this concentration can go up to 20–25 mg mL^{-1} when the homogenization step is performed with a larger amount of plant material.

Fast protein liquid chromatography (FPLC)

Size-exclusion FPLC using a Superose 6 column is a valuable technique for the characterization and the purification of the virus. The elution of material from the column is monitored by UV/Vis detection at two different wavelengths, $\lambda = 260$ nm for the RNA contribution and $\lambda = 280$ nm for the protein contribution in the sample. The FPLC chromatogram (Figure 3.5b) usually shows an elution peak at 1.1 mL and, in line with the UV/Vis spectroscopy data (Figure 3.5a), the absorbance at $\lambda = 260$ nm is higher than the absorbance at $\lambda = 280$ nm. The latter absorption is not only caused by the protein, but also contains a contribution from the RNA.

a)   **b)**

Figure 3.5 *Analysis of CCMV by UV/Vis spectroscopy and FPLC. a) Typical UV/Vis spectrum of a CCMV solution (c = 0.085 mg mL^{-1}) in acetate buffer of pH 5 at 25°C. b) FPLC chromatogram of a CCMV solution (c = 8.5 mg mL^{-1}) in acetate buffer of pH 5 at 25°C.*
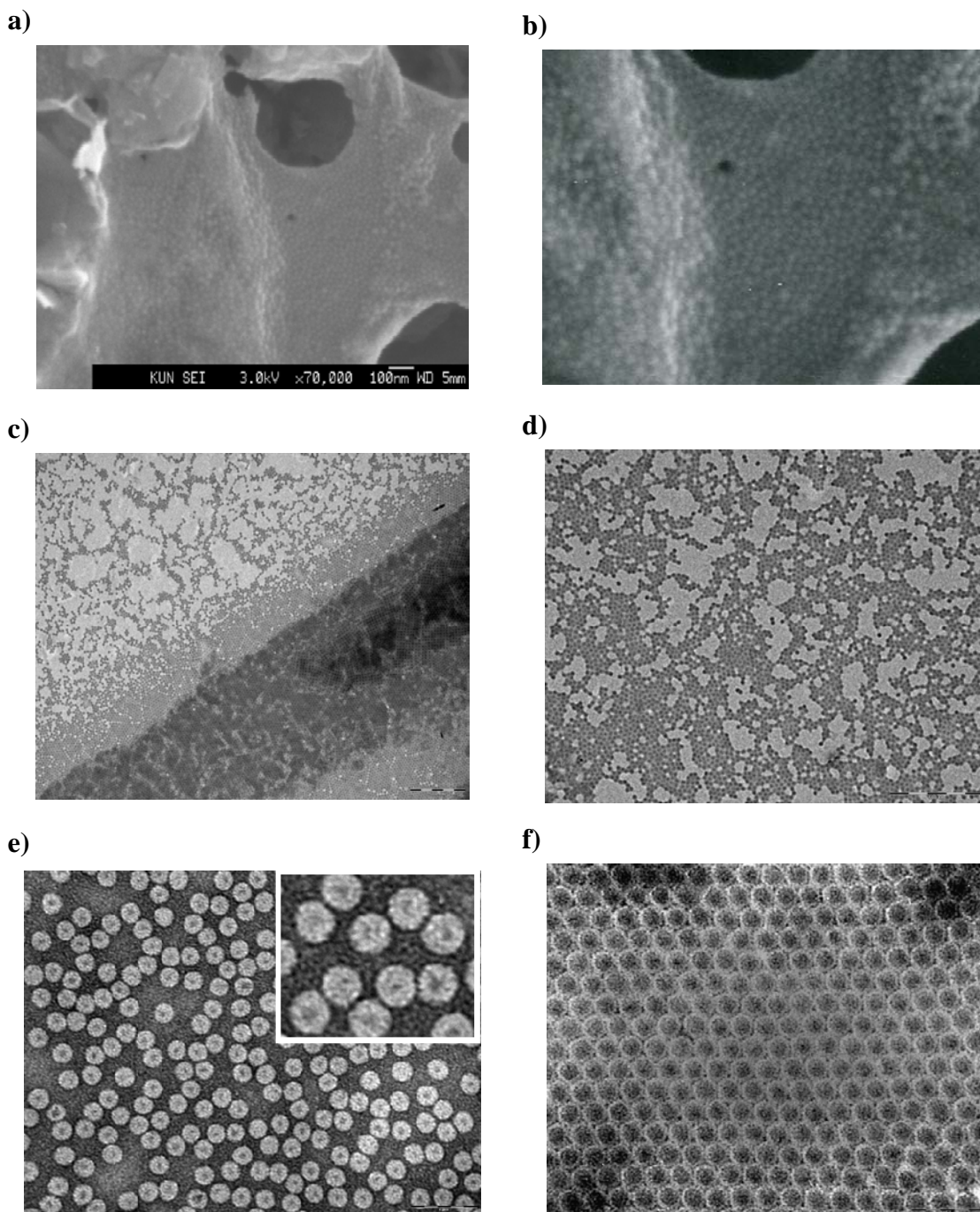

Microscopy studies[2]

CCMV was routinely analyzed by electron microscopy techniques, such as SEM and TEM. In one case we also used cryo-SEM to characterize the virus particles. This technique has not been used before in the literature for CCMV (Figure 3.6a and b). The first studies were directed towards finding the optimal conditions for sample preparation. The CCMV concentration, the type of grid, the deposition time, the kind of staining and its concentration, and so forth were varied. Typical TEM micrographs of the virus are shown in Figure 3.6c and d, in which a monolayer of CCMV can be observed with a hexagonal pattern in some areas. Depending on the preparation conditions, areas with multilayers can also be formed. The best conditions for sample preparation are as follows:

1) CCMV solution (5 μL; $c \approx 0.16$ mg mL^{-1}) was applied to a Formvar carbon-coated grid, previously made hydrophilic by glow discharge, and the solution was left for 1 min on the grid.
2) The excess buffer was blotted away with the help of filter paper.
3) A drop of uranyl acetate solution (0.2% in MilliQ filtered H_2O) was applied to the grid and the solution was left for 15 s (negative-staining step).
4) The excess liquid was blotted away with filter paper.
5) The samples were left to dry in air for 15 min.

---

[2] Part of the work described herein has been performed by Willem van Heugten as part of his Master degree under the supervision of the author.

By following these conditions the quality of the micrographs improved considerably and CCMV particles randomly distributed over the grid could be observed (Figure 3.6e) instead of the complete black particles that are obtained when higher concentrations of virus and staining reagent were applied (Figure 3.6c and d).The particles now displayed inner cavity, as revealed by the uranyl acetate solution (dark dot in the virus).

Figure 3.6 Microscopy studies on CCMV. a) Cryo-SEM micrograph of CCMV particles and b) magnification. c) First TEM micrographs of CCMV and d) magnification. e) TEM micrograph of CCMV particles under optimized conditions; inset magnification. f) TEM micrograph of CCMV particles organized in a hexagonal pattern (negative-staining carbon-film technique).

We also performed studies aimed at controlling the assembly of the virus on a surface, which can be very valuable for future applications of CCMV. To obtain monolayers of the virus organized in hexagonal patterns, the "negative-staining carbon-film technique" was used.[25,26] The procedure is schematically described in Figure 3.7. By following this protocol hexagonal arrays of CCMV particles on carbon could be successfully prepared (Figure 3.6f).

Freshly cleaved mica with CCMV solution. Liquid is drained with filter paper.

A very thin layer of carbon evaporated on specimen

Mica wafer is slowly immersed in an uranyl acetate solution

The floating carbon film is mounted on a grid
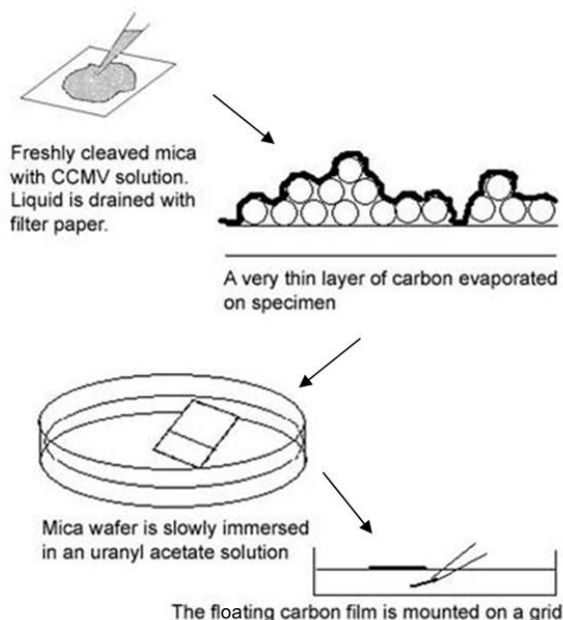
Figure 3.7 *Schematic drawing of the negative-staining carbon-film technique.*

 Gel electrophoresis

The CCMV samples were also characterized by SDS-PAGE. Purified CCMV particles were diluted with MilliQ filtered H_2O ($c = 0.1$ mg mL^{-1}) and mixed with an equal volume of SDS-PAGE gel loading buffer (1:1 v/v), and heated for five minutes in boiling water to denature the virus. The gel (see the Experimental Section for preparation, loading, and running conditions) usually shows a single coat-protein band, with a molecular weight of approximately 20 kDa, resulting from the 180 identical protein subunits (Figure 3.8a). In most cases no additional bands were observed, indicating that no degradation of the protein had occurred and no contamination was present. The protein could be visualized by using Coomassie Blue staining; for solutions containing very low virus concentrations, silver staining is an alternative. Agarose gel electrophoresis was also used to characterize the whole virus particle, in which case no previous denaturating step was applied. In this case, only one band was observed on the gel, which was stained by Commassie Blue (specific for proteins) and ethidium bromide (specific for nucleic acid). Both stains gave a spot at the same place, showing the co-migration of the protein and RNA on the gel. CCMV has a pI of 3.7 and contains RNA

that is negatively charged at neutral pH, which makes that the virus runs considerably on the gel from the cathodic (top) to the anodic (bottom) end.

a)   b)   c)
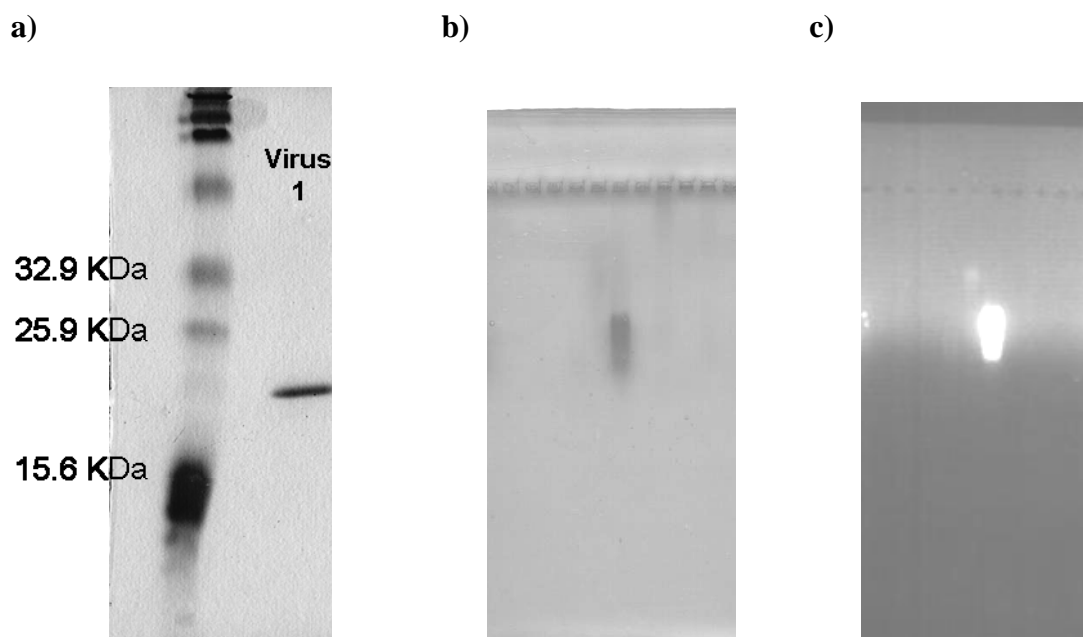
Figure 3.8 *Gel electrophoresis of CCMV. a) SDS-PAGE gel of the denatured CCMV stained with Coomassie Blue. b) Agarose gel of CCMV stained with Coomassie Blue. c) The same gel as that shown in (b) stained with ethidium bromide.*

Small-angle neutron scattering (SANS)

We also performed a SANS analysis of CCMV. Details are described in Chapter 5.

3.3 Conclusion

In this chapter the purification and characterization protocols for CCMV as worked out in our laboratories are described. Based on the variety of experiments CCMV particles can be obtained in good yields and high purity; allowing them to be used in a range of research projects.

3.4 Experimental Section

Materials

Reagents

Sodium acetate trihydrate (>99%), uranyl acetate dihydrate (≥98%), and PEG (MW = 6000 g/mol) were purchased from Fluka. Ethylenediaminetetraacetic acid (EDTA) disodium salt dihydrate (>99%), tris(hydroxymethyl)aminomethane (Tris) (>99%), calcium chloride dihydrate (>99%), L-(+)-ascorbic acid (>99%), sodium chloride (99.5%), sodium azide (99%), and cesium chloride (>99%) were purchased from Acros; ethanol (p.a.) was purchased from Merck; ethidium bromide (~95%), Orange G (≥80%), and dithiothreitol (DTT) (99%) were obtained from Sigma-Aldrich. Agarose (electrophoresis grade) was purchased from Invitrogen. All reagents used for SDS-PAGE electrophoresis were purchased from Bio-Rad Laboratories.

California Blackeye Cowpea Seeds were obtained from Main Street Seed and Supply, Co. (Michigan, USA) and from Groente & fruitspecialist "De Gezonde Apotheker" (The Netherlands). During storage they were kept dry in a cold room at 4°C. Carborundum (size 500) was obtained from Cats Import (Hoogvliet, The Netherlands). The potting soil (potting soil 4) was purchased from Hortimea groep (The Netherlands).

Buffers

The following aqueous buffers were used in the experiments:

Homogenization buffer: 0.2 M sodium acetate, 0.01 M ascorbic acid, 0.01 M disodium EDTA, buffered at pH = 4.8

Virus buffer: 0.1 M sodium acetate, 0.001 M disodium EDTA, 0.001 M sodium azide, buffered at pH = 5.0

Equipment

Plant pots with saucer (40–60, $d \approx 15$ cm)

Laboratory blender (1 L, Waring Laboratories)

Lamps for the growth room (model HS2000Medium, Hortilux Schreder)

Mortle and pestle

Household sprayer

Wooden garden stakes (approximately 50 cm in length)

Scissors

Cheesecloth (type KW 0023.0.14800, Henri Lampe BV, Sneek, The Netherlands).

Erlenmeyer flask (2 L)

Plastic funnel (25 cm diameter)

Centrifuge (Sorvall RC 5B plus, Sorvall)

Rotor SLA-1500 (Sorvall, bottle P.P. 250 mL)

Rotor SS-34 (Sorvall, tube P.P.-F 50 mL)

Ultracentrifuge (Sorvall Discovery 90, Sorvall)

Rotor Step Saver 70V6 (Sorvall, sealed tube PA 6 mL)

Cotton

Glass stirring rod (25 cm)

Blade

Plastic syringe with bent needle (10 mL)

Cold room

Growth room (16 h artificial light per day, $T \approx 25\ °C$)

Dialysis tubing (Spectra/Por 4, MWCO: 12–14 kD, Flat width: 25 mm, Spectrum Laboratories) or D-tube dialyzer (MWCO: 12–14 kD, volume: 1000–3000 µL, Novagen)

 Techniques for analysis

UV/Vis spectroscopy was performed on a Varian Cary 50 spectrophotometer at room temperature by using a 1 cm quartz cuvette (Hellma, light path: 1 cm). The reference spectrum of the corresponding buffer was subtracted from all UV/Vis spectra.

Fast protein liquid chromatography (FPLC) was performed on an Ettan Akta LC system equipped with a Superose 6 PC 3.2/30 column from Amersham Biosciences (flow rate 40 µL min^{-1}). Injections of 20-mL aliquots of the samples on the FPLC column at room temperature were monitored with the help of UV detection at $\lambda = 280$ and 260 nm.

Transmission electron microscopy (TEM) micrographs were recorded on a JEOL JEM-1010 instrument. Samples were prepared by drying a drop of the solution on a Formvar carbon-coated grid that had previously been made hydrophilic by glow discharge. The excess buffer on the grid was blotted away after 1 min with filter paper. Negative staining of the samples was achieved by applying a drop of uranyl acetate solution (0.2% in MilliQ filtered H_2O) onto the grid and blotting the excess liquid away after 15 s with filter paper. The samples were left to dry in air for 15 min before analysis.

Cryo-scanning electron microscopy (SEM) micrographs were recorded on a JEOL JSM-6330F microscope.

Gel electrophoresis was performed by using two different methods. SDS-polyacrylamide gel electrophoresis (SDS-PAGE) was performed by using a 4% stacking and a 15% running polyacrylamide gel containing 10% SDS. Samples were treated with β-mercaptoethanol and heated prior to loading onto the gel. Gels were stained with 0.05% (w/v) Coomassie Blue solution and destained with a solution of 5% (v/v) methanol and 7% (v/v) acetic acid in water (Coomassie Blue destainer). Agarose gel electrophoresis was performed by using gels that contained 1.25% agarose. To prepare

the gels, agarose (1.5 g) was dissolved in TAE buffer (120 mL; 40 mM Tris-acetate, 1 mM disodium EDTA, pH = 8). An aqueous solution of ethidium bromide (10 μL, 10 mg mL^{-1}) was used as a staining agent and Orange G as the sample buffer. The gel was run at 100 mV. Ethidium bromide stained nucleic acid on the gel was visualized with UV light. Furthermore, the gel was stained with 0.05% (w/v) Coomassie Blue solution and destained with 40% (v/v) methanol and 10% (v/v) acetic acid solution in water (complete Coomassie Blue destainer).

3.5 Notes and References

[1]   A. Ali, M. J. Roossinck, *J. Virol. Methods* **2007**, *141*, 84.

[2]   R. I. Hamilton, J. R. Edwardson, R. I. B. Francki, H. T. Hsu, R. Hull, R. Koenig, R. G. Milne, *J. Gen. Virol.* **1981**, *54*, 223.

[3]   R. W. Wyckoff, R. B. Corey, *Science* **1936**, *84*, 513.

[4]   R. W. G. Wyckoff, J. Biscoe, W. M. Stanley, *J. Biol. Chem.* **1936**, *117*, 57.

[5]   L. E. Kay, *Isis* **1986**, *77*, 450.

[6]   F. C. Bawden, N. W. Pirie, *P. Roy. Soc. B-Biol. Sci.* **1937**, *123*, 274.

[7]   H. Fraenkel-Conrat, R. C. Williams, *Proc. Natl. Acad. Sci. U.S.A.* **1955**, *41*, 690.

[8]   T. T. Hebert, *Phytopathology* **1963**, *53*, 362.

[9]   M. Zaitlin, P. Palukaitis, *Annu. Rev. Phytopathol.* **2000**, *38*, 117.

[10]   M. K. Brakke, *J. Am. Chem. Soc.* **1951**, *73*, 1847.

[11]   C. W. Kuhn, *Phytopathology* **1964**, *54*, 853.

[12]   J. B. Bancroft, G. J. Hills, R. Markham, *Virology* **1967**, *31*, 354.

[13]   E. Hiebert, J. B. Bancroft, C. E. Bracker, *Virology* **1968**, *34*, 492.

[14]   J. B. Bancroft, M. W. Rees, J. R. O. Dawson, G. D. McLean, M. N. Short, *J. Gen. Virol.* **1972**, *16*, 69.

[15]   R. Leberman, *Virology* **1966**, *30*, 341.

[16]   K. W. Adolph, P. J. Butler, *J. Mol. Biol.* **1974**, *88*, 327.

[17]   B. J. M. Verduin, *FEBS Lett.* **1974**, *45*, 50.

[18]   B. J. M. Verduin, *J. Gen. Virol.* **1978**, *39*, 131.

[19]   J. A. Speir, S. Munshi, T. S. Baker, J. E. Johnson, *Virology* **1993**, *193*, 234.

[20]   J. A. Speir, S. Munshi, G. J. Wang, T. S. Baker, J. E. Johnson, *Structure* **1995**, *3*, 63.

[21]   J. J. Bujarski, *Methods Mol. Biol.* **1998**, *81*, 183.

[22]   J. P. Michel, M. Gingery, L. Lavelle, *J. Virol. Methods* **2004**, *122*, 195.

[23]   X. Zhao, J. M. Fox, N. H. Olson, T. S. Baker, M. J. Young, *Virology* **1995**, *207*, 486.

[24]   S. Brumfield, D. Willits, L. Tang, J. E. Johnson, T. Douglas, M. Young, *J. Gen. Virol.* **2004**, *85*, 1049.

[25]   R. W. Horne, *Adv. Virus Res.* **1979**, *24*, 173.

[26]   R. W. Horne, I. P. Ronchetti, *J. Ultrastruct. Res.* **1973**, *47*, 361.

CHAPTER 4
CCMV Coat Protein Isolation and Assembly

4.1 Introduction

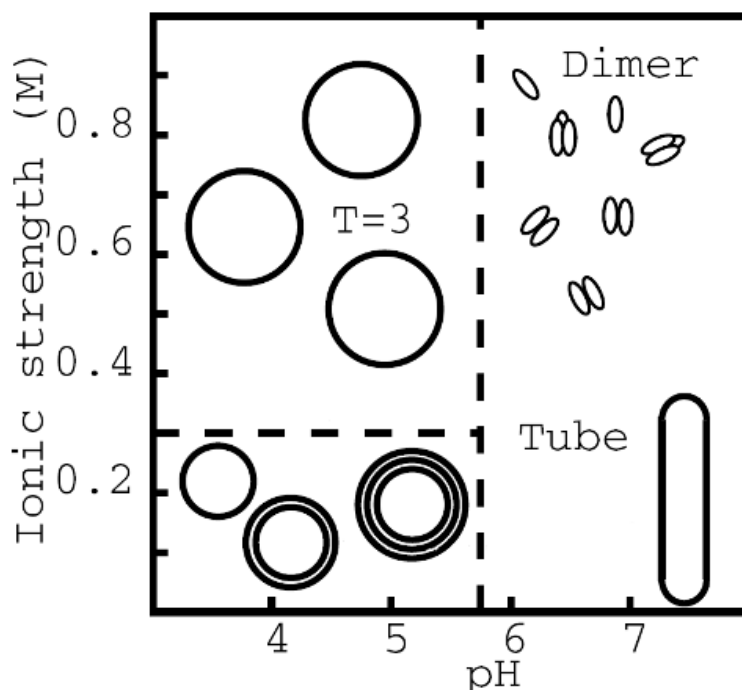**Assembly and disassembly of CCMV**

The reassembly of the tobacco mosaic virus (TMV) from its constituent components (protein and RNA) was published in 1955 by Fraenkel-Conrat and Williams, and it is the first example of the reconstitution of a virus.[1] TMV nucleic acid was recombined with its protein subunits at around pH 6 to form a nucleoprotein that still showed some virus activity. The reconstituted rod-like object appeared to be identical in shape and size to the intact TMV. The first time that attempts were made to reconstitute a spherical virus, that is, the cowpea chlorotic mottle virus (CCMV), was in 1967 by Bancroft and Hiebert.[2] CCMV was first disassembled and its components were isolated and purified. Afterwards, RNA and protein were mixed to form an infectious spherical nucleoprotein, which was similar in its general properties to the wild-type virus.

Since then self-assembly properties of CCMV have been thoroughly investigated by Bancroft and others,[3-5] and although a lot of information has been obtained about the different properties of the CCMV and its different forms of association, until to date, the mechanism of assembly has still not been completely elucidated. The CCMV particle can completely disassemble and subsequently reassemble in different morphologies depending on parameters such as pH, ionic strength, and temperature.

Assembly and disassembly of the CCMV coat protein

The viral RNA can be removed from CCMV and the coat protein (CP) subunits isolated and purified. These protein subunits can, under certain conditions, reaggregate and form structures that are identical or very similar to those of the original RNA-containing virus particle.[6] The self-assembly of the CCMV capsid devoid of RNA was first described by Bancroft *et al.* in 1968,[7,8] and has been thoroughly examined under a variety of conditions (different salt concentrations and different pH values) by him and other groups.[7-13] In Figure 4.1 the CCMV CP assembly as a function of pH and ionic strength, as proposed by Adolph and Butler in 1974 and later revised by Bruinsma *et al.* in 2003, is depicted.[10,14] The CPs can assemble and disassemble reversibly into many different structures: hollow single and multishell capsids, hexagonal sheets, and tubes.

A fairly monodisperse T = 3 capsid is encountered in the pH range between 3 and 5.5, whereas at neutral pH the dominant population consists of protein dimers.

Figure 4.1 *Equilibrium phase diagram of the capsid proteins as a function of pH and ionic strength.[14] Protein concentration varies between 0.5 and 1.0 mg mL^{-1}, T = 5°C.*

The assembly and disassembly of the CCMV CP has also been studied in the presence of various negatively charged species.[15-17] The goal was to explore their effect on capsid assembly and to investigate to what extent synthetic anionic templates are different from RNA. Various polyanions, with different lengths and sizes, for example, various polynucleotides,[15] nucleic acids from other viruses,[4] and negatively charged polymers such as polystyrene sulfonate,[16,17] were mixed with the CCMV CP and the assembly process was studied. The inclusion of various species in the viral capsid is further discussed in Chapter 5.

The understanding of the CCMV and coat-protein assembly has provided a lot of information about the ways to control the assembly process under different conditions. The construction of mutants by chemical modification of some of the CCMV CP amino acids, that is, by mutagenesis of wild-type CCMV RNA with nitrous acid, was the first attempt to control the properties of the virus, leading to the construction of temperature-sensitive CCMV and salt-stable CCMV.[18,19] Fox *et al.* have shown how a single amino acid change in the primary structure of the CP, obtained by genetic modification and expression in *Escherichia Coli*, can lead to tertiary interactions that stabilize the virion under high-salt-concentration conditions.[20]

In the previous chapter the synthesis, purification, and characterization of CCMV was described in detail. Having the best protocols at hand the next step was to carry out similar studies (*i.e.*, isolation, purification, and characterization) for the CCMV CP and to establish the conditions for their assembly and disassembly.

4.2 Results and Discussion
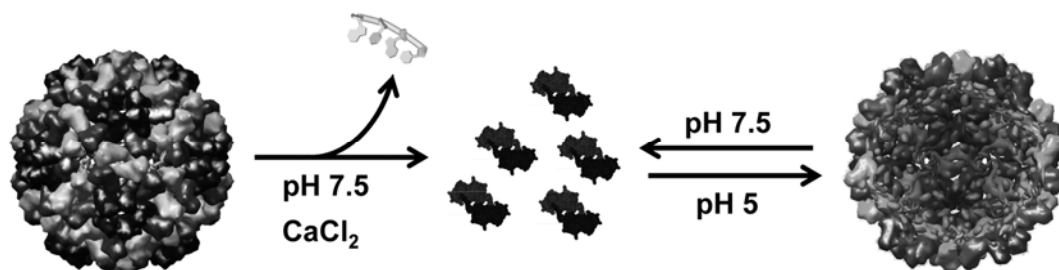
Coat protein isolation

The isolation of CCMV CP was first described by Bancroft *et al.*[2,4] They obtained CP by dialyzing the virus against a Tris buffer (20 mM, pH 7.4) containing 1 M NaCl and 1 mM dithiothreitol (DTT) and removing the RNA by centrifugation. The purity of the protein was determined by UV/Vis spectroscopy and by examining the ratio of A_{280nm}/A_{260nm}, which is indicative of the amount of residual RNA (Figure 4.2a). The assembly product of the CPs was analyzed by TEM, which showed mostly spheres of 28 nm diameter, which is the same dimension as that of the virus particles (Figure 4.2b).

a)   b)
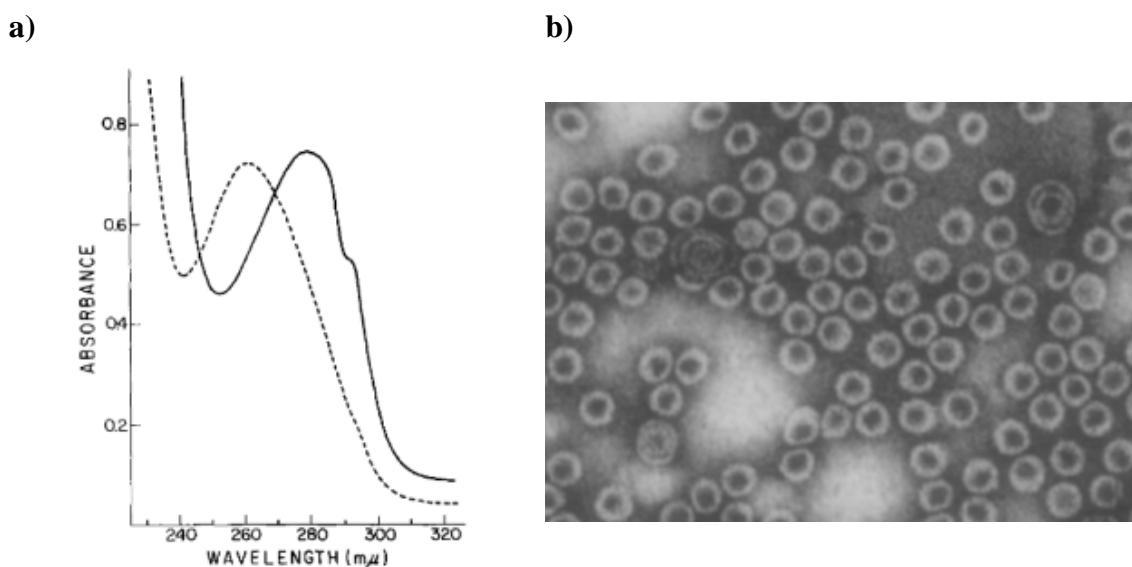
Figure 4.2 *Characterization of the first example of a CCMV capsid.[7] a) UV/Vis spectra of the CCMV virus (dashed) at 0.12 mg mL^{-1} and capsid at 0.73 mg mL^{-1}, both in 0.2 M NaCl, pH 5. b) Electron micrograph of the CCMV capsid in uranyl acetate (pH 4.7).*

To reduce the amount of residual RNA, different protocols to prepare viral protein were compared by Verduin.[21] Using spectroscopic techniques, the protein yield and the degree of contamination with nucleic acid (quantified by the absorbance ratio A_{280}/A_{260})

was examined for every protocol. The procedure that gave the best results is schematically depicted in Figure 4.3 and was used in our studies (see below).

Figure 4.3 *Schematic pathway for the isolation and assembly of the CCMV CP.*

The first step in the isolation of CCMV protein involves the removal of viral RNA from CCMV by dialyzing a virus suspension (10 mg mL^{-1} approximately) against a CaCl$_2$ and DTT-containing Tris-HCl buffer at pH 7.5. The Ca^{2+}ions combine with the phosphate groups of RNA and form an insoluble salt, precipitating the RNA as soon as the virus disassembles due to the neutral pH conditions (Figure 4.4). DTT is used as an antioxidant to avoid the oxidation of sulfhydryl groups of the protein molecules.[5] The RNA precipitate formed during dialysis was removed by ultracentrifugation and the supernatant was further dialyzed against Tris-HCl buffer (pH 7.5) containing NaCl and DTT, to remove all remaining RNA and CaCl$_2$. The dissociated CP, free of RNA, can be reassociated into spherical particles by dialyzing it against a pH 5 acetate buffer containing NaCl. This assembly/disassembly process is reversible (Figure 4.3).
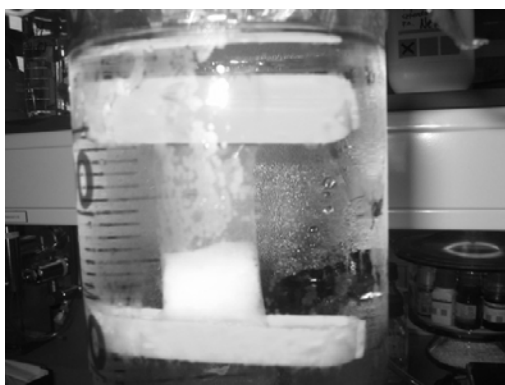
*Figure 4.4* *Precipitated RNA in the dialysis bag during the first step of the isolation of the CCMV CP.*

The removal of the RNA from the virus was followed with the help of FPLC (Figure 4.5). A main peak appearing at 1.8 mL indicates almost complete disassembly of the CP into dimers once the pH is increased and the RNA removed (Figure 4.5a). The reassembly of the dimers into an empty capsid of the same size as the virus upon

decreasing the pH is shown in Figure 4.5b. Characteristic is the appearance of a peak at the same retention volume as the virus (Figure 4.5c).
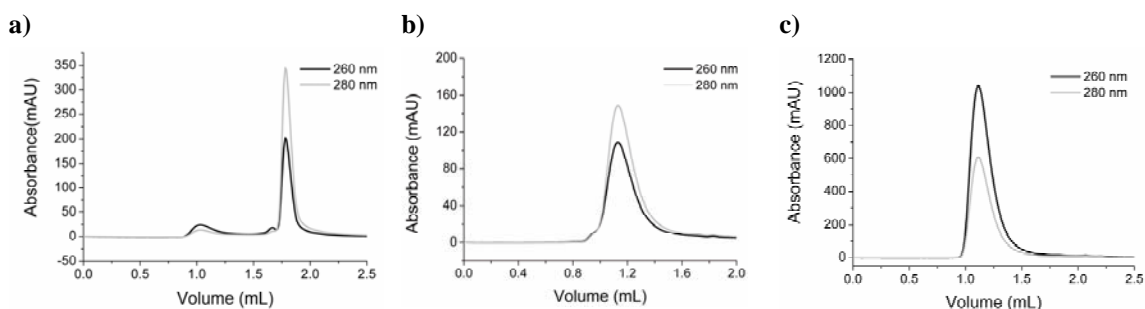
Figure 4.5 *FPLC traces showing the CP isolation and its reassembly to form the CCMV capsid; a) CCMV CP dimers, b) CCMV protein capsid, and c) CCMV itself. UV/Vis detection of the FPLC instrument was set at 260 and 280 nm.*

Isolation of the CCMV capsid particles could also be monitored by UV/Vis spectroscopy (Figure 4.6). As already observed in the FPLC traces (Figure 4.5), the absorbance ratio A_{280}/A_{260} changes drastically during the RNA removal process. Due to the high extinction coefficient of the RNA ($\varepsilon_{CCMV\ RNA} = 27.81 \times 10^6\,\mathrm{M^{-1}\,cm^{-1}}$), the CCMV virus has a maximum absorption at 260 nm (Figure 4.6a), whereas after RNA removal the maximum absorption shifts to 280 nm, the typical absorption of a protein, which has a much lower extinction coefficient ($\varepsilon_{CCMV\ CP} = 4.33 \times 10^6\,\mathrm{M^{-1}\,cm^{-1}}$) (Figure 4.6b). Hence, for both the assembled and nonassembled forms of the CCMV CP, the UV/Vis spectra are almost the same, only the absorbance minimum at 250 nm is different at pH 5 and pH 7.5 due to the difference in scattering produced by the capsids and the dimers (the former are larger particles).

The yield of the CCMV coat-protein isolation, and the purity of the protein, namely, the degree of contamination with RNA, can be obtained from the spectroscopic data, as already mentioned above. By comparing the initial protein content in the virus and the amount of final CP obtained, we could estimate that in our hands approximately 20–30% of the protein present in the virus is lost during the purification process (based on a protein content of the virus of 76% (w/w)). Furthermore, the absorbance ratio A_{280}/A_{260} was about 1.3 for most of the experiments, indicating a higher degree of RNA contamination in our samples than that described by Verduin.[21] The reason for this difference is not fully understood. The initial virus concentration that was routinely used by us was $10\,\mathrm{mg\,mL^{-1}}$, although concentrations of up to $20\,\mathrm{mg\,mL^{-1}}$ of virus occasionally were employed as well, giving the same results.

a)   b)
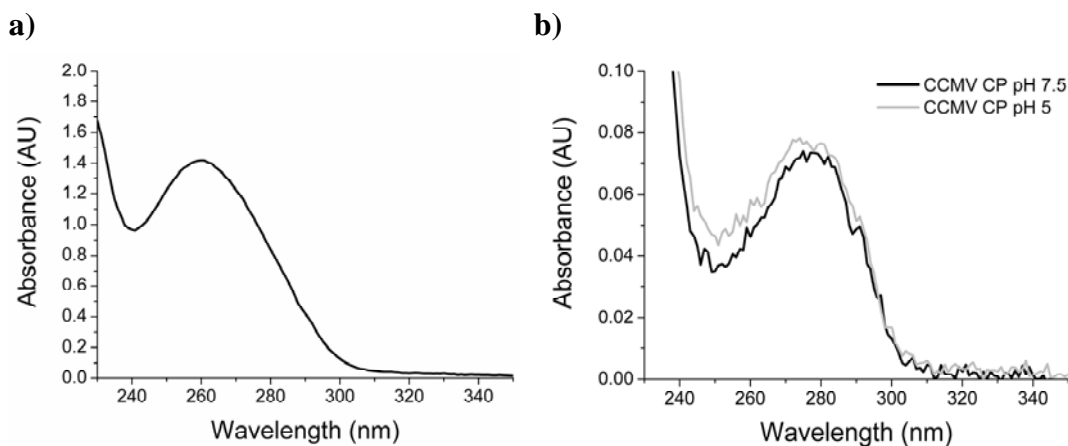
Figure 4.6 UV/Vis spectroscopic analysis of the removal of the RNA from CCMV. *UV/Vis spectra of: a) CCMV and b) the CCMV CP at pH 7.5 and 5.*

The removal of the RNA is also evident from TEM experiments (Figure 4.7). Since the RNA is removed the space in the capsid is larger than in the virus, which is reflected in the larger volume occupied by the staining dye compounds in the TEM pictures (Figure 4.7b). For the TEM experiments the capsid samples were prepared in the same way as the virus samples (see Chapter 3). The capsids appeared to be more difficult to visualize than the virus particles and hexagonally patterned monolayers could not be easily prepared with the empty capsids. This might indicate that they possess a less compact and more floppy structure than the virus, due to the absence of RNA.

a)   b)
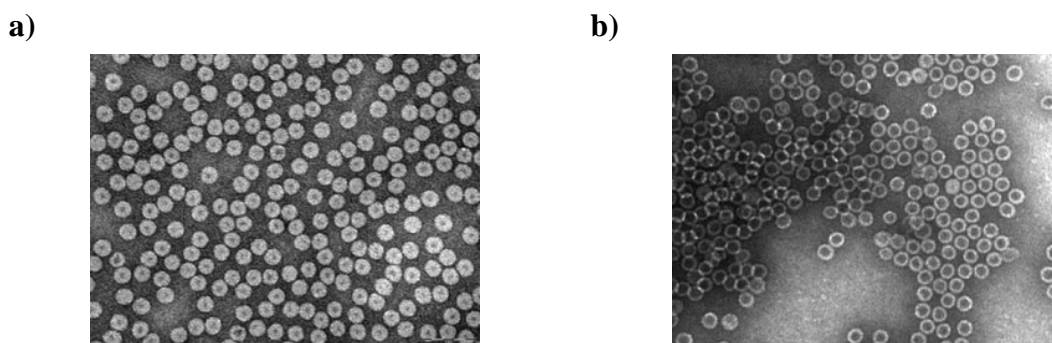
Figure 4.7 Microscopy studies on CCMV and capsid. *TEM micrographs of a) CCMV and b) capsid. The samples were negatively stained with 0.2% uranyl acetate.*

Unless used immediately the CCMV CP, once isolated, should be stored in assembled form at high salt concentration, that is, in acetate buffer of pH 5, at 1 M NaCl and at 4 °C, to avoid protein degradation. When stored in disassociated form at pH 7.5 the capsid protein molecules easily lose amino acid residues 1 to 36 (MW = 16,300 Da), as is visible in the SDS-PAGE gel (Figure 4.8a).[22] The concentration of degraded protein (indicated by a band at lower molecular weight) is the highest for the sample containing CP at pH 7.5 (lane 7). All other samples, namely, virus (lanes 2, 4 and 5) and capsid

(lanes 3 and 6), show little degradation and the most intense band is the one corresponding to the nondegraded CP (MW = 20 kDa). The presence of degraded protein in the reassembled capsid samples seems to cause the formation of smaller capsids (T = 1 and "T = 2" particles), which is inconvenient for our experiments (see Chapter 2).[22]

The virus, CP dimers, and capsid run differently in an agarose gel (Figure 4.8b). The virus at pH 5 runs relatively fast (lane 1), while the assembled protein capsid at the same pH does not run at all (lane 2). The disassociated CP, on the other hand, runs slower on the agarose gel than the virus (lane 3).

a)   **b)**
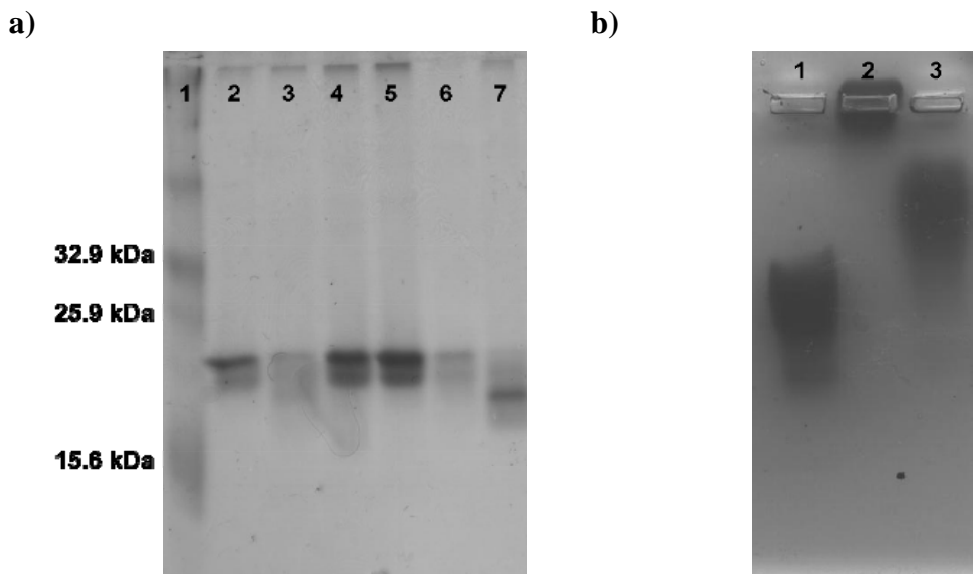
Figure 4.8 *Gel electrophoresis analysis of the removal of the RNA from the CCMV virus. a) SDS-PAGE gel of CCMV and the CCMV CP under different conditions and at different stages of the isolation process. Lanes: 1) marker, 2 and 4) CCMV at pH 5, 3 and 6) CCMV CP at pH 5, 5) CCMV at pH 7.5, 7) CCMV CP at pH 7.5. b) Agarose gel. Lanes: 1) CCMV, 2) CCMV CP at pH 5, 3) CCMV CP at pH 7.5. Both gels were stained with Coomassie Blue.*

As can be seen in the diagram in Figure 4.1, an ionic strength of 0.3 M is on the brink of the formation of the correct capsid assembly and the formation of larger assemblies. Initially, we carried out assembly experiments with an NaCl concentration of 0.3 M in a buffer of pH 5, giving well-assembled capsids from purified CCMV CP. Occasionally it was observed, however, that no capsid assembly occurred, as judged by TEM or FPLC. In later experiments we decided to use higher salt concentrations in the buffers. When NaCl concentrations of 0.5 or 1 M were used, the assembly of the capsid was always successful. This illustrates the importance of the salt concentration in the assembly process of the CCMV CP.

The formation of the larger assemblies was separately studied by FPLC and TEM (Figure 4.9). When the CP was assembled in a pH 5 buffer containing a salt concentration lower than 0.3 M NaCl, the appearance of a peak at low retention volume could be observed in the FPLC chromatograms (Figure 4.9a). This peak corresponds to the larger assemblies, such as double shell and lamellar structures (Figure 4.9b). When analyzed by UV/Vis spectroscopy, these large assemblies gave a clear increase in the absorbance minimum at 250 nm, probably due to an increased scattering of the solution. It is expected that not all of the larger assemblies can be distinguished separately by FPLC because of the exclusion limit of the column.

a)

b)
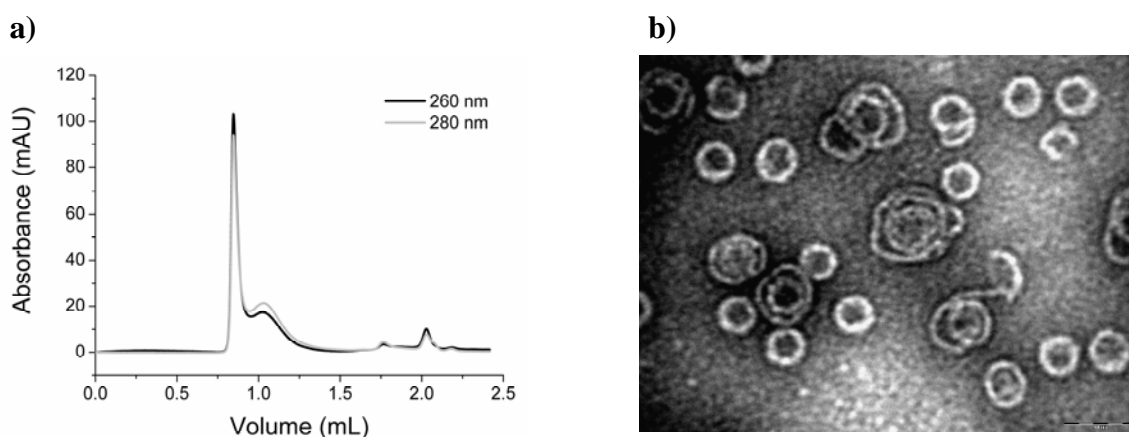
Figure 4.9 The formation of large CCMV CP assemblies. a) FPLC chromatogram and b) TEM micrograph of the CCMV CP assembled at pH 5 using an NaCl concentration of 0.2 M.

In Figure 4.10 the complete CCMV assembly process and the conditions used to reach each state in this process are summarized. It should be noted that manipulations with the capsid and the many times repeating of the assembly–disassembly cycle causes the appearance of the larger assemblies. It is also noteworthy that the capsid at pH 7.5 is very sensitive to degradation, leading to the formation of T = 1 or "T = 2" particles, when the CP is assembled.[22] These effects can be observed by FPLC and TEM, and are sometimes difficult to control.
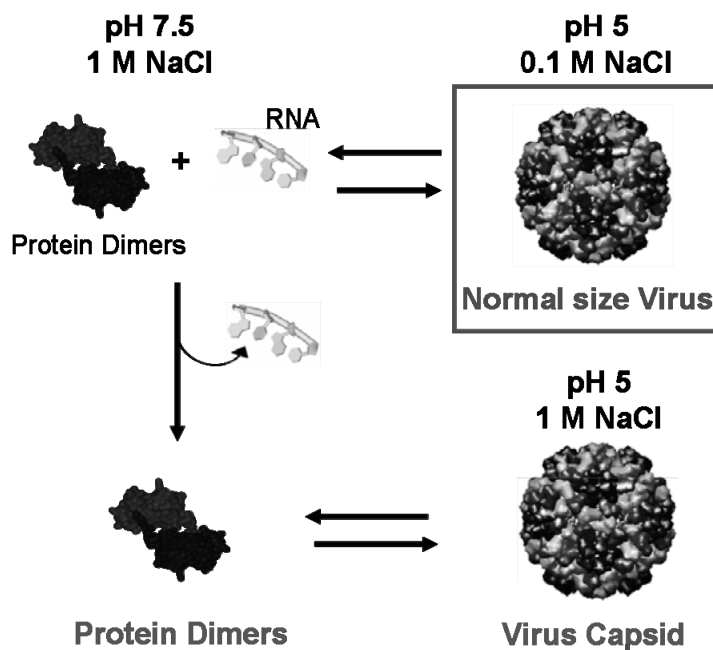
Figure 4.10 *Assembly pathway of the CCMV virus and the CCMV capsid depending on the pH and ionic strength.*

4.3 Conclusion

The CCMV capsid could be successfully isolated following the protocol described by Verduin,[21] that is, by precipitating the RNA with $CaCl_2$ at neutral pH. The adequate removal of the RNA and the assembly of the CP subunits to capsid was confirmed by several techniques, such as FPLC, UV/Vis spectroscopy, and TEM. Not only the pH but also the salt concentration turned to be an important parameter, which should be taken into account when performing the assembly process. Assembly buffers need to contain concentrations of NaCl higher than 0.3 M. In this way empty capsids 28 nm in diameter are formed, avoiding the formation of larger assemblies such as lamellar structures and double shells. The CP is susceptible to degradation, in particular when it is in the dimeric form at pH 7.5, as evidenced by SDS-PAGE. The CP should, therefore, be stored in its assembled form, that is, as a capsid in 1 M NaCl at pH 5 and at 4°C.

We have described the procedure to remove the RNA from CCMV and the techniques to monitor the process of obtaining the CP and the capsid itself. The study of the capsid assembly as a function of the pH and ionic strength has given us insight as to how to control the capsid association process. The latter is of key importance to achieve the main goal of this thesis, that is, the use of the CCMV capsid as a container for enzymes.

4.4 Experimental Section

Materials

Sodium acetate trihydrate (>99%) and uranyl acetate dihydrate (≥98%) were purchased from Fluka. Ethylenediaminetetraacetic acid (EDTA) disodium salt dihydrate (>99%), tris(hydroxymethyl)aminomethane (Tris) (>99%), calcium chloride dihydrate (>99%), sodium chloride (99.5%), sodium azide (99%), and cesium chloride (>99%) were purchased from Acros; ethanol (p.a.) was purchased from Merck; phenylmethanesulfonyl fluoride (PMSF) (≥98.5%), ethidium bromide (~95%), Orange G (≥80%), and dithiothreitol (DTT) (99%) were obtained from Sigma-Aldrich. Agarose (electrophoresis grade) was purchased from Invitrogen. All reagents used for SDS-PAGE electrophoresis were purchased from Bio-Rad Laboratories.

Instrumentation

UV/Vis spectroscopy was performed on a Varian Cary 50 spectrophotometer at room temperature using a 1 cm quartz cuvette (Hellma, light path: 1 cm). The reference spectra of the corresponding buffers were subtracted from all UV/Vis spectra.

Fast protein liquid chromatography (FPLC) was performed on an Ettan Akta LC system equipped with a Superose 6 PC 3.2/30 column from Amersham Biosciences (flow rate 40 μL min^{-1}). Injections (20-mL aliquots) of the samples on the FPLC column at room temperature were monitored by UV/Vis detection at 280 nm and 260 nm.

Transmission electron microscopy (TEM) micrographs were recorded on a JEOL JEM-1010 instrument. Samples were prepared by drying a drop of the solution on a Formvar carbon-coated grid, which had been previously made hydrophilic by glow discharge. The excess buffer on the grid was blotted away after 1 min with filter paper. Negative staining of the samples was achieved by applying a drop of uranyl acetate solution (0.2% in MilliQ) onto the grid and blotting the excess liquid away after 15 s with filter paper. The samples were left to dry in air for 30 min before analysis.

Gel electrophoresis. SDS-polyacrylamide gel electrophoresis (SDS-PAGE) was performed by using a 15% polyacrylamide gel containing 10% SDS. Samples were treated with β-mercaptoethanol and heated prior to loading onto the gel. Gels were stained with 0.05% (w/v) Coomassie Blue solution and destained with a solution of 5% (v/v) methanol and 7% (v/v) acetic acid in water (Coomassie Blue destainer). Agarose gel electrophoresis was performed by using gels with 1.25% agarose. To prepare the gels, agarose (1.5 g) was dissolved in TAE buffer (12 mL; 40 mM Tris-acetate, 1 mM disodium EDTA, pH = 8). Orange G was used as the sample buffer. The gel was run at 100 mV (from cathode to anode), stained with 0.05% (w/v) Coomassie Blue solution,

and destained with 40% (v/v) methanol and 10% (v/v) acetic acid solution in water (complete Coomassie Blue destainer).

Ultracentrifugation was performed using a Sorvall Micro (SM) ultracentrifuge (type RC-M150GX) with a S-120-AT2 type rotor. Thick-walled polycarbonate tubes (vol = 1 mL) provided by Sorvall were used.

Dialysis was performed by using dialysis tubing (Spectra/Por 4, MWCO: 12–14 kD, Flat width: 25 mm) purchased from Spectrum Laboratories, and D-tube dialyzer (MWCO: 12–14 kD, volume: 1000–3000 uL) from Novagen.

Buffers

The following aqueous buffers were used in the experiments:

Virus buffer: 0.1 M sodium acetate, 0.001 M disodium EDTA, 0.001 M sodium azide, buffered at pH = 5.0

RNA buffer: 0.05 M Tris-HCl, 0.5 M calcium chloride, 0.001 M dithiothreitol (DTT), buffered at pH = 7.5

Clean buffer: 0.05 M Tris-HCl, >0.3 M sodium chloride, 0.001 M dithiothreitol (DTT), buffered at pH = 7.5

Capsid storage Buffer: 0.05 M sodium acetate, 1 M sodium chloride, 0.001 M sodium azide, buffered at pH = 5.0

Isolation of the CCMV coat protein

A CCMV suspension (1–2 mL, c = 10 mg mL^{-1}) in virus buffer was dialyzed against RNA buffer (1000 times excess in volume). After dialyzing overnight at 4°C the white precipitate of RNA was collected by ultracentrifugation. This was realized with the help of a Sorvall Micro ultracentrifuge and the S-120-AT2 Sorvall rotor (2 h at 47,000 rpm, T = 10°C, Acc/Decc = 9). The top three-quarters of the supernatant were removed with a micropipette and the yellow-white pellet containing precipitated RNA was discarded. The solution was then dialyzed against three changes of clean buffer (100–1000 times excess in volume, 3 h per change). The obtained dissociated protein, free of RNA, was associated into spherical particles by dialysis using the capsid storage buffer (100–1000 times excess in volume, 3 h per change), and the protein was stored in this form at 4°C (no longer than 1 month) or dialyzed and used immediately, as explained in the next section.

Preparation of samples for assembly experiments

Assembled CP in storage buffer was dissociated back to protein dimers before being used for the assembly studies. To this end the assembled protein was dialyzed against three changes of Tris-HCl buffer (100–1000 times excess in volume, 0.05 M, pH 7.5) (3 h per change) containing varying concentrations of NaCl, depending on the

requirements needed for the assembly experiments. Assembly studies were performed by bringing the CP dimer solution to the required conditions of pH and ionic strength by dialysis (100–1000 times excess in volume, 3 h per change). All buffers used in the disassembly and assembly studies contained 1 mM EDTA, 10 mM $CaCl_2$, and 0.2 mM PMSF.

4.5 Notes and References

[1]   H. Fraenkel-Conrat, R. C. Williams, *Proc. Natl. Acad. Sci. U.S.A.* **1955**, *41*, 690.

[2]   J. B. Bancroft, E. Hiebert, *Virology* **1967**, *32*, 354.

[3]   J. B. Bancroft, G. J. Hills, R. Markham, *Virology* **1967**, *31*, 354.

[4]   E. Hiebert, J. B. Bancroft, C. E. Bracker, *Virology* **1968**, *34*, 492.

[5]   E. Hiebert, J. B. Bancroft, *Virology* **1969**, *39*, 296.

[6]   J. M. Fox, G. Wang, J. A. Speir, N. H. Olson, J. E. Johnson, T. S. Baker, M. J. Young, *Virology* **1998**, *244*, 212.

[7]   J. B. Bancroft, G. W. Wagner, C. E. Bracker, *Virology* **1968**, *36*, 146.

[8]   J. T. Finch, J. B. Bancroft, *Nature* **1968**, *220*, 815.

[9]   J. B. Bancroft, C. E. Bracker, G. W. Wagner, *Virology* **1969**, *38*, 324.

[10]   K. W. Adolph, P. J. Butler, *J. Mol. Biol.* **1974**, *88*, 327.

[11]   J. B. Bancroft, *Adv. Virus Res.* **1970**, *16*, 99.

[12]   J. E. Johnson, J. A. Speir, *J. Mol. Biol.* **1997**, *269*, 665.

[13]   B. Jacrot, *J. Mol. Biol.* **1975**, *95*, 433.

[14]   R. F. Bruinsma, W. M. Gelbart, D. Reguera, J. Rudnick, R. Zandi, *Phys. Rev. Lett.* **2003**, *90*, 248101.

[15]   J. B. Bancroft, E. Hiebert, C. E. Bracker, *Virology* **1969**, *39*, 924.

[16]   F. D. Sikkema, M. Comellas-Aragones, R. G. Fokkink, B. J. Verduin, J. J. L. M. Cornelissen, R. J. M. Nolte, *Org. Biomol. Chem.* **2007**, *5*, 54.

[17]   Y. F. Hu, R. Zandi, A. Anavitarte, C. M. Knobler, W. M. Gelbart, *Biophys. J.* **2008**, *94*, 1428.

[18]   J. B. Bancroft, M. W. Rees, J. R. O. Dawson, G. D. McLean, M. N. Short, *J. Gen. Virol.* **1972**, *16*, 69.

[19]   J. B. Bancroft, M. W. Rees, M. W. Johnson, J. R. O. Dawson, *J. Gen. Virol.* **1973**, *21*, 507.

[20]   J. M. Fox, X. Zhao, J. A. Speir, M. J. Young, *Virology* **1996**, *222*, 115.

[21]   B. J. M. Verduin, *FEBS Lett.* **1974**, *45*, 50.

[22]   J. Tang, J. M. Johnson, K. A. Dryden, M. J. Young, A. Zlotnick, J. E. Johnson, *J. Struct. Biol.* **2006**, *154*, 59.

CHAPTER 5

Structural Studies of CCMV and CCMV Capsid by Small-Angle Neutron Scattering and Dynamic Light Scattering

5.1 Introduction

Virus assembly

The three-dimensional structure of many spherical RNA viruses, such as the cowpea chlorotic mottle virus (CCMV) has been studied by different techniques including negative-staining electron microscopy (EM)[1] and X-ray crystallography.[2] In general CCMV is a well-studied virus and can be considered a model system for other spherical RNA viruses. CCMV with a diameter of 280 Å, swells at high pH in the absence of Ca^{II} ions, due to the repulsion between its carboxylate groups, while maintaining its overall structure. Under these conditions it displays pores 20 Å in diameter in its protein shell. The removal of RNA from CCMV and the reassembly of the empty capsid from the constituting coat proteins have been extensively studied under a variety of conditions such as pH and ionic strength, as is described in Chapter 4.[3-11] The capsid is an assembly of 180 identical protein units that assemble into stable dimers, which in turn organize themselves into a T = 3 structure of icosahedral symmetry, that is, a cluster with faces consisting of protein hexamers and pentamers. The removal of 25 to 34 amino acids from the N-terminal part of the CCMV protein, which contains mainly basic residues, can occur spontaneously and may lead to a considerable heterogeneity of species in the capsid assembly.[12] Recently, we and others have started to explore the potential of the empty capsid,[13] which is a well-defined nanocapsule of homogeneous size (diameter 280 Å), as a scaffold for mineralization,[14-16] for the encapsulation of non-nucleic acid materials such as single enzyme molecules,[17] and synthetic polymers, for example, polyanethole sulfonate,[18] and polystyrene sulfonate (PSS).[19,20] Techniques such as X-ray crystallography, electron microscopy, gel filtration (*e.g.*, fast protein liquid chromatography (FPLC)) and more recently mass spectrometry[21,22] and atomic force microscopy (AFM),[23,24] have proven to be valuable tools for the study of viruses and biohybrid assemblies of viruses. Although all of these techniques have yielded valuable and specific information, we felt that additional knowledge about the

size and shape of CCMV and the CCMV capsid might be obtained from solution scattering methods such as small angle neutron scattering (SANS) and dynamic light scattering (DLS).[25-28] In this chapter such SANS and DLS studies are described.

SANS

SANS has been used to study the solution structure of biological macromolecules for over three decades. Since the measurements are performed in solution, SANS can provide unique structural information under conditions that more closely mimic the molecules' natural environment than X-ray crystallography and non-cryogenic EM can do.[29,30] SANS also allows the effect of solution parameters such as pH and ionic strength to be assessed directly. Jacrot *et al*. were the first to study the protein–nucleic acid organization of a number of RNA viruses by SANS.[31] Their results confirmed the structure of the viruses obtained by other techniques, but furthermore provided a consistent set of data, from which low-resolution models could be built. It was concluded that there are differences between the viruses with respect to the degree of interpenetration of the RNA into the protein shells, related to the nature of the forces stabilizing the virus. Following this pioneering study, many other viral particles have been investigated by SANS,[32-40] of which the bromegrass mosaic virus (BMV)[41-43] is the virus most closely related to CCMV.

SANS is a technique that is similar to other scattering techniques, which are often complementary, namely, small-angle X-ray scattering (SAXS) and light scattering (LS). In each of these techniques radiation is elastically scattered by a sample and the resulting scattering pattern, which is represented by the intensity as a function of the scattering angle (recalculated as the scattering vector $q = (4\pi/\lambda)\sin(\theta/2)$ (Å^{-1})), is analyzed to provide information about the size and shape of the object. The type of radiation and the way in which this radiation interacts with matter are the main differences between these techniques. Light and X-rays are both scattered by the electrons surrounding the atomic nuclei, but neutrons are scattered by the nuclei themselves, a fact that has several important consequences.[30,44] The strength of the neutron–nucleus interaction varies completely irregularly with the atomic number Z; not even isotopes of the same element have the same neutron-scattering cross-section. The most significant isotopic variation is the one involving hydrogen and deuterium. The different scattering densities of these two isotopes is used in the so-called SANS "contrast variation method".

The contrast variation method

In complexes composed of two components with different neutron-scattering length densities, the scattering from one component can be separated from the other one by measuring the complex in water containing solvents with different H_2O/D_2O ratios

(Figure 5.1). This provides unique structural information about each individual component and the way the components interact with each other in the complex.[29,30] This method is very powerful for the investigation of the structure and dynamics of biological systems and related biomaterials.[45] Isotopic substitution of H for D is routinely used to change the scattering of a biomacromolecule without affecting its biochemistry. Often, this substitution is as simple as using D_2O instead of H_2O in the solvent to increase the contrast between the studied molecules and the solvent and to decrease the background due to the incoherent scattering by H. Because of the exchange of acidic protons with the solvent, water, the scattering length density of proteins and polynucleotides varies with the solvent (D_2O/H_2O) composition, whereas that of hydrocarbons like lipids and polystyrene ($\rho = 1.42 \times 10^{-14}$ cm Å^{-3}) does not.[44] It can be concluded from Figure 5.1 that in 100% D_2O, the contrast between solvent, protein, and hydrocarbon is optimal, whereas for RNA the contrast is better in 100 % H_2O.
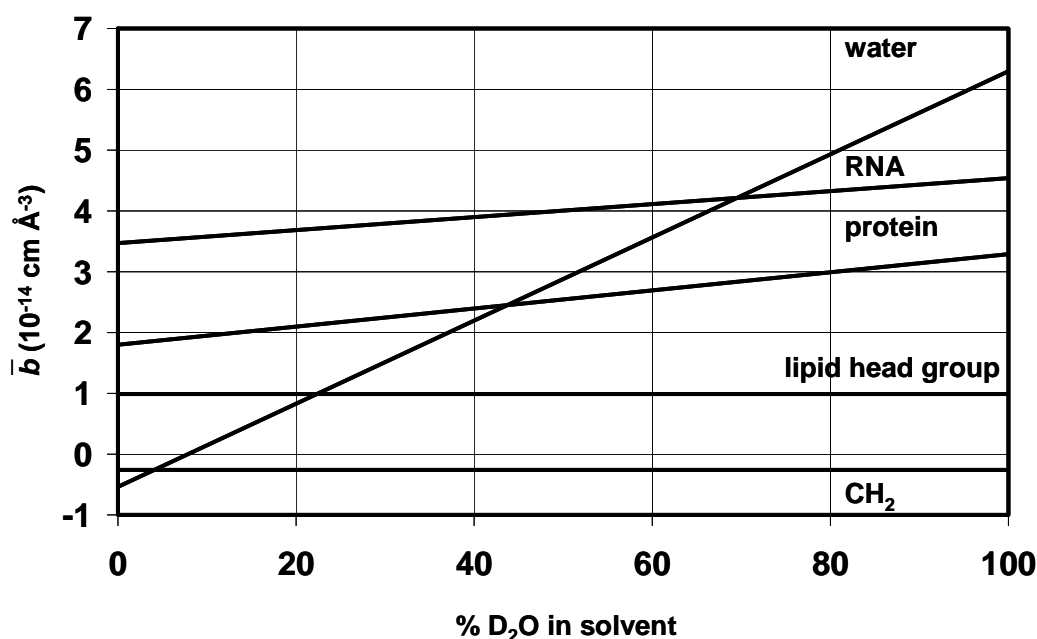
Figure 5.1 *The average scattering density for various biological molecules as a function of the D_2O concentration in the solution (adapted from the reference [46]). The crossing point of the water line with that of a solute is called the "matching" or isopicnic point.[30] The matching point corresponding to capsid protein and RNA are 43% and 68% D_2O/H_2O, respectively.*

SANS, using the contrast variation method, can nicely complement X-ray crystallographic studies to provide low-resolution information on the radial distribution of protein and RNA in a virus, and the possible reorganisation that occurs upon swelling or disassembly of the virus. The method is generally applicable and allows a simple systematic comparison between viruses.[31]

The structure of CCMV and its assembly properties have been described in the previous chapters. The different states of CCMV and the CCMV capsid, depending on the pH and ionic strength, were characterized by using several techniques, such as FPLC and TEM, and the results are schematically represented in Scheme 5.1. In the present chapter we describe SANS studies on CCMV, which were carried out to see whether this technique would confirm the structural data obtained by other techniques and whether it would provide us with additional information about the CCMV structure. Subsequently, we have used SANS, including the contrast variation method, to analyze a biohybrid assembly composed of the CCMV capsid and polystyrene sulfonate (PSS).[19] Furthermore, parallel to the SANS measurements, DLS studies have been performed to complement the SANS data and to support the postulated models. The combination of these two non-destructive techniques gives additional information about CCMV, its assembly properties, and the structure of the biohybrid particles.
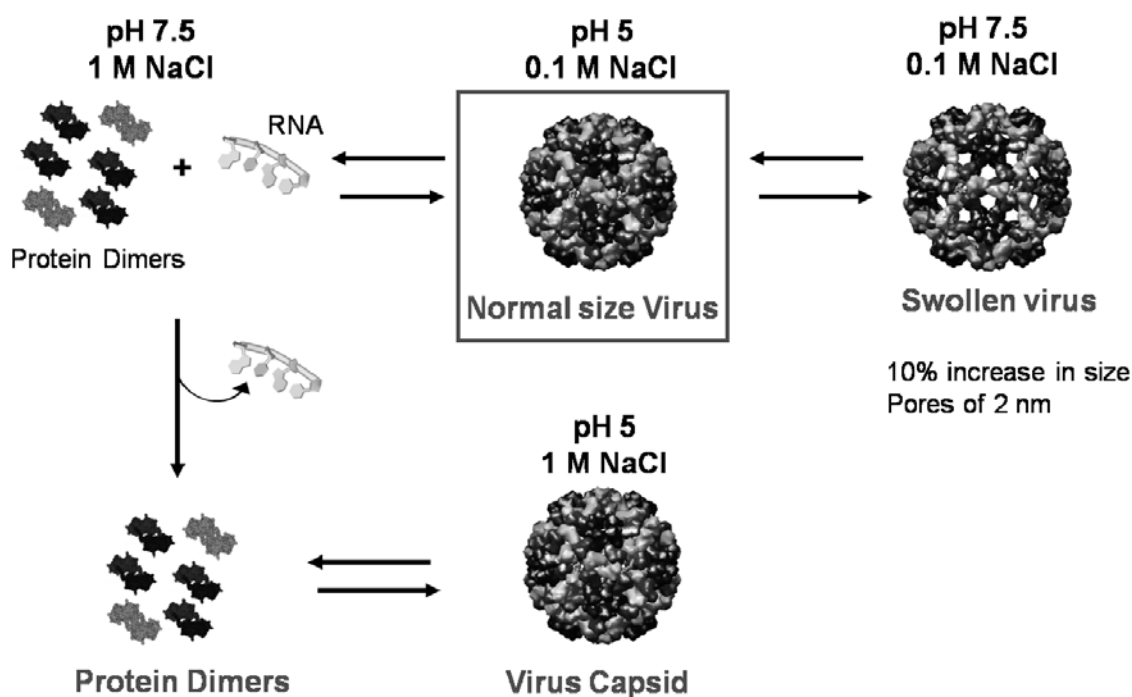
Scheme 5.1 *Assembly pathway of CCMV and the CCMV capsid depending on the pH and ionic strength.*

5.2 Results and Discussion

CCMV and CCMV capsid assembly as studied by conventional techniques

CCMV at pH 5 is a well-defined monodisperse particle of $d = 28$ nm as shown by TEM (Figure 5.2a). The swelling of the virus is clearly demonstrated by FPLC. The virus at pH 5 elutes at $V = 1.1$ mL, while at pH 7.5 a peak appears at a smaller elution volume,

corresponding to a larger particle (Figure 5.2b). The arrangement of the RNA chain within the virus particle and its interaction with the protein shell at pH 5 and 7.5, namely, for both the compact and swollen state, is not completely known. Studying the two states by SANS is therefore of high interest.

a)

b)
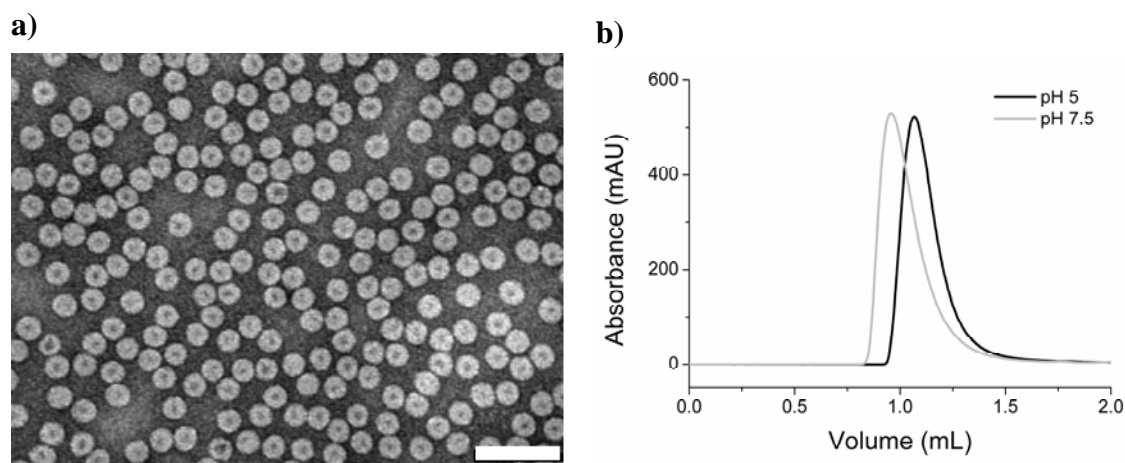
Figure 5.2 a) Negative-staining TEM micrograph of the CCMV virus at pH 5 (bar = 100 nm), b) FPLC of CCMV at pH 5 (compact form) and 7.5 (swollen form).

As described in Chapter 4, the viral RNA can be removed from CCMV and the coat protein (CP) isolated. The latter can then be reassembled at pH 5 in the presence of NaCl to form the CCMV capsid, which has dimensions identical to those of the virus. The structure of the reassembled capsid is highly dependent on the pH and salt concentration, as can be concluded from the FPLC and TEM results depicted in Figure 5.3. At pH 7.5 the capsid is mostly disassembled into protein dimers at salt concentrations between 0.2 and 1.0 M, whereas at pH 5 the salt concentration influences the assembly dramatically, in line with results from the literature (Figure 5.3a and c).[11,47] At low salt concentration (< 0.3 M NaCl), a rather polydisperse distribution of particles is obtained, containing different kinds of larger CP assemblies, that is, lamellar structures or larger capsids, which elute at $V = 0.8$ mL in the FPLC (Figure 5.3c and d). At high salt concentration (higher than $c = 0.3$ M), mainly well-defined capsids of $d = 28$ nm are formed, which, in TEM, show a larger cavity than the virus itself, presumably due to the absence of the RNA (Figure 5.3a and b). SANS and DLS are techniques that allow the direct study of these assemblies in solution at different pH values and salt concentrations while avoiding sample preparation steps.
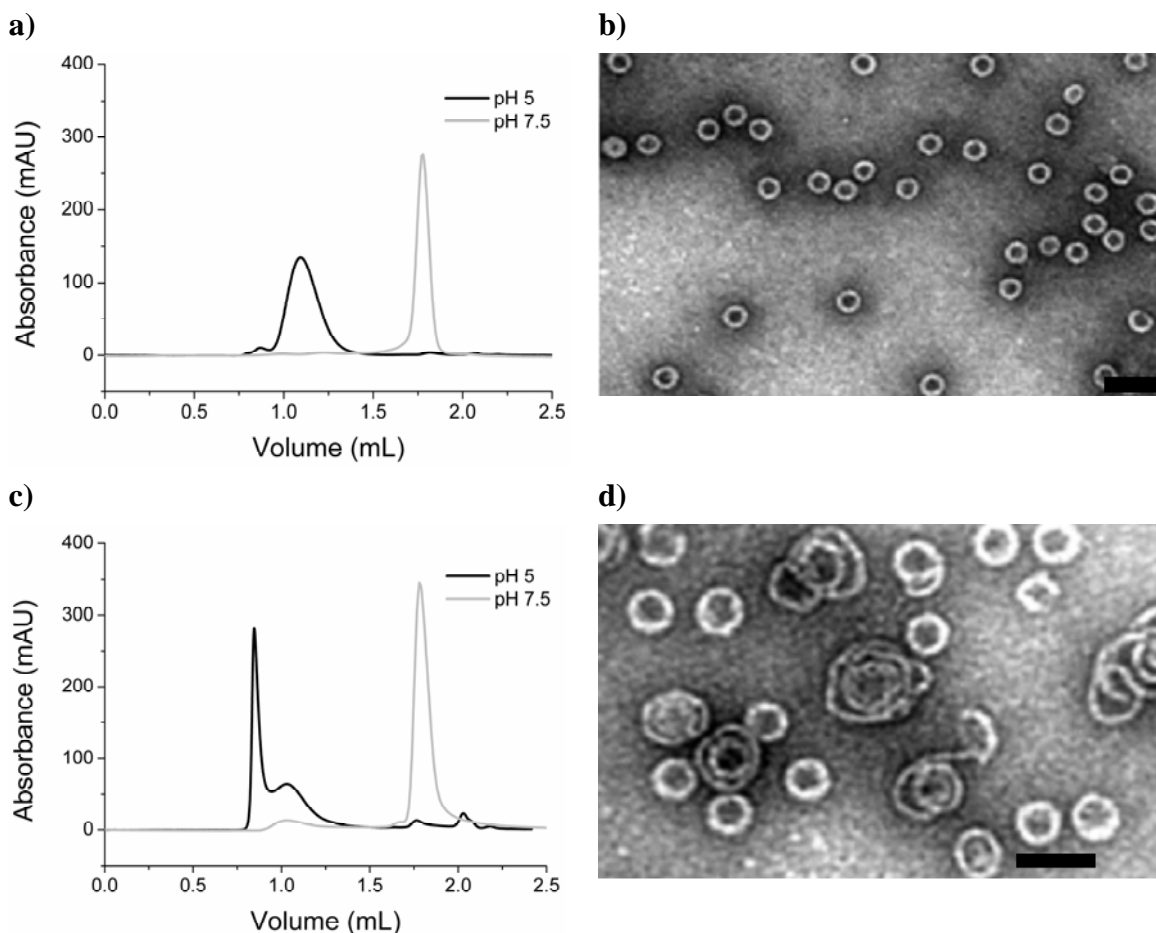
Figure 5.3 FPLC chromatograms of the CCMV CP assemblies at 1 M NaCl (a) and at 0.2 M NaCl (c), showing the traces at two different pH values. TEM micrographs (scale bar = 50 nm) corresponding to each of the samples at pH 5 at 1 M NaCl (b) and at 0.2 M NaCl (d).

Effect of D$_2$O on virus and capsid

As described in the Introduction, the presence of D$_2$O improves the contrast and therefore the information obtained from the SANS data. In order to be able to perform the SANS studies properly, it was felt necessary to study the influence of D$_2$O on the assembly behavior of CCMV and the CCMV capsid. The effect of D$_2$O was studied by FPLC and the results are shown in Figure 5.4. In the case of the CP (Figure 5.4a and b), the samples eluted at exactly the same time, which shows that the change from hydrogen to deuterium does not really affect the structure of the particles. However, in the case of the virus (Figure 5.4c and d), we observed that the D$_2$O solutions tended to elute later, although the difference was small. The appearance of the particles in TEM appeared not to be affected (not shown). The delayed elution would suggest a decrease in particle size in D$_2$O, but this is not confirmed with the SANS studies (see below).
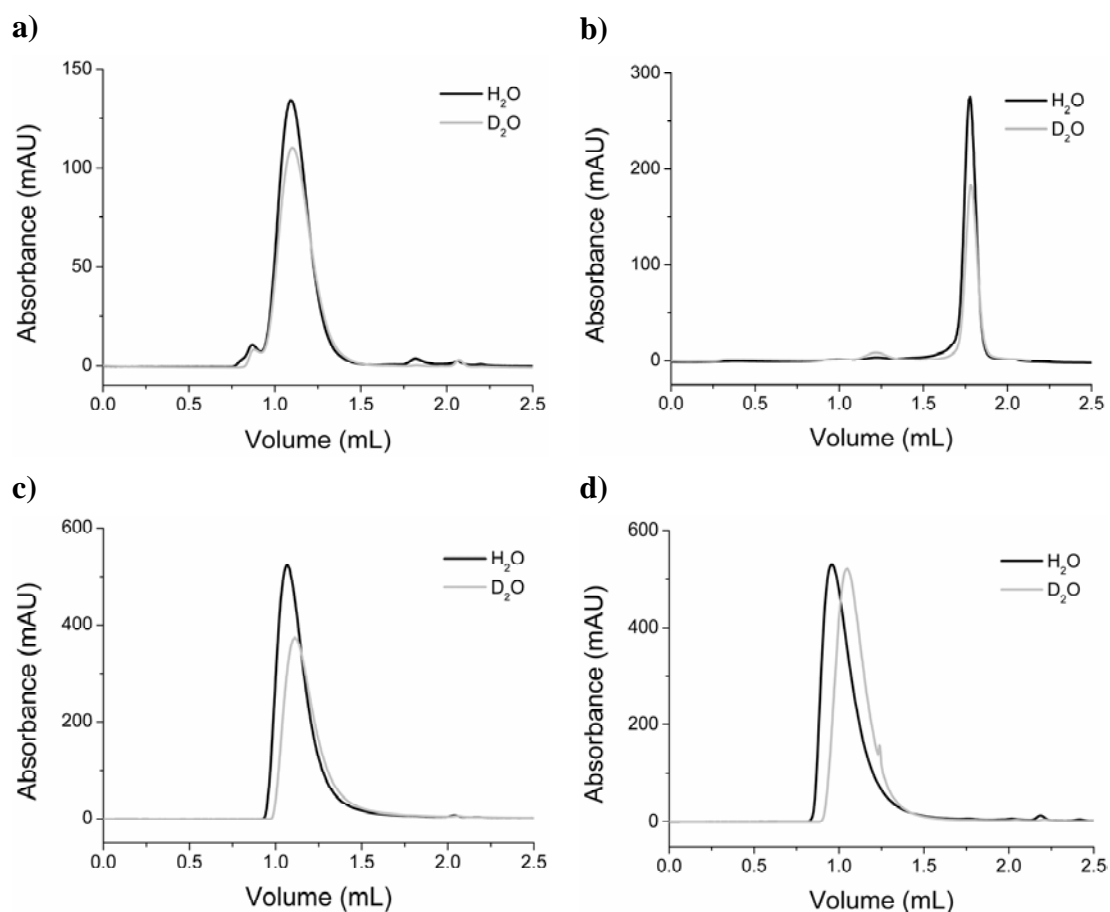
Figure 5.4 *FPLC chromatograms of CCMV CP at a) pH/pD 5 and b) pH/pD 7.5, and CCMV at c) pH/pD 5 and d) pH/pD 7.5, showing traces for both H_2O and D_2O solutions. The samples containing capsid protein contained 1 M NaCl whereas those containing CCMV contained no NaCl.*

Interpretation of SANS

It has recently been demonstrated that small-angle scattering (X-ray) data can be simulated with the help of the coordinates of the protein structure, for example, as determined by X-ray crystallography.[40] Such coordinates are available for the CCMV protein,[2] but not for the RNA and the polymer (see below) included in the viral cage. In our simulations of the SANS data we therefore approximated the virus structure by assuming that protein, polynucleotide, or polymer, and solvent shells were present with constant average scattering density lengths. The data was simulated with crude models and the parameters were subsequently refined with the programme FISH[48] to give the best agreement with the experimental traces. In this way the optimum values for parameters such as the radius of the particles and the size of the steps in the contrast in the scattering length densities can be determined. In this approximation, the shapes of the virus and capsid are approximated by spheres, although the virus is known to have a more complex symmetry, namely, that of an icosahedron. The first model to be applied

was a core–shell model, which is characterized by a core with a certain scattering length density ρ_1 (most probably solvent with encapsulated molecules) and a shell with inner and outer diameter r_1 and r_2 and scattering length density ρ_2 (capsid protein, with an RNA and/or polymer component), surrounded by a solvent region with scattering length density ρ_3 (Scheme 5.2a and c). In this model, the ρ_2/ρ_3 contrast step was always assumed to be that between protein and solvent ($\Delta\rho = 3.25$ for protein/D_2O), but the step ρ_1/ρ_2 was not fixed in the refinement, to see if the scattering length density of the core could be identified as solvent, RNA, polymer, or a mixture of these. A selected set of samples were refined with a more complex model (Scheme 5.2b and d) in which the core was surrounded by an inner and outer shell of different constant scattering length density. In these cases, the outer shell was always assumed to be protein, and the contrast step ρ_3/ρ_4 was chosen accordingly, whereas the inner shell could be RNA, polymer, or dilute ("wet") protein. The scattering curves are presented as the logarithm of the scattered intensity (log (I)) *versus* the scattering vector (q). This highlights the characteristic features at low q, but also amplifies the experimental noise at high q. The high q part of the scattering curve is used only to estimate the level of background scattering that should be incorporated in the simulation.

a)

b)

c)

d)
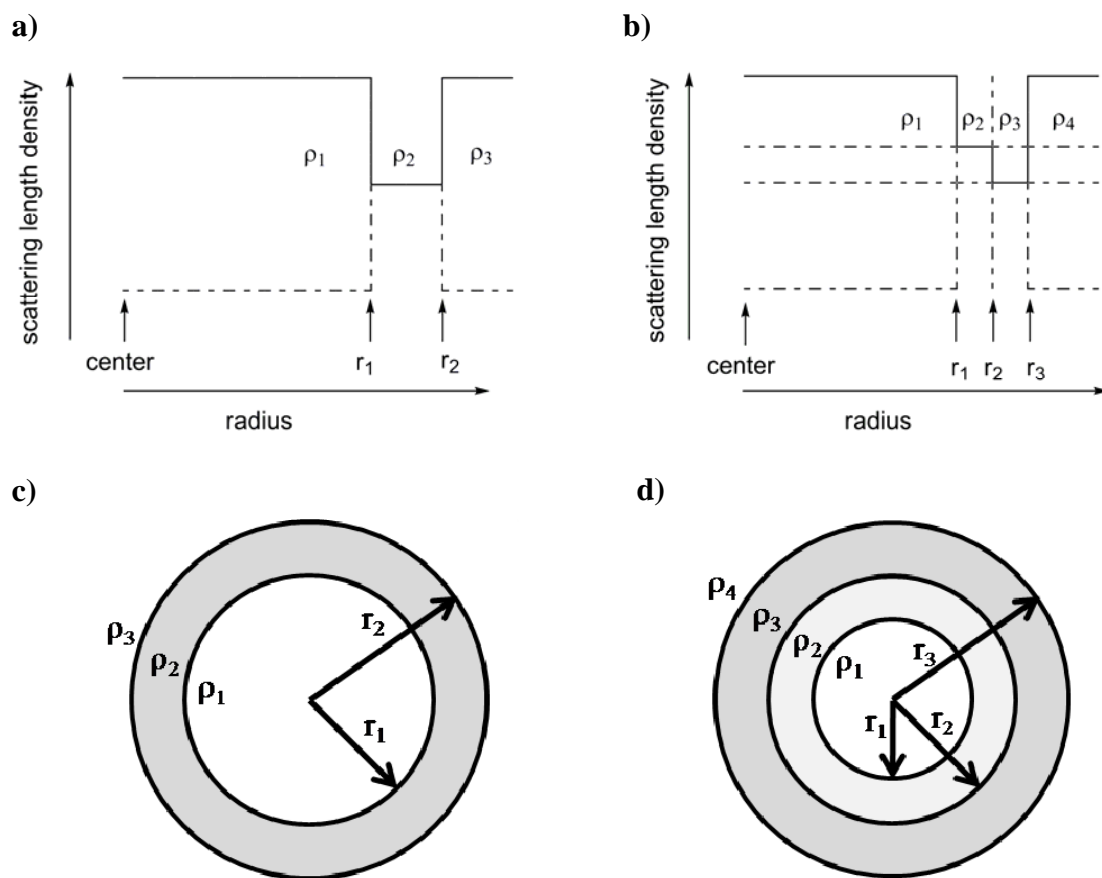
Scheme 5.2 *Schematic scattering length densities in a, c) core–shell and b, d) core–2-shell models. In b), the dashed lines from top to bottom indicate the levels of 68, 43, and*

0 % D$_2$O, where the solvent scattering length densities match those of RNA, protein, and H$_2$O, respectively (see also Figure 5.1).

In the next sections we will first discuss the effect of contrast variation in SANS studies on CCMV, followed by a core–shell interpretation of the scattering data of the virus at different pH values. Subsequently, the SANS results of the CCMV capsid at various salt concentrations and pH values using this same model, along with complementary DLS studies, will be discussed and compared with the data obtained for the virus. Finally, we will discuss core–2-shell models to interpret the neutron-scattering data of the virus, the empty capsid, and the capsid loaded with polystyrene sulfonate.

SANS and DLS studies on CCMV. The contrast variation method

The results for the contrast variation studies on CCMV are shown in Figure 5.5. The parameters derived from the simulations are given in Table 5.1. It can be seen that CCMV gives a scattering curve typical for a (near-)spherical particle such as a virus.[31] Solutions of virus in 43 and 68% D$_2$O were prepared to eliminate either the protein or the RNA contribution, respectively (see Figure 5.1).[31] At 68% a curve similar to that for 100% D$_2$O is obtained, as expected for the protein capsid; even the curve at 0% D$_2$O, where the contrast for RNA is expected to be larger than that for protein, resembles that in 100% D$_2$O. This apparent resemblance is corroborated by the similarities in the outer radii obtained from the refined simulations, which are between $r_2 = 130$ and 135 Å. The values found at the 68% D$_2$O level, where the RNA contribution is matched, are $r = 104.14$ and 130.06 Å for the inner and outer radii, respectively; this is in good agreement with the values found in the crystallographic study (average interior radius 104 Å, outer radius between 120 and 142 Å).[2] At 43% D$_2$O, where the contrast is expected to be optimal for RNA, the scattering curve is not well defined. This implies that the RNA structure is disordered to an extent that it cannot be approximated by a shell of the scattering length density of RNA, nor by any other simple structure. When a simulation was attempted, the outer radius refined to approximately the same value as that found for the protein shell, which suggests that a residual contrast for the protein contribution is being fitted rather than a genuine RNA contribution. In other viruses studied by SANS, some of which are closely related to CCMV, an RNA shell was clearly present.[31]

In a combined X-ray crystallography/EM study on CCMV in the literature,[2,18] it was found that the regions where the electron density of the RNA is well defined are close to the inner surface of the virus. Under the circumstances (100, 43, 0% D$_2$O) where the contrast is not optimized for the protein, the inner radius is significantly smaller than that found for 68% D$_2$O and the outer radius slightly larger; this indicates that in these

cases the innermost part, and even some of the outermost part, of the apparent protein shell has a high RNA content. Interestingly, in the case of 100 and 0% D_2O, the contrast step $\rho_1-\rho_2$ for the inner radius of the shell does not refine to the contrast step $\rho_2-\rho_3$ for the outer shell, which is fixed. This suggests that the core does not consist of pure buffer, but contains a significant amount of material with a higher scattering length density, namely, RNA. For 68% D_2O, where the contrast of the solvent is matched to that of RNA, $\rho_1-\rho_2$ refines almost to the value fixed for $\rho_2-\rho_3$, indicating a near-perfect match of the scattering length density of the core with that of the solvent; this is another indication that the core contains some "wet" RNA. The issue of the localization of the RNA in the virus is further discussed in the core–2-shell simulations section (see below). As the CCMV was found to give a better contrast in D_2O than in H_2O, it was decided to perform all further studies of the virus and capsid in D_2O.

Table 5.1 *Simulations (core–shell model;* r, *radius;* ρ, *contrast (10^{-14} cm Å^{-3}), PD, polydispersity) of SANS data obtained from experiments with CCMV in solutions of varying D_2O/H_2O composition.*

D_2O/H_2O (v/v)[a]	Expected contrast (see Figure 5.1)	$\rho_1-\rho_2$	r_1 (Å)	Δr (Å)	r_2 (Å)	$\rho_2-\rho_3$ (fixed)	PD (%)
100/0	protein>RNA	2.75	95.05	39.57	134.61	−3.25	4.09
68/32	protein	1.31	104.14	25.92	130.06	−1.33	3.59
43/57[b]	RNA	−1.33	91.84	40.75	132.58	+1.33	15.69
0/100	RNA>protein	−2.69	61.22	74.12	135.34	+3.66	23.52

a) Buffer: pH 5, 50 mM sodium acetate.

b) Data not fitted; simulation of core shell with low contrast and high polydispersity.
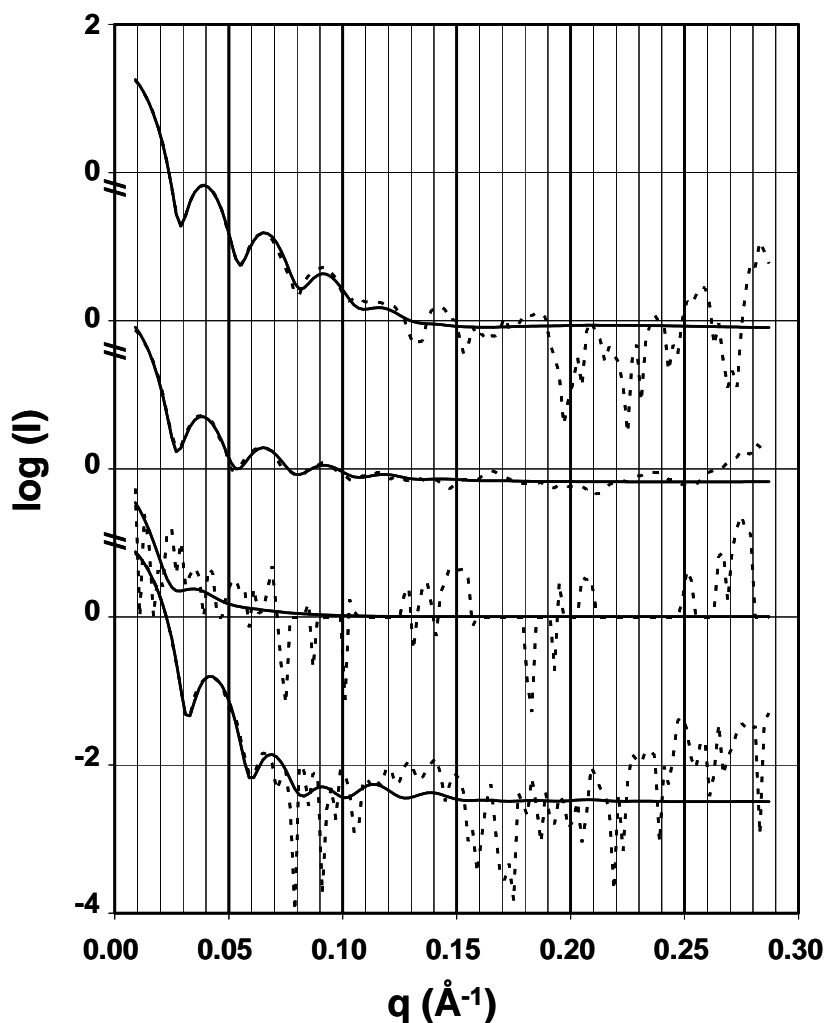
Figure 5.5 *SANS curves (dotted lines) of CCMV in solutions of varying D_2O/H_2O composition (buffer: pH 5, 50 mM sodium acetate) simulated (solid lines) with the parameters in Table 5.1. Top to bottom: 100, 68, 43, and 0% D_2O.*

Swelling of CCMV

In a separate set of SANS experiments with a new sample, the pH-dependent swelling of the virus was studied in detail. The results are shown in Figure 5.6 and the parameters of the corresponding simulations in Table 5.2. Although attention was taken to ensure the same experimental conditions of 100% D_2O was applied to the previous and present set of experiments, differences in r_2 and the PD were obtained (compare Table 5.1 and Table 5.2). The observed <2% deviation should be noted but is likely to be a result of the experimental settings and since data sets within one series of data collections are compared, it is not likely to be of significant influence on the interpretation of the SANS results.

Under the conditions mentioned in Table 5.2, the swelling of CCMV was detectable by SANS, as is the case for other viruses,[35,43,49] as a shift in the position of the subsidiary

maxima to lower q, indicating an increase in the virus radius. This increase (131.35 to 137.12 Å for the outer radius, 95.67 to 101.18 Å for the inner radius) is smaller (4.3% for outer, 5.8% for inner radius) than the 10% swelling observed in earlier X-ray crystallography/EM studies.[2] Complementary DLS results, which we performed and are shown in Figure 5.7, also indicated a larger swelling (152.85 to 172.95 Å) than that derived from the SANS data.

Table 5.2 *Simulations (core–shell model;* r, *radius;* ρ, *contrast; PD, polydispersity) of SANS data obtained from experiments on CCMV at different pH values.*

Experiment[a]	Expected result[b]	$\rho_1-\rho_2$	r_1 (Å)	Δr (Å)	r_2 (Å)	$\rho_2-\rho_3$ (fixed)	PD (%)
pD 7.5	Swollen virus	2.81	101.18	35.95	137.12	−3.25	7.05
pD 5	Virus, d = 280 Å	2.80	95.67	35.68	131.35	−3.25	6.27

a) Buffers: pD 5, 50 mM sodium acetate; pD 7.5, 50 mM Tris-HCl.

b) Expected on the basis of complementary studies in H_2O.
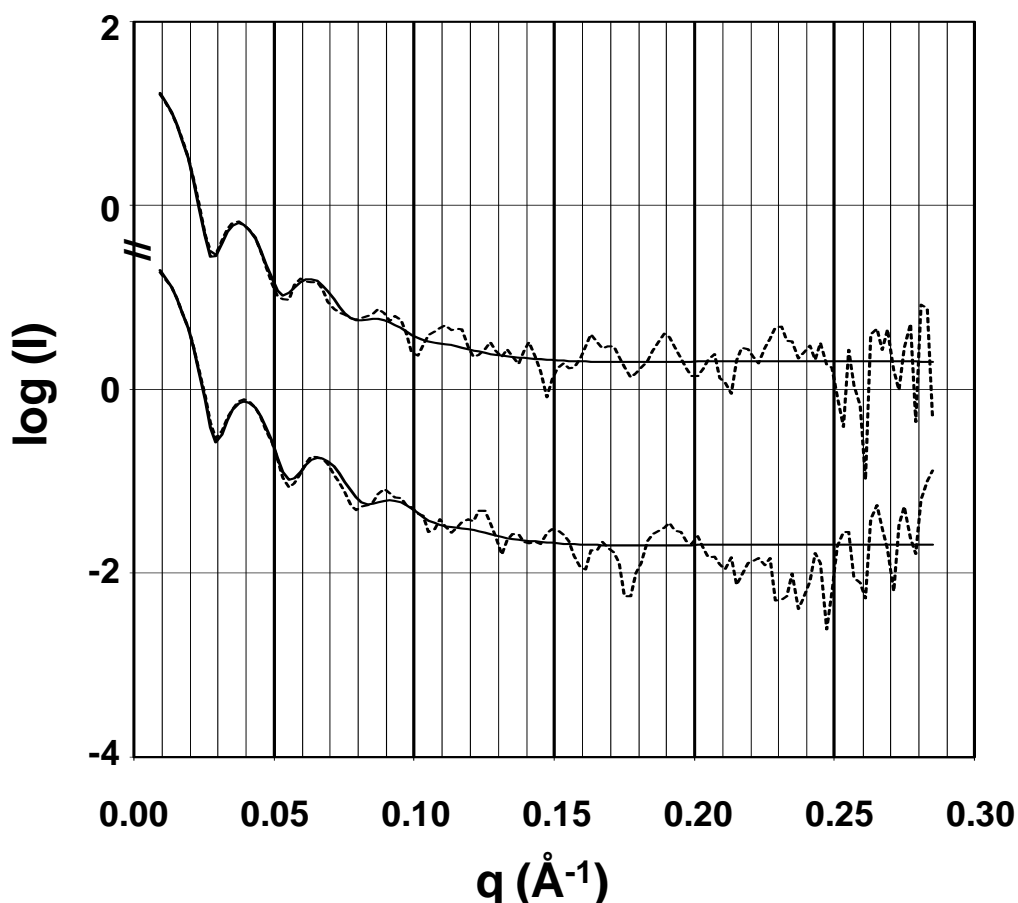
Figure 5.6 *SANS curves (dotted lines) of experiments performed with CCMV in 100% D_2O at different pH values. The solid lines are simulated curves with the parameters in Table 5.2. Top virus at pD 7.5, bottom virus at pD 5.0.*
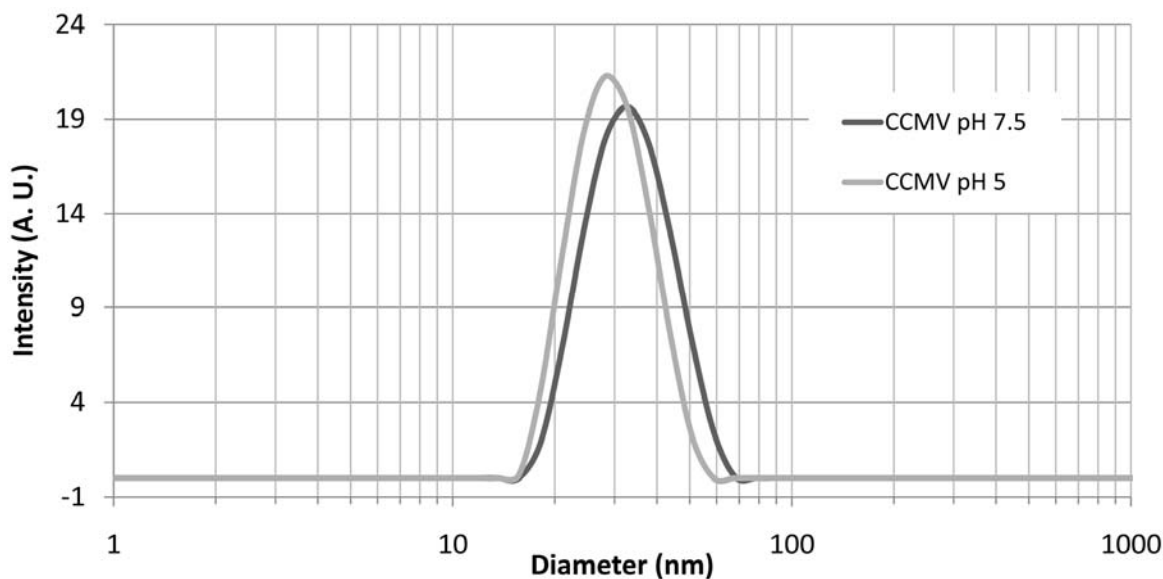
Figure 5.7 *Size analysis of DLS patterns obtained for CCMV in H_2O, at pH 5.0 (50 mM sodium acetate) and at pH 7.5 (50 mM Tris-HCl).*

SANS and DLS studies on the CCMV coat protein at 0.3 M NaCl

SANS experiments on the CCMV capsid, which is expected to dissociate into CP dimers at higher pH, were initially performed at a salt concentration of 0.3 M NaCl. The results are depicted in Figure 5.8, and the parameters of the corresponding simulations are presented in Table 5.3.

At pH 5, the capsid has a thinner shell than the virus and it has a slightly larger and shorter inner and outer radius, namely, 99 and 131 Å, respectively. This result is quite close to that obtained for the virus at optimum protein contrast (Figure 5.5); the structure of the remaining protein shell is the same when in the simulations the contribution of the RNA to the scattering is minimized either by removing it or by matching the solvent scattering length density. In the case of the virus, as noted in the contrast study, the contrast step $\rho_1-\rho_2$ for the inner radius of the shell does not refine to the contrast step $\rho_2-\rho_3$ for the outer shell, which suggests the presence of some dissolved RNA in the core of the virus (Table 5.1). For the capsid, however, at pH 5 and 6.5, $\rho_1-\rho_2$ refines to almost the same value as fixed for $\rho_2-\rho_3$, suggesting that the core contains pure solvent, as expected.

At higher pH, a tendency of the maxima in the scattering curve to shift to higher q values was observed, indicating a decrease in particle diameter. Concomitant with this shift, smearing, which indicates a higher polydispersity, was found. The results of the simulations reflected this decrease in particle radius and the values (pH 5, 131 Å; pH 6.5, 115 Å, pH 7.5, 85 Å) would point to the occurrence of capsids with T = 3 (180 protein units), "T = 2" (120 units) and T = 1 (60 units) icosahedral symmetry, respectively (see Chapter 2 and Appendix).[12] Such a result would be unprecedented,

since all other results (see above) point to a dissociation of the capsid at high pH into CP dimers and not to the formation of "T = 2" and T = 1 particles. The only report in the literature[18] that might be relevant for the present study suggests a swelling of the capsid not a shrinking. We decided therefore to investigate the samples by DLS to determine if smaller particles were present or not.

Table 5.3 *Simulations (core–shell model; r, radius; ρ, contrast; PD, polydispersity) of SANS data obtained from experiments on CCMV CP at different pH values (0.3 M NaCl).*

Experiment[a]	Expected result[b]	$\rho_1-\rho_2$	r_1 (Å)	Δr (Å)	r_2 (Å)	$\rho_2-\rho_3$ (fixed)	PD (%)
pD 5	Capsid d = 280 Å	3.07	99.41	31.94	131.35	−3.25	7.54
pD 6.5	(no data)	3.17	92.02	22.47	114.49	−3.25	13.38
pD 7.5[c]	CP dimers	3.63	67.44	17.30	84.75	−3.25	23.52

a) Buffers: pD 5, 50 mM sodium acetate; pD 6.5, 50 mM ammonium acetate; pD 7.5, 50 mM Tris-HCl. Buffers contained 0.3 M NaCl.

b) Expected on the basis of complementary studies in H_2O.

c) Core–shell model not applicable.
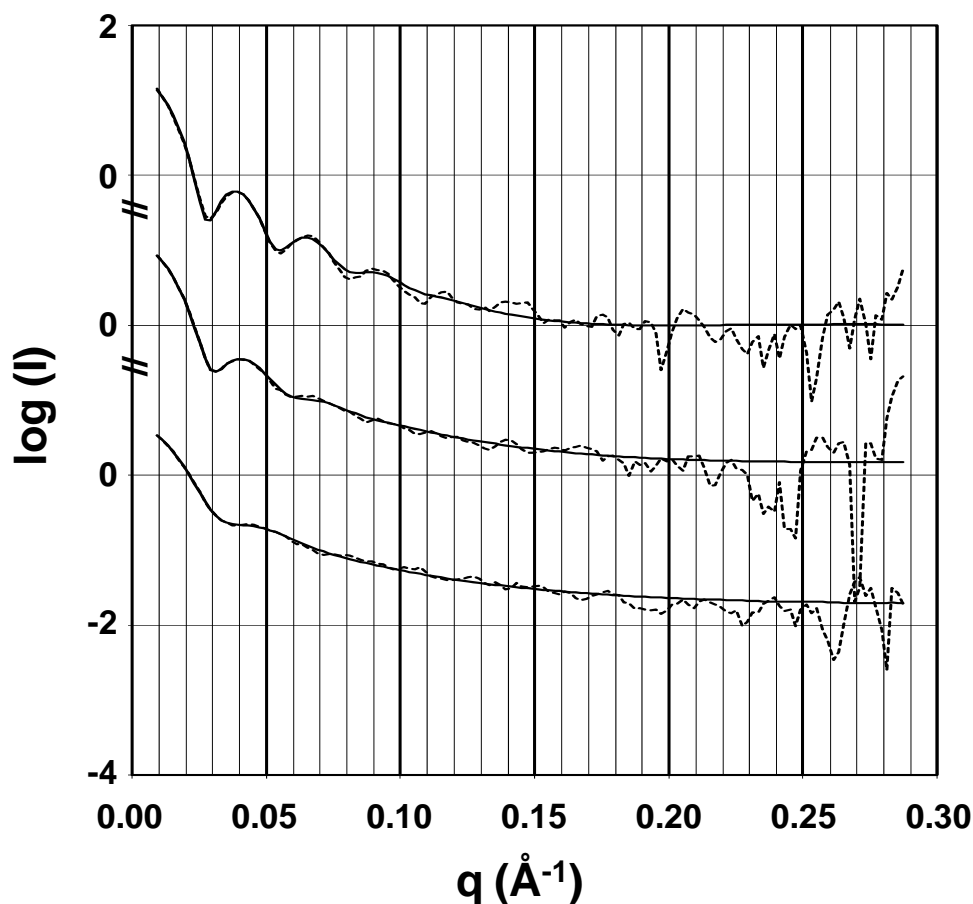
Figure 5.8 *SANS curves (dotted lines) for the CCMV capsid (0.3 M NaCl) in 100% D$_2$O. The solid lines are curves simulated with the parameters in Table 5.3. Top to bottom: capsids at pD 5.0, 6.5, and 7.5.*

The results of the DLS measurements on the CCMV capsid at 0.3 M NaCl are presented in Figure 5.9. At pH 5, the capsid shows a close to perfect homogenous size distribution, in line with the EM data and the SANS results. The hydrodynamic radius determined from DLS (r = 192.1 Å) is somewhat larger than the 130–135 Å value found with SANS for the outer radius of the protein shell. At pH 6.5, a bimodal distribution is found by DLS, with maxima at diameters of about 80 and 300 Å, indicating the coexistence of whole T = 3 capsids and CP dimers. However, because the curve was not corrected for the fact that the DLS intensity is proportional to the size of the object ($I \propto d^3$), it can be concluded that the solution contains mainly CP dimers, whereas the core–shell simulation for the corresponding SANS would indicate the presence of capsids with a diameter of 230 Å. It has to be noted that the polydispersity in the SANS simulation refines to a relatively high value (13.38%). This might be an indication that the SANS sample also in fact has a bimodal distribution. This is difficult to establish since the contribution of the CP dimers to the SANS curve is not as easy to predict as that of a near-spherical capsid particle. At pH 7.5, the DLS pattern showed a bimodal

distribution and again we assume that the solution contains mainly CP dimers (d = 70–90 Å). This agrees with the results obtained by size-exclusion chromatography (SEC), whereas the core–shell simulation of the SANS data suggested the presence of particles with a diameter of 170 Å, albeit with an ever higher polydispersity (23.52%) than the assembly of particles at pH 6.5. Again it is difficult to decide whether the SANS results at this pH should also be interpreted with a bimodal distribution. An indication that the SANS simulations are problematic in this case is the fact that $\rho_1-\rho_2$ refines to a higher absolute value than the one fixed for $\rho_2-\rho_3$, which is physically not realistic.

From the results presented above it can be concluded that the SANS and DLS studies at 0.3 M NaCl are not very conclusive. pH/Ionic strength phase diagrams based on EM studies in the literature[11,47] have shown that an ionic strength of 0.3 M NaCl is at an experimental condition where the T = 3 capsids may be converted to multilamellar capsids at low pH and the dimers to tubes at high pH. Hence at this ionic strength the coexistence of various species is very likely, and this is not a favorable starting point for the interpretation of the SANS experiments. We decided therefore to continue our studies at an ionic strength of 1 M NaCl, where T = 3 capsids and CP dimers are expected to exist at low and high pH, respectively. For the experiments with polystyrene sulfonate (PSS) (see below), a salt concentration of 0.5 M NaCl was chosen in line with the conditions reported in literature.[19,20]
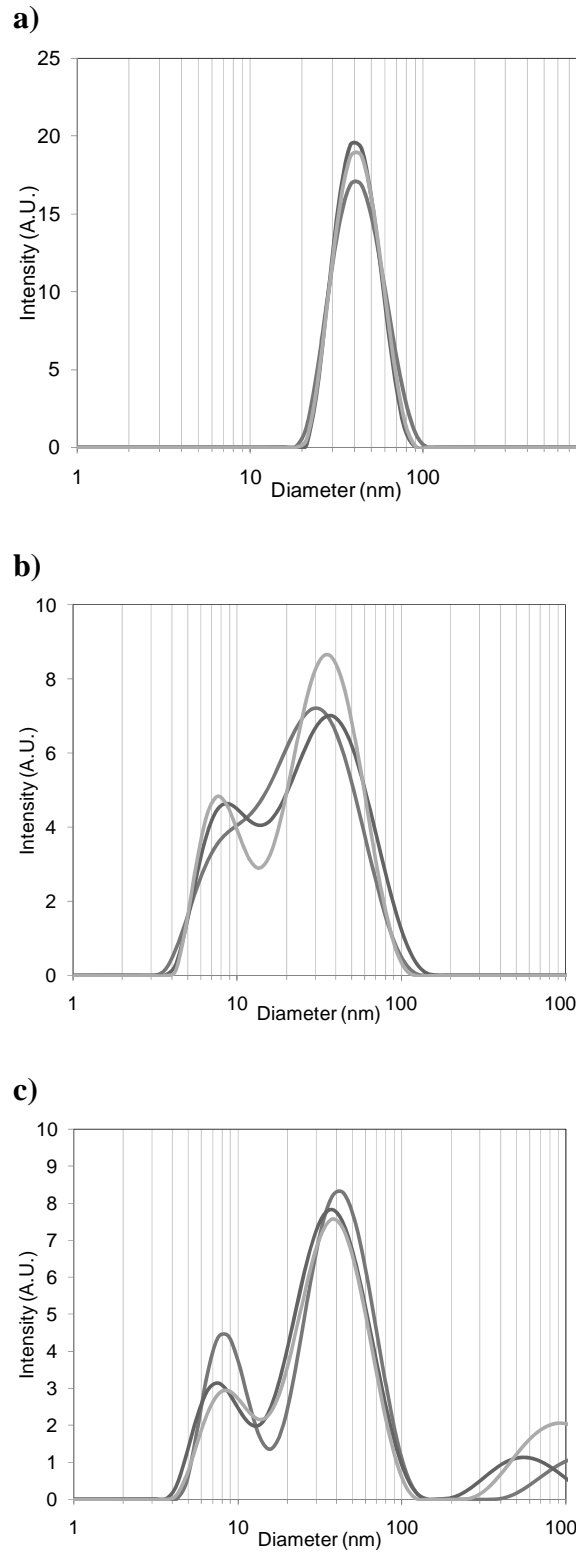
Figure 5.9. *pH dependence of the DLS patterns obtained for the CCMV CP in 100% H$_2$O, 0.3 M NaCl. Buffers: a) pH 5, 50 mM sodium acetate ;b) pH 6.5, 50 mM ammonium acetate, and c) pH 7.5, 50 mM Tris-HCl.*

SANS and DLS studies on the CCMV capsid at high salt concentration

The SANS results for the capsid at high salt concentration, that is, 1 M NaCl, at pH 5.0 and 7.5 are shown in Figure 5.10, with the corresponding parameters derived from the refined simulations in Table 5.4. At pH 5 and 1 M NaCl, the empty capsid is comparable in size to that of the virus, although its outer diameter appears to be significantly reduced. The SANS curve of the empty capsid at pH 7.5 is almost featureless and attempts to simulate it on the basis of a core–shell model gave unreliable results, which is clear from the high polydispersity and the anomaly in the contrast steps. This strongly indicates that the capsid, unlike the virus, does not swell at high pH, but instead dissociates into particles that are too small to be observed by SANS, presumably CP dimers. This is consistent with the observations described in Chapter 4.

Table 5.4 *Simulations (core–shell model;* r, *radius;* ρ, *contrast; PD, polydispersity) of SANS data obtained from experiments on CCMV CP at different pD values (1 M NaCl).*

Experiment[a]	Expected result[b]	$\rho_1 - \rho_2$	r_1 (Å)	Δr (Å)	r_2 (Å)	$\rho_2 - \rho_3$ (fixed)	PD (%)
pD 5	Capsid $d = 280$ Å	3.23	94.75	33.22	127.98	−3.25	8.83
pD 7.5[c]	CP dimers	3.74	54.37	7.42	61.80	−3.25	31.11

a) Buffers: pD 5, 50 mM sodium acetate; pD 7.5, 50 mM Tris-HCl. Capsid buffers contained 1 M NaCl.

b) Expected on the basis of complementary studies in H_2O.

c) Core–shell model not applicable.
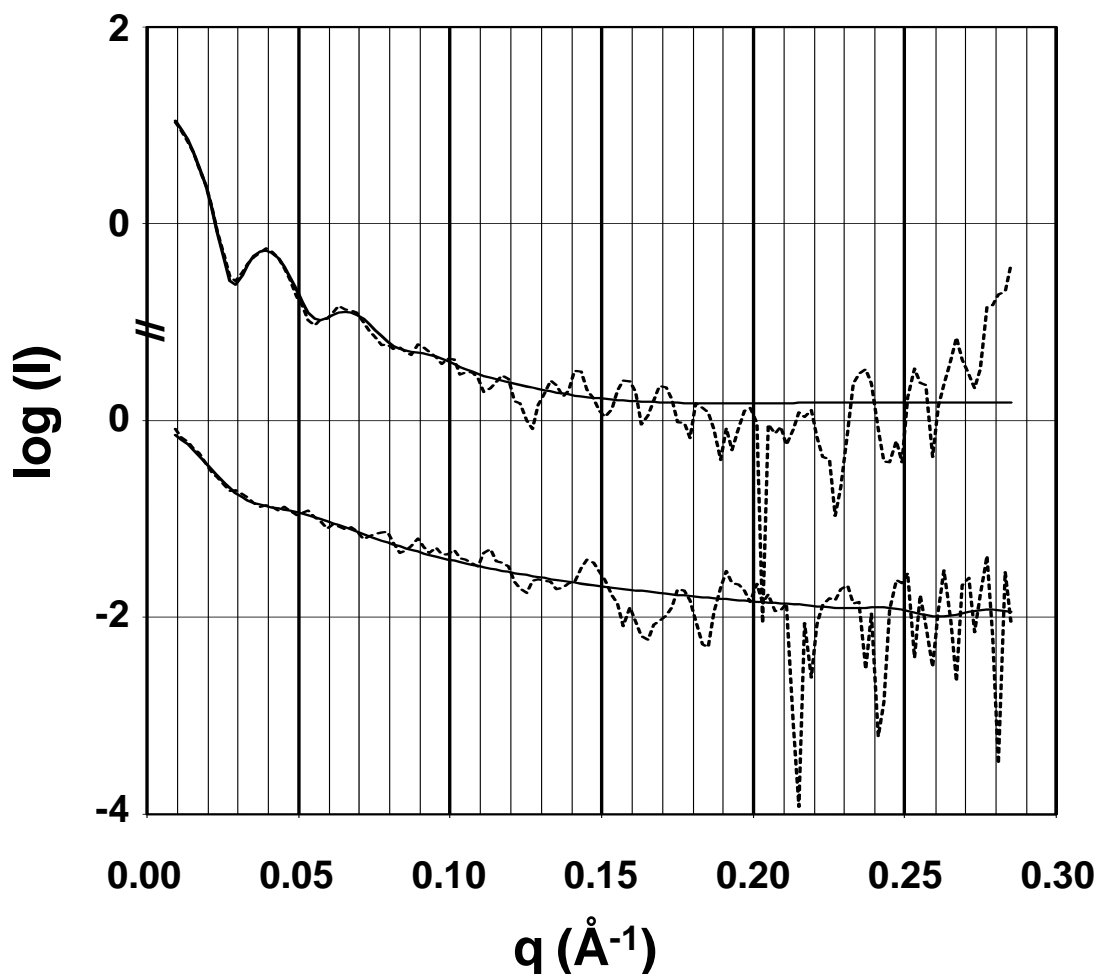
Figure 5.10 *SANS curves (dotted lines) of the CCMV capsid (1 M NaCl) in 100% D$_2$O. The solid lines are simulated curves using the parameters in Table 5.4. Top capsid at pD 5.0, bottom capsid at pD 7.5.*

In order to better compare the SANS results at high and low salt concentrations and to obtain more information it was decided to carry out additional experiments at an NaCl concentration of 0.2 M. The results for the capsid at pH 5 and at the various salt concentrations are compared in Table 5.5 and in Figure 5.11. When the salt concentration is lowered, a decrease in the shell width of the capsid (Δr) is observed and an increase in the outer radius (r_2). This is in agreement with what was observed in Chapter 4 and is shown in Figure 5.3, that is, that high salt concentrations stabilize the formation of monodisperse T = 3 capsids at pH 5, whereas low salt concentrations induce the formation of larger assemblies.

Table 5.5 *Simulations (core–shell model;* r, *radius;* ρ, *contrast; PD, polydispersity) of SANS data obtained from experiments on CCMV CP at pD 5 and different salt concentrations.[a]*

NaCl (M)	$\rho_1-\rho_2$	r_1 (Å)	Δr (Å)	r_2 (Å)	$\rho_2-\rho_3$ (fixed)	PD (%)
1	3.23	94.75	33.22	127.98	−3.25	8.83
0.3	3.07	99.41	31.94	131.35	−3.25	7.54
0.2	2.84	114.00	21.76	135.76	−3.25	13.04

a) Buffer: pH 5, 50 mM sodium acetate.
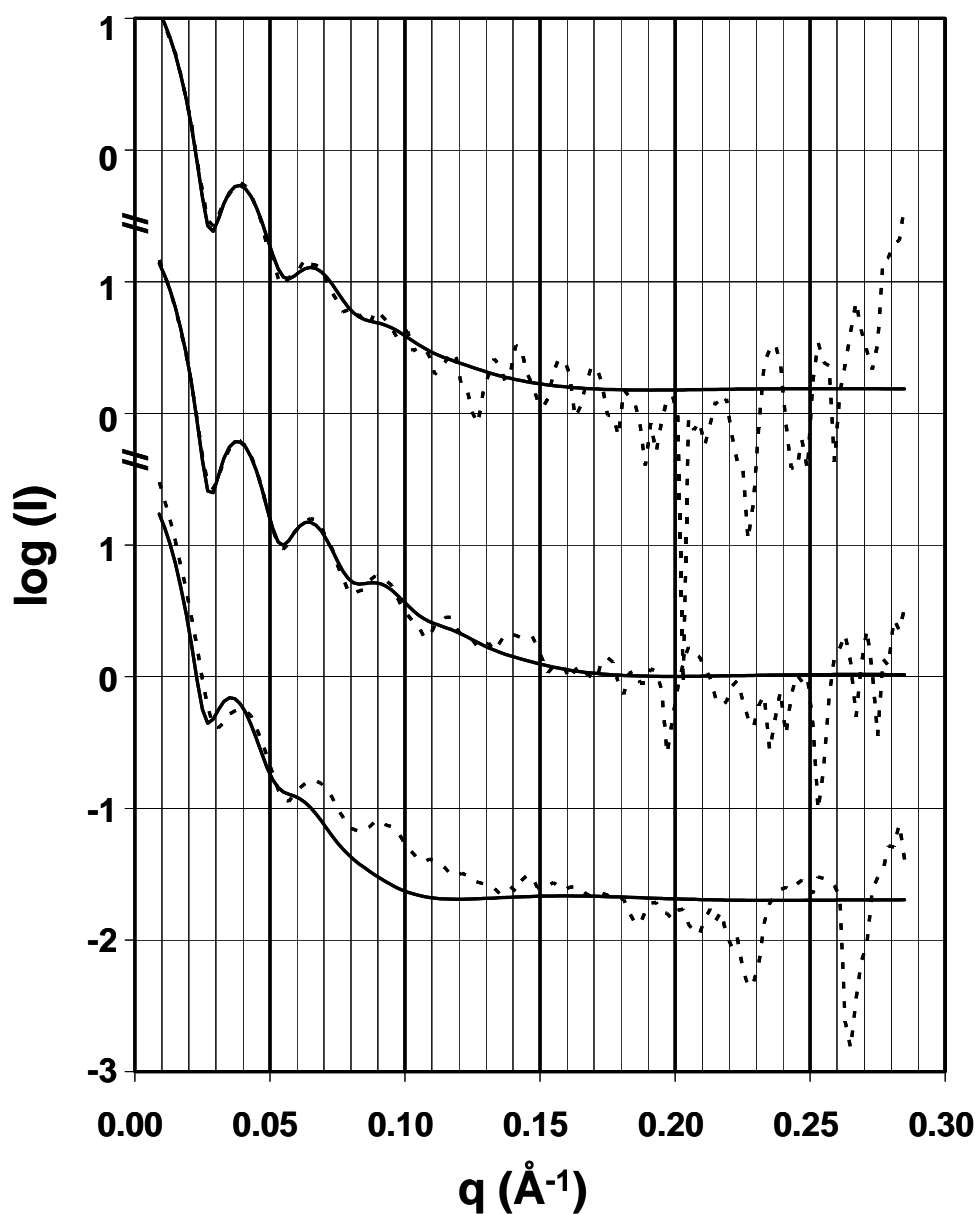
Figure 5.11 *SANS curves (dotted lines) of the CCMV capsid in 100% D_2O, pD 5, at different salt concentrations. The solid lines are curves simulated with the parameters in Table 5.5. Top to bottom: 1, 0.3, 0.2 M NaCl.*

Since the SANS data for the sample containing 0.2 M NaCl could not be fitted very well, we also performed DLS experiments at this ionic strength. In Figure 5.12 the DLS results for the various salt concentrations are compared. The DLS data shows the same trend as the SANS results, except that the capsid diameter shows a clearer increase in size, namely, from 289.9 to 384.2, and further to 490.9 Å, going from 1 to 0.3 and then to 0.2 M NaCl. Unexpectedly, in the DLS analysis all samples seem to have a highly monodisperse size distribution, opposite to what was observed by TEM (Figure 5.3). In the latter case, at low salt concentrations a mixture of species with different shapes and dimensions was observed. A possible explanation is that low salt concentrations weaken the interactions between the protein subunits, inducing the formation of larger capsids with thinner shells that are more susceptible to disassembly. During the sample preparation for TEM imaging, this might result in damage and the generation of a variety of species. DLS analysis of CCMV CP at pH 5 containing an even lower concentration of salt (0.1 M NaCl) did show a highly polydisperse mixture of species of different sizes that were not stable over time. After several minutes a clear scattering curve could no longer be observed and a white precipitate was formed. This points to the formation of large assemblies which, as we checked, were undetectable by FPLC, since their size was beyond the exclusion limit of the FPLC column (Superose 6).
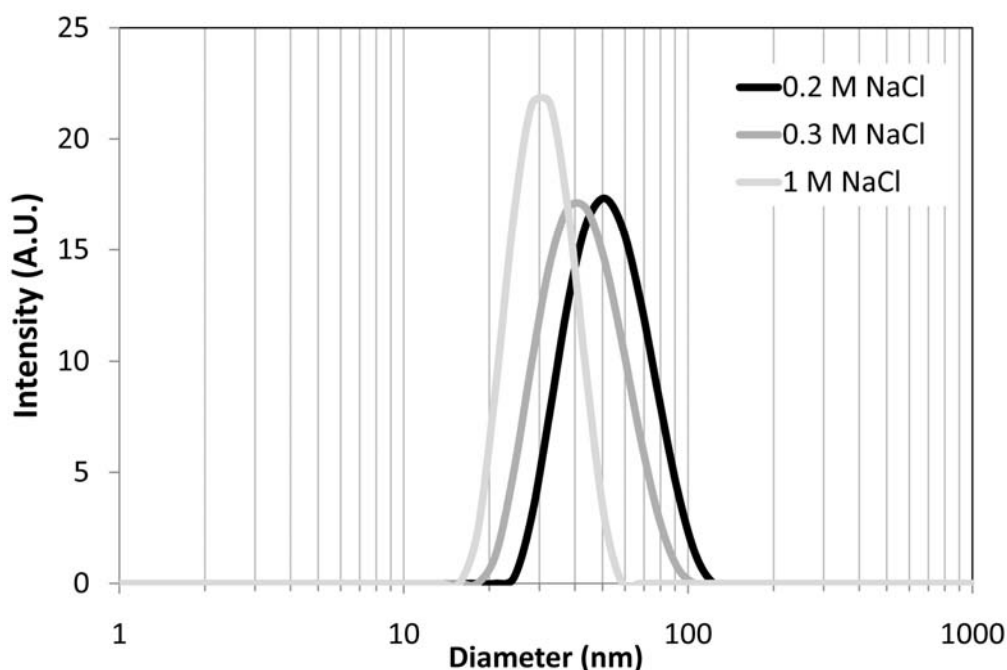
Figure 5.12 *DLS curves of CCMV CP at pH 5 and at different salt concentrations.*
a) 0.2 M NaCl, b) 0.3 M NaCl, and c) 1 M NaCl.

### SANS core–2-shell simulations for CCMV and CCMV capsid

The core–shell model used for the interpretation of the SANS experiments so far has led to satisfactory simulations for the virus and the capsid under various circumstances, and has given interesting information on the size of the shell, which is dominated by the capsid protein. As for the RNA component of the virus, it has given only indirect information, derived from the differences in the thickness and volume of the shell, and the discrepancy in the inner and outer contrast steps. It was considered to be of interest to see if the RNA structure could be defined better by simulating the SANS data with a core–2-shell model, consisting of a core, a weakly scattering inner shell (presumably containing dilute RNA and/or protein), and a more strongly scattering outer shell consisting of protein (Scheme 5.2b).

In Figure 5.13, the experimental traces and the core–2-shell simulations of the SANS data for CCMV and the CCMV capsid are compiled together with the results obtained for capsids with encapsulated PSS (see next section). The corresponding parameters are given in Table 5.6, and the corresponding radial scattering length density profiles for CCMV, CCMV capsid, and one of the CCMV capsid-PSS samples in Figure 5.14.

For the virus (Figure 5.13, Figure 5.14, and Table 5.6), the outcome of the core–2-shell simulation approach is a weakly ($\rho_{1,2} = -0.59$) scattering inner shell (40–100 Å) and an outer protein shell (100–130 Å). The latter has an outer diameter that is virtually identical to that found in the core–shell simulation (Table 5.2), but the inner diameter is approximately 5 Å larger. The weakly scattering inner shell can be interpreted as being the result of a dilute solution of RNA bound to the inner surface of the capsid protein.

Table 5.6 *Simulations (core–2-shell model; r, radius; ρ, contrast; Δ, thickness; PD, polydispersity) of SANS data of the experiments shown in Figure 5.13.*

Sample	r_1	$\rho_{1,2}$	Δ_{inner}	r_2	$\rho_{2,3}$	Δ_{outer}	r_3	$\rho_{3,4}$	PD
V 5	40.53	−0.59	59.80	100.33	−2.66	29.83	130.16	3.25	6.28
V 7.5	44.96	−0.58	62.16	107.12	−2.67	28.40	135.52	3.25	7.10
C 5	84.25	−0.71	15.98	100.23	−2.54	26.32	126.55	3.25	9.04
P 10	49.85	−5.20	21.82	71.67	+1.95	11.53	83.20	3.25	15.72
P 2	51.36	−4.74	15.46	66.82	+1.49	10.14	76.96	3.25	17.50
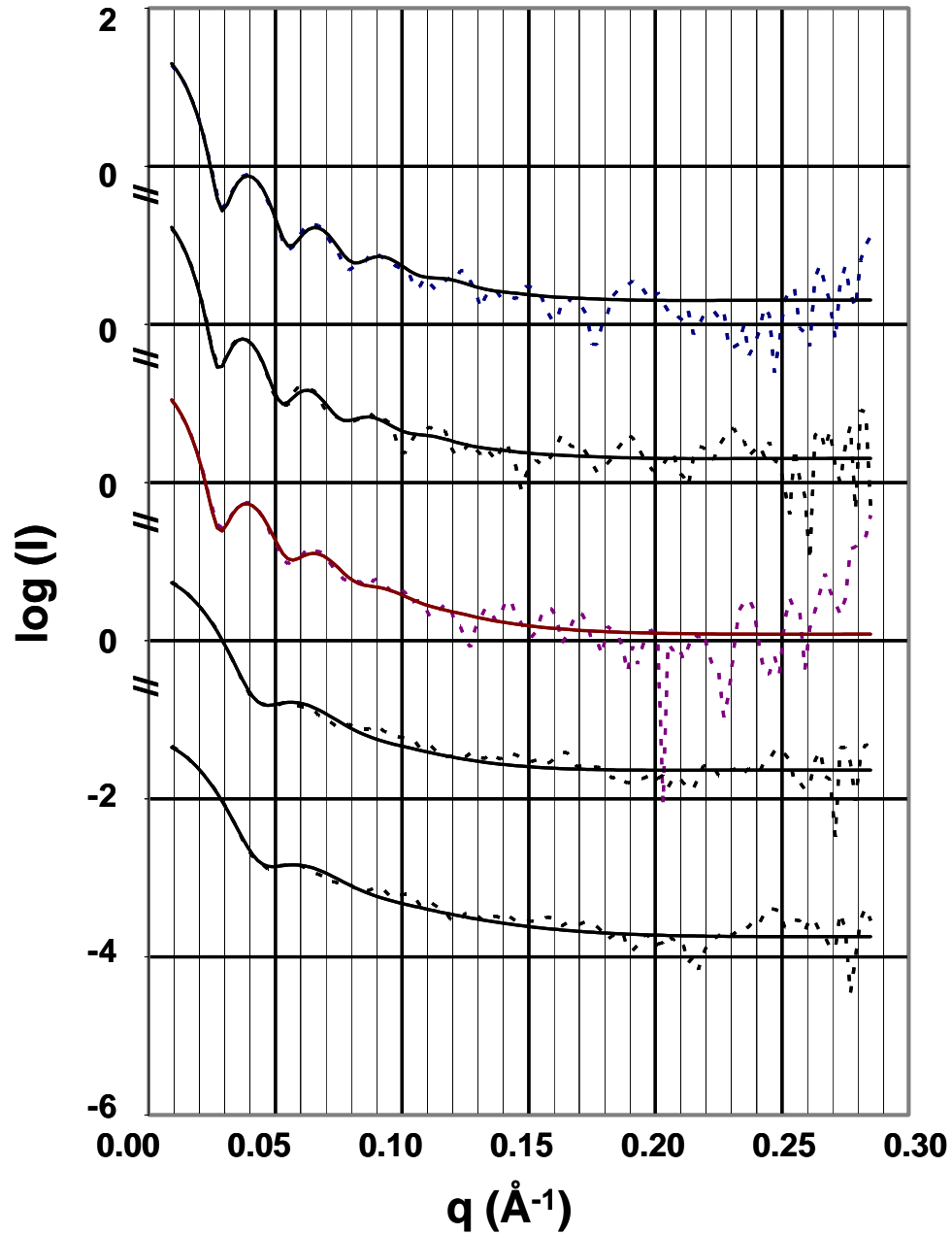
Figure 5.13 SANS curves (dotted lines) of various CCMV and CCMV capsid samples in
100% D₂O and pD 5. The solid lines are simulated curves using the parameters in
Table 5.6. Top to bottom: V 5, V 7.5, C 5, P 10, and P 2.
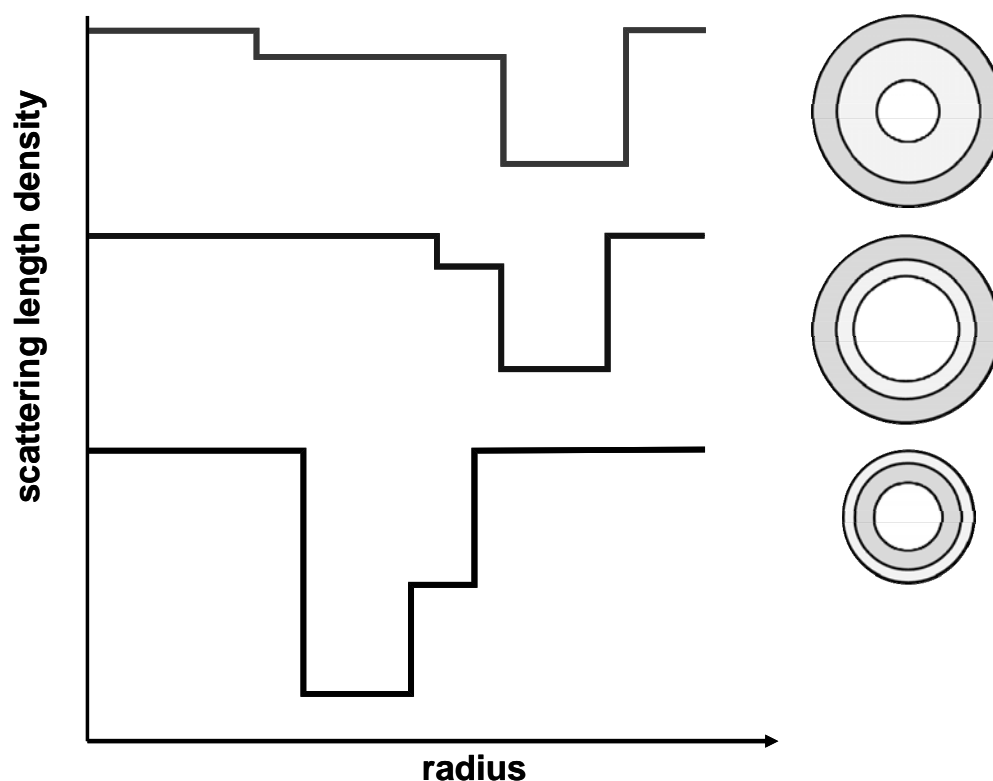
Figure 5.14. *Scattering length density profiles derived from the core–2-shell simulations carried out on SANS data obtained for (top) CCMV, (middle) CCMV capsid, and (bottom) CCMV capsid loaded with PSS.*

Analysis of the pH-induced swelling of the virus by the core–2-shell model (compare V5 and V7.5 in Figure 5.13 and Table 5.6) reveals that the aqueous core and the wet RNA shell increase by approximately 4 and 2 Å in diameter and thickness, respectively. The thickness of the protein shell decreases slightly but its volume still increases somewhat because of the increase in diameter. Presumably, the basic N-terminal part of the capsid protein, the electron density of which is not well defined in the crystal structure,[2] plays a role in the binding of the RNA. Interestingly, simulation of the CCMV capsid with the core–2-shell model (Figure 5.13, Figure 5.14, and Table 5.6) reveals the presence of a thin (10–15 Å) weakly scattering inner shell, which could be protein. The protein nature of this inner shell is corroborated by the finding that the core–2-shell analysis of the empty capsid (0.3 M NaCl) gives the same outcome for measurements performed at 68 (protein contrast selected) and 100% D_2O (Figure 5.15 and Table 5.7).

Table 5.7 *Simulations (core–2-shell model; r, radius; ρ, contrast; Δ, thickness; PD, polydispersity) of SANS data of the experiments shown in Figure 5.15.*

Experiment	r_1	$\rho_{1,2}$	Δ_{inner}	r_2	$\rho_{2,3}$	Δ_{outer}	r_3	$\rho_{3,4}$	PD
pD 5 0.3 M NaCl	95.28	−1.42	9.38	104.66	−1.66	26.28	130.94	3.25	7.56
pD 5 68%D_2O, 0.3 M NaCl	92.12	−0.57	9.07	101.19	−0.74	28.87	130.06	1.33	10.13
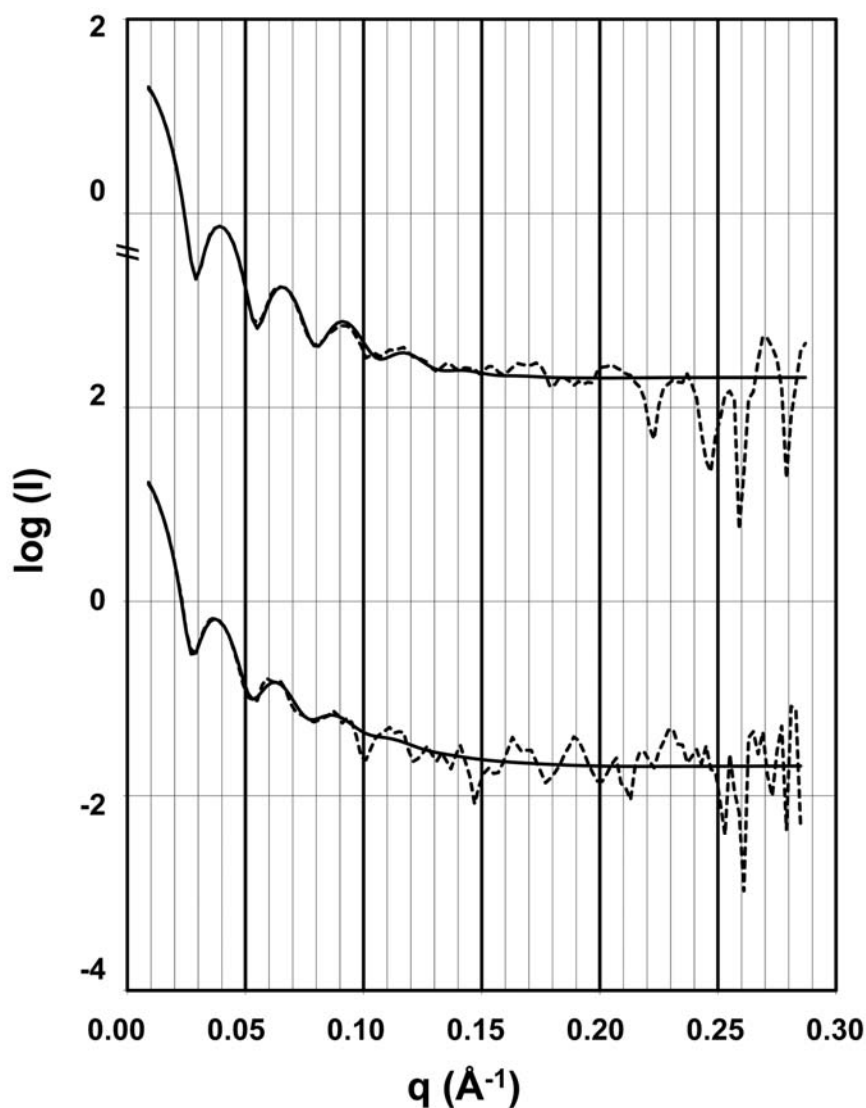
Figure 5.15. *SANS curves (dotted lines) of CCMV and the CCMV capsid at pD 5.0. The solid lines are simulated with the parameters shown in Table 5.7. Top CCMV capsid, 100% D_2O, 0.3 M NaCl; bottom CCMV capsid, 68% D_2O, 0.3 M NaCl.*

107

SANS studies on CCMV capsid loaded with PSS by using a core–2-shell model

In our group, Sikkema *et al.* have demonstrated that the self-assembling properties of CCMV CP lacking part of its N terminus can be employed to create a monodisperse 160 Å T = 1 icosahedral nanoparticle upon encapsulation of a disperse polymer at pH 7.5.[19]

For the analysis of the SANS data of the capsid with encapsulated PSS,[19] it turned out that a core–2-shell model approach was vital; these data, therefore, were simulated with a core–2-shell model where the inner shell was a strongly scattering polymer shell and the outer shell a comparatively weakly scattering protein shell. In the initial simulations of this type, the contrast steps were restrained so that $\rho_1 - \rho_2$ and $\rho_2 - \rho_3$ steps together were equal to the $\rho_3 - \rho_4$ step (which is the protein/D_2O contrast step, Scheme 5.2), and, in the case of the capsid–PSS system, the $\rho_2 - \rho_3$ and $\rho_3 - \rho_4$ steps together were equal to the $\rho_1 - \rho_2$ step. This situation was kept in the final simulations, in which such restraints were removed, indicating that the core–2-shell simulations adequately describe a situation where the scattering length density of the core (ρ_1) is equal to that of the surrounding solvent (ρ_4). In Figure 5.13, the experimental traces and the core–2-shell simulations of the SANS data for capsids with encapsulated PSS are shown. The corresponding parameters are given in Table 5.6, and the corresponding radial scattering length density profile of one of the CCMV capsid-PSS samples in Figure 5.14.

The SANS experiments show that the incorporation of the PSS in the CCMV capsid leads to much smaller and much more polydisperse particles than is the case for the virus and capsid (Figure 5.14); the outer radii calculated for the two samples (P10 and P2) are in the 75–85 Å range and the polydispersities range from 15 to 18%. This is in line with the earlier conclusion from EM and DLS that the incorporation of PSS presumably leads to the formation of T = 1 rather than T = 3 capsids.[19] The SANS data allow us to define the polymer and protein shells more precisely. There is an inner solvent core with a radius of around 50 Å. This core is surrounded by a polymer shell of 15 Å in the case of the PSS of molecular weight M_r 2000 (P2), and 22 Å for the PSS of molecular weight M_r 10,000 (P10), and a protein shell of 10 Å in both cases. Interestingly, the PSS appears to have a much stronger effect on the capsid structure than RNA; a more condensed structure than the original virus appears, which, however, still has a well-defined but thinner shell of protein with a smaller outer diameter.

5.3 Conclusion

SANS has allowed us to study the CCMV structure in solution under various pH and salt concentration conditions. The optimum contrast was achieved in D_2O buffers, and

the protein component could be defined as a separate shell in the core–shell simulations (outer radius 130 Å). Only indirect information could be obtained on the way the RNA molecules are arranged in the virus. There are parts of RNA intercalated with the protein shell and even parts protruding from the protein shell to the outside of the virus, and there is dilute "wet" RNA associated with the inside of the protein shell. Complementary DLS studies were performed in cases for which a bimodal size distribution was obtained. The expected swelling of the virus upon changing the pH from pH 5 to 7.5 was detectable, but not as strong as the 10% swelling derived from DLS, EM, and X-ray crystallography. The empty capsid was of a size comparable to that of the virus (marginally smaller), and was found to dissociate into dimers upon increasing the pH. Incorporation of PSS in the CCMV capsid led to the formation of smaller capsids (outer radius 80 Å) corresponding to T = 1 geometry, with a solvent core, a polymer inner shell, and a protein outer shell.

5.4 Experimental Section

Materials
Sodium acetate trihydrate (>99%) and uranyl acetate dihydrate (≥98%) were purchased from Fluka. Ethylenediaminetetraacetic acid (EDTA) disodium salt dihydrate (>99%), tris(hydroxymethyl)aminomethane (Tris) (>99%), calcium chloride dihydrate (>99%), sodium chloride (99.5%), and sodium azide (99%) were purchased from Acros. Phenylmethanesulfonyl fluoride (PMSF) (≥98.5%) and dithiothreitol (DTT) (99%) were obtained from Sigma-Aldrich.

Instrumentation
UV/Vis spectroscopy was performed on a Varian Cary 50 spectrophotometer at room temperature using a 1 cm quartz cuvette (Hellma, light path: 1 cm). The reference spectrum of the corresponding buffers were subtracted from all UV/Vis spectra.

Fast protein liquid chromatography (FPLC) was performed on an Ettan Akta LC system equipped with a Superose 6 PC 3.2/30 column from Amersham Biosciences (flow rate 40 μL min^{-1}). Injections of 20 mL aliquots of the samples on the FPLC column at room temperature were monitored by UV/Vis detection at 280 and 260 nm.

Transmission electron microscopy (TEM) micrographs were recorded on a JEOL JEM-1010 instrument. Samples were prepared by drying a drop of the solution on a Formvar carbon-coated grid, which had been previously made hydrophilic by glow discharge. The excess buffer on the grid was blotted away after 1 min with filter paper. Negative staining of the samples was achieved by applying a drop of uranyl acetate solution

(0.2% in MilliQ) onto the grid and blotting the excess liquid away after 15 s with filter paper. The samples were left to dry in air for 30 min before analysis.

Dialysis was performed by using dialysis tubing (Spectra/Por 4, MWCO: 12–14 kD, Flat width: 25 mm) purchased from Spectrum Laboratories, and D-tube dialyzer (MWCO: 12–14 kD or 6–8 kDa, volume: 1000–3000 μL) from Novagen.

Dynamic light scattering (DLS) measurements were carried out on native CCMV or coat-protein solutions at different pH and/or salt concentrations. The concentration ranged from 0.16 to 1.6 mg mL^{-1} for the CCMV samples and from 0.13 to 1.3 mg mL^{-1} for the CP samples. The acquisition was performed at 15 °C at an angle of 173° (backscattering mode) with a Zetasizer Nano S from Malvern using a 4mW He-Ne laser at 633 nm. Analysis of the data was performed using the Nano DTS v.5.10 software. Reported values and graphs have been selected from the experiments in an equilibrium state, that is, when no further change was observed after one day.

SANS measurements were performed using a 12 mm diameter neutron beam on the LOQ beam line at the ISIS pulsed neutron source (CCLRC Rutherford-Appleton Laboratory, Didcot, UK). LOQ uses pulses of neutrons of wavelengths between 2.2 Å and 10 Å which are separated by time-of-flight and detected by a 64×64 cm, two-dimensional detector at 4.1 m from the sample. Wavelength-dependent corrections were made to allow for the incident spectrum, detector efficiencies, and measured sample transmissions to create a composite SANS pattern (see reference [50] for a more detailed description). This gives a scattering vector $q = (4\pi/\lambda) \sin (\theta/2)$ in the range of $q = 0.010-0.028$ Å^{-1}. Comparisons with scattering from a partially deuterated polystyrene standard allowed absolute scattering cross sections to be determined with an error of $\pm 2.0\%$. Quartz cuvettes with a light path of 2 mm (type 110-QS, Hellma) were used to perform most SANS measurements, except the the swelling studies, in which case banjo cells (disk shape cells, 12 mm) were used. Cuvettes of 1 mm light path were used for samples containing H$_2$O.

SANS data analysis.

The SANS scattering curves were simulated with crude models based on a core–shell or a core with 2 shells, as described in the text and Scheme 5.2, using the SANS simulation programme FISH.[48] The parameters were refined to give the best agreement with the experimental traces, to extract the optimum values for parameters such as the radius of the particles and the size of the steps in the contrast in the scattering length densities.

Isolation of CCMV and CCMV CP

The purification of the CCMV and the CCMV CP isolation was performed as described in Chapters 3 and 4. The approximate concentrations of the virus and the capsid in the initials stock solutions were $c = 10–15$ mg mL^{-1} and $c = 4–8$ mg mL^{-1}, respectively. Two different sets of SANS experiments were performed by using two different virus

and capsid batches. The concentrations were intended to be as similar as possible within the range described above.

Preparation of CCMV and CCMV capsid samples under different pH and ionic strength conditions

To prepare the SANS samples, different aliquots of CCMV and CCMV capsid stock solutions ($V \approx 500 \, \mu L$) were dialyzed against the corresponding buffer in H_2O (see buffer conditions in Table 5.8). Part of these solutions was kept for analysis of the samples in H_2O and the rest was dialyzed against the same buffer prepared in D_2O. In all cases, the samples were dialyzed against a minimum of two changes of buffer ($V \approx 400 \, mL$; 3 h per change). The background solutions were taken from the last dialysis buffer after the last change, to have exactly the same H_2O/D_2O ratio in the sample and in the background solution. For those buffers containing D_2O, the pH was corrected and corresponded to $pD = pH + 0.3314 \, n + 0.0766 \, n^2$, in which n is the volume fraction of D_2O and pH is the pH meter reading.[35] Buffers and samples were stored at 4 °C and the dialyses were performed in a cold room at 4 °C.

Table 5.8 *Buffer conditions used for the different virus and capsid samples.*

Samples	Buffer Conditions[a]		
Virus pH 5	50 mM sodium acetate		
Virus pH 7.5	50 mM Tris-HCl		
Capsid pH 5	50 mM sodium acetate 200 mM NaCl	50 mM sodium acetate 300 mM NaCl	50 mM sodium acetate 1 M NaCl
Capsid pH 6.5		50 mM ammonium actetate 300 mM NaCl	
Capsid pH 7.5		50 mM Tris-HCl 300 mM NaCl	50 mM Tris-HCl 1 M NaCl

a) All buffers used in the assembly studies additionally contained 1 mM EDTA, 10 mM $CaCl_2$, and 0.2 mM PMSF.

Preparation of PSS-containing particles

CCMV capsid samples with encapsulated PSS were prepared and characterized as decribed previously.[19] For the SANS experiments, capsid protein and PSS were dissolved in 100 % D_2O buffered at pD 7.5 containing 0.5 M NaCl and mixed to a final concentrations of 3.6×10^{-4} and 2.7×10^{-4} M for protein and polymer, respectively.

5.5 References and Notes

[1]   A. C. Steven, P. R. Smith, R. W. Horne, *J. Ultrastruct. Res.* **1978**, *64*, 63.

[2]   J. A. Speir, S. Munshi, G. J. Wang, T. S. Baker, J. E. Johnson, *Structure* **1995**, *3*, 63.

[3]   B. J. M. Verduin, *FEBS Lett.* **1974**, *45*, 50.

[4]   J. B. Bancroft, E. Hiebert, *Virology* **1967**, *32*, 354.

[5]   J. B. Bancroft, G. J. Hills, R. Markham, *Virology* **1967**, *31*, 354.

[6]   E. Hiebert, J. B. Bancroft, C. E. Bracker, *Virology* **1968**, *34*, 492.

[7]   E. Hiebert, J. B. Bancroft, *Virology* **1969**, *39*, 296.

[8]   J. M. Fox, G. Wang, J. A. Speir, N. H. Olson, J. E. Johnson, T. S. Baker, M. J. Young, *Virology* **1998**, *244*, 212.

[9]   J. B. Bancroft, G. W. Wagner, C. E. Bracker, *Virology* **1968**, *36*, 146.

[10]   J. T. Finch, J. B. Bancroft, *Nature* **1968**, *220*, 815.

[11]   R. F. Bruinsma, W. M. Gelbart, D. Reguera, J. Rudnick, R. Zandi, *Phys. Rev. Lett.* **2003**, *90*, 248101.

[12]   J. Tang, J. M. Johnson, K. A. Dryden, M. J. Young, A. Zlotnick, J. E. Johnson, *J. Struct. Biol.* **2006**, *154*, 59.

[13]   M. Young, D. Willits, M. Uchida, T. Douglas, *Annu. Rev. Phytopathol.* **2008**, *46*, 361.

[14]   T. Douglas, M. Young, *Adv. Mater.* **1999**, *11*, 679.

[15]   T. Douglas, E. Strable, D. Willits, A. Aitouchen, M. Libera, M. Young, *Adv. Mater.* **2002**, *14*, 415.

[16]   A. de la Escosura, M. Verwegen, F. D. Sikkema, M. Comellas-Aragones, A. Kirilyuk, T. Rasing, R. J. M. Nolte, J. J. L. M. Cornelissen, *Chem. Commun.* **2008**, 1542.

[17]   M. Comellas-Aragones, H. Engelkamp, V. I. Claessen, N. A. J. M. Sommerdijk, A. E. Rowan, P. C. M. Christianen, J. C. Maan, B. J. M. Verduin, J. J. L. M. Cornelissen, R. J. M. Nolte, *Nat. Nanotechnol.* **2007**, *2*, 635.

[18]   T. Douglas, M. Young, *Nature* **1998**, *393*, 152.

[19]   F. D. Sikkema, M. Comellas-Aragones, R. G. Fokkink, B. J. Verduin, J. J. L. M. Cornelissen, R. J. M. Nolte, *Org. Biomol. Chem.* **2007**, *5*, 54.

[20]   Y. F. Hu, R. Zandi, A. Anavitarte, C. M. Knobler, W. M. Gelbart, *Biophys. J.* **2008**, *94*, 1428.

[21]   C. Uetrecht, C. Versluis, N. R. Watts, W. H. Roos, G. J. Wuite, P. T. Wingfield, A. C. Steven, A. J. Heck, *Proc. Natl. Acad. Sci. U.S.A.* **2008**, *105*, 9216.

[22] C. Uetrecht, C. Versluis, N. R. Watts, P. T. Wingfield, A. C. Steven, A. J. Heck, *Angew. Chem. Int. Ed.* **2008**, *47*, 6247.

[23] J. P. Michel, I. L. Ivanovska, M. M. Gibbons, W. S. Klug, C. M. Knobler, G. J. Wuite, C. F. Schmidt, *Proc. Natl. Acad. Sci. U.S.A.* **2006**, *103*, 6184.

[24] W. S. Klug, R. F. Bruinsma, J. P. Michel, C. M. Knobler, I. L. Ivanovska, C. F. Schmidt, G. J. Wuite, *Phys. Rev. Lett.* **2006**, *97*, 228101.

[25] J. Witz, F. Brown, *Arch. Virol.* **2001**, *146*, 2263.

[26] H. H. J. Bink, C. W. A. Pleij, *Arch. Virol.* **2002**, *147*, 2261.

[27] P. Dobos, R. Hallett, D. T. Kells, O. Sorensen, D. Rowe, *J. Virol.* **1977**, *22*, 150.

[28] Y. Panyukov, I. Yudin, V. Drachev, E. Dobrov, B. Kurganov, *Biophys. Chem.* **2007**, *127*, 9.

[29] S. Krueger, *Physica B* **1998**, *241-243*, 1131.

[30] B. Jacrot, *Rep. Prog. Phys.* **1976**, *39*, 911.

[31] B. Jacrot, C. Chauvin, J. Witz, *Nature* **1977**, *266*, 417.

[32] C. Chauvin, B. Jacrot, J. Witz, *Virology* **1977**, *83*, 479.

[33] C. Chauvin, B. Witz, B. Jacrot, *J. Mol. Biol.* **1978**, *124*.

[34] S. Cusack, A. Miller, *J. Mol. Biol.* **1981**, *145*, 525.

[35] J. Krüse, P. A. Timmins, J. Witz, *Virology* **1982**, *119*.

[36] C. R. Wobbe, S. Mitra, V. Ramakrishnan, *Biochem.* **1984**, *23*, 6565

[37] S. Cusack, R. W. H. Ruigrok, P. C. J. Krygsman, J. E. Mellema, *J. Mol. Biol.* **1985**, *186*, 565.

[38] J. Krüse, P. Timmins, J.Witz, *Virology* **1987**, *159*, 166.

[39] D. A. Kuzmanovic, I. Elashvili, C. Wick, C. O'Connell, S. Kreuger, *Structure* **2003**, *11*, 1339.

[40] P. Zipper, H. Durchschlag, *J. Appl. Crystallogr.* **2007**, *40*, S153.

[41] M. Cuillel, C. Berthet-Colominas, P. A. Timmins, M. Zulauf, *Eur. Biophys. J.* **1987**, *15*, 169.

[42] M. Leimkühler, A. Goldbeck, M. D. Lechner, J. Witz, *J. Mol. Biol.* **2000**, *296*, 1295.

[43] C. Chauvin, P. Pfeiffer, J. Witz, B. Jacrot, *Virology* **1978**, *88*, 138.

[44] S. M. King, *Small-angle Neutron Scattering in: Modern Techniques for polymer characterisation*, John Wiley & Sons Ltd., Chichester, UK, **1999**.

[45] J. K. Blasie, P. Timmins, *MRS Bulletin* **1999**, 40.

[46] K. E. v. Holde, W. C. Johnson, P. S. Ho, *Principles of Physical Biochemistry*, Prentice Hall: Upper Saddle River, New Jersey **1998**.

[47] K. W. Adolph, P. J. Butler, *J. Mol. Biol.* **1974**, *88*, 327.

[48] R. K. Heenan, *Fish Data Analysis Program: Report RAL-89-129*, Rutherford Appleton Laboratory: Didcot, Oxfordshire, **1989**.

[49] J. Krüse, K. M. Krüse, J. Witz, C. Chauvin, B. Jacrot, A. Tardieu, *J. Mol. Biol.* **1982**, *162*, 393.

[50] R. K. Heenan, J. Penford, S. M. King, *J. Appl. Cryst.* **1997**, *30*, 1140.

CHAPTER 6

Encapsulation of Proteins in the CCMV Capsid

6.1 Introduction

Protein cages

Nature has developed a variety of self-assembled protein cages that can act as spatially well-defined host systems. Examples include viral capsids, ferritins, heat shock proteins, and the recently described "encapsulins".[1,2] Protein-cage architectures provide three surfaces (interior, exterior, and subunit interfaces) to which one can impart function by design. Atomic-resolution structural information, in conjunction with genetic and chemical modification, allows the rational incorporation of small molecules, for example, peptides, or metallic particles at precise locations in the protein cage and on its surface. In recent years, protein cages have increasingly been investigated and used in the laboratory as scaffolds for metallization and the growth of minerals, resulting in metalized or mineralized nano-objects. They have also been used as nanocages for the entrapment of compounds and as nanoreactors.[1,3-5]

In 1991 Mann and co-workers showed, for the first time, that protein cages have the potential to act as a constrained reaction environment in the synthesis of inorganic materials of nanometer dimensions.[6,7] They used the mineralization properties of ferritin to produce metal particles from metal ions other than the natural hydrates of iron(III) oxide. Since then, ferritin has been applied as a size-constrained reaction vessel for the production of different types of metal nanoparticles,[8-10] and even to produce ferromagnetic nanocrystals leading to the construction of a magnetic protein.[11-13] A similar approach was followed to prepare a magnetic ferritin that was further engineered to act as a cell-specific targeting device, opening the possibility of employing protein cages in the field of biomedicine.[14] Furthermore, the metal–nanocluster formed in the ferritin protein was shown to work as a catalyst in different types of reactions.[15,16] For example, a Pd–nanocluster was encapsulated in the apoferritin cavity by *in situ* reduction of Pd^{II} ions. Subsequently, the catalytic activity of this complex in the hydrogenation of olefins was evaluated and it was found that the catalytic system is capable discriminating between substrates via the pores in the protein mantle (Scheme 6.1).[17]
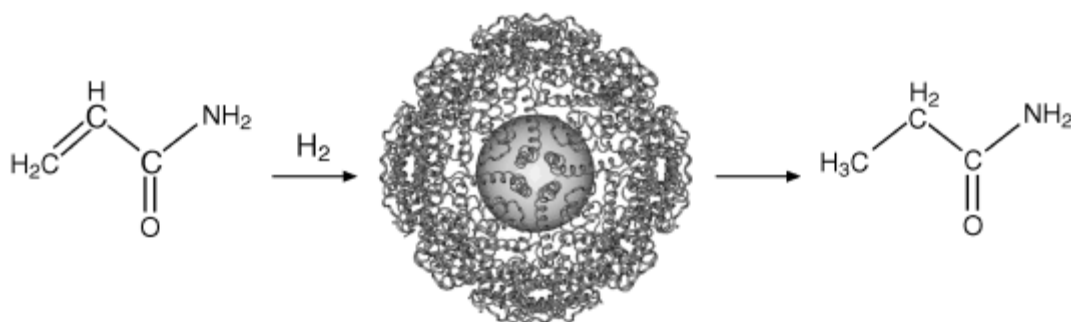
Scheme 6.1 *Size-selective catalytic hydrogenation of olefins by the Pd–apoferritin hybrid.[17]*

The investigations on ferritin paved the way for the use of other proteins and virus capsids as size- and shape-constrained reaction vessels. The hollow self-assembled protein structure of lumazine synthase, a bacterial enzyme, and the small heat shock protein cage from *Methanococcus jannaschii* (MjHsp) were also shown to be a suitable mineralization template for the formation of iron oxide particles,[18,19] which in some cases have also been used for catalytic reactions.[20] Furthermore, a genetically modified MjHsp protein cage was shown to have the ability to house and selectively release the antitumor agent doxorubicin.[21]

In materials science, viruses are currently increasingly applied as scaffolds for chemical synthesis. Molecules of interest are connected to the viral surface by means of bioconjugation chemistry or molecular-biology approaches. In this way, nanoparticles of viral origin can be fabricated that show a defined number and arrangement of functional molecules on their surface.[22-24] Some viruses can be conveniently disassembled and reassembled by changing the environmental conditions, such as the pH of the medium. This feature provides the unique possibility to use viruses for encapsulation, which is appropriate for the design of size-constrained nanocontainers and nanoreactors. One of the most explored virus with these characteristics is CCMV (which is discussed separately below), however, other viruses have been used as well. For example, the MS2 bacteriophage, which has the possibility of forming genome-free, empty capsid shells, has been chemically modified on both the outer and inner surface.[25,26] An alternative approach for the encapsulation of nanoparticles in protein cages has been to direct the assembly of viral capsid subunits around a preformed nanoparticle. For example, the interaction between oligonucleotides attached to gold nanoparticles and the positive N terminus of coat protein subunits has been used to entrap these particles within the capsids of the red clover necrotic mosaic virus (RCNMV),[27] the brome mosaic virus (BMV),[28,29] and the animal virus alphavirus.[30] By using similar approaches, magnetic nanoparticles have also been encapsulated within the BMV virus.[31]

CCMV as a host

By making use of its reversible assembly–disassembly properties, CCMV has been applied as a host for the reversibly gated entrapment of organic and inorganic compounds.[32] The entrapment of different guest compounds has been carried out by taking advantage of the positively charged inner cavity of the CCMV protein capsid and the pH-dependent gating.[5] For example, it has been used for directing the nucleation of mineralization reactions to form spatially constrained nanoparticles of polyoxometalate salts (tungstates, molybdates, and vanadates).[33] Subsequently, through a combination of protein design and genetic engineering, the charge on the interior surface of the CCMV capsid has been altered from positive to negative, which provided an adequate environment for directing the mineral nucleation of transition-metal oxides.[34] Recently, Prussian blue salts have been synthesized *in situ* within the cavity of the CCMV capsid, yielding highly monodisperse nanoparticles of this mineral.[35]

Inclusion of polyanions in the CCMV capsid has been shown to give a variety of structures, including nanotubes and spheres of various sizes.[36-39] Polystyrene sulfonate (PSS) has been shown to produce $T = 1$ particles at neutral pH[40] and capsids with "$T = 2$" or $T = 3$ symmetry at pH 5, depending on the molecular weight of the polymer.[41] Moreover, tubular structures with tunable lengths have also been observed, namely when double-stranded DNA (dsDNA) was used as the macromolecular polymeric cargo.[42]

In Chapter 4 properties of the CCMV capsid were studied in detail and the conditions for its assembly and disassembly established. In the present chapter and in Chapter 7 we will use this knowledge to encapsulate proteins and enzymes in the capsid interior, the objective being to construct a viral nanoreactor. As a proof of principle and to optimize the procedure of protein encapsulation, first different model proteins were included in the CCMV capsid. Some important issues to consider are i) what approach should be followed to encapsulate the guest protein, ii) what are the best techniques to characterize the system once it contains the guest protein, and iii) how efficient can the process be made. The volume of the internal cavity of the viral capsid is very small, and as a result the amounts of encapsulated guest will be low. Hence it will be difficult to characterize viral host–guest systems making that sufficiently sensitive techniques are needed.

6.2 Results and Discussion

The approach that was followed to encapsulate proteins is depicted in Scheme 6.2. It involves the statistical encapsulation of the guest by disassembling and subsequently reassembling the capsid in the presence of the protein. The encapsulation efficiency of the process, namely, the number of guest proteins per capsid, is determined by the

starting concentration of the protein. The capsid disassembles into protein dimers by raising the pH from 5 to 7.5. An excess of guest material was added to the dimer solution at different guest protein/dimer ratios, depending on the protein used, and the pH was lowered to 5 by dialysis against a buffer of pH 5. As mentioned in Chapter 4, this process can be monitored by FPLC and TEM, and in this way it is possible to follow the complete disassembly of the capsid into dimers and examine the correct formation of the capsid once the guest protein is encapsulated.

Empty Capsid   **Protein Dimers**   **Filled Capsid**
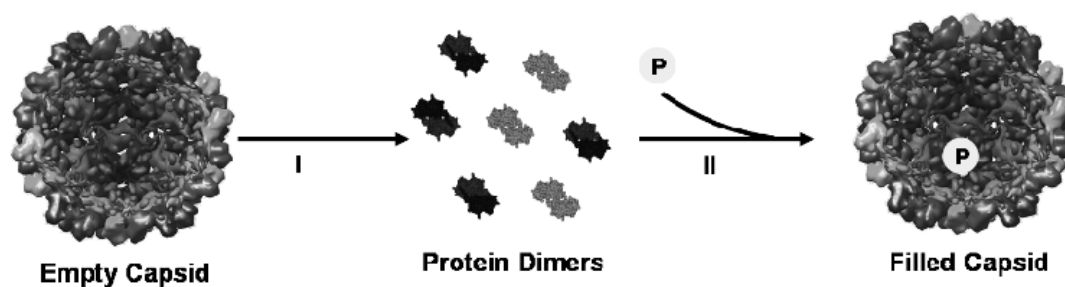
Scheme 6.2 Schematic pathway for the inclusion of a protein in the CCMV capsid. After disassembling the CCMV capsid into dimers (step I, pH 7.5), the guest protein (P) is added and the CCMV capsid is assembled again by decreasing the pH (step II, pH 5).

Control experiments were carried out simultaneously to determine the extent of protein adsorption to the outer surface of the capsid. In the first control experiment, the capsid and guest protein, using the same concentration as described for the encapsulation experiment, were mixed in sodium acetate buffer (0.05 M, pH 5), and subsequently dialyzed against the same pH 5 buffer. Disassembly of the initial capsid does not take place under these conditions and any detected protein is therefore the result of protein adsorption to the outer surface of the capsid or inclusion in the protein shell.

Two further control experiments were carried out following the same procedure as described above for the protein encapsulation experiments, but omitting either the guest protein or the capsid protein.

Proof of concept: encapsulation of myoglobin

Myoglobin (Mb) was the first model protein that was chosen to be encapsulated in the CCMV capsid. Ample experience with this protein in our laboratory, its low price, small size, together with the fact that it has an easily detectable chromophore in the form of a heme group, makes myoglobin a good choice for a proof of principle experiment.

The encapsulation was carried out by using 500 equivalents of myoglobin per capsid particle (one capsid particle corresponds to 90 capsid protein dimers) with a capsid concentration of 15 mg mL^{-1}. The formation of the capsid in the presence of myoglobin was confirmed by FPLC and TEM (Figure 6.1). The reassembled, filled capsid (Figure 6.1b) eluted at the same retention volume as the initial capsid (Figure 6.1a) when

analyzed by FPLC, indicating that both capsids have the same size and shape. Also TEM micrographs (Figure 6.1a and b, insets) proved that the capsids were formed in the presence of protein. Concentrated fractions from the FPLC corresponding to the peak at 1.1 mL were analyzed by UV/Vis spectroscopy. These fractions are free from nonencapsulated myoglobin because the protein elutes at a higher retention volume ($V = 1.9$ mL) than the capsid (Figure 6.1b and c). The myoglobin-containing capsid displayed a signal at $\lambda = 409$ nm in the UV/Vis spectrum, characteristic of the myoglobin-heme group, indicating the successful inclusion of the protein (Figure 6.1d).
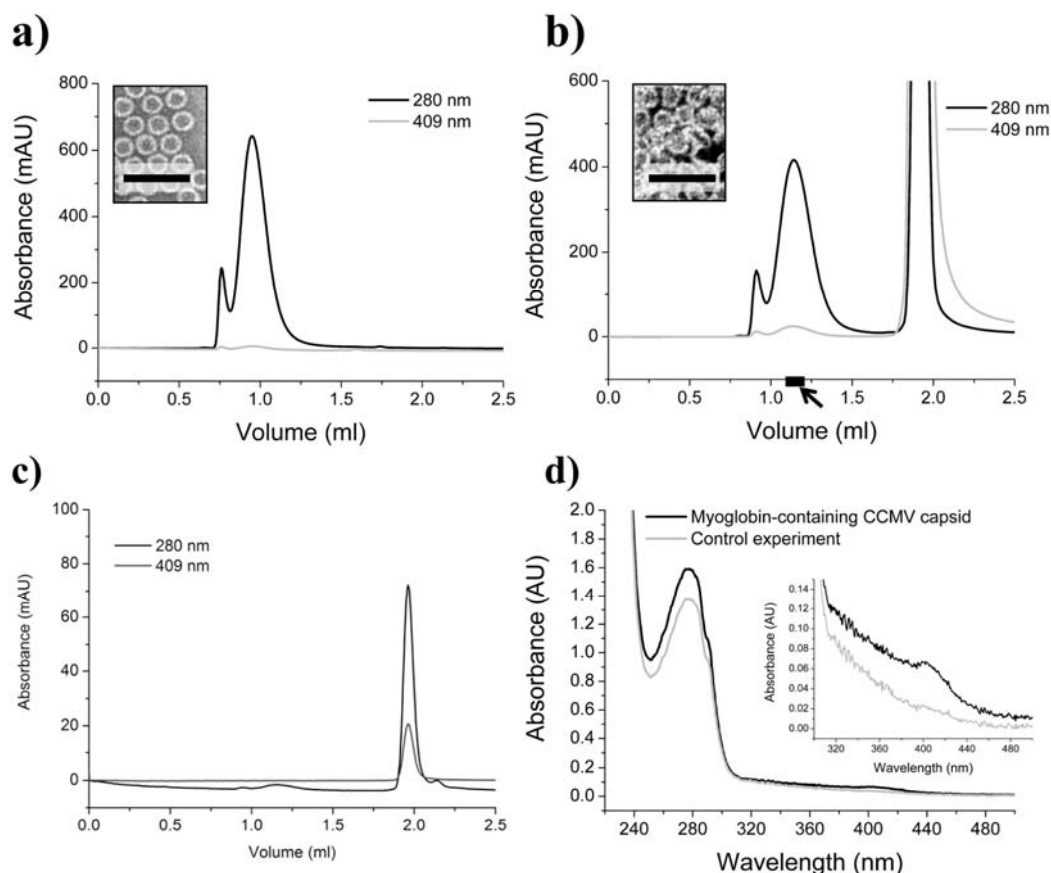
Figure 6.1 Inclusion of myoglobin in the CCMV capsid. a) FPLC chromatogram of the CCMV capsid. Inset: TEM (negative staining) image of the CCMV capsid (scale bar = 100 nm). b) FPLC chromatogram of the myoglobin-containing CCMV capsid. Inset: TEM (negative staining) image of the myoglobin-containing CCMV capsid (scale bar = 100 nm). c) FPLC chromatogram of myoglobin. d) UV/Vis spectra of the myoglobin-containing CCMV fraction (see arrow in panel b) and the corresponding fraction of the control experiment. Inset: magnification of the traces at λ = 409 nm.

From the UV/Vis absorption data of the capsid (at $\lambda = 280$ nm) and the myoglobin (at $\lambda = 409$ nm), and the corresponding extinction coefficients, we could calculate the final guest/host ratio corresponding to this experiment (Equation 6-1). Under the applied

experimental conditions, it was calculated that an average of two myoglobin molecules were encapsulated within a single CCMV capsid. This result is in reasonable agreement with the ratio calculated for a statistical process, in which there is no driving force to encapsulate the protein. Taking into account the initial concentration of myoglobin in the mixture and the volume of the capsid inner cavity, it was calculated that an average of 3.5 myoglobin molecules would be encapsulated per capsid. The initial myoglobin concentration in the mixture is expected to be lower due to some protein precipitation, explaining the slight deviation in encapsulation efficiency.

Equation 6-1

$$\mathrm{Mb\,/\,CCMVcapsid} = \frac{c(\mathrm{Mb})}{c(\mathrm{CCMVcapsid})} = \frac{A(\mathrm{Mb},\,409\ \mathrm{nm})\,/\,\varepsilon_{409\,\mathrm{nm}}(\mathrm{Mb})}{A(\mathrm{CCMVcapsid},\,280\ \mathrm{nm})\,/\,\varepsilon_{280\,\mathrm{nm}}(\mathrm{CCMVcapsid})}$$

Enhancing the detection sensitivity: encapsulation of dronpa

Although the encapsulation of myoglobin was confirmed by UV/Vis spectroscopy, the obtained signal intensity was very low (Figure 6.1d). To improve the UV/Vis signal we had three options: i) to increase the amount of encapsulated protein, which was difficult because inclusion is a statistical process (as mentioned above), ii) to increase the myoglobin-containing capsid concentration in the fraction to be analyzed, and iii) to use a more sensitive technique to monitor the encapsulation process, which would also mean the use of a probe molecule. The second option was tested for myoglobin but higher concentrations were difficult to obtain for experimental reasons. The third option appeared to be the most realistic one and we decided to use the protein dronpa as a model protein for inclusion in the CCMV capsid. Dronpa is an engineered mutant of a green fluorescent protein (GFP)-like protein that was cloned from the *Pectiniidae* species of coral and exhibits reversible photoswitching behavior (Figure 6.2a).[43,44] The latter led to the naming "Dronpa," after "dron," a ninja term for vanishing, and "pa," which stands for photoactivation. This protein has an absorption maximum at $\lambda = 503$ nm and emits bright fluorescence at $\lambda = 518$ nm. It has photochromic behavior because its fluorescence can be switched on and off by using two different wavelengths of light. Although the highest fluorescence quantum yield occurs at high pH, at pH = 5 the protein still shows enough fluorescence to be used as a fluorophore in our inclusion experiments (Figure 6.2b).[1]

---

[1] Because of the photochemical properties of dronpa interesting physical phenomena can be expected when the protein is encased in the small volume of a virus particle.[43] This feature is beyond the scope of this thesis.

a)

b)
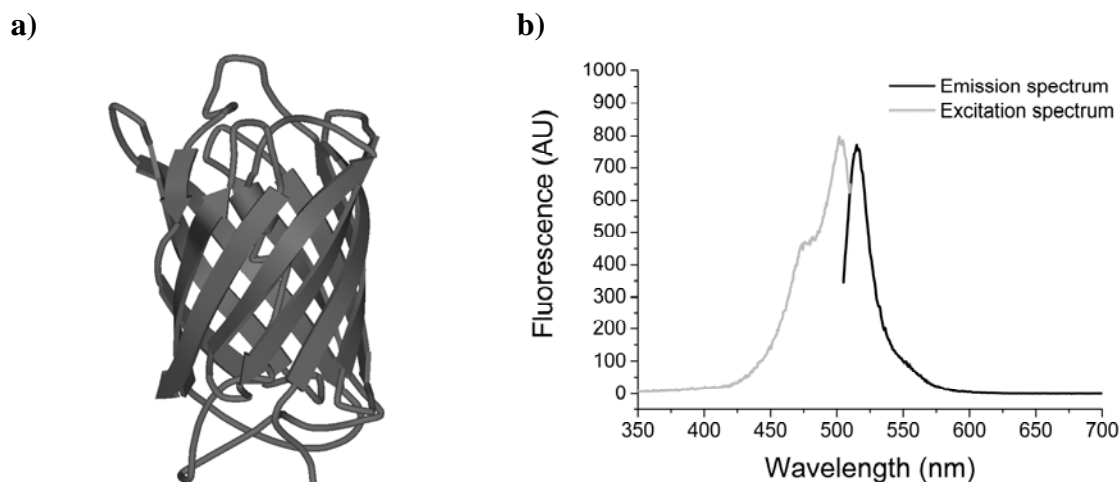
Figure 6.2 The engineered mutant dronpa. a) Crystallographic structure of dronpa represented in ribbon format.[45] b) Excitation (λ_{em} =518 nm) and emission (λ_{exc} =503 nm) spectra of dronpa at pH = 5 (c = 1.3 $\times$ 10^{-6} M in buffer solution).

The encapsulation of dronpa was carried out by following the same procedure as used for the protein myoglobin and its inclusion in the CCMV capsid was investigated by fluorescence spectroscopy and SDS-PAGE (SDS-polyacrylamide gel electrophoresis). The concentrated CCMV capsid samples obtained through purification by FPLC, showed strong emission when excited at λ = 503 nm (Figure 6.3a), which indicated that dronpa molecules co-eluted with the CCMV capsids. The protein appeared to be mainly included inside the cavities of the capsids and was not adsorbed on the capsid outside surface, as was concluded from the low emission obtained in the control experiment, in which no disassembly–assembly cycle was applied (Figure 6.3a). The samples were analyzed by SDS-PAGE to further prove the protein encapsulation (Figure 6.3b). Two different bands were observed for the samples of the inclusion experiments, corresponding to the molecular weight of dronpa (29,200 Da) and that of the CCMV protein subunits. The control experiment containing only CCMV capsid (lanes 2, 4, and 6) showed a band corresponding to the viral protein subunits (20,212 Da) and multiple lower-molecular-weight bands due to protein degradation (typical in old capsid samples, see Chapter 4). The sample containing only dronpa (29,200 Da) showed a single band (lane 7). Both the inclusion experiment (lane 3) and the control experiment, in which no disassembly–assembly cycle was applied (lane 5), showed multiple bands corresponding to the CCMV capsid, but the dronpa band was only present in the former experiment (lane 3). The smeared bands in lanes 3 and 5 are due to intentional overloading of the samples to improve the detection of dronpa.

a)

b)
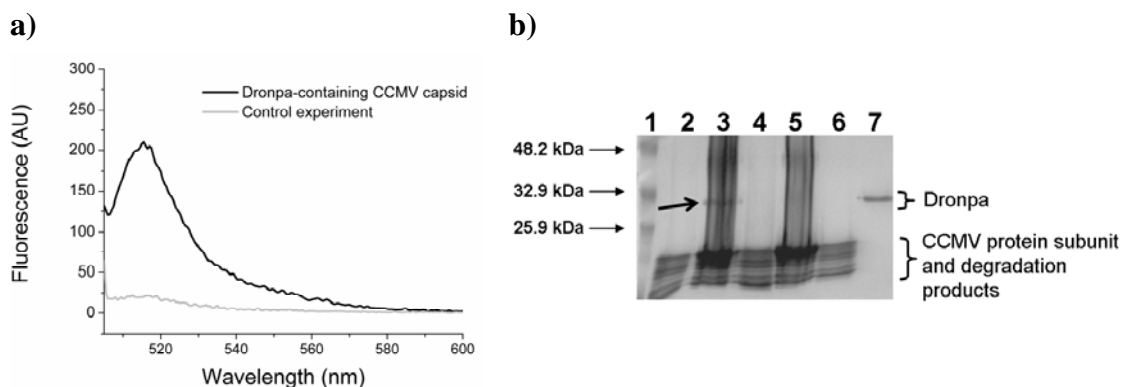
Figure 6.3 *Inclusion of the protein dronpa in the CCMV capsid. a) Emission spectra (λ_{exc} = 503 nm) of the dronpa-containing CCMV capsid fraction and the corresponding fraction of the control experiment in which no disassembly–assembly cycle was applied. b) SDS-PAGE gel of the CCMV capsid (lanes 2, 4, and 6), the dronpa-containing CCMV capsid (lane 3), the control containing the mixture for which no disassembly–assembly cycle was applied (lane 5), and dronpa (lane 7).*

The above two experiments with myoglobin and dronpa prove that the encapsulation of a protein inside the cavity of the CCMV capsid is possible and show the techniques that can be used to monitor this process. This opens the way to the encapsulation of enzymes and the study of the substrate conversion by an enzyme-containing capsid, which will be discussed in Chapter 7. Towards this goal, the access of substrate to the cavity of the viral capsid is an important issue that needs to be investigated. Therefore, the porosity of the CCMV capsid was studied by using the streptavidin–biotin system. Following the same procedure employed for myoglobin and dronpa, it was possible to encapsulate the protein streptavidin in the CCMV capsid. Biotin is known to strongly bind to streptavidin and by labeling both biomolecules, FRET experiments can be used to monitor the occurrence of biotin transport across the capsid wall. These experiments are described in the next section.

Encapsulation of streptavidin: study of the diffusion of biotin molecules through the CCMV capsid pores[2]

Streptavidin (SAv) is a homotetrameric protein, which is expressed in the bacterium *Streptomyces avidinii*.[46] It has a molecular weight of approximately 60 kDa and a size of $5.4 \times 5.8 \times 5.8$ nm.[47] Every subunit has one binding site and each of them can independently bind one biotin (Bt) molecule. The resulting SAv–Bt complex has the

---

[2] Part of the work described herein has been performed by Laura Osorio Planes as part of her Master degree under the supervision of Dr. Andrés de la Escosura and the author.

highest interaction between a protein and a ligand known in nature (ka = 2.5×10^{13} M^{-1}).[48]

The strong interaction between Bt and SAv has found broad applications in biotechnology. It is also of interest to note that Bt-modified virus particles have been combined with SAv as a linker molecule to form self-assembled layer structures on a surface through a layer-by-layer approach.[49,50] In the present case the encapsulation of SAv in the CCMV capsid aims to create a molecular trap for the binding of Bt (and its derivatives). When Bt is added to a solution containing capsids with entrapped SAv molecules, its binding to this protein is a measure for the porosity of the capsid membrane.

The encapsulation of SAv was carried out by following the same procedure as described for myoglobin and dronpa. SAv was labeled with the Alexa-Fluor 488 dye to monitor the inclusion by fluorescence spectroscopy; 1.6 equivalents of SAv per capsid particle were added, a much smaller amount than in the encapsulation of myoglobin (see above). After purification of the complex by using FPLC, co-elution of the capsid and SAv was demonstrated by fluorescence spectroscopy, that is, a distinct emission at λ = 520 nm was observed. The control experiment (no disassembly–assembly cyclus) yielded a much lower fluorescence intensity. The observed residual fluorescence is probably due to SAv molecules that are adsorbed to the outside surface of the capsid. These experiments indicate that the protein was successfully included inside the capsid. The correct reassembly of the SAv-containing capsid was confirmed by TEM experiments (not shown), but due to the low concentration of protein and its low extinction coefficient no additional evidence for SAv inclusion could be obtained by UV/Vis spectroscopy and SDS-PAGE.

To study complex formation between CCMV encapsulated SAv and externally added Bt, initially a 4'-hydroxyazobenzene-2-carboxylic acid (HABA)–SAv assay was carried out.[51] This spectroscopic assay allows one to study the displacement of the dye HABA bound to SAv by Bt. Unfortunately, the concentration of SAv inside the CCMV capsid was so low that no differences could be detected between bound and unbound HABA by UV/Vis spectroscopy. A more sensitive approach is to use biocytin Alexa-Fluor 546 (Bt-546), which is a commercially available Bt-labeled fluorescent dye that allows the monitoring of the SAv–Bt interaction by fluorescence spectroscopy (so-called Förster resonance energy transfer (FRET) experiment).

When Bt-546 is in close proximity to SAv-488 and the complex is excited at λ = 494 nm (λ_{exc} of the Alexa Fluor 488), energy transfer between the two chromophores occurs, causing a decrease in the emission at λ = 520 nm (λ_{em} of the Alexa Fluor 488) and the concomitant appearance of a new signal at λ = 566 nm (λ_{em} of the Bt-546).[52] SAv-488-containing capsids were titrated with Bt-546 and a clear quenching was found to occur already after the addition of 0.5 equivalents of Bt-546 per SAv binding site (Figure 6.4

a). The same procedure was followed for the control experiment (CCMV capsid mixed with SAv-488 at pH 5 followed by purification) and in this case almost no quenching was observed (Figure 6.4b).

The occurrence of FRET could be also shown by SDS-PAGE, in which case the gel was loaded with different SAv-488 samples to which Bt-546 was added or not (Figure 6.4c). The gel was developed with a Fuji FLA-5100 fluorescence scanner operating at an excitation wavelength of $\lambda_{exc} = 473$ nm and provided with an LPB (510 nm) detection filter. In these experiments no band is expected when Bt-546 binds to SAv-488, see lanes 2, 4, and 10. Lane 10 shows a small residual band probably due to the large excess of Bt-546, which was used. This compound partially absorbs at $\lambda = 473$ nm.

The above experiments show that Bt can pass the protein shell of the CCMV capsid. Although SAv is not catalytically active, such a system might be used for the inclusion within the capsid of catalysts that are attached to Bt. Such a possibility makes the SAv-containing CCMV capsid an interesting object for further investigation.

a)

b)
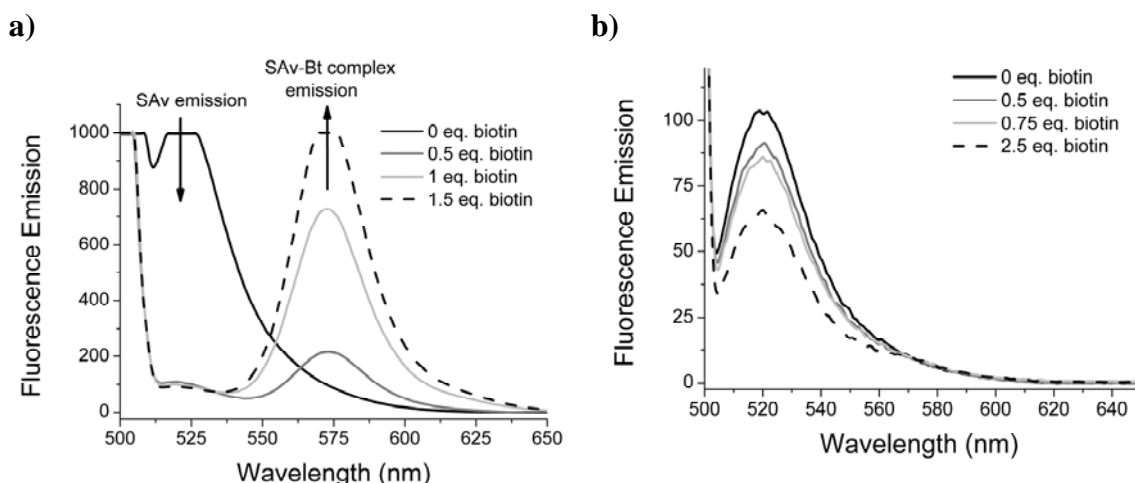
c)
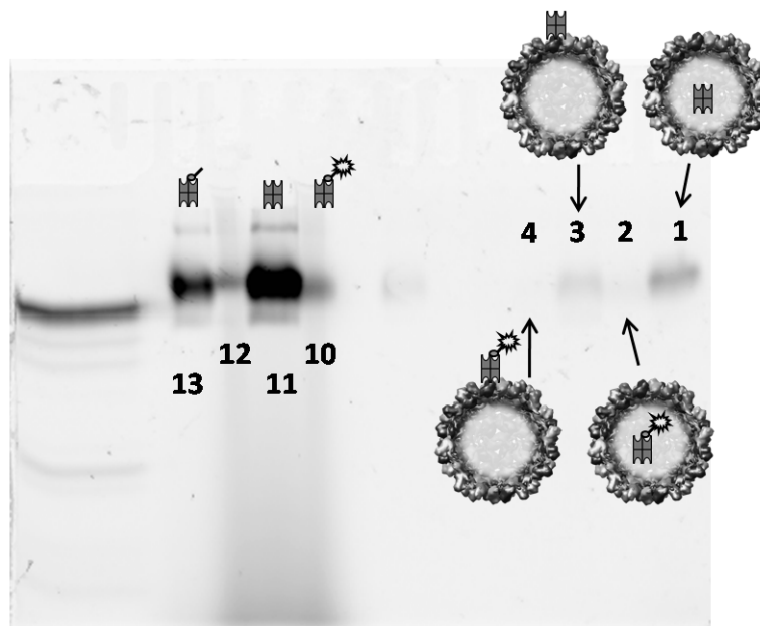
Figure 6.4 *Analyses of Sav-488 and Bt-546 mixing and encapsulation experiments.*
a) Fluorescence spectra (λ_{exc} = 494 nm) of SAv-488-containing capsids after the
addition of different equivalents of the quenching agent Bt-546 (the numbers
correspond to Bt-546 per SAv binding site). b) Fluorescence spectra (λ_{exc} = 494 nm) of
the control experiment, in which SAv-488 was mixed with the capsids and no
disassembly–assembly cycle was applied. Several equivalents of the quenching agent
Bt-546 (the numbers correspond to Bt-546 per SAv binding site) were added. c) Native
SDS-PAGE visualized by using a fluorescence scanner (λ_{exc} = 473 nm, λ_{em} > 510 nm).
The different lanes correspond to SAv-488-containing capsid before (lane 1) and after
(lane 2) the addition of Bt-546 (10 equiv); the control experiment before (lane 3) and
after (lane 4) the addition of Bt-546(10 equiv); SAv-488 after (lane 10) and before
(lane 11) the addition of Bt-546 (100 equiv); unlabeled SAv after the addition of Bt-546
(10 equiv) (lane 12), and SAv-488 after the addition of unlabeled Bt (lane 13). Lanes 5–
9 were not loaded and lane 14 is to the marker.

6.3 Conclusion

The assembly–disassembly properties of the CCMV coat protein studied in Chapter 4
were used to encapsulate different proteins in the capsid. The encapsulation of
myoglobin, dronpa, and SAv was successfully achieved and in the case of myoglobin it
was shown that on average not more than two proteins were entrapped per capsid.
Fluorescence spectroscopy in contrast to UV/Vis spectroscopy proved to be a sensitive

technique to monitor the encapsulation of the proteins, in particular for dronpa. For this reason nonfluorescent proteins, such as SAv, need to be labeled with a fluorophore.

The successful encapsulation of proteins within the CCMV capsid, and the fact that the capsid is permeable for small molecules, as shown by the diffusion of Bt across the protein shell of the SAv-containing capsid, allows for the construction of a viral nanoreactor. In such a system an enzyme is encapsulated in the CCMV capsid and substrate and product molecules can diffuse freely in and out of the reactor (see Chapter 7).

6.4 Experimental Section

Materials

Sodium acetate trihydrate (>99%) and uranyl acetate dihydrate (≥98%) were purchased from Fluka. Ethylenediaminetetraacetic acid (EDTA) disodium salt dihydrate (>99%), Tris(hydroxymethyl)aminomethane (Tris) (>99%), calcium chloride dihydrate (>99%), sodium chloride (99.5%), sodium azide (99%), and cesium chloride (>99%) were purchased from Acros. Ethanol (p.a.) was purchased from Merck. Myoglobin from equine heart (Product number: M1882, ≥90%), streptavidin (Product number: S4762), biotin (Product number: 14400, ≥99%), phenylmethanesulfonyl fluoride (PMSF) (≥98.5%), ethidium bromide (~95%), Orange G (≥80%), 4'-hydroxyazobenzene-2-carboxylic acid (HABA) (Product number: H5126, ≥98%), and dithiothreitol (DTT) (99%) were obtained from Sigma-Aldrich. Streptavidin was labeled with Alexa Fluor® 488 via carboxylic acid TFP ester bis(triethylammonium salt) of this dye, following the protocol provided with the labeling kit by the supplier (Molecular Probes, Invitrogen). Agarose (electrophoresis grade) and Alexa Fluor 546 biocytin (Catalog number: A12923) were purchased from Invitrogen. All reagents used for SDS-PAGE electrophoresis were purchased from Bio-Rad Laboratories. Dronpa was kindly provided by Prof. Johan Hofkens, University of Leuven (Belgium).

Instrumentation

UV/Vis spectroscopy was performed on a Varian Cary 50 spectrophotometer at room temperature using a 1 cm quartz cuvette (Hellma, path length $l = 1$ cm) or a 45 μL quartz fluorescence cuvette (Hellma, path length $l = 3$ mm). The reference spectrum of the corresponding buffers was subtracted from all UV/Vis spectra.

Fluorescence spectroscopy was performed on a Perkin-Elmer LS 50B fluorescence spectrophotometer. Experiments were carried out at $T = 10°C$ by using a 45 μL quartz fluorescence cuvette (Hellma, path length $l = 3$ mm).

Fast protein liquid chromatography (FPLC) was performed on an Ettan Akta LC system equipped with a Superose 6 PC 3.2/30 column from Amersham Biosciences (flow rate: 40 μL min^{-1}). Injections of 20–100 mL aliquots of the samples on the FPLC column at room temperature were monitored by using UV/Vis detection at $\lambda = 280$ nm and the wavelength corresponding to the chromophore present in the guest protein.

Transmission electron microscopy (TEM) micrographs were recorded on a JEOL JEM-1010 instrument. Samples were prepared by drying a drop of the solution on a Formvar carbon-coated grid, which had been previously made hydrophilic by glow discharge. The excess buffer on the grid was blotted away after 1 min with filter paper. Negative staining of the samples was achieved by applying a drop of uranyl acetate solution (0.2% in MilliQ) onto the grid and blotting the excess liquid away after 15 s with filter paper. The samples were left to dry in air for 30 min before analysis.

SDS-polyacrylamide gel electrophoresis (SDS-PAGE) was performed by using a 4% stacking and 15% running polyacrylamide gel containing 10% SDS (1% SDS in the case of native conditions). Samples for gels under non-native conditions were treated with β-mercaptoethanol and heated prior to loading onto the gel. Gels were stained with 0.05% (w/v) Coomassie Blue solution and destained with a solution of 5% (v/v) methanol and 7% (v/v) acetic acid in water (Coomassie Blue destainer).

A Fuji FLA-5100 fluorescence scanner ("1 laser 1 image" mode), was used for gel analysis when the gels were loaded with fluorescent samples ($\lambda_{exc} = 473$ nm, detection filter LPB (510 nm)).

Dialysis was performed by using dialysis tubing (Spectra/Por 4, MWCO: 12–14 kD, flat width: 25 mm) purchased from Spectrum Laboratories, or D-tube dialyzer (MWCO: 6–8 kD, volume: 50 to 800 μL) from Novagen.

Protein encapsulation experiments

The purification of the CCMV virus and the isolation of the coat protein were performed as described in Chapters 3 and 4. The coat protein was used immediately after isolation to avoid degradation. Occasionally, it was used from a coat protein sample stored in capsid storage buffer (0.05 M sodium acetate, 1 mM NaCl, 1 mM sodium azide, pH 5) kept at 4°C. Such a solution was never more than two-weeks old and it was always checked for degradation before use.

A solution containing the CCMV coat protein (see Table 6.1) in sodium acetate buffer (0.05 M, pH 5) was dialyzed against three changes of Tris–HCl buffer (500 mL, 0.05 M, pH 7.5) (3 h per change). When the solution had reached pH 7.5, the guest protein solution (see table below) in Tris–HCl (0.05 M, pH 5) was added in excess, and the resulting solution was incubated for 1 to 2 h. Dialysis of the incubated solution against the initial sodium acetate buffer was carried out under the same dialysis conditions as described above. The samples were concentrated and the free guest protein was

removed using centrifugal filter devices (Centricon YM-100, Millipore). Samples were further purified by FPLC and concentrated when needed by using centrifugal filter devices (Centricon YM-100, Millipore).

All buffer solutions contained 1 mM EDTA, 300 mM NaCl, 10 mM $CaCl_2$, and 0.2 mM phenylmethylsulphonyl fluoride (PMSF). Buffers were stored at 4°C, and the dialysis was performed in a cold room at 4°C. In later experiments better results were obtained when 500 mM of NaCl instead of 300 mM was used. An increase in the amount of salt enhances the stability of the assembled capsid (for further details about the assembly process, see Chapter 4).

Table 6.1 *Concentrations and volumes of guest proteins used in the experiments*

Guest protein	Guest protein solution		Capsid solution		Guest protein in final solution		
	Conc. (M)	Added volume (mL)	Conc. (M)	Added volume (mL)	Added equiv per capsid	Final conc. (M)	Guest protein per capsid[a)]
Mb	1.16×10^{-2}	0.1	4.37×10^{-6}	0.5	532	1.94×10^{-3}	3.57
dronpa	3.50×10^{-4}	0.18	4.37×10^{-6}	0.3	48	1.31×10^{-4}	0.24
SAv	3.38×10^{-6}	0.29	2.03×10^{-6}	0.3	1.6	1.66×10^{-6}	3×10^{-3}

a) Considering the fact that the encapsulation is a statistical process, the guest proteins per capsid were calculated by multiplying the concentration of guest protein in the final solution by the inner volume of the capsid ($V = 3.05 \times 10^{-15}$ μL) and by Avogadro's number ($N_A = 6.022 \times 10^{23}$).

The final average guest protein/capsid ratio could only be calculated by UV/Vis spectroscopy for the protein myoglobin. For practical reasons myoglobin allowed us to work with this protein in higher concentration than with the other two proteins and as a result a higher number of guest protein molecules could be encapsulated and detected by UV/Vis spectroscopy. Once encapsulated, the dronpa and the labeled SAv could be easily detected by fluorescence spectroscopy. Unfortunately, because of the low concentration and the low extinction coefficient of both chromophores, no peak was observed by UV/Vis spectroscopy, therefore, no guest protein/capsid ratio could be calculated.

Control encapsulation experiments

For the control experiments, in which guest protein and capsid are mixed without performing a disassembly–assembly cycle, the next procedure was followed: Guest protein solution in sodium acetate buffer (0.05 M, pH 5) was added to a solution containing CCMV coat protein in sodium acetate buffer (0.05 M, pH 5), using the same volumes and concentrations as described for the encapsulation experiment. The mixture was subsequently dialyzed against three changes of the same sodium acetate buffer (500 mL, 0.05 M, pH 5) (3 h per change).

Two further control experiments were carried out by following the same procedure as described above for the protein encapsulation experiments, but omitting either the guest protein or the capsid protein.

All buffer solutions contained 1 mM EDTA, 300 mM NaCl, 10 mM $CaCl_2$, and 0.2 mM PMSF. Buffers were stored at 4°C and the dialysis was performed in a cold room at 4°C. Later experiments showed better results when 500 mM of NaCl were used instead of 300 mM. An increase in the amount of salt enhances the stability of the assembled capsid (for further details about the assembly process, see Chapter 4).

FRET experiments. Study of biotin–546 transport across the CCMV-capsid shell.
In a first series of test experiments titrations were carried out in which labeled and unlabeled biotin were added to SAv-488 in solution. In subsequent experiments, aliquots ($V = 1$ µL) of a Bt-546 solution ($c = 5.68 \times 10^{-5}$ M) were added to a sample ($V = 40$ µL) of SAv-488-containing CCMV capsid (c (SAv) $\approx 9.47 \times 10^{-7}$ M). For the control experiments, aliquots ($V = 1$ µL) of a Bt-546 solution ($c = 7.58 \times 10^{-6}$ M) were added to a sample ($V = 40$ µL) in which no disassembly–assembly cycle was applied (c (SAv) $\approx 3.79 \times 10^{-7}$ M).

All spectra were corrected for dilution and the solutions were prepared in 0.05 M sodium acetate buffer (pH 5).

6.5 Notes and References

[1]   D. M. Vriezema, M. Comellas Aragones, J. A. A. W. Elemans, J. J. L. M. Cornelissen, A. E. Rowan, R. J. M. Nolte, *Chem. Rev.* **2005**, *105*, 1445.

[2]   M. Sutter, D. Boehringer, S. Gutmann, S. Gunther, D. Prangishvili, M. J. Loessner, K. O. Stetter, E. Weber-Ban, N. Ban, *Nat. Struct. Mol. Biol.* **2008**, *15*, 939.

[3]   M. Fischlechner, E. Donath, *Angew. Chem. Int. Ed.* **2007**, *46*, 3184.

[4]   T. Douglas, M. Young, *Science* **2006**, *312*, 873.

[5]   M. Uchida, M. T. Klem, M. Allen, P. Suci, M. Flenniken, E. Gillitzer, Z. Varpness, L. O. Liepold, M. Young, T. Douglas, *Adv. Mater.* **2007**, *19*, 1025.

[6]   S. Mann, F. C. Meldrum, *Adv. Mater.* **1991**, *3*, 316.

[7]   F. C. Meldrum, V. J. Wade, D. L. Nimmo, B. R. Heywood, S. Mann, *Nature* **1991**, *349*, 684.

[8]   J. Polanams, A. D. Ray, R. K. Watt, *Inorg. Chem.* **2005**, *44*, 3203.

[9]   M. T. Klem, J. Mosolf, M. Young, T. Douglas, *Inorg. Chem.* **2008**, *47*, 2237.

[10]   M. J. Parker, M. A. Allen, B. Ramsay, M. T. Klem, M. Young, T. Douglas, *Chem. Mater.* **2008**, *20*, 1541.

[11]   F. C. Meldrum, B. R. Heywood, S. Mann, *Science* **1992**, *257*, 522.

[12] K. K. W. Wong, T. Douglas, S. Gider, D. D. Awschalom, S. Mann, *Chem. Mater.* **1998**, *10*, 279.

[13] M. T. Klem, D. A. Resnick, K. Gilmore, M. Young, Y. U. Idzerda, T. Douglas, *J. Am. Chem. Soc.* **2007**, *129*, 197.

[14] M. Uchida, M. L. Flenniken, M. Allen, D. A. Willits, B. E. Crowley, S. Brumfield, A. F. Willis, L. Jackiw, M. Jutila, M. J. Young, T. Douglas, *J. Am. Chem. Soc.* **2006**, *128*, 16626.

[15] I. Kim, H. A. Hosein, D. R. Strongin, T. Douglas, *Chem. Mater.* **2002**, *14*, 4874.

[16] D. Ensign, M. Young, T. Douglas, *Inorg. Chem.* **2004**, *43*, 3441.

[17] T. Ueno, M. Suzuki, T. Goto, T. Matsumoto, K. Nagayama, Y. Watanabe, *Angew. Chem. Int. Ed.* **2004**, *43*, 2527.

[18] W. Shenton, S. Mann, H. Cölfen, A. Bacher, M. Fischer, *Angew. Chem. Int. Ed.* **2001**, *40*, 442.

[19] M. L. Flenniken, D. A. Willits, S. Brumfield, M. J. Young, T. Douglas, *Nano Lett.* **2003**, *3*, 1573.

[20] Z. Varpness, J. W. Peters, M. Young, T. Douglas, *Nano Lett.* **2005**, *5*, 2306.

[21] M. L. Flenniken, L. O. Liepold, B. E. Crowley, D. A. Willits, M. J. Young, T. Douglas, *Chem. Commun.* **2005**, 447.

[22] P. S. Arora, K. Kirshenbaum, *Chem. Biol.* **2004**, *11*, 418.

[23] C. E. Flynn, S.-W. Lee, B. R. Peelle, A. M. Belcher, *Acta Mater.* **2003**, *51*, 5867.

[24] E. Strable, D. E. Prasuhn, Jr., A. K. Udit, S. Brown, A. J. Link, J. T. Ngo, G. Lander, J. Quispe, C. S. Potter, B. Carragher, D. A. Tirrell, M. G. Finn, *Bioconjugate Chem.* **2008**, *19*, 866.

[25] J. M. Hooker, E. W. Kovacs, M. B. Francis, *J. Am. Chem. Soc.* **2004**, *126*, 3718.

[26] E. W. Kovacs, J. M. Hooker, D. W. Romanini, P. G. Holder, K. E. Berry, M. B. Francis, *Bioconjugate Chem.* **2007**, *18*, 1140.

[27] L. Loo, R. H. Guenther, V. R. Basnayake, S. A. Lommel, S. Franzen, *J. Am. Chem. Soc.* **2006**, *128*, 4502.

[28] J. Sun, C. DuFort, M. C. Daniel, A. Murali, C. Chen, K. Gopinath, B. Stein, M. De, V. M. Rotello, A. Holzenburg, C. C. Kao, B. Dragnea, *Proc. Natl. Acad. Sci. U.S.A.* **2007**, *104*, 1354.

[29] C. Chen, M. C. Daniel, Z. T. Quinkert, M. De, B. Stein, V. D. Bowman, P. R. Chipman, V. M. Rotello, C. C. Kao, B. Dragnea, *Nano Lett.* **2006**, *6*, 611.

[30] N. L. Goicochea, M. De, V. M. Rotello, S. Mukhopadhyay, B. Dragnea, *Nano Lett.* **2007**, *7*, 2281.

[31] X. Huang, L. M. Bronstein, J. Retrum, C. Dufort, I. Tsvetkova, S. Aniagyei, B. Stein, G. Stucky, B. McKenna, N. Remmes, D. Baxter, C. C. Kao, B. Dragnea, *Nano Lett.* **2007**, *7*, 2407.

[32] T. Douglas, M. Young, *Adv. Mater.* **1999**, *11*, 679.

[33] T. Douglas, M. Young, *Nature* **1998**, *393*, 152.

[34] T. Douglas, E. Strable, D. Willits, A. Aitouchen, M. Libera, M. Young, *Adv. Mater.* **2002**, *14*, 415.

[35]   A. de la Escosura, M. Verwegen, F. D. Sikkema, M. Comellas-Aragones, A. Kirilyuk, T. Rasing, R. J. M. Nolte, J. J. L. M. Cornelissen, *Chem. Commun.* **2008**, 1542.

[36]   J. B. Bancroft, G. J. Hills, R. Markham, *Virology* **1967**, *31*, 354.

[37]   B. J. Verduin, J. B. Bancroft, *Virology* **1969**, *37*, 501.

[38]   J. B. Bancroft, E. Hiebert, C. E. Bracker, *Virology* **1969**, *39*, 924.

[39]   X. Zhao, J. M. Fox, N. H. Olson, T. S. Baker, M. J. Young, *Virology* **1995**, *207*, 486.

[40]   F. D. Sikkema, M. Comellas-Aragones, R. G. Fokkink, B. J. Verduin, J. J. L. M. Cornelissen, R. J. M. Nolte, *Org. Biomol. Chem.* **2007**, *5*, 54.

[41]   Y. F. Hu, R. Zandi, A. Anavitarte, C. M. Knobler, W. M. Gelbart, *Biophys. J.* **2008**, *94*, 1428.

[42]   S. Mukherjee, C. M. Pfeifer, J. M. Johnson, J. Liu, A. Zlotnick, *J. Am. Chem. Soc.* **2006**, *128*, 2538.

[43]   R. Ando, H. Mizuno, A. Miyawaki, *Science* **2004**, *306*, 1370.

[44]   S. Habuchi, R. Ando, P. Dedecker, W. Verheijen, H. Mizuno, A. Miyawaki, J. Hofkens, *Proc. Natl. Acad. Sci. U.S.A.* **2005**, *102*, 9511.

[45]   P. G. Wilmann, K. Turcic, J. M. Battad, M. C. Wilce, R. J. Devenish, M. Prescott, J. Rossjohn, *J. Mol. Biol.* **2006**, *364*, 213.

[46]   L. Chaiet, F. J. Wolf, *Arch. Biochem. Biophys.* **1964**, *106*, 1.

[47]   P. C. Weber, D. H. Ohlendorf, J. J. Wendoloski, F. R. Salemme, *Science* **1989**, *243*, 85.

[48]   N. M. Green, *Adv. Protein Chem.* **1975**, *29*, 85.

[49]   N. F. Steinmetz, G. Calder, G. P. Lomonossoff, D. J. Evans, *Langmuir* **2006**, *22*, 10032.

[50]   P. A. Suci, M. T. Klem, F. T. Arce, T. Douglas, M. Young, *Langmuir* **2006**, *22*, 8891.

[51]   N. M. Green, *Biochem. J.* **1965**, *94*, 23C.

[52]   J. R. Lakowicz, *Principles of Fluorescence Spectroscopy*, 2nd ed., Plenum Publishing Corporation, **1999**.

CHAPTER 7

A Virus-Based Single-Enzyme Nanoreactor

7.1 Introduction

Most enzyme studies are carried out in bulk aqueous solution, at the so-called ensemble level, but more recently, studies have appeared in which enzyme activity is measured at the level of one single molecule, revealing previously unseen properties.[1-8] To this end, enzymes have been chemically or physically anchored to a surface, which is often disadvantageous because it may lead to denaturation. In their natural environment, enzymes are present in a confined reaction space, which inspired us to develop a generic method to carry out single-enzyme experiments in the restricted spatial environment of a virus capsid. In recent reports, protein capsids and viruses have been studied as containers, as potential reaction vessels,[9-12] as well-defined hosts,[13-16] as nanotemplates,[17-22] and as synthetic platforms.[23-25] To the best of our knowledge, no enzyme-loaded nanocontainer has been assembled and studied at the single-enzyme level.

The reversible pH-dependent assembly–disassembly properties of the CCMV capsid provide a unique molecular gating mechanism for controlling the containment and release of entrapped material.[15,26] The use of the CCMV capsid as a protein container was first optimized with the proteins myoglobin, dronpa, and streptavidin to control the encapsulation and characterization process (Chapter 6). By using the same approach, this chapter reports the incorporation of an individual horseradish peroxidase (HRP) enzyme molecule in the cavity of the CCMV capsid (Scheme 7.1). Furthermore, single-molecule studies on the enzymatic behavior of the HRP-containing capsid by using confocal fluorescence microscopy are described. We aim to use this HRP-containing CCMV capsid as a model system to investigate single-enzyme processes in a more natural environment than in previous studies.[6]
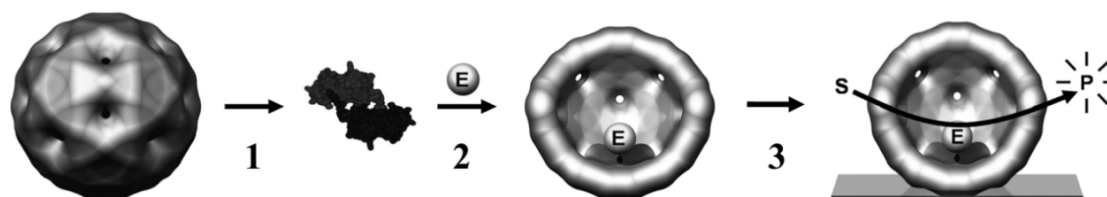
Scheme 7.1 *Schematic pathway for the assembly of a viral nanoreactor. After disassembling the CCMV capsid into coat protein dimers (step 1, pH 7.5), the enzyme (E) is added and the CCMV capsid is reassembled again by decreasing the pH (step 2, pH 5). The HRP-containing capsid is spin-coated on a cover glass and its catalytic activity is studied by using a confocal fluorescence microscope after the addition of a substrate (S) that it is converted into a fluorescent product (P) by the enzyme (step 3).*

Single-molecule fluorescence microscopy: instrumentation and analysis

In contrast with ensemble measurements that only yield information on average properties, single-molecule experiments provide information on individuals, such as distributions and time trajectories of properties that would otherwise be hidden. During the last 15 years the spectroscopic study of single molecules has become an almost routine task for researchers in different scientific fields, from fundamental physics through material sciences to biology. While successful approaches to detect and study single atoms or molecules on surfaces have used near-field interactions with tunneling electrons (scanning tunneling microscopy (STM)) or forces from sharp tips (atomic force microscopy (AFM)), optical methods have the advantage that they enable the observation of single molecules from a certain distance and unperturbed by these tips.[6,7,27] Moreover, advances in optical spectroscopy and microscopy have made it possible not only to detect and identify immobilized or freely diffusing fluorescent molecules, but also to realize spectroscopic measurements on these molecules and monitor their dynamic behavior. Currently the only feasible way to detect a single molecule optically is through fluorescence, and hence, this method is known as single-molecule fluorescence spectroscopy (SMFS); it combines ultrasensitivity with the required high time resolution for in situ measurements.

Nowadays, confocal fluorescence microscopy has become one of the most widely used modes for the detection of single molecules.[27] The typical setup of a confocal fluorescence microscope is depicted in Figure 7.1. The excitation light of a laser beam is focused through an oil- or water-immersion objective lens in a diffraction-limited focus onto the sample. The fluorescence generated by a single molecule residing in the confocal volume is collected by the same objective lens and the emission light is separated from the excitation light by a dichroic mirror. Before reaching the detector, the fluorescence light passes appropriate filters and a small pinhole (50–100 μm in

diameter), rejecting background fluorescence and out-of-focus light, respectively (Figure 7.1a). The emitted fluorescence can be measured by a point detector, such as an avalanche photodiode (APD), which detects photons very efficiently while having a low dark current, resulting in a good signal-to-noise ratio. When using the confocal technique for SMFS, one molecule is studied at a time and when imaging of extended areas is required, this is possible by scanning the sample with respect to the laser focus point or *vice versa*.[27,28]

a)   **b)**
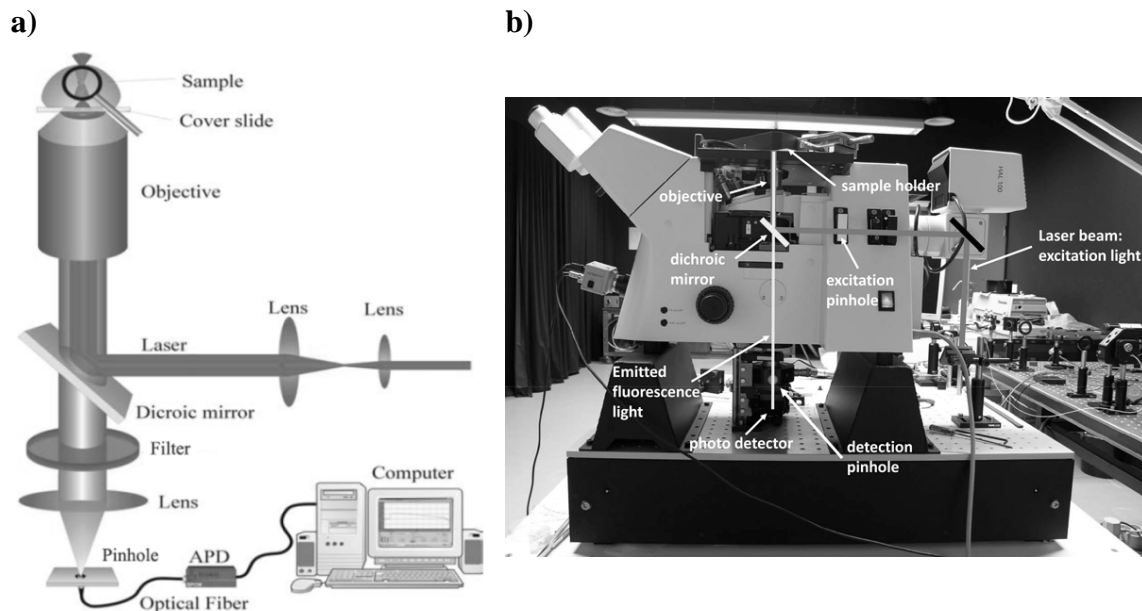
Figure 7.1 *a) Schematic experimental setup of a single-molecule confocal fluorescence microscopy experiment. b) Confocal fluorescence microscope used for the single-molecule studies of the HRP-containing CCMV capsid.*

Fluorescence correlation spectroscopy

Fluorescence correlation spectroscopy (FCS) is one of the many different methods for the high-resolution spatial and temporal analysis of extremely dilute concentrations of biomolecules.[27-30] To enhance detection sensitivity and background suppression, Rigler et al. combined, for the first time, FCS with a confocal setup[31] and in the following years the analytical and diagnostic potential of this methodology was demonstrated. The basic principle behind FCS is that the detected fluorescence will fluctuate, which can be due to *in situ* chemical reactions or diffusion of each fluorescent species in and out of the sampling volume. A correlation analysis of the fluctuating intensity signal yields the diffusion constant of the system under study. By recording and correlating the fluorescence fluctuations of singly labeled or fluorescent molecules excited by laser beam, FCS gives information on molecular mobility and photophysical and photochemical reactions.

By applying SMFS to the HRP-containing CCMV capsid, we intend to obtain information on the catalytic activity of the enzyme and on the influence of the confined space of the viral capsid on the enzymatic activity.

7.2 Results and Discussion

Encapsulation of HRP in the CCMV capsid

The study of the inclusion of myoglobin and dronpa, described in Chapter 6, provided us with the optimal experimental conditions for the statistical encapsulation of a protein within the CCMV capsid and with the methodology to monitor the process. The loading of HRP was carried out by the pH-dependent disassembly−assembly protocol (Scheme 7.1), which was monitored by TEM and FPLC. Initially, the capsid was transformed into protein dimers, indicated by a peak at $V = 1.78$ mL in the FPLC. After addition of HRP, the capsid was reassembled while incorporating the guest enzyme. Because the objective was to perform single-enzyme studies, the concentration of the enzyme was selected to be such that there was only one or no molecules of enzyme present per capsid. As follows from the experiments on myoglobin and dronpa in Chapter 6, the final HRP per capsid ratio will only depend on the concentration of HRP in solution; the amount of capsid or the HRP/capsid ratio do not influence the degree of inclusion. By multiplying the concentration of guest protein in the final solution by the inner volume of the capsid, and by Avogadro's number, we could calculate that on average 0.37 HRP units would be encapsulated per capsid.

Co-elution of the guest protein and the capsid was observed in the HRP encapsulation experiment. Detailed FPLC, TEM, and fluorescence spectroscopic analyses of HRP encapsulation are shown in Figure 7.2. FPLC traces of the HRP-containing CCMV capsid pointed to the successful reassembly of the viral cage after the encapsulation process (Figure 7.2b), showing the same elution volume ($V = 1.12$ mL) as the original capsid (Figure 7.2a). The signal at $V = 1.8$ mL in Figure 7.2b corresponds to the elution volume of free HRP (Figure 7.2c; the high absorbance at 403 nm is due to the heme group present in the protein). The material eluting at $V = 0.9$ mL in Figure 7.2a and b corresponds to the elution volume of larger aggregates formed by the viral coat protein, as described in detail in Chapter 4. The correct reassembly of the capsids with and without HRP was further proven by cryo-TEM analysis (Figure 7.2a and b, insets). In both cases identical particles were observed. Additional evidence for co-elution of the capsid and HRP ($V = 1.12$ mL) comes from analysis of the concentrated fractions of FPLC by fluorescence spectroscopy. Although HRP has a heme group that gives a UV/Vis band at $\lambda = 403$ nm, the experiments with myoglobin and dronpa (Chapter 6) showed that fluorescence was a better technique to monitor the encapsulation of guest

proteins. Therefore, the HRP utilized in the experiments was labeled with the fluorescent dye Alexa Fluor 532 (λ_{exc} = 530 nm). The FPLC fraction corresponding to the CCMV capsid containing this guest enzyme (see the arrow in Figure 7.2b) displayed significant emission when excited at λ = 530 nm, indicating that inclusion of the enzyme had occurred (Figure 7.2d).
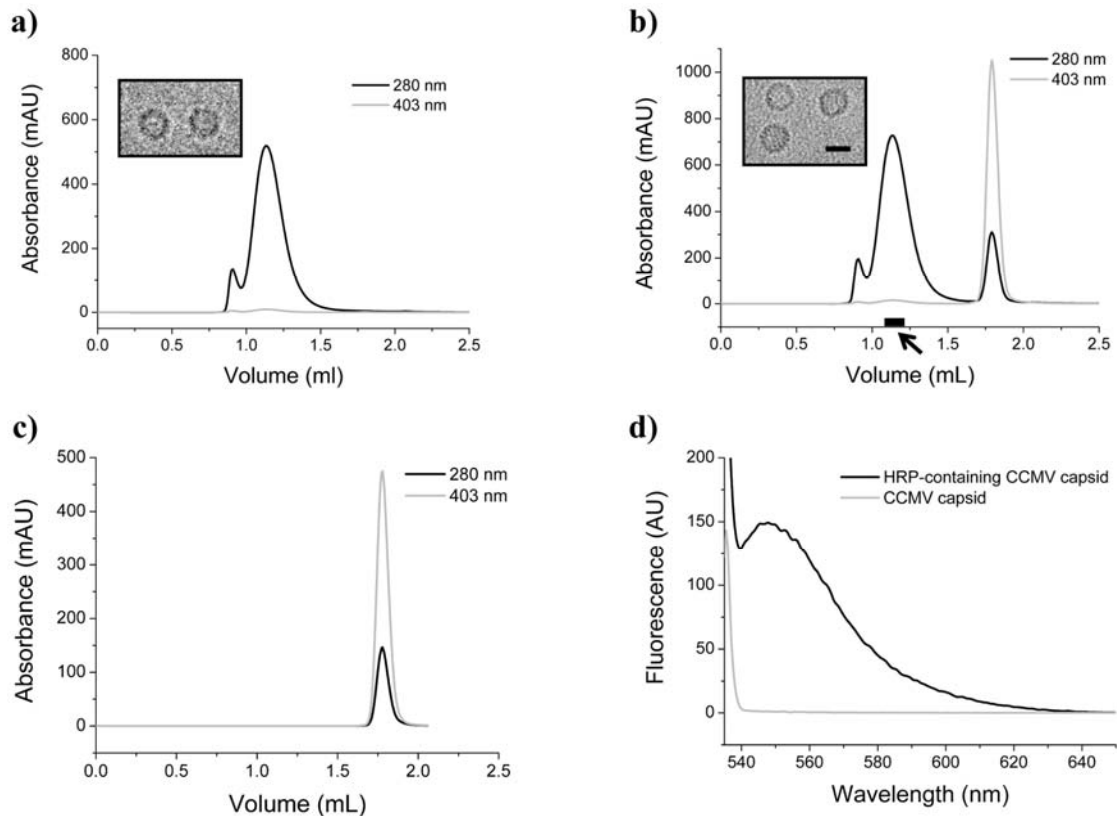
Figure 7.2 Inclusion of HRP in the CCMV capsid. a) Size-exclusion FPLC of the CCMV capsid with the absorbance of eluted materials monitored at two different wavelengths. Inset: cryo-TEM image of the CCMV capsid (scale bar = 20 nm). b) Size-exclusion FPLC of the HRP-containing CCMV capsid. The peak at an elution volume of 1.8 mL corresponds to free HRP (see part c)). The arrow points to a fraction that was collected for further analysis (see part d)). Inset: cryo-TEM image of the HRP-containing CCMV capsid (bar = 20 nm). c) Size-exclusion FPLC of HRP. d) Emission spectra (λ_{exc} = 530 nm) of the HRP-containing CCMV capsid fraction collected from FPLC experiments (as indicated in part b)) and the corresponding fraction of the CCMV capsid devoid of HRP obtained in an analogous fashion.

As in the case of myoglobin, dronpa, and streptavidin (Chapter 6), an additional experiment was performed to compare the encapsulation product with a control experiment in which no assembly/disassembly cycle was applied to investigate the

extent of protein adsorption to the outer surface of the capsid. In this case HRP was labeled with an Alexa Fluor 488 fluorescent dye (λ_{exc} = 494 nm). The capsid and HRP, using the same concentration as that for the encapsulation experiment, were mixed at pH 5, and subsequently, dialyzed against the same pH 5 buffer. After FPLC purification, the fractions corresponding to both the experiment and the control were analyzed by fluorescence spectroscopy (Figure 7.3a). In the case of the control experiment, some emission at λ = 520 nm was present, which indicates that a minor amount of the enzyme is adsorbed to the capsid outer surface. Test experiments using the ABTS colorimetric assay (ABTS = 2,2´-azino bis(3-ethylbenzthiazoline-6-sulphonic acid)) revealed that the HRP-containing CCMV capsid still possessed substantial enzymatic activity (Figure 7.3b).

a)

b)
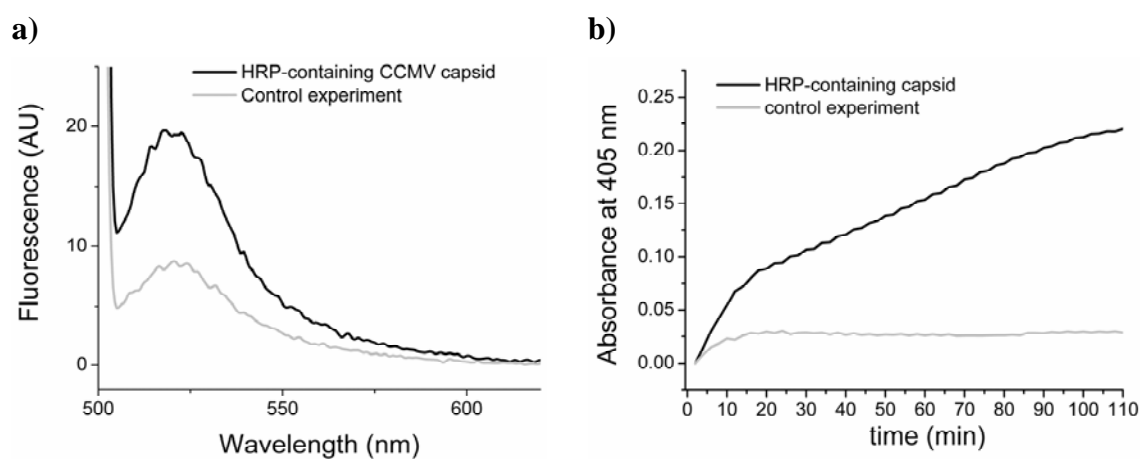
Figure 7.3 *a) Emission spectra (λ_{exc} = 494 nm) of the HRP-containing CCMV capsid fraction and the corresponding fraction of the control experiment. The HRP was labeled with the fluorescent probe Alexa Fluor 488 (λ_{exc} = 494 nm). b) Activity experiment on HRP encapsulated within the CCMV capsid using an ABTS/H_2O_2 assay and the control experiment in which no disassembly/assembly cycle was applied. The H_2O_2 was generated* in situ *by the glucose oxidase/glucose couple.*

Single molecule analysis of the HRP-containing CCMV capsid

The enzymatic activity of the HRP molecules inside the CCMV capsid was examined at the single-molecule level with a confocal fluorescence microscope using the fluorogenic substrate dihydrorhodamine 6G.[1] Dihydrorhodamine 6G acts as a hydrogen donor in the enzymatic reduction of hydrogen peroxide by HRP, yielding the highly fluorescent product rhodamine 6G, which can be easily monitored (Scheme 7.2).
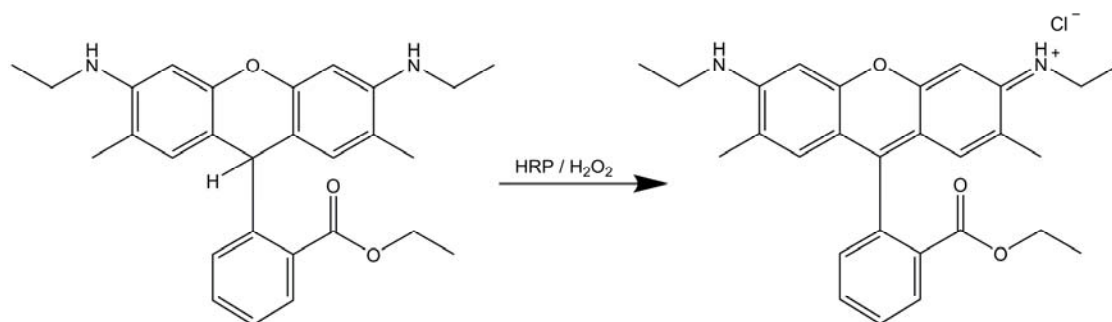
Scheme 7.2 *The substrate dihydrorhodamine 6G is turned into rhodamine 6G in the presence of HRP and hydrogen peroxide.*

Two solutions were prepared: one containing HRP encapsulated inside some of the CCMV capsids and a control solution containing a mixture of empty CCMV capsids and free HRP. Additional control solutions were prepared in which either no HRP or no capsid was present. The solutions were deposited on separate hydrophilic cover slips and, after the addition of a mixture of substrate and hydrogen peroxide, were examined with a laser scanning confocal microscope. The two experiments are schematically depicted in Figure 7.4a and b. Typical images of the activity of HRP inside the CCMV capsid after 10 min of incubation of the mixture are shown in Figure 7.4c. Bright diffraction-limited spots are clearly visible, which are attributed to diffusion of the substrate through the capsid pores, conversion, and accumulation of product molecules inside the capsid. During scanning of several images a decrease in fluorescence intensity due to photobleaching and an increase in the background fluorescence became visible (Figure 7.4e), which points to the continuous formation of product molecules slowly diffusing out of the capsids into the solution. The increase of background fluorescence can also be partially due to some auto-oxidation of the substrate present in solution. Furthermore, by determining the number of capsids per unit area by AFM and comparing it with the number of fluorescent (active) particles, as determined by fluorescence confocal microscopy (Figure 7.4c and inset) in the same area, we confirmed that approximately 1 in every 130 capsids contains an active HRP. This fraction is smaller than that calculated statistically (see above) and would indicate that only part of the encapsulated enzymes retain their activity.

An image of the analysis of the control solution containing the mixture of nonencapsulated HRP and empty CCMV capsid is shown in Figure 7.4d. Localized fluorescence is again observed, but at a much reduced intensity; however, no indication of accumulation of product molecules is detected in this case. In both experiments the localized fluorescence is the result of the continuous formation of the enzyme–product complex,[3] but when the enzyme is encased inside the virus capsid the disappearance of the fluorescence is delayed because of product accumulation in the capsid. Interestingly, in the blank experiment in which HRP was deposited in the absence of the CCMV

capsid, no fluorescence was observed, probably as a result of denaturation of the enzyme on the glass surface.
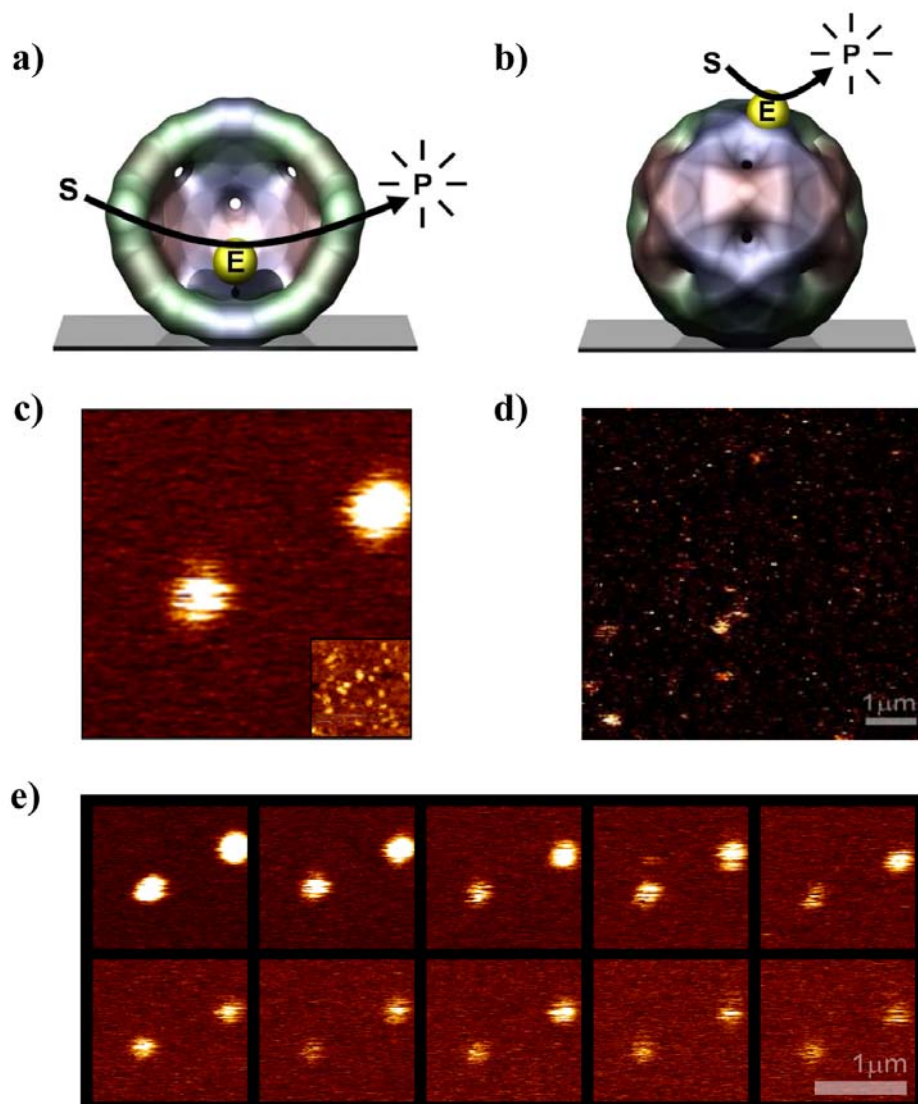
Figure 7.4 HRP enzyme activity in the presence of single CCMV capsids. a) When HRP is encapsulated inside a capsid, substrate molecules (S) diffuse into the capsid and are subsequently converted into product molecules (P), which accumulate before diffusing out through the capsid pores. b) If HRP is adsorbed on the outside of a capsid, diffusion of S or P in or out of the capsid has no effect on the activity of the enzyme. c) A typical confocal fluorescence image (1.68 μm × 1.68 μm) showing the formation of a fluorescent product (rhodamine 6G) from a nonfluorescent substrate (dihydrorhodamine 6G) by HRP encapsulated inside a capsid. Inset: AFM image (to scale) at the same sample location, showing that only a small fraction of the capsids contain an active enzyme molecule. d) A mixture of nonencapsulated HRP and CCMV capsid shows localized activity; no product accumulation is observed. e) Consecutive scanning confocal fluorescence images of HRP encapsulated in CCMV capsid during the catalytic conversion of dihydrorhodamine 6G. The first image shows accumulated

product molecules, which, over time, are bleached until a constant level is obtained. During this time the background fluorescence level increases. The time interval between the images is 144 s.

To further prove that the bright fluorescent spots in Figure 7.4c are the result of enzymatic activity localized inside the capsid, the fluorescence of one of these bright spots was followed over time (Figure 7.5a). A strongly fluctuating intensity trace was clearly visible over time, whereas a time trace at a dark area away from the capsid showed only poissonian background fluorescence. In the case of the nonencapsulated enzyme in the presence of empty capsid, time traces measured at the fluorescent spots (Figure 7.5b) also showed a strongly fluctuating behavior. The enzyme traces were characterized by alternating bursts of fluorescence, followed by relatively long periods of background noise. Initially, we intended to investigate the enzyme behavior by analyzing the individual turnovers, as previously performed in our group for the study of the catalytic activity of single lipase enzymes by using confocal fluorescence microscopy.[6,8] However, this was not a possibility because in the case of the encapsulated HRP the time trace does not reach the background level after each turnover and this is required to apply statistics to the turnovers measured. Therefore, another approach was followed to analyze the above observations, namely, by using FCS. Autocorrelation curves $G(t)$ were calculated from the time traces in Figure 7.5a and b, according to Equation (1):

$$G(t) = \frac{\sum_i (I_i - \bar{I})(I_{i+t} - \bar{I})}{\sum_i (I_i - \bar{I})^2}.$$

(1)

The curves are plotted in Figure 7.5c, and interestingly, the two curves show completely different signatures. The curve for the HRP-included CCMV complex (red squares in Figure 7.5c) fits well with the simple diffusion model given in Equation (2):

$$G(t) = \frac{1}{\bar{N}} \frac{1}{1 + (t/\tau_D)},$$

(2)

in which $\bar{N}$ is the average number of fluorescent product molecules in the observed volume and τ_D is the characteristic diffusion time.[32] In the present example, the best fit is obtained for $\tau_D = 19.5$ ms. For rhodamine in pure water, a τ_D value of 0.04 ms is reported,[33] a difference of almost three orders of magnitude compared with the HRP-containing CCMV capsid. We attribute this difference in τ_D to the hampered diffusion of the product molecules through the pores in the CCMV capsid wall. Although the

diffusion model appears to fit the data nicely, apart from the aimed conversion, processes such as auto-oxidation also probably play a role. Despite this simplification, the model provides solid information about the timescales of the processes that occur and the accumulation of product within the capsid.

The simple diffusion model in Equation (2) could not describe the autocorrelation curve for the nonencapsulated HRP enzyme. In this case, the curve was fitted best by using Equation (3),

$$G(t) = Ae^{-t/\tau},$$

(3)

which is a model for a thermodynamic equilibrium[34] between a fluorescent and a non-fluorescent state, in this case the steady-state equilibrium

enzyme → enzyme–substrate complex → fluorescent enzyme
–product complex* → enzyme.
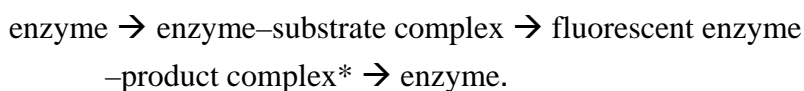
In Equation (3), A is a pre-exponential constant and τ is the turnover time; this, together with the observation that the activity is localized, leads us to conclude that the HRP enzyme molecules are adsorbed to the outside of the capsid.
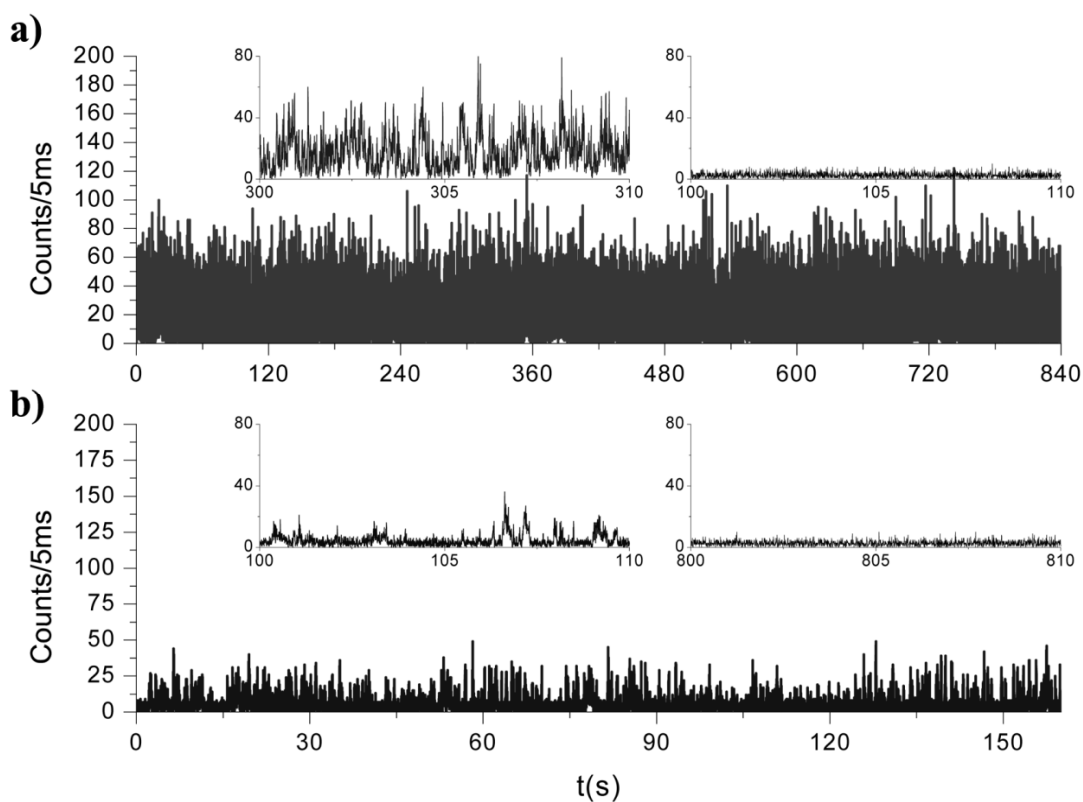
c)
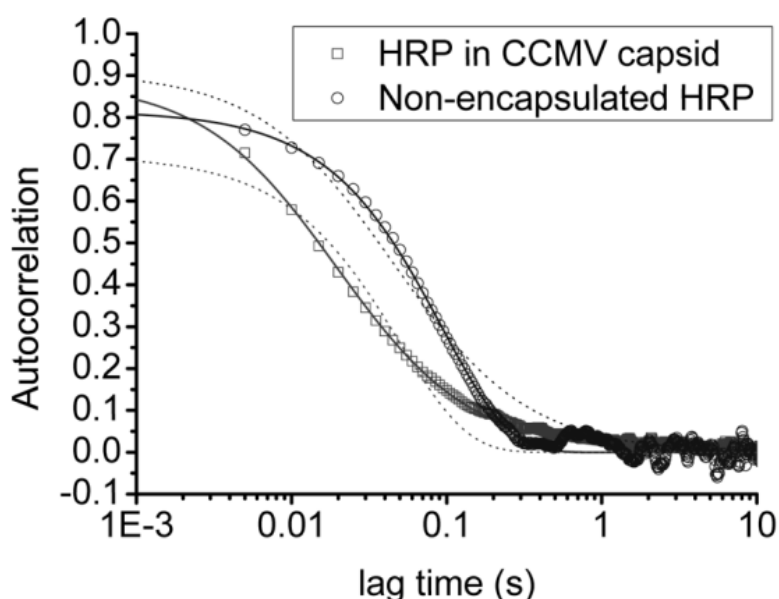
Figure 7.5 Single-capsid experiments. a,b) Fluorescence intensity time traces measured on bright spots in the confocal fluorescence images obtained from samples in which HRP is either a) encapsulated inside a capsid (as depicted in Figure 7.4a) or b) simply mixed with empty CCMV capsids (as depicted in Figure 7.4b). Insets: left, 10 s zoom-in; right, background fluorescence measured at dark areas of the images. c) Fluorescence autocorrelation curves of the traces in a and b. Squares: Fluorescence autocorrelation curve of the HRP–CCMV capsid inclusion complex during catalysis. The continuous line is the best fit obtained by using a diffusion model. Circles: fluorescence autocorrelation curve of the mixture of non-encapsulated HRP and the CCMV capsid. The continuous line is the best fit obtained by using a model for a chemical equilibrium.[34] To emphasize the difference between the two models, each curve is also fitted with the model used for the other case (dotted lines), yielding very poor fits.

Confocal analysis of the CCMV capsid permeability when varying pH

The pore size of the intact CCMV is known to depend on the pH.[35] At pH 5 the virus is compact with small pores (< 2 nm), but at pH 7.5 it is swollen and contains pores of ≥ 2 nm. Upon standing at this pH, depending on the salt concentration, the virus slowly disassembles into dimers such information on pore size is not available in the literature for the CCMV capsid. To investigate the influence of the pore size on the behavior of the capsid nanoreactor, the apparent diffusion times τ_D of one single capsid at several pH values were measured (Figure 7.6). After addition of substrate and having localized a fluorescent spot corresponding to a single capsid, aliquots of NaOH solution were added to the sample on the glass support. Two minutes after every addition, time traces were collected, always on the same spot. The time traces were subsequently autocorrelated

143

for every pH value (Figure 7.6a) and all curves fitted well with a diffusion model. The diffusion time τ_D clearly decreased when the pH was increased and revealed a step at around pH 5.7, as observed in the plot in Figure 7.6b. This experiment indicates that the permeability of the capsid wall increases by a factor of 2–3 when the pH increases, which is probably associated with the formation of larger pore sizes. We can rule out the possibility that the decrease of τ_D by increasing the pH is due to an effect of the pH on the HRP activity. The optimum pH for HRP is in the range of 6.0 to 6.5, and the activity at 7.5 is 84% of the maximum activity, which means that upon increasing the pH fewer products are formed per unit of time. These observations, furthermore, indicate that the monitored processes take place inside the capsid cavity.
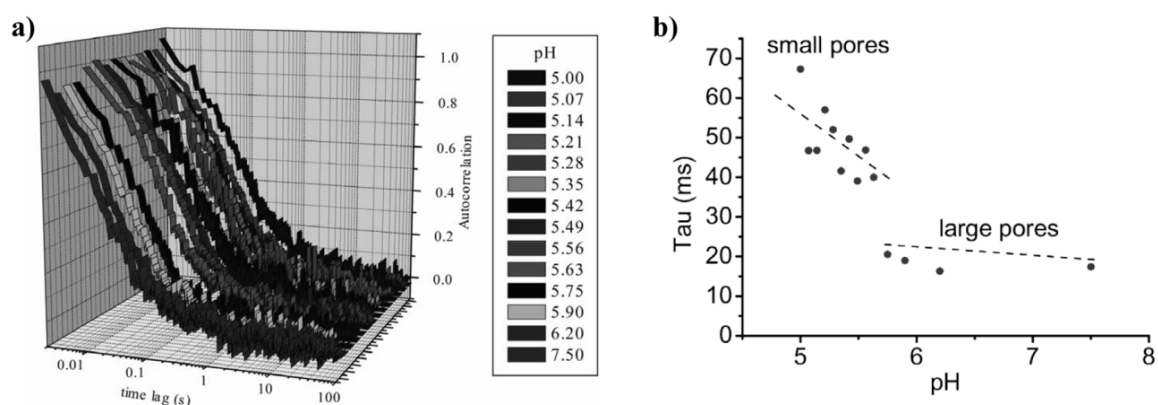
Figure 7.6 a) Fluorescence autocorrelation curves obtained when studying the permeability of the HRP-containing CCMV capsid is studied as a function of pH. b) Measured correlation times τ_D as a function of pH during the enzymatic formation of rhodamine 6G by the HRP–CCMV capsid inclusion complex showing a step at pH 5.7, indicating a sudden increase in pore size.

7.3 Conclusion

The assembly–disassembly properties of CCMV allowed us to encapsulate HRP in the CCMV capsid by using the inclusion protocol described in Chapter 6 for different proteins. In this way we were able to construct the first enzyme-loaded viral nanoreactor. The inclusion of HRP is a statistical process in which the number of encased enzymes is determined by the starting concentration of the enzyme. Under the applied experimental conditions, it can be assumed that, as intended, not more than one HRP enzyme molecule was encapsulated within a CCMV particle. The activity of the encapsulated enzyme was studied at the single-capsid level by using confocal fluorescence microscopy. The resulting data provided information about the location of

the enzyme, that is, in the CCMV capsid or on the capsid outer surface, and about the permeability of the viral capsid when changing the solution conditions, namely, pH.

7.4 Experimental Section

Materials

Sodium acetate trihydrate (>99%) and uranyl acetate dihydrate (≥98%), D-(+)-glucose monohydrate (≥99.5%), and ABTS (≥99%) were purchased from Fluka. Ethylenediaminetetraacetic acid (EDTA) disodium salt dihydrate (>99%), tris(hydroxymethyl)aminomethane (Tris) (>99%), calcium chloride dihydrate (>99%), and sodium chloride (99.5%) were purchased from Acros. Type XII HRP (E.C. 1.11.1.7), type X-S from Aspergillus niger glucose oxidase (E.C. 1.1.3.4), and phenylmethanesulfonyl fluoride (PMSF) (≥98.5%) were purchased from Sigma Aldrich. HRP was labeled by using Alexa-Fluor 532 succinimidyl ester or Alexa Fluor 488 carboxylic acid TFP ester, bis(triethylammonium salt), following the protocol provided with the labeling kits by the supplier (Molecular Probes, Invitrogen). Dihydrorhodamine 6G was purchased from Molecular Probes, Invitrogen.

Instrumentation

UV/Vis spectroscopy was performed on a Varian Cary 50 spectrophotometer at room temperature using a 45 μL quartz fluorescence cell (Hellma, light path: 3 mm). The reference spectrum of the corresponding buffers were subtracted from all UV/Vis spectra.

Fluorescence spectroscopy was performed on a Perkin–Elmer LS 50B fluorescence spectrophotometer. Experiments were carried out using a 45 μL quartz fluorescence cell (Hellma, light path: 3 mm) at 10 °C.

Fast protein liquid chromatography (FPLC) was performed on an Ettan Akta LC system equipped with a Superose 6 PC 3.2/30 column from Amersham Biosciences (flow rate: 40 μL min^{-1}). Injections of 20 μL aliquots of the samples on the FPLC column at room temperature were monitored by UV/Vis detection at 403 nm, 280 nm, and 260 nm.

Dialysis was performed by using dialysis tubing (Spectra/Por 4, MWCO: 12–14 kD, Flat width: 25 mm) purchased from Spectrum Laboratories and a D-tube dialyzer (MWCO: 12–14 kD, volume: 1–3 mL) from Novagen.

Cryo-transmission electron microscopy images were obtained by applying small aliquots (3 μl) of the solutions to Quantifoil grids (R2/2 Quantifoil Jena) within the environmental chamber (relative humidity 100%) of an automated vitrification robot, namely, an FEI Vitrobot™ Mark III at 22 °C. The Quantifoil grids were treated with a

surface plasma treatment using a Cressington 208 carbon coater operating at 5 mA for 40 s prior to the sample preparation and vitrification procedure. The sample vitrification procedure consisted of automated blotting and plunging into liquid ethane. After vitrification the grids were transferred to a Gatan cryo-holder operating at approximately $-170\,°C$. TEM was performed under low-dose conditions on an FEI Titan Krios equipped with a field emission gun (FEG) operating at 300 kV. Images were recorded by using a Gatan GIF energy filter and a $2k \times 2k$ Gatan CCD camera.

Confocal fluorescence microscope setup: Laser light (Spectra-Physics 2080 argon ion laser, 488 nm) was coupled into a single-mode optical fibre, passed through a 488-nm interference filter, reflected by a dichroic beam splitter (Chroma, 505dcxr) and focused on the sample by an oil immersion ×100 objective lens (Karl Zeiss, NA = 1.30), which was mounted on a Karl Zeiss Axiovert 200 inverted microscope. The confocal volume of the sample beam was determined to be 0.5 fl. The power density at the sample was $1–2\,kW\,cm^{-2}$. Fluorescent light emitted from the focal volume was collected by the same objective, passed through the dichroic beamsplitter, filtered (Chroma, HQ500lp), guided through a 50 μm pinhole, and finally focused on an avalanche photo diode (Perkin–Elmer SPCM-AQR-14), which was coupled to a National Instruments PCI-6036E data acquisition card operating at 20 MHz. The sample was mounted onto a JPK TAO nanopositioner. Data collection and analyses were carried out with programs written in National Instruments LabVIEW 7.1.

Atomic force microscopy (AFM) measurements were performed on a JPK (Berlin, DE) Nanowizard machine with a 100×100 μm XY scanner and a TAO (tip-assisted optics) module. Experiments were carried out with 125 μm long silicon tips (Nanoworld [Neuchatêl, CH] NCH 20 POINTPROBE) with average nominal resonant frequencies of 320 kHz and average nominal force constants of $42\,N\,m^{-1}$. Scanning was performed in the tapping mode at a speed of 1 line s^{-1} with amplitude setpoints of 0.7 V. JPK SPM software was used to control the AFM and to process (linear leveling) the data. The sample was prepared by spin-coating onto a thoroughly cleaned objective glass after which the measurements were carried out.

HRP encapsulation experiment

HRP encapsulation in the CCMV capsid: The purification of CCMV and the isolation of its coat protein were performed as described in Chapters 3 and 4. A solution containing the proteins that comprise the CCMV coat (300 μl, 22.1 mg mL^{-1}) in sodium acetate buffer (0.05 M, pH 5) was dialyzed against three changes of Tris–HCl buffer (500 mL, 0.05 M, pH 7.5) (3 h per change). When the solution had reached pH 7.5, the guest enzyme solution (300 μl) in Tris–HCl buffer (0.05 M, pH 7.5) was added in excess (66 equiv of HRP per capsid particle—one capsid particle corresponds to 90 capsid protein dimers) and the resulting solution was incubated for 1.5 h. Dialysis of the

incubated solution against the initial sodium acetate buffer was carried out under the same dialysis conditions as above. The samples were concentrated and the free guest enzyme was removed by using centrifugal filter devices (Centricon YM-100, Millipore). The samples obtained from the encapsulation and control experiments were analyzed and purified by FPLC. Injections of 20 μl aliquots of the samples on the FPLC column at room temperature were monitored by using UV detection at 280 and 403 nm. Fractions of 60 μl were collected and those corresponding to the purified HRP-containing CCMV capsid, were further analyzed by fluorescence spectroscopy and TEM. The HRP used in the experiments was labeled with Alexa Fluor 532 dye (λ_{exc} = 530 nm).

All buffer used solutions contained 1 mM EDTA, 300 mM NaCl, 10 mM $CaCl_2$, and 0.2 mM phenylmethylsulphonyl fluoride. Buffers were stored at 4 °C, and the dialysis was performed in a cold room at 4 °C. Later experiments showed better results when 500 mM of NaCl was used instead of 300 mM. An increase in the amount of salt enhances the stability of the assembled capsid (for further details about the assembly see Chapter 4).

 Activity of HRP-containing CCMV capsids in bulk: The purified fractions of the HRP-containing CCMV capsids obtained after FPLC were subjected to the HRP activity assay. An ABTS/glucose oxidase (GOx)/glucose solution was prepared in a sodium acetate buffer (1 mL, 0.05 M, pH 5) with [ABTS] = 0.26 mM, [GOx] = 10–6 mM, and [glucose] = 41 mM. Subsequently, an aliquot (5 μL) of the fraction containing HRP encapsulated in the CCMV capsid, or the corresponding fraction of the control experiment, was added to 115 μL of the solution. The enzyme activity was monitored by measuring the absorbance at 405 nm using UV/Vis spectroscopy on a Perkin-Elmer Wallac 1420 Victor multilabel counter. A similar experiment was performed for free HRP in solution.

Confocal fluorescence microscopy studies

Study of the encapsulated HRP activity at the single-molecule level by confocal fluorescence microscopy: A solution of the HRP-containing CCMV capsid (10 μl, 3 μg L^{-1}) was spin-coated at 4000 r.p.m. on a clean, hydrophilic cover glass after which the glass was quickly rinsed with 4×1 mL of MilliQ water while spinning. After mounting the sample on the microscope, 200 μl of a solution containing 120 μM of H_2O_2 and 0.5 μM of dihydrorhodamine 6G was added. Dihydrorhodamine 6G acts as a hydrogen donor in the enzymatic reduction of hydrogen peroxide by HRP, yielding the highly fluorescent product rhodamine 6G. As a control experiment for the activity studies at the single-molecule level, a mixture of nonencapsulated HRP and CCMV capsid solution was prepared and analyzed by confocal fluorescence microscopy in the same way as described above for the HRP-containing CCMV capsid.

Study of the CCMV capsid permeability by confocal fluorescence microscopy: To investigate the influence of the pH on the behaviour of the viral nanoreactor, the apparent diffusion times τ_D of a single capsid at several pH values were measured. Samples were prepared in the same way as described above. After the addition of the substrate and having localized a fluorescent spot corresponding to a single HRP-containing capsid, 2-μL aliquots of a NaOH solution (0.1 M) were added every 5–7 min. The volume of the aliquots was chosen based on the results on larger scale experiments, in which the pH was monitored by using a pH-meter. During the confocal experiments, the pH was confirmed with the help of pH indicator paper. After every addition, the area where the spot was localized was scanned to check its position and a 2 min time trace was measured, always on the same spot. The autocorrelation curves were calculated from the time traces for every pH and the diffusion time τ_D was deduced for every one of them. All curves fitted well with the diffusion model, but the correlation time τ_D varied upon changing the pH.

7.5 References

[1]   L. Edman, Z. Foldes-Papp, S. Wennmalm, R. Rigler, *Chem. Phys.* **1999**, *247*, 11.

[2]   G. De Cremer, M. B. Roeffaers, M. Baruah, M. Sliwa, B. F. Sels, J. Hofkens, D. E. De Vos, *J. Am. Chem. Soc.* **2007**, *129*, 15458.

[3]   O. Flomenbom, K. Velonia, D. Loos, S. Masuo, M. Cotlet, Y. Engelborghs, J. Hofkens, A. E. Rowan, R. J. M. Nolte, M. Van der Auweraer, F. C. de Schryver, J. Klafter, *Proc. Natl. Acad. Sci. U.S.A.* **2005**, *102*, 2368.

[4]   W. Min, B. P. English, G. Luo, B. J. Cherayil, S. C. Kou, X. S. Xie, *Acc. Chem. Res.* **2005**, *38*, 923.

[5]   H. P. Lu, L. Xun, X. S. Xie, *Science* **1998**, *282*, 1877.

[6]   H. Engelkamp, N. S. Hatzakis, J. Hofkens, F. C. De Schryver, R. J. M. Nolte, A. E. Rowan, *Chem. Comm.* **2006**, 935.

[7]   P. Tinnefeld, M. Sauer, *Angew. Chem. Int. Ed.* **2005**, *44*, 2642.

[8]   N. S. Hatzakis, H. Engelkamp, K. Velonia, J. Hofkens, P. C. M. Christianen, A. Svendsen, S. A. Patkar, J. Vind, J. C. Maan, A. E. Rowan, R. J. M. Nolte, *Chem. Comm.* **2006**, 2012.

[9]   D. M. Vriezema, M. Comellas Aragones, J. A. A. W. Elemans, J. J. L. M. Cornelissen, A. E. Rowan, R. J. M. Nolte, *Chem. Rev.* **2005**, *105*, 1445.

[10]   T. Douglas, D. P. E. Dickson, S. Betteridge, J. Charnock, C. D. Garner, S. Mann, *Science* **1995**, *269*, 54.

[11]   F. C. Meldrum, B. R. Heywood, S. Mann, *Science* **1992**, *257*, 522.

[12]   T. Ueno, M. Suzuki, T. Goto, T. Matsumoto, K. Nagayama, Y. Watanabe, *Angew. Chem. Int. Ed.* **2004**, *43*, 2527.

[13] F. P. Seebeck, K. J. Woycechowsky, W. Zhuang, J. P. Rabe, D. Hilvert, *J. Am. Chem. Soc.* **2006**, *128*, 4516.

[14] Z. Varpness, J. W. Peters, M. Young, T. Douglas, *Nano Lett.* **2005**, *5*, 2306.

[15] T. Douglas, M. Young, *Nature* **1998**, *393*, 152.

[16] T. Douglas, E. Strable, D. Willits, A. Aitouchen, M. Libera, M. Young, *Adv. Mater.* **2002**, *14*, 415.

[17] T. Douglas, M. Young, *Science* **2006**, *312*, 873.

[18] C. E. Flynn, S.-W. Lee, B. R. Peelle, A. M. Belcher, *Acta Mater.* **2003**, *51*, 5867.

[19] W. Shenton, T. Douglas, M. Young, G. Stubbs, S. Mann, *Adv. Mater.* **1999**, *11*, 253.

[20] E. Dujardin, C. Peet, G. Stubbs, J. N. Culver, S. Mann, *Nano Lett.* **2003**, *3*, 413.

[21] C. B. Mao, D. J. Solis, B. D. Reiss, S. T. Kottmann, R. Y. Sweeney, A. Hayhurst, G. Georgiou, B. Iverson, A. M. Belcher, *Science* **2004**, *303*, 213.

[22] N. Carette, H. Engelkamp, E. Akpa, S. J. Pierre, N. R. Cameron, P. C. Christianen, J. C. Maan, J. C. Thies, R. Weberskirch, A. E. Rowan, R. J. M. Nolte, T. Michon, J. C. Van Hest, *Nat. Nanotechnol.* **2007**, *2*, 226.

[23] P. S. Arora, K. Kirshenbaum, *Chem. Biol.* **2004**, *11*, 418.

[24] Q. Wang, T. R. Chan, R. Hilgraf, V. V. Fokin, K. B. Sharpless, M. G. Finn, *J Am Chem Soc* **2003**, *125*, 3192.

[25] J. M. Hooker, E. W. Kovacs, M. B. Francis, *J. Am. Chem. Soc.* **2004**, *126*, 3718.

[26] A. de la Escosura, R. J. M. Nolte, J. J. L. M. Cornelissen, *J. Mater. Chem.* **2009**, *19*, 2274.

[27] D. Woll, E. Braeken, A. Deres, F. C. De Schryver, H. Uji-i, J. Hofkens, *Chem. Soc. Rev.* **2009**, *38*, 313.

[28] M. A. Medina, P. Schwille, *Bioessays* **2002**, *24*, 758.

[29] E. Haustein, P. Schwille, *Annu. Rev. Biophys. Bio.* **2007**, *36*, 151.

[30] W. W. Webb, *Appl. Optics* **2001**, *40*, 3969.

[31] R. Rigler, U. Mets, J. Widengren, P. Kask, *Eur. Biophys. J. Biophy.* **1993**, *22*, 169.

[32] O. Krichevsky, G. Bonnet, *Rep. Prog. Phys.* **2002**, *65*, 251.

[33] M. Kinjo, R. Rigler, *Nucleic Acids Res.* **1995**, *23*, 1795.

[34] S. Wennmalm, L. Edman, R. Rigler, *Proc. Natl. Acad. Sci. U.S.A.* **1997**, *94*, 10641.

[35] J. A. Speir, S. Munshi, G. J. Wang, T. S. Baker, J. E. Johnson, *Structure* **1995**, *3*, 63.

CHAPTER 8

Controlled Integration of Polymers into Viral Capsids

8.1 Introduction

Based on their reciprocal relationship, biology and chemistry are converging more and more into a new discipline called chemical biology. This discipline aims to understand biological issues at the chemical level, for instance, by the probing of biomolecules with synthetic compounds that interact with them. An opposite trend is also receiving much attention, namely, the synthesis of new materials and catalytic systems inspired by biological structures and pathways.[1,2] In this context viruses are also playing a role as a biological object that can be chemically modified. Viruses are biological entities that operate at the interface of non-living and living matter and as such they occupy a special and unique position.[3] Although they are structurally complex, viruses do not have a metabolism of their own and their chemical machinery is relatively simple to manipulate. The size and shape of viruses, as well as the number and location of the functional groups on their inner and outer surfaces, are precisely defined. A new emerging field uses viruses as platforms for the controlled positioning of chemical species with different functions at the nanoscopic level.[4,5]

The decoration of the outer surfaces of icosahedral and rod-like viruses, using genetic and chemical manipulation has been explored in recent years by a number of groups. Different moieties, including metal nanoparticles, fluorescent dyes, biotin, histidine tags, carbohydrates, DNA, peptides, proteins, conducting compounds, and luminescent quantum dots, have been attached to a variety of viruses.[4-8] Also the use of the hollow cavities of icosahedral viral capsids and other protein cages has been explored, for example, as nanocontainers. For instance, inorganic nanoparticles, can be easily synthesized by nucleating mineralization reactions inside nucleic acid free viral capsids of different sizes.[9,10] The catalysis of organic reactions within these nanocontainers is also possible. Reactions catalyzed by encapsulated metal clusters,[11-14] palladium complexes,[15] and enzymes, have been reported in the literature.[16]

The covalent attachment of natural[17,18] and synthetic organic polymers to the exterior surface of a virus particle is an interesting approach to broaden the applications of viruses in medicine and nanotechnology.[19] Such modification might change the stability of the viral cages. Synthetic polymers may also impart solubility in organic solvents and new self-assembling properties to the virus particles. To date only three examples of the functionalization of the outer surface of viral capsids with synthetic polymers are known in the literature. The outer surfaces of the tobacco mosaic virus (TMV),[20] the cowpea mosaic virus (CPMV),[21-23] and the bacteriophage MS2[24] have been modified with poly(ethylene glycol) (PEG) and the resulting conjugates were found to display new solubility properties and altered immunogenicity, consistent with the known chemical and biological properties of PEG.[25,26]

The encapsulation of synthetic polymers inside viral capsids allows the formation of so-called virus-like particles (VLPs), which have the potential to be used as new building blocks for the preparation of nanostructured materials.[27] Given their large size, macromolecules cannot penetrate a virus through its pores, requiring that the virus particle displays the ability to reversibly disassemble/assemble to allow the polymer molecule to be encapsulated. One of the most widely studied viruses in this context is the cowpea chlorotic mottle virus (CCMV).[28] The icosahedral capsid of CCMV has an outer diameter of 28 nm and a well-defined inner cavity with a diameter of 18 nm. It is formed from 90 homodimers of 20 kDa coat protein (CP) subunits arranged with $T = 3$ Caspar-Klug symmetry around a central RNA strand. The CP consists of 189 amino acids with nine basic residues at the N-terminal RNA binding domain. An interesting property of CCMV is its reversible disassembly–assembly behavior depending on the pH and ionic strength.[29] By varying these conditions, CCMV virions can be disassembled *in vitro* into protein dimers and, after removal of the RNA, re-assembled again to form empty capsids. This pH-dependent behavior, has been used to encapsulate a number of species, such as proteins,[16] inorganic nanoparticles,[30,31] and polymers.[32,33]

Despite the fact that the CCMV capsid was assembled *in vitro* for the first time more than 40 years ago,[34] the mechanistic understanding of the assembly process is still not completely clear, especially with regards to the occurrence of polymorphism when the viral proteins are assembled in the presence of different types of cargoes. The CCMV coat protein can form, depending on the conditions, a variety of structures including tubes and icosahedral capsids with Caspar-Klug triangulation numbers of $T = 1, 3, 4$, and 7 (see Appendix).[35,36] Inclusion of negatively charged polymers strongly influences the CP self-assembly process, giving rise to the formation of VLPs with only one of the above-mentioned symmetries. Polystyrene sulfonate (PSS), for example, is able to produce $T = 1$ particles at neutral pH[32] and particles with a $T = 2$ or 3 geometry at pH 5,[33] whereas tubular structures are obtained when double-stranded DNA is used

as the polymeric cargo.[37] The covalent modification of the protein molecules on the outer surface of CCMV capsids is also expected to alter their stability and assembly properties in a similar way as observed for other types of viruses.[38] This may be particularly relevant when organic polymers are used as decoration motifs, owing to the characteristic phase behavior of these polymers. Understanding the interplay between the different effects that the incorporation of organic polymers, either inside the viral capsid or covalently attached to the outer surface, can have on the stability and assembly of VLPs appears to be a crucial factor in the design and preparation of virus–polymer hybrid materials.

As part of our efforts to develop methodologies that enable the precise positioning of different synthetic polymers in viral architectures, we describe herein the controlled attachment of PEG to the outer surface of the CCMV capsid and the incorporation of PSS into the inner cavity of this virus. Our strategy relies on the combined use of the assembly–disassembly properties of the viral protein and the successive incorporation of the two polymers (Scheme 8.1). First, the native CCMV is modified by the covalent binding of PEG chains to its surface. At this stage the interfering functionalization of internal lysine and arginine residues is blocked because they strongly interact with the viral nucleic acid that is still present inside the capsids. After complete dissociation of the modified virus into protein subunits and precipitation of the RNA, the addition of PSS results in the formation of VLPs. PSS does not only play the role of guest during the encapsulation process, but also acts as a template for the assembly. The electrostatic interactions between PSS and the positive N termini of the CPs are the driving force to overcome the lower tendency of PEG-functionalized protein subunits to associate with each other.
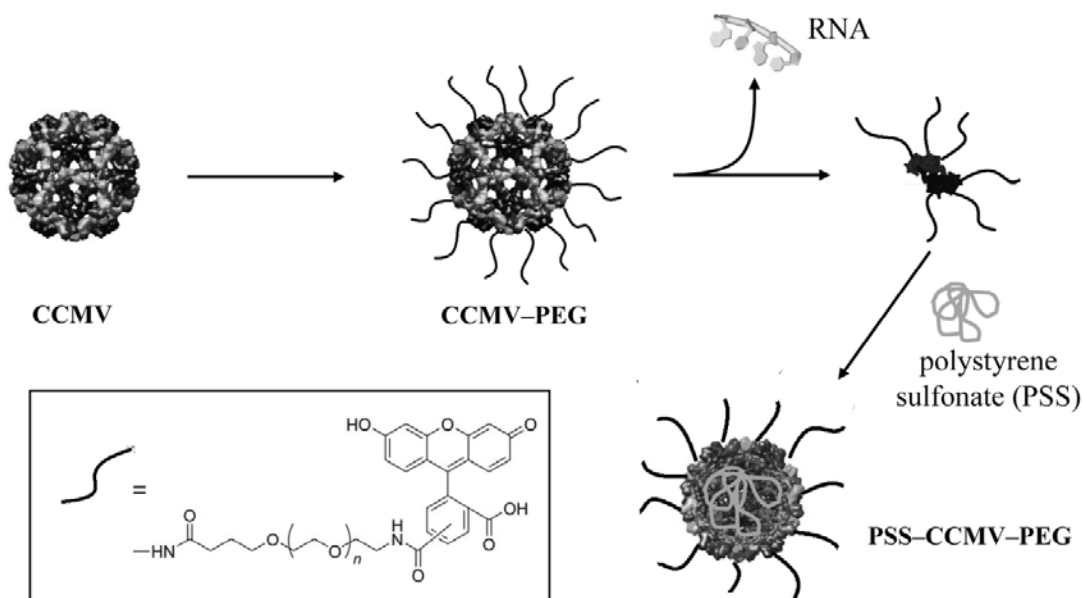
Scheme 8.1 *Schematic pathway for the formation of PSS–CCMV–PEG virus-like particles.*

8.2 Results and Discussion

Formation of PEG-functionalized CCMV

According to the crystallographic data of the CCMV structure, there are four lysine groups per subunit accessible on the exterior surface, from which only three seem to be available for functionalization.[39,40] This abundance of reactive amine groups on the virus surface allows for facile and high-yielding modification by using *N*-hydroxysuccinimide (NHS) esters. Hence, the current study began with the synthesis of α-NHS ester ω-fluorescein-functionalized PEG with $M_n = 3000$ Da (compound **1** in Scheme 8.2). Labeling with a fluorescein moiety was used as a means to advance the characterization of the CCMV–PEG hybrids.

In the first step α-amine ω-carboxylic acid PEG ($M_n = 3000$) was treated with fluorescein carrying an NHS-activated ester moiety to obtain polymer **2** (Scheme 8.2). Complete conversion was indicated by ^{1}H NMR spectroscopy, which showed that the signals corresponding to the protons next to the amine moiety ($\delta = 3.1$ ppm) in the polymer had disappeared, confirming the successful attachment of the fluorescent dye. Subsequently, the remaining carboxylic acid functionality of PEG was converted into an activated ester by 1-ethyl-3-(3-dimethylaminopropyl) carbodiimide hydrochloride (EDC) coupling with NHS. The stoichiometry was chosen such that only the α-carboxylic acid group of PEG was activated and not the carboxylic acid moiety on the fluorescein. ^{1}H NMR spectroscopy and MALDI-TOF analysis confirmed the formation of compound **1**.
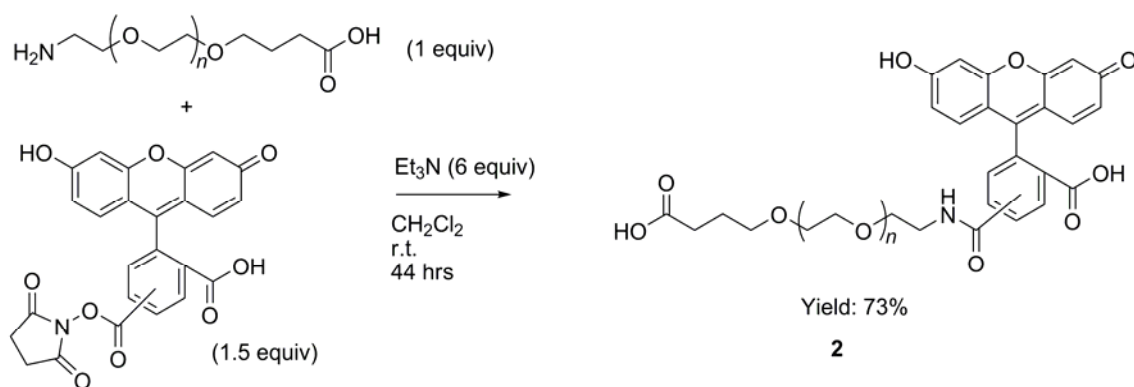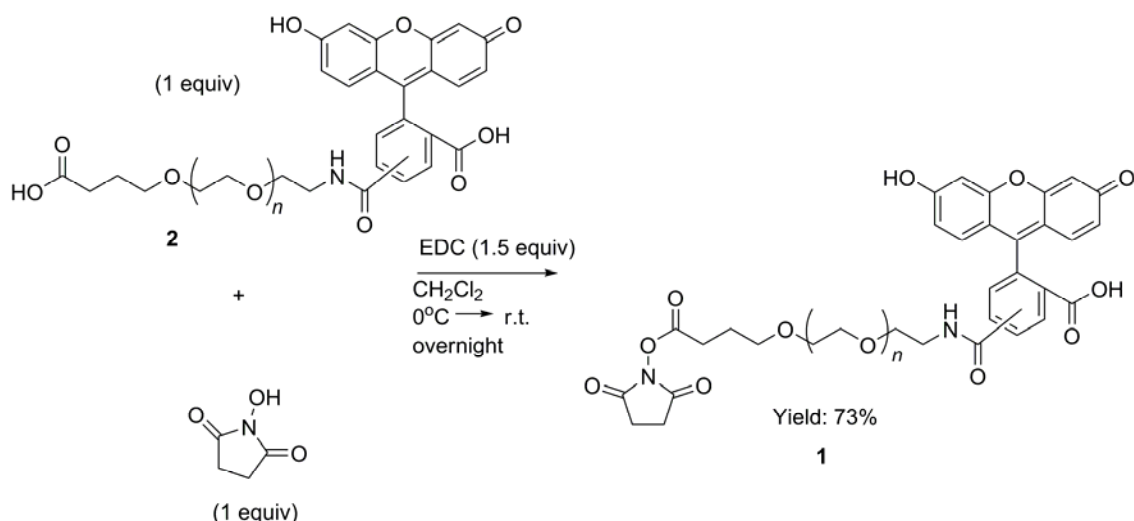
Scheme 8.2 *Synthesis of α-NHS ester ω-fluorescein-functionalized PEG (**1**).*

The attachment of PEG chains to CCMV was accomplished by mixing compound **1** with a solution of this virus in phosphate buffer (pH 7.5) (Scheme 8.3) at various CCMV CP / PEG molar ratios (samples **A** (1:50), **B** (1:25), **C** (1:10), and **D** (1:1)). The mixtures were incubated for 2 h at room temperature and subsequently kept overnight at 4 ℃. As a control experiment CCMV was mixed with α-carboxylic acid ω-fluorescein functionalized PEG-3000 (**2**) (Scheme 8.2), the unactivated polymer derivative, in a CP / PEG molar ratio of 1:50. In all cases, the virus–polymer products were purified by SEC using a Sephadex G-100 preparative column. A clear separation between the functionalized virus and the excess polymer was observed for the samples containing **1**.
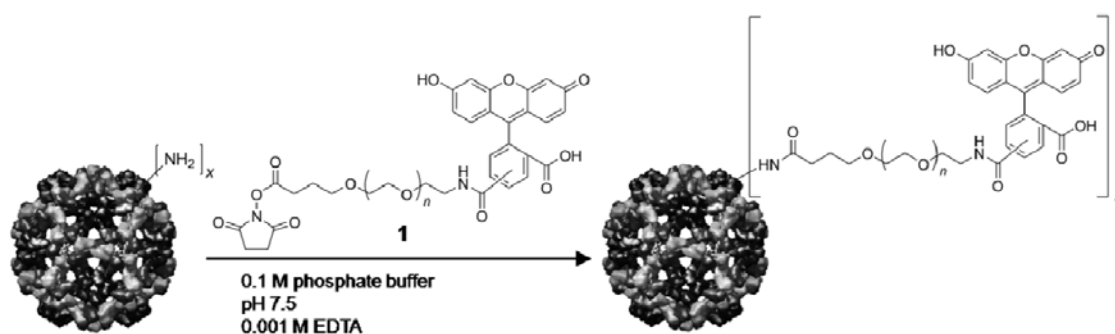
Scheme 8.3 *Functionalization of the CCMV surface-exposed amine groups with **1**.*

The presence of virus–polymer conjugates was confirmed by UV/Vis spectroscopy, fast protein liquid chromatography (FPLC), transmission electron microscopy (TEM), and gel electrophoresis (Figure 8.1). The FPLC chromatograms of all samples (**A**–**D**) showed peaks at a retention volume of $V = 0.90$ mL, which is lower than the characteristic elution volume of the virus under the same conditions ($V = 1.06$ mL) (Figure 8.1a), suggesting the formation of larger particles.[41] The formation of

polymer–virus conjugates was further evidenced by the clear absorption at $\lambda = 490$ nm (for the peak at $V = 0.90$ mL) resulting from the fluorescein moiety attached to the polymer. The UV/Vis spectra of fractions taken directly from the FPLC column at $V = 0.90$ mL showed absorption bands from both the polymer ($\lambda = 490$ nm) and the virus ($\lambda = 260$ nm), corroborating the FPLC results.

The same conclusion could be drawn from agarose gel experiments, in which the virus–polymer conjugates were found to run slower than the native virus (Figure 8.1b). SDS-polyacrylamide gel electrophoresis (SDS-PAGE) confirmed the covalent attachment of several polymeric chains to the protein subunits, namely, the presence of additional bands above the underivatized capsid proteins (Figure 8.1c and d). The average number of PEG chains per protein subunit could be estimated from the ratio of the absorbance values at $\lambda = 490$ and 260 nm for the FPLC fractions at $V = 0.90$ mL. A good correlation with the initial ratios of protein and polymeric material used to prepare the reaction mixtures was observed. A maximum number of 2–3 PEG chains per protein subunit were found in the case of a 1:50 initial CP / PEG ratio (Figure 8.1e), which is in good agreement with the anticipated number of available amine groups on the outer surface of CCMV. The SDS-PAGE results suggest that the degree of functionalization of the coat protein is similar for all samples **B**–**D** (Figure 8.1c), while sample **A** contains small amounts of protein having a higher degree of functionalization (Figure 8.1d). The varying ratios of PEG / CP observed in Figure 8.1e likely originate from differences in the amount of PEG-functionalized CP subunits in the conjugates rather than to their different degrees of functionalization. According to Figure 8.1e and taking in account that there is always a mixture of PEG-functionalized and non-functionalized CP in all samples, the degree of functionalization for samples **B**–**D** corresponds to a CP monomer functionalized with 3 PEG tails.

The CCMV–PEG particles were deposited on a carbon-coated copper grid and studied with TEM (Figure 8.1a, inset). The measured virus particle diameters were in agreement with the diameter of the wild-type virus (ca. 28 nm). None of the above techniques showed evidence for the formation of CCMV–PEG conjugates in the control experiment.
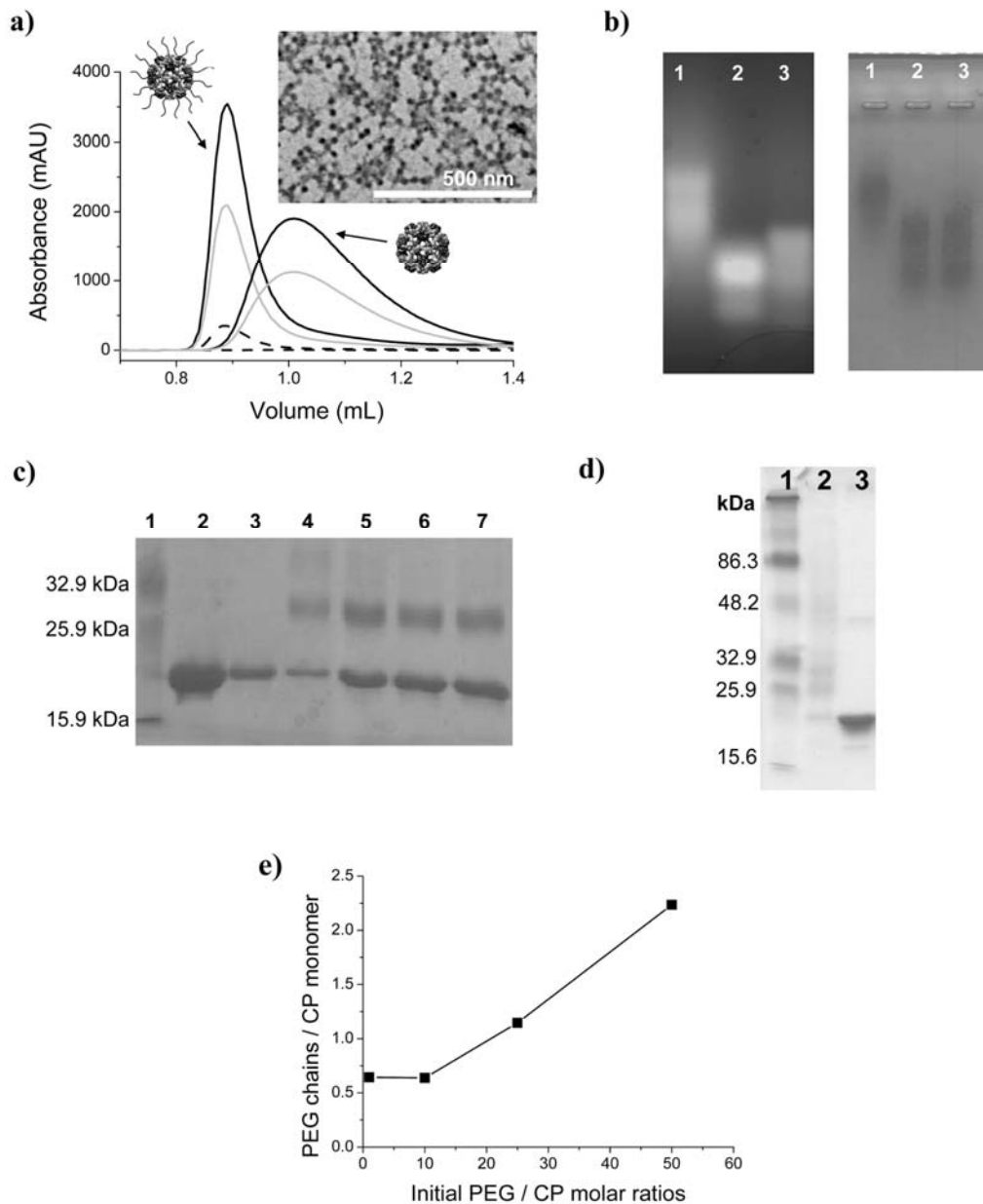
Figure 8.1 *Analysis of the CCMV–PEG conjugates. a) FPLC chromatograms of SEC-purified sample **B** (1:25), and wild-type CCMV under the same conditions of pH and ionic strength (detection at 280 nm (grey), at 260 nm (black), and at 490 nm (dash)). Inset: TEM micrograph of the FPLC fraction corresponding to the CCMV–PEG conjugate. b) Agarose gels showing the CCMV–PEG conjugates (lane 1), CCMV virus (lane 2), and CCMV + inactivated polymer **2** (lane 3) visualized under a fluorescence image analyzer. RNA detection (left) and protein detection (Coomassie Blue staining, right). c) SDS-PAGE gel showing the protein size marker (lane 1), CCMV virus (lane 2), CCMV + inactivated polymer **2** (lane 3), and samples **A** (1:50; lane 4), **B** (1:25; lane 5), **C** (1:10; lane 6), and **D** (1:1; lane 7), all visualized using Coomassie Blue staining. d) SDS-PAGE gel showing the protein size marker (lane 1), different batch of sample **A** (1:50; lane 2), and CCMV + inactivated polymer (**2**) (lane 3), all visualized using Coomassie Blue staining. The bands that appear above 40 kDa*

observed for 2 and 3, correspond to dimers that have not been completely released during the denaturation process. e) Plot showing the estimated number of PEG chains per CP subunit versus the initial PEG / CP molar ratios used to prepare the reaction mixtures.

Stability of PEG-functionalized CCMV

During the characterization of samples **A**–**D** by FPLC it was observed that a substantial decrease in the intensity of the peak at $V = 0.90$ mL occurred after successive injections of the same sample. It seemed from these data that the grafting of PEG chains onto CCMV forced, to a certain degree, the disassembly of its capsid. To unravel the details and extent of this process, the stability of the CCMV–PEG assemblies was systematically studied over time. All samples showed the same behaviour, therefore, only the results for sample **B** are shown (Figure 8.2). The mixture obtained after the reaction and the preliminary SEC purification (Sephadex G-100) was analyzed by FPLC at different times over a three week period. Besides the peak at $V = 0.90$ mL, two additional peaks were initially present in every FPLC chromatogram (Figure 8.2a), which seem to correspond to polymer aggregates ($V = 1.60$ mL) and the polymer itself ($V = 1.95$ mL), which in addition co-elutes with non assembled derivatized and underivatized CP (see below). Their assignment is discussed in the Experimental Section in detail (see Section 8.4). A decrease in the intensity of the peak at $V = 0.90$ mL, recorded by following the absorbance at $\lambda = 280$ nm, was observed over time (Figure 8.2b). Simultaneously, the intensity of the peak at $V = 1.95$ mL increased, while the peak at $V = 1.65$ mL stayed more or less constant. This result points to the disassembly of the conjugates into species that elute at similar retention volumes as the polymer.

To obtain more insight into the disassembly process, the fraction at $V = 0.90$ mL from the FPLC chromatogram in Figure 8.2a, which contains the pure CCMV–PEG conjugates, was also re-injected at different time intervals. The evolution of the pure CCMV–PEG conjugates over time showed the same tendency as that observed for the original samples **A**–**D**. Whereas only the peak associated with the conjugates ($V = 0.90$ mL) appeared in the FPLC chromatograms after one day, the intensity of this peak rapidly decreased over time, concomitantly with the formation of a new peak at $V = 1.95$ mL (Figure 8.2c). This process can be illustrated by plotting the ratio of the intensities of the two peaks at various wavelengths as a function of time (Figure 8.2d). Analysis by SDS-PAGE, UV/Vis, and infrared spectroscopy confirmed the presence of both protein and polymer in the fraction corresponding to the 1.95 mL peak (Figure 8.6 in the Experimental Section). The elution volume of the peak is larger than that of the unfunctionalized CP dimers ($V = 1.78$ mL), suggesting that PEG-functionalized CP monomers and not dimers are generated during the disassembly. Nevertheless, it cannot

be excluded that the peak consists of both functionalized and unfunctionalized CP subunits.

a)

b)

c)

d)
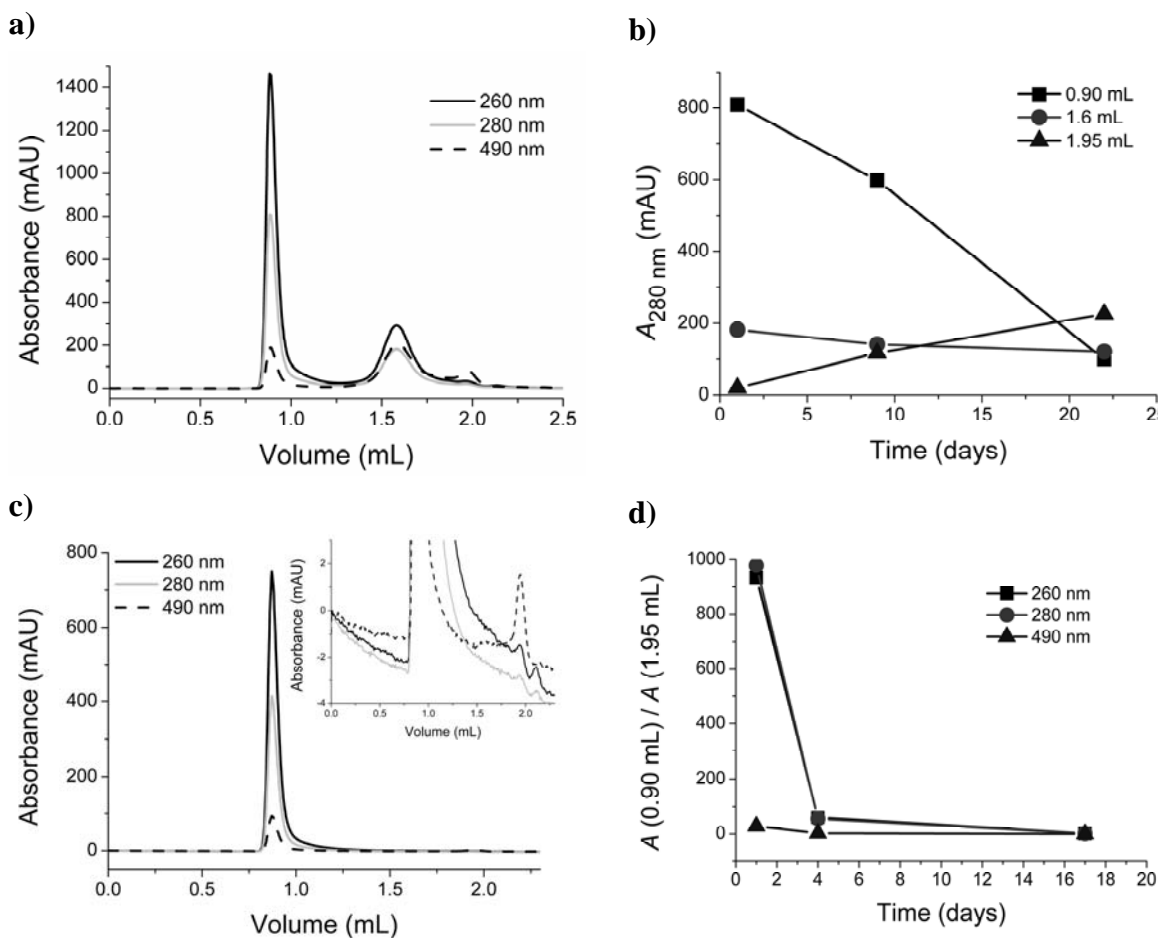
Figure 8.2 *Stability studies on sample **B** (sample was first purified on Sephadex G-100). a) FPLC chromatogram after 1 day. b) Absorbance at λ = 280 nm as a function of time for the different peaks observed after injection of sample **B**. c) FPLC chromatogram of the re-injected fraction at V = 0.90 mL in a) one day after the first injection. Inset: magnification of the peak at V = 1.95 mL. d) Plot of the ratio of intensities of peaks at V = 0.90 and 1.95 mL for the re-injected fraction as a function of time.*

The whole set of experiments suggests a scenario for the disassembly of CCMV–PEG conjugates as depicted in Scheme 8.4. The slow but irreversible dissociation of the CCMV–PEG conjugates is probably a consequence of the disruption of protein–protein interactions caused by steric interference due to the presence of the PEG chains. The influence that organic substituents can exert on the assembly of viral capsids has previously been studied for the hepatitis B virus (HBV), the assembly process of which was misdirected to the formation of much larger particles than that of the native virus.[38] The stability studies described above provide more information on this kind of phenomenon. The tendency of the CCMV–PEG conjugates to dissociate should be taken into account as a very likely side process if one aims to decorate CCMV with

organic polymers. The potential instability of these CCMV assemblies, however, does not exclude further experiments, as described below.
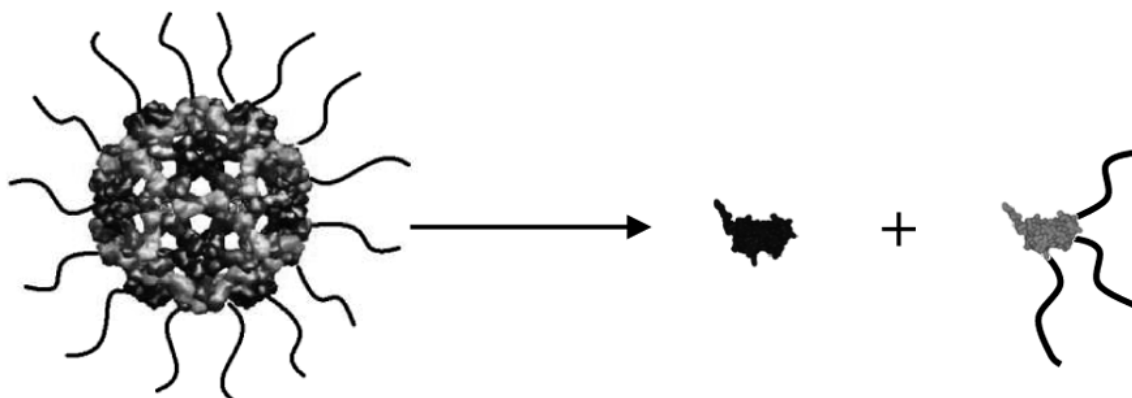
Scheme 8.4 *Tentative scenario proposed for the disassembly of CCMV–PEG conjugates into CP bearing PEG chains and nonfunctionalized CP.*

Assembly of PSS–CCMV capsid–PEG virus-like particles

Before studying the reassembly of the PEG-functionalized coat proteins into virus-like particles, the RNA, which was still present, had to be removed. Dialysis of samples **A–D** against Tris-HCl buffer (pH 7.5, 1.0 M NaCl) allowed the viral genomic material to precipitate. After ultracentrifugation and collection of the supernatant, the samples were free from RNA, as evidenced by the absence of the characteristic absorption at $\lambda = 260$ nm (Figure 8.3a). SDS-PAGE analysis of the supernatant revealed that both functionalized and unfunctionalized CP subunits were isolated (Figure 8.3b). Furthermore, it could be concluded from their high elution volume in the FPLC chromatograms (Figure 8.3c) that the CP subunits were still present in their monomeric form.

a)   b)   c)
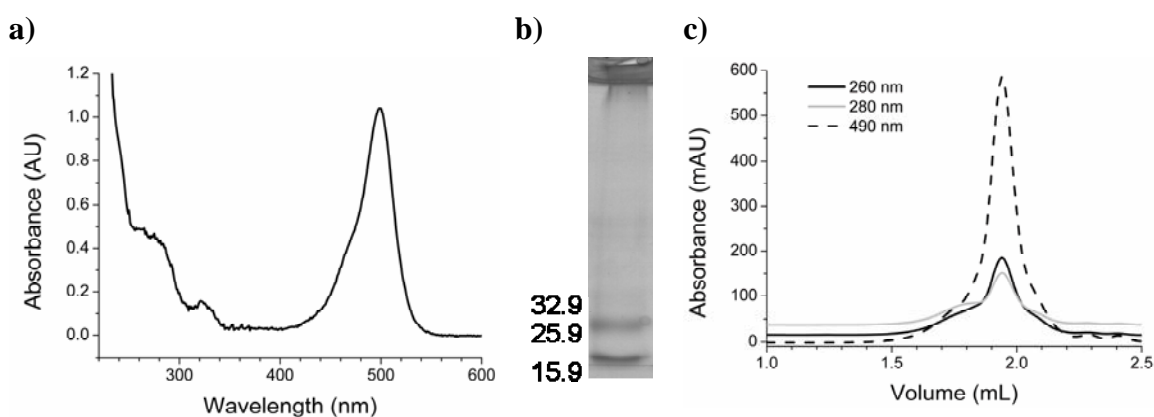
Figure 8.3 *Analysis of the isolated product after RNA removal from the CCMV–PEG conjugates. a) UV/Vis spectrum of the supernatant. The usually high absorbance value at $\lambda = 260$ nm, due to the presence of RNA, is now shifted to $\lambda = 280$ nm, the characteristic wavelength maximum of the protein. b) SDS-PAGE of the isolated PEG–CP (supernatant after ultracentrifugation). c) FPLC chromatogram of the supernatant.*

By following the approach described by Sikkema et al.,[32] the isolated PEG-functionalized coat proteins were re-assembled using PSS (M_w = 70,000 g mol^{-1}) as the template. The assembly was performed at pH 7.5 with a ratio of approximately 15 PSS repeating units per CP, which is within the optimal range of values described for the formation of T = 1 particles.[42] One interesting question is what effect the presence of PEG chains attached to the CP will have on the assembly process. A convenient way to evaluate this would be to assemble mixtures that have different compositions of functionalized and unfunctionalized CP to test the extent to which the particles are formed as well as their degree of coverage with PEG chains. To this end, five different mixtures of CP and PEG–CP (samples **E**–**I**, containing 0, 25, 50, 75, and 100% PEG–CP, respectively), in the presence of PSS, were prepared and studied. The unfunctionalized CP was prepared as described in Chapter 4.

After mixing the components of samples **E**–**I** at pH = 7.5 and incubating for 30 min at room temperature, the mixtures were purified by FPLC chromatography and further analyzed by fluorescence spectroscopy, SDS-PAGE, and TEM (Figure 8.4). A peak at V = 1.35 mL in the FPLC chromatograms indicated the formation of T = 1 particles for the various CP / PEG-CP ratios employed in the experiment (Figure 8.4a and b). All samples gave similar chromatograms, and differed only in the intensity of this peak at different wavelengths. Moreover, the presence of an absorbance at λ = 280 and 490 nm demonstrated that both the CP and polymer were constituents of the material eluting at V = 1.35 mL. This result was further confirmed by the fluorescence spectrum of this FPLC fraction, which showed a clear emission at λ = 520 nm when excited at λ = 490 nm (Figure 8.4c) due to the presence of the fluorescein dye. On the contrary, no absorption at λ = 490 nm and fluorescence at λ = 520 nm were detected for sample **A**, which contained no PEG–CP. In addition to the peak at V = 1.35 mL, there were peaks of other material eluting at higher volumes in the chromatograms. The nature of this material is as yet unknown, although it probably consists of highly PEG-functionalized CP monomers and residual polymer, which are not able to assemble around the PSS.

Interestingly, the FPLC chromatograms of samples **E**–**I** did not change over time. It therefore seems that the PSS–CCMV capsid–PEG particles are more robust than their CCMV–PEG conjugate predecessors. The particles were also found to be stable at pH 5.0 because dialysis against an acetate buffer at this pH value did not lead to substantial changes in the FPLC results. The electrostatic interactions between the negative charges of PSS and the positively charged N terminus of the coat protein molecules are likely to be the reason for this remarkable increase in robustness.

The degree of coverage of the PSS–CCMV capsid–PEG particles with PEG chains, when using different CP / PEG-CP ratios, was evaluated by plotting the emission at λ = 522 nm (λ_{exc} = 490 nm) of the FPLC fractions at V = 1.35 mL, normalized to the

total concentration of CP present, versus the amount of PEG–CP used in the initial assembly mixture. An almost linear relationship was obtained, which showed statistical incorporation of PEG onto the $T = 1$ capsids (Figure 8.4d).

a)

b)

c)

d)

e)

f)

g)

h)
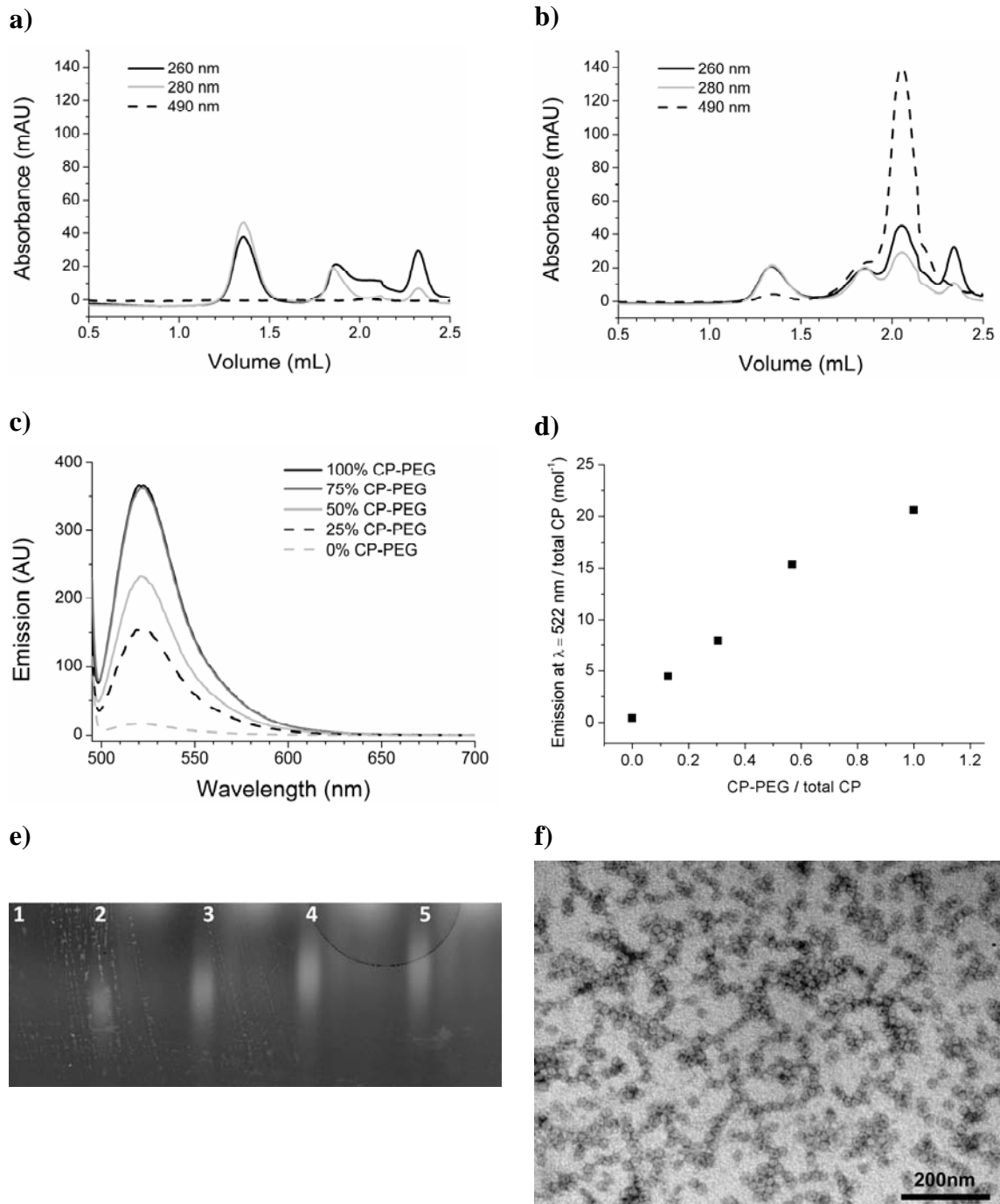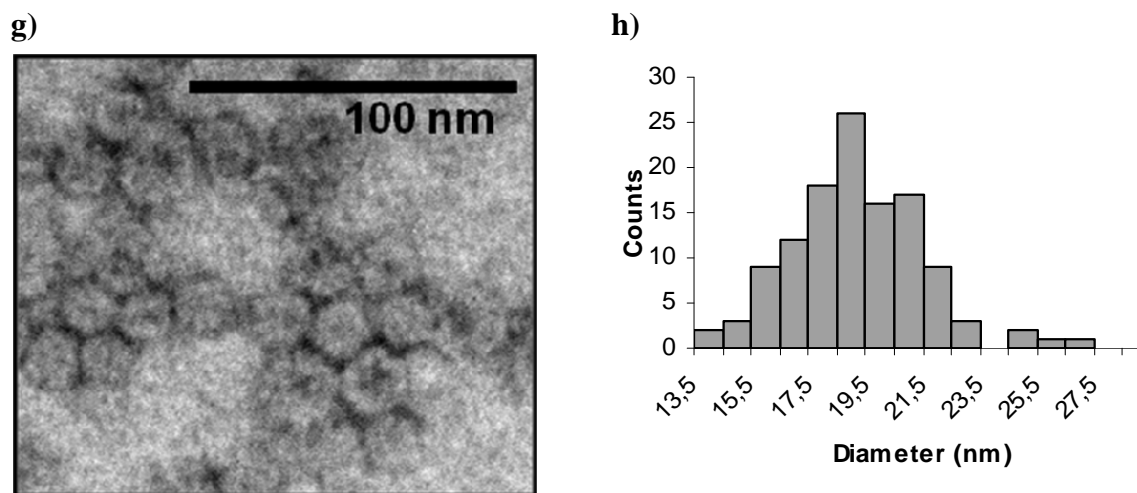
*Figure 8.4 Characterization of PSS–CCMV capsid–PEG assemblies. FPLC chromatogram of the PSS–CCMV capsid–PEG assemblies formed using a) 0% PEG–CP sample (**E**) and b) 100% PEG–CP sample (**I**). c) Emission spectra (λ_{exc} = 490 nm) of the FPLC fractions at V = 1.35 mL of the PSS–CCMV capsid–PEG samples **E**–**I** prepared with different CP / PEG–CP ratios. d) Emission at λ = 522 nm (λ_{exc} = 490 nm) of the FPLC fractions at V = 1.35 mL versus the amount of PEG–CP used for the assembly in samples **E**–**I**. e) Agarose gel of pure PSS–CCMV capsid–PEG T = 1 particles (purified by FPLC) prepared from mixtures with different PEG–CP content having different amounts of PEG chains: 0 (lane 1), 25 (lane 2), 50 (lane 3), 75 (lane 4), and 100% PEG–CP (lane 5). The gel was visualized with a fluorescence scanner. f) TEM micrograph of the PSS–CCMV capsid–PEG T = 1 particles taken from sample **G** (50% PEG–CP). g) Zoom in on the TEM micrograph shown in (f). h) Size distribution of the PSS-CCMV-PEG T = 1 particles shown in (f).*

Samples **E**–**I** and their FPLC fractions at V = 1.35 mL were further characterized by agarose gel electrophoresis (Figure 8.4e). The gel was visualized with the help of a fluorescence scanner to detect the fluorescein-labeled PEG chains. The FPLC fractions showed single bands running faster than those of the wild-type virus, as expected for smaller particles. The fact that these bands are visible by fluorescence is a strong proof that PEG is present on the outside of the T = 1 capsids (note the absence of such a band in the case of sample **E**, 0% PEG-CP, lane 1). The degree to which PEG-functionalization of the particles occurred could even be inferred from the dependence of their running speed in the gel on the initial amount of PEG–CP used in the assembly mixtures (Figure 8.4e).

Finally, the PSS–CCMV–PEG particles were studied by TEM (Figure 8.4f–h). This study confirmed that the particles are monodisperse spherical capsids with an average diameter of 18.5 nm. The particles showed a slightly larger size than the T = 1 particles

reported by Sikkema et al.,[32] probably caused by the presence of the PEG tails attached to the outer surface of the protein cage.

8.3 Conclusion and Outlook

Based on its reversible pH-dependent disassembly/assembly behavior, the CCMV capsid is a suitable nanocontainer for the encapsulation of proteins, inorganic nanoparticles, and organic polymers.[19] The external functionalization of this capsid with synthetic organic polymers will broaden the field of potential applications, for example, its use as a nanoreactor or as a building block for the preparation of nanostructured materials. We have shown that the covalent attachment of polymer tails to the outer surface of the CCMV capsid leads to some thermodynamic instability, which forces the virus to disassemble over a period of days. The irreversible dissociation of CP dimers, probably due to steric interference between the protein–protein subunits as a result of the proximity of the PEG chains, is responsible for the shift of the equilibrium to complete disassembly of the viral particles. This effect limits the potential application of the CCMV–polymer biohybrids, however, this problem can be overcome if a PSS guest is present in the modified viral capsids. The methodology described herein allows for complete control over the amount of PEG chains attached to the PSS–CCMV capsid–PEG particles. Moreover, there is a remarkable increase in their robustness compared with the CCMV–PEG conjugates; an important requirement if VLPs are to be used in nanotechnology. The polymers chosen for this work are not yet functional, but the approach exemplifies a possible future strategy for the design and preparation of more sophisticated VLPs. Any negatively charged synthetic polymer could in principle be used as a template to direct the viral capsid assembly towards the formation of a stable and precisely defined architecture. The use of functional polymers both on the inside and the outside of the capsids may impart new properties to the particles. Our strategy implies that these properties can be tuned by the proper choice of the external polymer and the polymer template. In this regard, the controlled integration of polymers with viral capsids represents a promising approach for the synthesis of nanostructured materials.

8.4 Experimental Section

Materials

Uranyl acetate dihydrate (≥98%) and 1-ethyl-3-(3-dimethylaminopropyl) carbodiimide hydrochloride (EDC) (≥98%) were purchased from Fluka. Sodium dihydrogen phosphate monohydrate (≥99%) and disodium hydrogen phosphate dihydrate (≥99%) were purchased from Merck. Fluorescein-NHS (>99%) was purchased from Pierce. Ethylenediaminetetraacetic acid (EDTA) disodium salt dihydrate (>99%), Tris(hydroxymethyl)aminomethane (Tris) (>99%), triethylamine (99%), and sodium chloride (99.5%) were purchased from Acros. Ethidium bromide (~95%), Orange G (≥80%), N-hydroxysuccinimide (98%), dithiothreitol (DTT) (99%), and poly(sodium 4-styrene sulfonate) (M_n = 70,000) were obtained from Sigma-Aldrich. Agarose (electrophoresis grade) was purchased from Invitrogen. All reagents used for SDS-PAGE electrophoresis were purchased from Bio-Rad Laboratories. HOOC-PEG-NH$_2$ (M_n = 3000 Da) was purchased from Rapp Polymere. CH_2Cl_2 was distilled from CaH_2 under nitrogen

Instrumentation

Nuclear magnetic resonance (NMR) spectra were recorded on a Varian Inova 400 spectrometer at 298 K. 1H NMR shifts (δ) are reported in parts per million (ppm) relative to the residual proton peak of the solvent, δ = 7.26 for CDCl3. Multiplicities are reported as s (singlet), d (doublet), t (triplet), q (quartet), m (multiplet), and dd (doublet of doublets). The number of protons for a given resonance is shown as nH and are derived from spectral integration.

Matrix-assisted laser desorption/ionisation time-of-flight (MALDI-TOF) mass spectra were measured on a Bruker Biflex III spectrometer. Indole acrylic acid (IAA) was used as a matrix. Samples were prepared by mixing 45 µL of a solution of matrix (20 mg mL−1) in THF with 5 µL of a solution of polymer (2 mg mL−1) in THF. From this mixture, 1 µL of the sample was spotted onto the target plate.

Infrared spectroscopy was performed on a Thermo Mattson IR300 spectrometer equipped with a Harrick ATR. Samples were prepared by evaporating the solvent (water), re-dissolving the residue in THF, depositing a drop in the measuring plate, and leaving it to dry for 2 min in a nitrogen stream.

Fluorescence spectroscopy measurements were performed on a Perkin-Elmer LS 55 fluorescence spectrophotometer. Experiments were carried out using a 40 µL quartz fluorescence cuvette (Hellma, path length: 3 mm) or a 1 mL quartz fluorescence cuvette (Hellma, path length: 4 mm).

UV/Vis spectroscopy measurements were performed on a Varian Cary 50 spectrophotometer using a 1 mL quartz fluorescence cuvette (Hellma, path length: 4 mm) and a 40 μL quartz fluorescence cuvette (Hellma, path length: 3 mm).

Fast protein liquid chromatography (FPLC) was performed on an Ettan Akta LC system equipped with a Superose 6 PC 3.2/30 column from Amersham Biosciences (flow rate 40 μL min^{-1}). Injections of 50 μL aliquots of the samples were monitored by using UV detection at λ = 260, 280, and 490 nm. Fractions of 60 μL were collected and further analyzed when necessary.

SDS-polyacrylamide gel electrophoresis (SDS-PAGE) was performed using a 10% polyacrylamide gel containing 10% SDS. The samples were treated with β-mercaptoethanol and heated before being loaded onto the gel. Gels were visualized by Coomassie Blue staining or in cases when the protein concentration was low by silver staining.

Agarose gel electrophoresis was performed from a 1.2% agarose solution mixed with 10 μL of an ethidium bromide solution (10 mg mL^{-1}). Samples (20 μL) were mixed with DNA-loading buffer (6 μL) and loaded onto the gel. Gels were run at 100 V for 1.5 h. Gels were analyzed with the help of a FLA-5100 fluorescence scanner. The used excitation wavelengths were λ = 473 and 532 nm. Gels were also stained using Coomassie Blue.

Transmission electron microscopy (TEM) micrographs were recorded on a JEOL JEM-1010 instrument. CCMV–PEG samples were prepared by drying a drop of the solution on a carbon-coated or hydrophilized (by glow discharge) formvar-carbon-coated copper grid. The excess buffer on the grid was blotted away after 3 min by using filter paper. PSS–CCMV capsid–PEG samples were prepared in the same way, but on hydrophilized (by glow discharge) formvar carbon grids and blotting the excess solution away after 1 min. Negative staining of the samples was achieved by application of a drop of a uranyl acetate solution (0.2% in MilliQ) onto the grid and blotting the excess liquid away after 15 s with filter paper. The samples were left to dry in air for 30 min before analysis.

Ultracentrifugation was performed in a Sorvall Micro (SM) ultracentrifuge (type RC-M150GX) with a S-120-AT2 type rotor. Thick-walled polycarbonate tubes (V = 1 mL) provided by Sorvall were used.

Dialysis was performed by using dialysis tubing (Spectra/Por 4, MWCO: 12–14 kDa, Flat width: 25 mm) purchased from Spectrum Laboratories or D-Tubes Dialyzers (MWCO: 6–8 kDa or 12–14 kDa) from Calbiochem.

Synthesis

α-Carboxylic acid ω-fluorescein functionalized PEG (2)
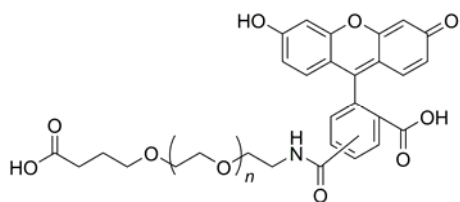
All glassware was flame dried and the reaction was performed under an argon atmosphere. Triethylamine (450 μL, 3.24 mmol) was added to a solution of HOOC-PEG-NH$_2$ (1.63 g, 0.54 mmol) in anhydrous CH$_2$Cl$_2$ (30 mL). After stirring for 15 min NHS-fluorescein (328 mg, 0.69 mmol) was added and the mixture was stirred for an additional 44 h at room temperature. Upon dilution with CH$_2$Cl$_2$, the mixture was sequentially washed with a 10% aqueous citric acid solution and a saturated aqueous solution of NaHCO$_3$. The organic phase was dried over anhydrous Na$_2$SO$_4$, filtered, and concentrated under reduced pressure to afford an orange solid (1.37 g, 73%). ^{1}H NMR (CDCl$_3$, 400 MHz): δ = 1.9 (t, 2H), 2.6 (t, 2H), 3.5–3.7 (m, protons PEG + 4H (CH$_2$CH$_2$CH_2O)), 6.5–6.8 (m, 6H), 8.1 (m, 1H), 8.3 (m, 1H), 8.6 (s, 1H).

α-NHS ester ω-fluorescein functionalized PEG (1)
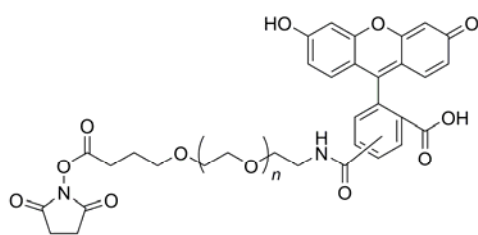
All glassware was flame dried and the reaction was performed under an argon atmosphere. Compound **2** (1.0 g, 0.29 mmol) and *N*-hydroxysuccinimide (37 mg, 0.32 mmol) were dissolved in anhydrous CH$_2$Cl$_2$ (40 mL). The mixture was cooled to 0 °C in an ice bath and EDC (85 mg, 0.44 mmol) was added. After stirring for 1 h at 0 °C, the reaction mixture was warmed to room temperature and it was allowed to stir overnight. The mixture was then diluted with CH$_2$Cl$_2$ and washed with an aqueous saturated solution of NH$_4$Cl. After drying over anhydrous Na$_2$SO$_4$, the organic phase was concentrated under reduced pressure to afford an orange solid (753 mg, 73%). ^{1}H NMR (CDCl$_3$, 400 MHz): δ = 2.0 (m, 2H), 2.7 (t, 2H), 2.8 (s, 4H), 3.5–3.7 (m, protons PEG + 2H (CH$_2$CH$_2$CH_2O)), 6.5–6.7 (m, 6H), 8.1 (m, 1H), 8.3 (m, 1H), 8.6 (s, 1H); MALDI-TOF (IAA): *m*/*z* calcd for [*M*+H]$^+$: 3597.9 (for *n* = 68); found: 3598.4.

Coupling of 1 to CCMV.

A CCMV solution (8.48 mg mL^{-1}, 2.5 mL) in sodium acetate buffer (0.05 M, 1.0 M NaCl, pH 5.0) was dialyzed against phosphate buffer (0.1 M, 0.001 M EDTA, pH 7.5) over a period of 9 h (with buffer changes every 3 h, *T* = 4 °C) using a 12–14 kDa MWCO dialysis membrane. Samples **A**–**D** with different CP / **1** ratios (1:50 (**A**), 1:25 (**B**), 1:10 (**C**) and 1:1 (**D**)) were prepared by the addition of variable aliquots of a stock solution of compound **1** (0.081 M) in the same phosphate buffer to the CCMV solution

(500 uL, 1.61×10^{-4} mmols) (Table 8.1). Additional phosphate buffer was added, when necessary, to provide final volumes of 600 μL for all samples. A control sample was prepared in the same way as that used for sample **A** with compound **2** instead of **1**.

Table 8.1 *Preparation of CCMV–PEG conjugates using different CP / **1** ratios. Amount of compound **1** added to the CCMV solution for every sample.*

Experiment	Molar ratio CP / **1**	Concentration of **1** in final solution (mmol)	Volume of stock solution of **1** (μL)
A	1 : 50	8.10×10^{-3}	100
B	1 : 25	4.03×10^{-3}	50
C	1 : 10	1.61×10^{-3}	20
D	1 : 1	1.61×10^{-4}	2

Samples **A–D** were incubated on a roller mixer for 2 h at room temperature and subsequently overnight at 4 °C. The samples were protected from light at all times. The excess fluorescein-functionalized PEG was removed by size-exclusion chromatography (SEC, Sephadex G-100) with the same phosphate buffer as eluent. The PEG-functionalized virus (orange in color) eluted before the excess of **1** (bright yellow). All fractions were analyzed by FPLC, SDS-PAGE, TEM, and UV/Vis spectroscopy.

Isolation of the PEG-functionalized CCMV coat protein (removal of the viral RNA)

A purified PEG-functionalized CCMV solution (ca. 5 mg mL^{-1}, 1 mL; sample **C**) was extensively dialyzed overnight against Tris-HCl buffer (0.02 M, 1 M NaCl, 0.001 M DTT, pH 7.5) using a 6–8 kDa MWCO dialysis membrane. The solution was ultracentrifuged at 45000 rpm for 16 h at 4 °C. The top three-quarters of the supernatant was removed with a micropipette and analyzed by FPLC, SDS-PAGE, and UV/Vis spectroscopy. The unfunctionalized coat protein obtained from CCMV, as described in the literature, [16,43,44] was used as a control.

Assembly of PSS-CCMV capsid-PEG virus-like particles

Two different solutions of CP (600 μL, 0.82 mg mL^{-1}) and PEG–CP (300 μL, 1.20 mg mL^{-1}, isolated from sample **C**), both in the same Tris-HCl buffer (0.02 M, 1.0 M NaCl, 0.001 M DTT, pH 7.5), were dialyzed separately against phosphate buffer (0.1 M, 0.3 M NaCl, 0.001 M EDTA, pH 7.5). PSS (M_n = 70000 Da, 17 mg, 2.42×10^{-4} mmol) was dissolved into the same phosphate buffer (170 μL) and diluted 50 times to obtain a PSS stock solution (2.86×10^{-5} M).

The assembly mixtures, containing different relative amounts of CP and PEG–CP (samples **E** (0% PEG–CP), **F** (25% PEG–CP), **G** (50% PEG–CP), **H** (75% PEG–CP) and **I** (100% PEG–CP)), were prepared by adding volumes of the stock solutions of both components, according to Table 8.2, to the PSS stock solution (20 μL, 1.94×10^{-4} mmol repeating units). A CP / PSS repeating unit ratio of approximately 1:40 was used in all cases. The samples were protected from light and incubated on a roller mixer for 30 min at room temperature, followed by storage at 4 °C. The characterization of samples **E–I** was performed by FPLC and agarose gel electrophoresis, and the purified FPLC fractions were further analyzed by fluorescence spectroscopy, TEM, SDS-PAGE, and agarose gel electrophoresis.

Table 8.2 Amounts of PEG–CP and CP used for the different experiments to form PEG-functionalized T = 1 CCMV capsid particles containing PSS in their interior.

Experiment	PEG–CP (% (v/v))	PEG–CP solution (μL)	CP solution (μL)	Approximate amount of CP present in the final mixture (mmol)
E	0	–	100	4.1×10^{-6}
F	25	25	75	4.6×10^{-6}
G	50	50	50	5.0×10^{-6}
H	75	75	25	5.5×10^{-6}
I	100	100	-	6×10^{-6}

Analysis of the peaks at V *= 1.60 and 1.95 mL in the FPLC chromatograms of the CCMV–PEG conjugates.*

A solution of **1** was injected in the FPLC column to facilitate the assignment of the peaks at $V = 1.60$ and 1.95 mL observed in the FPLC chromatograms of the CCMV–PEG samples **A–D**. Three different peaks appeared in the FPLC chromatogram of polymer **1** (Figure 8.5a). These peaks were also present, in small proportion, in the FPLC chromatograms of the CCMV–PEG samples **A–D** (Figure 8.2a), indicating that the excess of polymer **1** could not be completely removed during the preliminary purification by SEC on Sephadex G-100. Only the smallest species eluting at $V = 2.1$ mL was totally eliminated. After comparing the UV/Vis (Figure 8.5b) and IR (not shown) spectral data of the FPLC fractions corresponding to these three peaks with data of non-injected compound **1**, the species could be identified. The fraction at $V = 2.1$ mL contained PEG that was not functionalized with a fluorescein moiety, which

was evident from the absence of absorbance at $\lambda = 490$ nm in the FPLC chromatogram (Figure 8.5a). The fraction at $V = 1.95$ mL contained the fluorescein-functionalized PEG from which the NHS ester (1715 cm^{-1}) had been hydrolyzed. The peak at $V = 1.60$ mL was the most difficult one to elucidate. The IR spectrum of this FPLC fraction showed the presence of NHS-functionalized polymer. In addition, the low elution volume and low absorbance value at $\lambda = 490$ nm (self-quenching of the fluorescein dye to aggregation) suggested that this peak was related to polymer aggregates, although other possibilities, such as the oligomerization of PEG (**1**) by esterification of the NHS-activated carboxylic acid with the hydroxyl group of the fluorescein moiety, cannot be excluded.

a)   b)
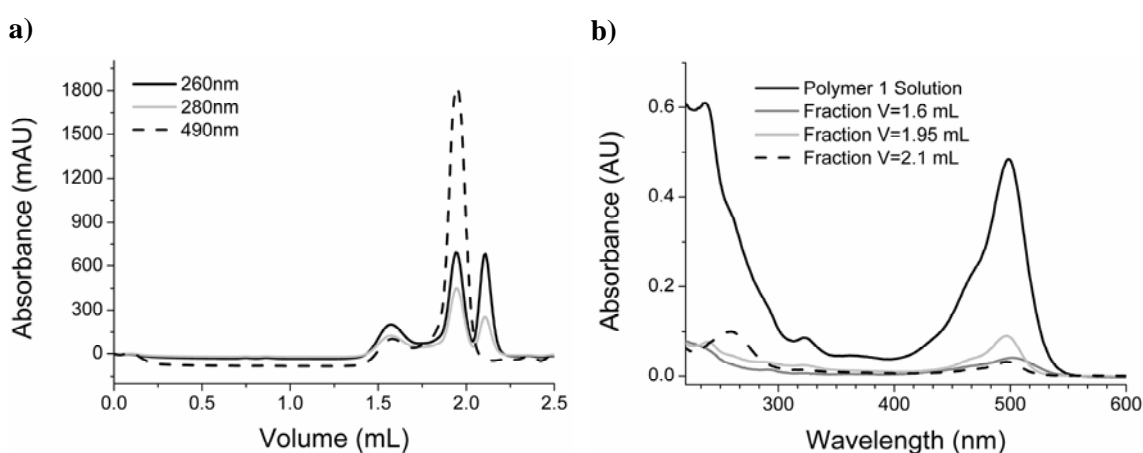
Figure 8.5 *a) FPLC chromatogram of **1** (c = 12.4 mg mL^{-1}, injected volume = 20 μL). b) UV/Vis spectra of nonpurified **1** (c = 0.25 mg mL^{-1}, l = 4 mm) and of the fractions collected after injection of **1** into the FPLC column (corresponding to the 3 peaks in the chromatogram in (a)).*

The fractions corresponding to the peaks at $V = 1.60$ and 1.95 mL in the FPLC chromatograms of the CCMV–PEG samples **A**–**D** (Figure 8.2a) contained the same species as those described above for polymer **1**, as suggested by their similar elution volumes and UV/Vis absorbance values in the chromatograms. SDS-PAGE and IR spectroscopy analysis, however, also showed the presence of protein in the fraction at $V = 1.95$ mL (Figure 8.6). It therefore seems that the CCMV–PEG conjugates disassemble into CP monomers over time, which elute at similar elution volumes as those found for polymer **1** and related species. Furthermore, the content of protein compared with polymer increases with time in this fraction due to the slow disassembly of the conjugates, as shown in Figure 8.2.

Figure 8.6 *SDS-PAGE of the FPLC fraction (V = 1.95 mL) isolated after the injection of a two-week-old CCMV–PEG conjugate sample (sample **A**) on the FPLC column.*

8.5 Notes and References

[1]   C. M. Niemeyer, *Angew. Chem. Int. Ed.* **2001**, *40*, 4128.

[2]   V. M. Rotello, *J. Mater. Chem.* **2008**, *18*, 3739.

[3]   T. Douglas, M. Young, *Science* **2006**, *312*, 873.

[4]   M. Fischlechner, E. Donath, *Angew. Chem. Int. Ed.* **2007**, *46*, 3184.

[5]   M. Uchida, M. T. Klem, M. Allen, P. Suci, M. Flenniken, E. Gillitzer, Z. Varpness, L. O. Liepold, M. Young, T. Douglas, *Adv. Mater.* **2007**, *19*, 1025.

[6]   Q. Wang, T. Lin, L. Tang, J. E. Johnson, M. G. Finn, *Angew. Chem. Int. Ed.* **2002**, *41*, 459.

[7]   S. Sen Gupta, J. Kuzelka, P. Singh, W. G. Lewis, M. Manchester, M. G. Finn, *Bioconjugate Chem.* **2005**, *16*, 1572.

[8]   M. Young, D. Willits, M. Uchida, T. Douglas, *Annu. Rev. Phytopathol.* **2008**, *46*, 361.

[9]   D. M. Vriezema, M. Comellas Aragones, J. A. A. W. Elemans, J. J. L. M. Cornelissen, A. E. Rowan, R. J. M. Nolte, *Chem. Rev.* **2005**, *105*, 1445.

[10]   I. Yamashita, *J. Mater. Chem.* **2008**, *18*, 3813.

[11]   T. Ueno, M. Suzuki, T. Goto, T. Matsumoto, K. Nagayama, Y. Watanabe, *Angew. Chem. Int. Ed.* **2004**, *43*, 2527.

[12]   D. Ensign, M. Young, T. Douglas, *Inorg. Chem.* **2004**, *43*, 3441.

[13]   M. Tominaga, A. Ohira, A. Kubo, I. Taniguchi, M. Kunitake, *Chem. Commun.* **2004**, 1518.

[14]   Z. Varpness, J. W. Peters, M. Young, T. Douglas, *Nano Lett.* **2005**, *5*, 2306.

[15]   S. Abe, J. Niemeyer, M. Abe, Y. Takezawa, T. Ueno, T. Hikage, G. Erker, Y. Watanabe, *J. Am. Chem. Soc.* **2008**, *130*, 10512.

[16] M. Comellas-Aragones, H. Engelkamp, V. I. Claessen, N. A. J. M. Sommerdijk, A. E. Rowan, P. C. M. Christianen, J. C. Maan, B. J. M. Verduin, J. J. L. M. Cornelissen, R. J. M. Nolte, *Nat. Nanotechnol.* **2007**, *2*, 635.

[17] J. Johnson, T. Lin, G. Lomonossoff, *Annu. Rev. Phytopathol.* **1997**, *35*, 67.

[18] N. F. Steinmetz, T. Lin, G. P. Lomonossoff, J. E. Johnson, *Curr. Top. Microbiol. Immunol.* **2009**, *327*, 23.

[19] A. de la Escosura, R. J. M. Nolte, J. J. L. M. Cornelissen, *J. Mater. Chem.* **2009**, *19*, 2274.

[20] T. L. Schlick, Z. Ding, E. W. Kovacs, M. B. Francis, *J. Am. Chem. Soc.* **2005**, *127*, 3718.

[21] K. S. Raja, Q. Wang, M. G. Finn, *ChemBioChem* **2003**, *4*, 1348.

[22] Q. Wang, K. S. Raja, K. D. Janda, T. Lin, M. G. Finn, *Bioconjugate Chem.* **2003**, *14*, 38.

[23] N. F. Steinmetz, M. Manchester, *Biomacromolecules* **2009**, *10*, 784.

[24] E. W. Kovacs, J. M. Hooker, D. W. Romanini, P. G. Holder, K. E. Berry, M. B. Francis, *Bioconjugate Chem.* **2007**, *18*, 1140.

[25] G. Pasut, F. M. Veronese, *Polymer Therapeutics I: Polymers as Drugs, Conjugates and Gene Delivery Systems* **2006**, *192*, 95.

[26] J. M. Harris, R. B. Chess, *Nature Rev. Drug Disc.* **2003**, *2*, 214.

[27] S. E. Aniagyei, C. DuFort, C. C. Kao, B. Dragnea, *J. Mater. Chem.* **2008**, *18*, 3763.

[28] J. A. Speir, S. Munshi, G. J. Wang, T. S. Baker, J. E. Johnson, *Structure* **1995**, *3*, 63.

[29] J. E. Johnson, J. A. Speir, *J. Mol. Biol.* **1997**, *269*, 665.

[30] T. Douglas, M. Young, *Nature* **1998**, *393*, 152.

[31] A. de la Escosura, M. Verwegen, F. D. Sikkema, M. Comellas-Aragones, A. Kirilyuk, T. Rasing, R. J. M. Nolte, J. J. L. M. Cornelissen, *Chem. Commun.* **2008**, 1542.

[32] F. D. Sikkema, M. Comellas-Aragones, R. G. Fokkink, B. J. Verduin, J. J. L. M. Cornelissen, R. J. M. Nolte, *Org. Biomol. Chem.* **2007**, *5*, 54.

[33] Y. F. Hu, R. Zandi, A. Anavitarte, C. M. Knobler, W. M. Gelbart, *Biophys. J.* **2008**, *94*, 1428.

[34] J. B. Bancroft, E. Hiebert, *Virology* **1967**, *32*, 354.

[35] R. F. Bruinsma, W. M. Gelbart, D. Reguera, J. Rudnick, R. Zandi, *Phys. Rev. Lett.* **2003**, *90*, 248101.

[36] J. Tang, J. M. Johnson, K. A. Dryden, M. J. Young, A. Zlotnick, J. E. Johnson, *J. Struct. Biol.* **2006**, *154*, 59.

[37] S. Mukherjee, C. M. Pfeifer, J. M. Johnson, J. Liu, A. Zlotnick, *J. Am. Chem. Soc.* **2006**, *128*, 2538.

[38] S. J. Stray, C. R. Bourne, S. Punna, W. G. Lewis, M. G. Finn, A. Zlotnick, *Proc. Natl. Acad. Sci. U.S.A.* **2005**, *102*, 8138.

[39] E. Gillitzer, D. Willits, M. Young, T. Douglas, *Chem. Commun.* **2002**, 2390.

[40] http://viperdb.scripps.edu/index.php

[41] Experiments with PEG of other chain lengths have also been carried out (PEG-750 and PEG-10000). The functionalization reaction was successful in both cases. However, no

significant changes in the FPLC chromatogram were observed for the derivatization with PEG-750, whereas precipitation seemed to occur when PEG-10000 was used.

[42]   Considering that there are 8-9 cationic residues in the N terminus of each coat protein subunit, approximately 2 equivalents of PSS repeating units are used.

[43]   B. J. M. Verduin, *FEBS Lett.* **1974**, *45*, 50.

[44]   B. J. M. Verduin, *J. Gen. Virol.* **1978**, *39*, 131.

Appendix

1.   Triangulation number

Triangulation numbers (T numbers) are commonly used in virology to describe the geometry of icosahedral viruses. The basic principles were outlined by Caspar and Klug (1962) who extended mathematical knowledge to biological structures.[1]

As noted by Crick and Watson, the capsids of viruses are formed from a minimum number of gene products given the small size of viral genomes. On this basis, spherical viruses have the symmetry of regular polyhedra of which all faces are identical perfect polygons and all protein units sit in identical environments. The largest shell of this kind is an icosahedron consisting of 60 equivalent subunits. An icosahedron is a polyhedral structure that has 20 equilateral triangles arranged around the face of a sphere (Figure 1a) and is defined by having 2-, 3-, and 5-fold axes of symmetry (Figure 1b). Many viral capsids display icosahedral symmetry, but are formed by more than 60 subunits. To understand the structure of such viruses it is necessary to rely on the quasi-equivalent assembly geometric principle developed by Caspar & Klug.

a)

b)
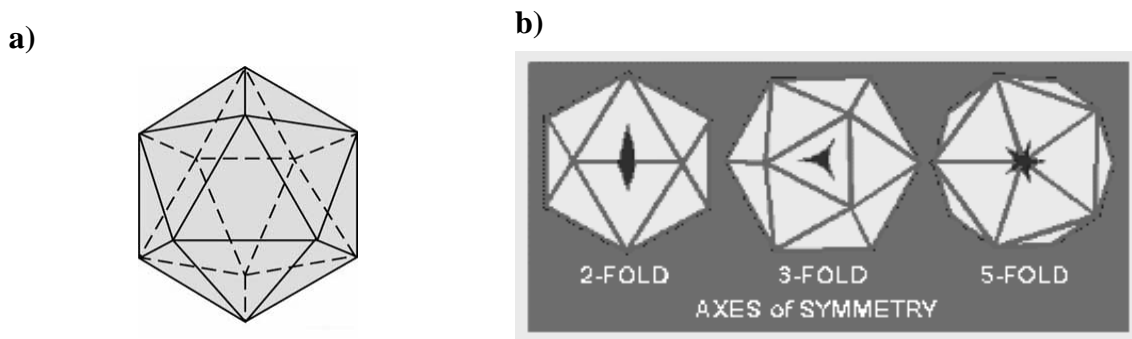
Figure 1 a) Structure of an icosahedron. b) The three different symmetry axes of an icosahedron.

Caspar and Klug proposed a geometrical scheme for the general construction of icosahedral shells with an arbitrarily large number of subunits. Capsid proteins can usually be grouped into ''capsomers'' of either hexamer/pentamer units or trimer units. The conceptual basis for viral quasi-equivalence is the interchangeable formation of hexamers and pentamers by the same protein molecule. Closed icosahedral structures can be built up from pentamers and hexamers as indicated in Figure 2.[2] The structures can be constructed from a sheet of hexamers in which pentamers are inserted in place of certain hexamers according to selection rules described by a "trangulation" (T) number.

Each triangular face of the icosahedrons contains 3T subunits where $T = \mathbf{h}^2 + \mathbf{hk} + \mathbf{k}^2$ and $\mathbf{h}$ and $\mathbf{k}$ correspond to the indices for the hexamer chosen to define the equilateral triangle. T adopts special integer values such as 1, 3, 4, 7, and 13, and the number of proteins constituting an icosahedral shell equals 60T (Figure 2c). Electron and x-ray diffraction studies have confirmed that the *T*-number classification applies to almost all sphere-like viruses.[3]
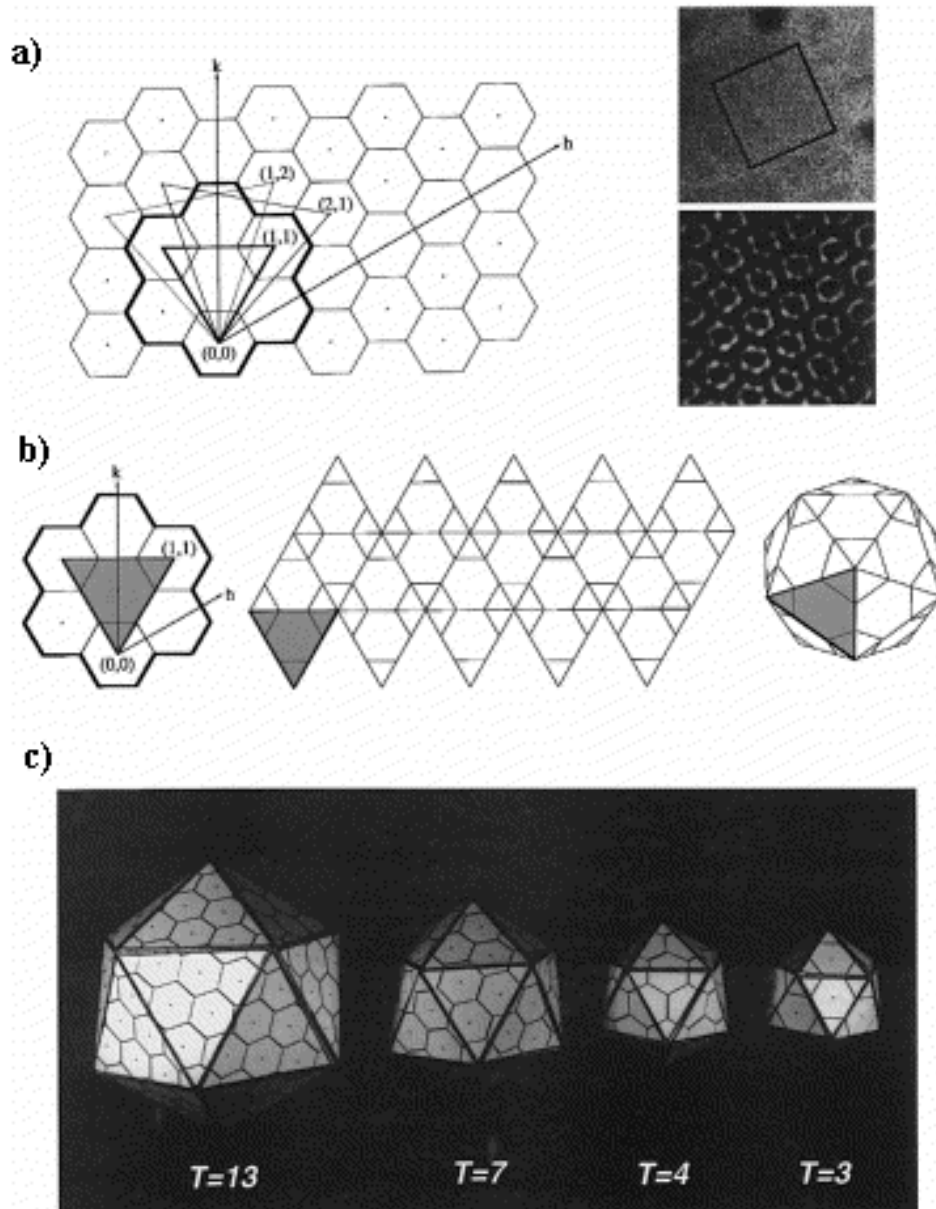
Figure 2 *Geometric principles for generating icosahedral quasi-equivalent surface lattices. a) Hexamers are initially considered planar (an array of hexamers forms a flat sheet as shown) and pentamers are considered convex; they introduce curvature into the sheet of hexamers when they are inserted. The closed icosahedral shell, composed of hexamers and pentamers, is generated by inserting 12 pentamers at the appropriate positions in the hexamer net. b) Seven hexamer units (bold outline in (a)) defined by the*

T=3 lattice are shown. The icosahedral asymmetric unit is one-third of this face and it contains three quasi-equivalent units (two units from the hexamer that coincides with the 3-fold axis and one unit from the pentamer). A three-dimensional model of the lattice can be generated by arranging 20 identical faces of the icosahedron as shown; this can then be folded into a quasi-equivalent icosahedron. c) Cardboard models of several icosahedral quasi-equivalent surface lattices constructed by using the method described above.[2]

References

[1]   D. L. Caspar, A. Klug, *Cold Spring Harbor Symp. Quant. Biol.* **1962**, *27*, 1.

[2]   J. E. Johnson, J. A. Speir, *J. Mol. Biol.* **1997**, *269*, 665.

[3]   R. F. Bruinsma, W. M. Gelbart, D. Reguera, J. Rudnick, R. Zandi, *Phys. Rev. Lett.* **2003**, *90*, 248101.

2.   List of terms and abbreviations

ABTS	2,2´-azino bis(3-ethylbenzthiazoline-6-sulphonic acid)
AFM	atomic force microscopy
Bt	biotin
CCMV	cowpea chlorotic mottle virus
CP	coat protein
CPMV	cowpea mosaic virus
DLS	dynamic light scattering
DNA	deoxyribonucleic acid
Dps	DNA-binding proteins from starved cells
DTT	dithiothreitol
EDC	1-ethyl-3-(3-dimethylaminopropyl) carbodiimide hydrochloride
EDTA	ethylenediaminetetraacetic acid
EM	electron microscopy
FCS	fluorescence correlation spectroscopy
FPLC	fast protein liquid chromatography
FRET	fluorescence resonance energy transfer
HABA	4'-hydroxyazobenzene-2-carboxylic acid
HRP	horseradish peroxidase
HSFn	horse spleen apoferritin
sHsp	small heat shock protein
IR	infrared (spectroscopy)
MALDI-TOF	matrix-assisted laser desorption / ionization time of flight

Mb	myoglobin
MRI	magnetic resonance imaging
NHS	*N*-hydroxy succinimide
NMR	nuclear magnetic resonance (spectroscopy)
PAGE	polyacrylamide gel electrophoresis
PEG	poly(ethylene glycol)
PMSF	phenylmethanesulfonyl fluoride
POD	pentamer of dimers
PSS	polystyrene sulfonate
RNA	ribonucleic acid
ssRNA	single stranded ribonucleic acid
SANS	small-angle neutron scattering
SAv	streptavidin
SEC	size exclusion chromatography
SEM	scanning electron microscopy
TEM	transmission electron microscopy
THF	tetrahydrofuran
TMV	tobacco mosaic virus
Tris	tris(hydroxymethyl)aminomethane
UV/Vis	ultraviolet-visual (spectroscopy)
VLP	virus-like particle

Summary

Viruses are commonly composed of an outer protein shell (capsid) that encapsulates the infectious genetic material. Many kinds of viruses exist and they offer a large repertoire of structures with different sizes and shapes within the nanometer range. Furthermore, they are highly monodisperse and relatively easy to modify both chemically and genetically to introduce designed functionality to the capsid; these features make them very attractive as building blocks in nanotechnology. This thesis describes the approach to construct a virus-based nanoreactor by the encapsulation of enzymes within the cowpea chlorotic mottle virus (CCMV), benefitting from the unique assembly properties of this virus. The motives for using virus particles in nanotechnology and an overview of work that has been carried out to date is given in Chapters 1 and 2.

CCMV is a spherical plant virus that consists of 180 identical coat protein (CP) subunits, which assemble around single-stranded RNA. The virus is isolated from cowpea plants and purified following different extraction and precipitation steps. A detailed protocol of the procedure performed in our laboratory is described in Chapter 3. Transmission electron microscopy (TEM), UV/Vis spectroscopy, and fast protein liquid chromatography (FPLC) are the most common techniques used to characterize the virus and to determine its purity in terms of shape, size, and RNA/protein content.

CCMV has special assembly properties, that is, its structure can assemble and disassemble depending on the pH and the ionic strength of the solution. These properties allowed us to remove the genetic material from the CCMV particles and to isolate the CPs. The CPs can be subsequently reassembled to form a protein capsid with the same size as the original virus, but without the RNA encapsulated. This capsid can be reversibly disassembled into the CP dimers and reassembled again by simply changing the pH. The procedure to remove the RNA from the CCMV and the study of the CP assembly properties are described in Chapter 4.

Furthermore, solution scattering techniques, such as dynamic light scattering (DLS) and small-angle neutron scattering (SANS) allowed us to study the structure of CCMV and the CCMV capsid under different pH and ionic strength conditions, as described in Chapter 5. Since the measurements are performed in solution, in contrast to TEM and FPLC, these techniques provide structural information under conditions that more closely mimic the natural environment of the molecules. The SANS measurements, performed at the ISIS facility (U.K.), provided information on how the RNA and the

proteins are arranged in different viral assemblies. Additionally, it provided structural information on particles that were derived by the incorporation of polystyrene sulfonate (PSS) in the CCMV capsid.

With their unique assembly properties, the potential of CCMV capsids to host enzymes and function as nanoreactors was studied by the encapsulation of three different model proteins, namely, myoglobin, dronpa, and streptavidin. The model proteins were mixed with the disassembled CP at pH 7.5 and the mixture was brought to pH 5, driving the CP to assemble into a capsid that incorporates the model protein in its interior. The results derived from the inclusion of the model proteins, described in Chapter 6, are the basis for the construction of an actual viral nanoreactor prepared by encapsulating the enzyme horseradish peroxidase in the CCMV capsid. This is described in Chapter 7. Diluted statistical encapsulation of the process allowed the inclusion of a maximum of one enzyme per capsid. By using confocal fluorescence microscopy, we could study the assembly and the enzymatic activity of the nanoreactor and we were able to distinguish whether the enzyme is inside the capsid or adsorbed on the outer surface.

The CCMV protein surface offers a diversity of functional groups for further functionalization. Chapter 8 describes how the outer surface of CCMV was modified with polyethylene glycol (PEG) at the amine groups from the exposed lysine residues. Although CCMV was successfully functionalized, the protein architecture turned out to be unstable over time. A more stable structure was obtained when, after removal of the RNA, the negatively charged polymer PSS was used as a template to assemble the isolated PEG-functionalized CP into a PSS-containing PEG-decorated capsid.

The studies reported in this thesis describe the first fundamental steps in the construction of a nanoreactor by encapsulating enzymes in the viral protein capsid. CCMV was chosen because of its unique assembly properties. This thesis not only describes the investigations in which CCMV is used as a platform for nanotechnology, but also reports in detail the procedures used to purify the virus and basic studies of its assembly properties, which are required to carry out such investigations. Furthermore, the controlled integration of two different synthetic polymers at the outer surface and in the core of the CCMV capsid, yielding tunable hybrid systems, offers many new possibilities in the fields of nanotechnology and biomedicine.

Samenvatting

De meeste virussen zijn opgebouwd uit een eiwitmantel (capside), die ervoor zorgt dat het infectueuze genetische materiaal ingekapseld is. De grote variëteit aan virussen biedt een grote verscheidenheid aan capsules met dimensies in de orde van tien nanometer, in allerlei soorten en vormen. Virussen bezitten vaak een hoge mate van monodispersiteit en zijn bovendien eenvoudig chemisch of genetisch te modificeren, zodat een gewenste functionaliteit aan het capside gegeven kan worden. Deze specifieke eigenschappen maken virussen bijzonder aantrekkelijk om te gebruiken als bouwstenen in nanotechnologie. In dit proefschrift wordt een methode beschreven om een nano-reactor te maken die gebaseerd is op virussen. Het virus dat daarvoor gekozen is, is het cowpea chlorotic mottle virus (CCMV); dit virus bezit unieke en reversibele assemblage eigenschappen waardoor het mogelijk is om een enzym op te sluiten in het virus. In Hoofdstukken 1 en 2 wordt, naast een motivatie voor het gebruik van virussen in nanotechnologie, de recente literatuur besproken, omtrent het onderzoek dat is beschreven in dit proefschrift.

CCMV wordt geïsoleerd vanuit geïnfecteerde planten en wordt, volgens het protocol dat uitvoerig beschreven is in Hoofdstuk 3, gezuiverd met behulp van verschillende extractie en precipitatie stappen. Het sferische virus bestaat uit 180 identieke mantel eiwitten, die assembleren om enkelstrengs RNA. Met behulp van verschillende technieken, zoals transmission electron miscroscopy (TEM), UV/Vis spectroscopy en fast protein liquid chromatography (FPLC), kunnen de eigenschappen van het virus bepaald worden. Bovendien geven deze technieken inzicht in de zuiverheid, vorm, grootte en de verhouding RNA/eiwit van het virus.

Een unieke eigenschap van CCMV is dat het kan assembleren en uiteenvallen afhankelijk van de pH en ion sterkte van de oplossing. Dit biedt de mogelijkheid om het virus te ontleden in de manteleiwitten en het RNA en dus om het genetische materiaal te verwijderen. De manteleiwitten kunnen dan onafhankelijk geïsoleerd worden om opnieuw te assembleren in een deeltje (een eiwit capside) met een vergelijkbare structuur als het oorspronkelijke virus, maar waarin geen RNA opgesloten zit. Het assembleren en uiteenvallen van de capside is een reversibel proces: door eenvoudig de pH te veranderen, kunnen of de mantel eiwitten afzonderlijk worden verkregen of de capside in zijn geheel. Deze studies zijn beschreven in Hoofdstuk 4.

Om gedetailleerde informatie te krijgen in de structuren van CCMV en de CCMV capside zijn verstrooiingstechnieken, zoals dynamic light scattering (DLS) en small-angle neutron scattering (SANS) uitgevoerd (Hoofdstuk 5). Met deze technieken kunnen onder verschillende condities (bijvoorbeeld wat betreft pH en ion sterkte) *en* in oplossing structurele studies uitgevoerd worden. Dit heeft als grote voordeel dat de moleculen in hun natuurlijke omgeving bestudeerd worden. De SANS metingen, die zijn uitgevoerd bij de ISIS faciliteit in het Verenigd Koninkrijk, geven informatie over de ordening van het RNA en de eiwitten in de verschillende virale assemblages. Door het negatief geladen polymeer polystyreensulfonaat (PSS) op te sluiten in het CCMV capside werd een nieuw virusdeeltje verkregen, waarvan de structurele eigenschappen ook met behulp van SANS konden worden bestudeerd.

De assemblage eigenschappen van de CCMV capside bieden ook de unieke gelegenheid om een nanoreactor te construeren. Drie verschillende modeleiwitten, te weten myoglobine, dronpa en streptavidine werden ingesloten in de CCMV capside gastheer. Deze insluiting werd bewerkstelligd door: de model eiwitten te mengen met de afzonderlijke manteleiwitten bij pH 7.5 en vervolgens de pH te verlagen naar pH 5, waar de manteleiwitten assembleren tot het capside waarin het modeleiwit ingesloten is. De resultaten van dit onderzoek staan beschreven in Hoofdstuk 6. Deze succesvolle modelstudies vormden de basis voor de constructie van een werkende virale nanoreactor, die uiteindelijk werd verkregen door insluiting van het enzym horseradish peroxidase in het CCMV capside (Hoofdstuk 7). Door verdunde statistische incapsulatie kon een maximum van één enzym per capside verkregen worden. Met confocale microscopie werden de assemblage eigenschappen en de activiteit van de nanoreactor bestudeerd en kon worden vastgesteld of het enzym ingesloten was *in* het capside of aan de buitenkant van de capside geadsorbeerd was.

In Hoofdstuk 8 wordt beschreven op welke manier de buitenkant van CCMV gemodificeerd kan worden. Vrije amine groepen van lysine residuen die zich aan de buitenkant van CCMV bevinden, werden verbonden met polyethyleenglycol (PEG) derivaten. Hoewel de CCMV functionalisatie succesvol verliep, bleek de PEG-CCMV hybride architectuur niet stabiel. Om een meer stabiele structuur te creëren werd het RNA verwijderd uit de PEG-CCMV, dat vervolgens werd ontleed in de manteleiwitten. De PEG gefunctionaliseerde manteleiwitten werden daarna, met behulp van het negatief geladen PSS, weer geassembleerd om een stabiel capside te vormen dat gedecoreerd is met PEG moleculen.

Het onderzoek dat beschreven is in dit proefschrift laat de eerste fundamentele stappen zien die nodig zijn om een nanoreactor te construeren, in dit geval door het incapsuleren

van enzymen in het CCMV capside. Op basis van zijn unieke assemblage eigenschappen is CCMV gekozen als werkpaard. Dit proefschrift beschouwt niet alleen de onderzoeken en experimenten waarin CCMV als platform voor nanotechnologie gebruikt wordt, maar ook de gedetailleerde protocollen en procedures om het virus zuiver in handen te krijgen. Dergelijke studies zijn van groot belang en dienen als basis voor het toekomstig werk in dit onderzoeksgebied. Eenvoudig varieerbare hybride systemen zijn beschikbaar door de gecontroleerde integratie van twee verschillende synthetische polymeren aan de buitenzijde en in de kern van de CCMV capside. Deze modulaire materialen geven een scala aan mogelijkheden op het gebied van nanotechnologie en biomedicijnen.

Resum

Els virus són agents infecciosos de mida microscòpica que necessiten la maquinària biosintètica d'una cèl.lula hoste per multiplicar-se. En general, estan formats per un àcid nucleic, ARN o ADN, envoltat per una càpsida proteica. Existeixen molts tipus de virus, i presenten una morfologia molt diversa. A més a més, molts virus poden ser manipulats tan genètica com químicament i així introduir una determinada funcionalitat a la càpsida. Aquestes propietats fan dels virus estructures molt interessants en el camp de la nanotecnologia. Aquesta tesi descriu la recerca duta a terme per construir un nanoreactor a partir de l'encapsulació d'un enzim dins la càpsida proteica d'un virus. El virus escollit és el *cowpea chlorotic mottle virus* (CCMV). En el capítol 1 i 2 d'aquesta tesi es pot trobar una descripció dels avantatges d'utilitzar partícules víriques en nanotecnologia i una ressenya de la recerca realitzada per altres grups d'investigació durant els últims anys sobre aquest tema.

El CCMV és un virus esfèric que infecta plantes. Està format per 180 unitats proteiques idèntiques que formen un embolcall al voltant de l'ARN. Aquest virus s'ailla de mongeteres infectades i es purifica seguint diferents processos d'extracció i precipitació. Un protocol detallat del procediment dut a terme en el laboratori està descrit en el capítol 3. Les tècniques més comunes utilitzades per a caracteritzar el virus i determinar la seva puresa són espectroscòpia d'ultraviolat i visible, microscopia electrònica i cromatografia d'exclusió molecular.

El CCMV té unes propietats peculiars ja que la seva estructura pot ensamblar-se o desensemblar-se en funció del pH i de la concentració de sal de la solució. Són aquestes propietats les que permeten extreure el material genètic del CCMV i obtenir les unitats proteiques pures. Aquestes unitats proteiques es poden reensamblar per formar una càpsida proteica de la mateixa mida i forma que el virus, però sense ARN encapsulat. Variant les condicions de pH podem, aleshores, formar i trencar aquesta càpsida de forma reversible. El procediment pel qual s'ha extret l'ARN del virus i els estudis de l'ensamblatge de les unitats proteiques aïllades del virus estan descrits en el capítol 4.

Les diferents estructures que presenta el CCMV i la seva càpsida han estat investigades en detall utilitzant SANS (*small-angle neutron scattering*) i DLS (*dynamic light scattering*), que són tècniques que permeten fer aquests estudis en dissolució. Els resultats d'aquest anàlisi, en diferents condicions de pH i de força iònica, es poden trobar en el Capítol 5.

El potencial de la càpsida del CCMV per acollir enzims en el seu interior i funcionar així com a nanoreactor va ser investigat i els resultats estan descrits en el capítol 6 i 7 d'aquesta tesi. L'encapsulació de l'enzim dins la càpsida del CCMV va ser duta a terme utilitzant les propietats d'ensamblatge del virus: l'enzim es va barrejar a pH 7.5 amb les unitats proteiques del CCMV que en aquest pH es troben en dissolució (no ensamblades). Tot seguit, el pH de la mescla es va abaixar a pH 5 provocant, d'aquesta manera, l'ensamblatge de les unitats proteiques resultant en una càpsida que ha incorporat l'enzim en el seu interior. Mitjançant el microscopi confocal de fluorescència, l'activitat enzimàtica de l'enzim encapsulat dins la càpsida vírica ha estat investigada.

La superfície externa del CCMV ofereix una gran diversitat de grups funcionals. El capítol 8 descriu la modificació de la superfície externa del virus amb el polímer sintètic polietilè glicol (PEG). El virus va ser funcionalitzat amb PEG amb èxit, però l'estructura del virus va resultar ser inestable. Es va obtenir una estructura més estable mitjançant l'extracció de l'ARN del complex PEG–CCMV i utilitzant el polianió poliestirè sulfonat (PSS) per ensamblar les unitats proteiques víriques funcionalitzades. D'aquesta manera es va poder obtenir una càpsida proteica que conté dos polímers sintètics, un adherit a la superfície externa i l'altre inclòs en el seu interior.

La feina descrita en aquesta tesi mostra els primers passos per construir un nanoreactor format per una càpsida vírica que encapsula un enzim. Però aquesta tesi també descriu en detall els procediments duts a terme per obtenir i purificar el CCMV i l'estudi de les propietats d'ensamblatge del virus. A més a més, la integració controlada de dos polímers sintètics a la superfície externa i a l'interior de la càpsida del CCMV resulta en materials híbrids que ofereixen moltes possiblitats noves en el camp de la nanotecnologia i la biomedicina.
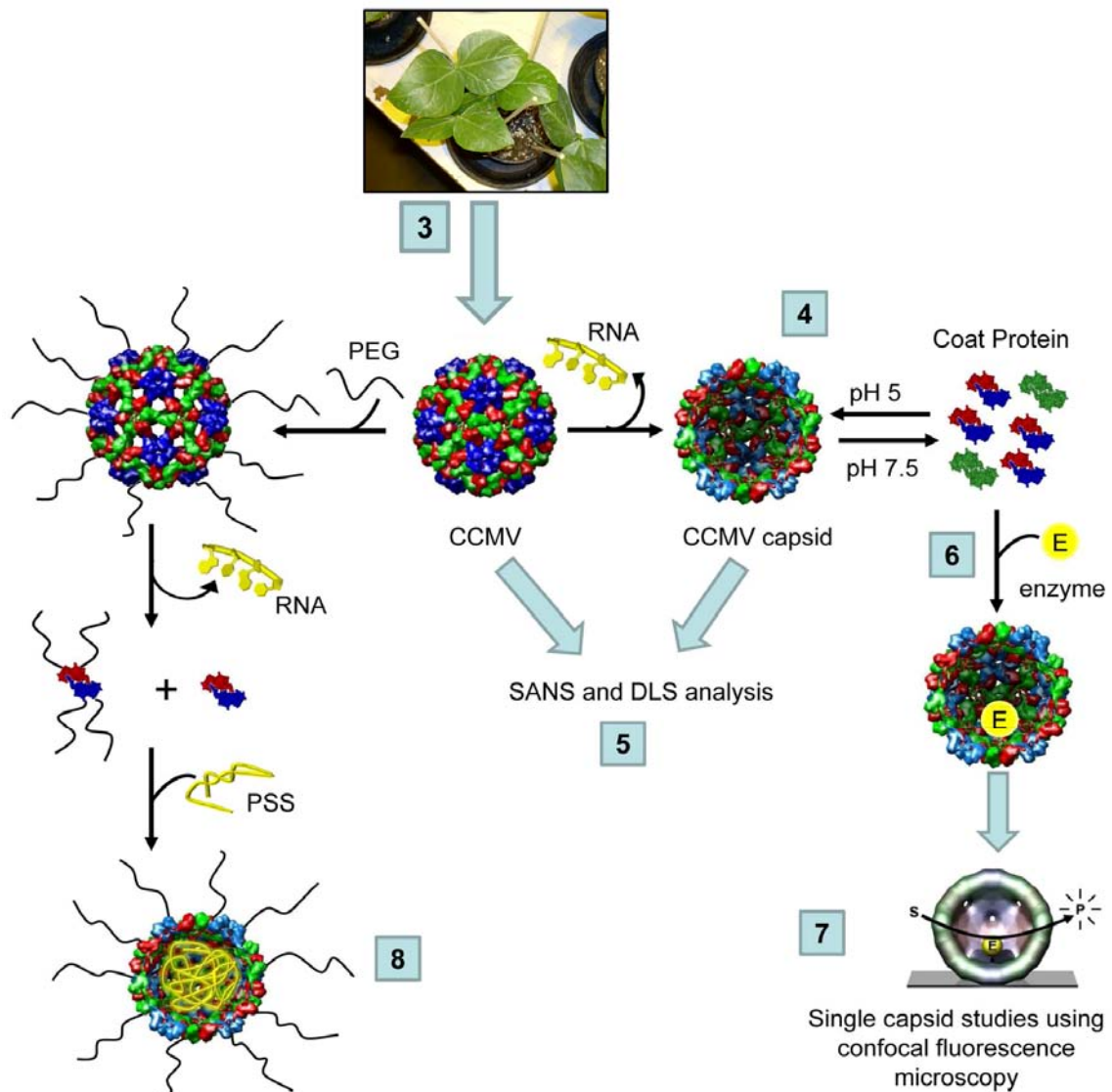
Schematic summary of the processes and species described in this thesis. *The blue squares indicate the chapter in which the research is described.*

Schematische weergave van de processen and virusdeeltjes beschreven in dit proefschrift. *De blauwe blokjes geven het hoofdstuk aan waarin het desbetreffende onderzoek is beschreven.*

Resum esquemàtic dels processos i les espècies descrites en aquesta tesi. *Els quadres blaus indiquen el capítol en el que es descriu la recerca indicada.*

Acknowledgements

It was Marjolijn who advised me to talk to Lee, "he is always good at helping to make decisions" she told me. So I went to Lee, and he said, in his particular Lee-way, "go for it, sure!", and I decided to go for it and start a Ph.D. project. Now I am very happy and proud for having done it. Working on a Ph.D. and doing it in a foreign country has been a very worthwhile experience and a perfect opportunity for me to learn about myself both as a scientist and as a person. It also allowed me to live in a new culture, have many different experiences, and above all, make many great friends. Thank you Lee and Marjolijn for this last kick! However, as Lee also said to me, "once you start your Ph.D., you don't get rid of it until the day of your defense"... I am looking forward to this day!

Prof. Jan van Hest also played an important role in my decision to pursue a Ph.D. Jan, the six months I worked in your group were a big pleasure and they gave me the self-confidence and security I needed to work on a Ph.D. Thank you for your trust and advice at that time, but also for your help and guidance every time I needed it during all these years.

I started my Ph.D. studies, together with Friso Sikkema, on a new project with viruses that would be supervised by Prof. Jeroen Cornelissen and Prof. Roeland Nolte. The fact that it was a new project made it both scary and challenging, but looking back I think we did a great job. Roeland, I want to thank you for the opportunity you gave me to start this new project that I know was very important to you, especially considering that I was not 100% convinced at the beginning. Although you have a busy agenda, I really appreciate that during all these years you always had the door open for me when I had questions, worries, complaints, or good results. I will always be thankful that you watered the plants during Christmas while I was in Barcelona.

Jeroen, thank you for the trust you always had in me to accomplish this thesis. Your confidence in me has always been higher than my own self-confidence; this helped sometimes. I really appreciate the help and supervision you gave me during the first years of my research, which provided the basis for the success of this project. Thanks for always being open to hearing my ideas, criticisms, or opinions. I am happy we could always talk open with each other.

The first problem Friso and I encountered at the beginning of our Ph.D. careers was to obtain the virus, which was quite essential, since all our research was based on it. The isolation and purification of the virus would have never been possible without the help

of Dr. Dick Verduin from Wageningen University. Dick, thank you for teaching us the procedure to isolate and purify CCMV and for all your good advice during the "virus meetings" and by email, which has been extremely useful at many critical moments during these years. Furthermore, I would also like to thank you, together with Prof. Jan van Hest and Prof. Gijs Wuite, for reading my thesis as part of the manuscript committee.

The second problem we had with obtaining the virus was "how to get an infrastructure to isolate a plant virus in an Organic Chemistry lab?" It was necessary to use the resources and facilities of several departments within the university to carry out the whole CCMV purification protocol, which includes growing more than 100 plants and using three different kind of centrifuges. This would not have been possible without the help of the people from the Experimental Plant Ecology department who gave advice on how to build a growth room, the people in the Green House of the university who took care of the bean plants and facilitated us with all the material that we needed, and the Plant Cell Biology group, and the Biomolecular Chemistry and Molecular Biology groups (in the NCMLS) who helped with using the centrifuges and ultracentrifuges.

A very special thanks to the people from the Gemeenschappelijk Instrumentarium, not only for your help with my research, but also for your *gezelligheid* every time I was in the department. Rien, Liesbeth, Huub, Geert-Jan, and Jelle, thank you very much for your patience and kindness, and for helping me all these years with the FPLC, TEM, ultracentrifuges, ICP-MS, and Elisa Reader. Good luck to all of you in the future!

I cannot imagine the department without the presence of Désirée, Jacky, and Peter van Dijk. Thank you Peter for helping me to get all these "things for the virus" that in the beginning I didn't even know what they were used for. Thanks for your always-there-smile and for your care and kindness. Jacky, Désirée, hartstikke bedankt voor jullie hulp en goede zorgen.

One of the greatest pleasures during the years I worked on my Ph.D. has been the supervision of students. Thank you very much for this opportunity! It is true that some of you did not arrive at the best moment for me, and sometimes I could not find enough time for supervision. Sorry about that. But I have learned a lot from you and I had many moments of fun and joy. Furthermore, without you working on this project this thesis would have never been what it is now, and I am very proud that it is so. Willem, your work, enthusiasm, and patience gave very nice results on the imaging of the CCMV particles, as can be seen in Chapter 3. Lots of luck with your Ph.D. work in Wageningen! Raquel, no hi va haver gaire temps per arrodonir els resultats però va ser un plaer que a part dels soparillos, xerrades i festes vàries també et fes il.lusió treballar en el meu projecte. Laura, la teva perseverància, eficiència i energia van quedar més que

190

demostrades durant l'any que vas treballar en el projecte. Vas descobrir el pitjor de la recerca: la frustració. Malgrat això, no et vas rendir mai i finalment els teus resultats són part del capítol 7 d'aquesta tesi. Sé que faràs un doctorat excel·lent a l'ICIQ. Molta sort, guapa! Anna, va ser un plaer tenir-te d'estudiant i és un plaer tenir-vos a tu i el Jordi entre els meus amics. Vas treballar sempre amb l'empenta que et caracteritza, disposada a aprendre i entendre fins l'últim detall, i la teva feina, unida a la de l'Anne, ha resultat en una publicació i en el capítol 8 d'aquesta tesi. Em fa moltíssima il.lusió poder compartir una publicació amb vosaltres. Anne, you did a great job! Your work during the two internships with us, under the supervision of Andrés, Ton, and me, showed the great scientist in you. You are critical, organized, efficient, and enthusiastic, a perfect combination to develop a successful Ph.D. thesis. I am sure you will do great in Twente! Thanks for your important contribution to Chapter 8, which recently became a very nice and complete publication. I don't want to forget the four groups of MLW students that I supervised for two weeks, most of the times together with Ton. It was always great fun those intense days carrying out a crazy project, plus a poster, plus a presentation, plus...

Next, I also want to thank the people who have in one way or another contributed to this work, either with their advice or with their expertise. Friso, although the way we approached our work did not always coincide, I think we found a good balance and it was always a lot of fun to work next to you. Thank you very much for your collaboration resulting in Chapter 5, in which many of the measurements are carried out by you. At the moment I thought that I would never be able to encapsulate a protein in the CCMV capsid, Dr. Nikos Hatzakis was of great support. Nikos, thank you very much for your help with the encapsulation of myoglobin, and your advice when I most needed it. Ton, our crazy ideas for the MLW students did not always bring the expected results, but sometimes they did and now these are in Chapter 8 and appear in a nice paper in Biomacromolecules. It was great to collaborate with you. Hans, only your expertise with the confocal fluorescence microscope made the paper in *Nature Nanotechnology* (Chapter 7) possible. It was not easy, but it was worth the effort! Victor, thank you also for your contribution in it. I will not forget our perfect synchronization in measuring while doing at the same time the pH titration (S**t! I lost the spot!). The SANS measurements described in Chapter 5 were performed at the ISIS facility in the U.K. I would like to thank Dr. Ann Terry, Dr. Steve King, Dr. Dirk Visser, and Dr. Richard Heenan who collaborated in this project and showed us how to perform SANS. I also want to thank Dr. Martin Feiters, who made possible this collaboration with ISIS and has spent many hours fitting the curves and interpreting the results. Guillaume, thank you for your contribution in Chapter 5 performing the DLS measurements. Andrés, ha sido un placer trabajar contigo y a tu lado. Este *paper* nos lo hemos currado! Gracias por estas charlas sobre química y temas varios en la "intimidad" de los *cubicles*. Inge, Linda, dank jullie wel voor alle hulp omtrent de biochemische procedures. I would also like to thank Prof. Alan Rowan for his

collaboration in terms of (crazy) ideas, corrections, and optimism during my Ph.D. years.

During all these years working at the University of Nijmegen I have met many people with whom I shared not only work but much more: Spanish/Promotion/Birthday/4-daagse/House-warming/etc. parties, borrels, whisky tasting experiences, IMM sport days, volleyball evenings, het Keldertje, Dollars, vettehap borrels, scary AiO rooms, the most amusing jokes with tubes, videos, and masks, Lunteren, de Onderwereld, Tarragona/Barcelona study-tour, meetings, coffee breaks, cakes, BBQ, Christmas dinners, Nolte–Meijer Cups... To all the people of the department, thank you for all these moments that make the life of a Ph.D. student much easier. Special thanks to Femke (my sweet supervisor), Jurry (my other supervisor), Pieter (thank you for your compliments every time we meet), Johan (I admit it, I was afraid to go into the AiO room), Gerald, Hans, Ruud, Aurelie, Marjolijn, Lee, Matthijs (thanks for the laughs and the good spirit you always brought to the department), Irene, Joost, Richard, Paul T., Paul v.G. (thank you for all the dinners and deep talks!), Jaap, Dennis, Paula, Mark (I should have played volleyball more often...), Inge, Linda, Friso, Alexander, Sander, Rosalie (it was nice to share so many conferences with you!), Ton, Onno, Nico (thank you for your very comforting hugs), Paul K. (thank you very much for your help with the last bits of this thesis), Jasper, Suzanne (let's go to het Keldertje!), Joris, Roel, Jorge, Marco, Guillaume (the man with the sweetest speech :-)), Erik, Mauri, Christine, Nikos M., Heather (thanks for all the doubts you solved via Skype), Rosalyne (thank you very much for having corrected the thesis not only once, but twice), Daniel (esperando oir cual será la próxima aventura a la que te apuntarás), Dani (el que nunca se enfada ;-)), Pili, Michal (the *calimocho* man), Johny, Matthieu (I have never heard somebody playing the accordion as you, thanks for this pleasure), Stephan (the finger-man), Ismael (mucha suerte con ese postdoc!), Paco, Andrés, and Nikos H. Also to the Erasmus students coming from Madrid, Barcelona, and Castellón, who brought the Spanish atmosphere to the department every year: Irene, María M., Eva, Evutxi, Silvia, Marta, Carol, Edgar, Gloria, Vicent, Luis, Mònica, Maria, Isa, Gemma, Ribera, Núria, Raquel, Anna, Laura, Eli, Andrea, Elena, and Edu.

These years in the Netherlands would not have been the same without the people that have been part of my life outside the university. Those persons who, in one way or another, at some time during these years, have made The Netherlands my home. Without them I would not have made it. Thank you very much! Especially Judith (my first "vriendin van mij"), Thamar, Stijn, Cuca, the flamenco troupe (Annelies, Sanne, Marco, Gabi), and the Lent family, Laura (the best vegetarian cook, next to Erik, of course! ;-)), Maarten (the man of the house), Dzenita (I am looking forward to your defense!), María (mi chica Almódovar), Álex (con tu fantástica risa), Henar, and Ozan (the expert in Marta-is-not-here-parties ;-)). I also want to mention Valeria, Andrés,

Heather, Bea, Dora, Pascale, Daniel, Dani, Alberto, Paula, Nico, Cristina, Amadeo, Giorgia, Claudio, Gerhild, Virginie, Núria, Marjolijn, Dani B., Anna A., Ribera, Rosalyne, and Anna F. For all that we shared and lived together, thank you!

Molt especialment vull donar les gràcies a la gent de Barcelona, als amics de tota la vida que no han fallat mai i per qui la distància no ha estat mai un obstacle per a mantenir l'amistat de sempre. Gràcies per la vostra confiança i pel vostre suport sempre que l'he necessitat. Gràcies per venir-me a veure a Nijmegen i per acollir-me quan vinc a Barcelona com si no hagués marxat mai. Moltíssimes gràcies Quim, Cinta, Vicenç, Jordi, Elena, Bernat, David, Jordi d'Alella, Baldiri, Funollet, Montse, Tomàs, Anna, Ferran, Eko, Marina, Neus, Ramon, Cesc i Gabriel. Gràcies també a la Flora, la Fina, el Jaume, l'Àngels, i a la meva família, padrins, avis, tiets, i cosins que, d'una manera o altra, estan sempre pendents de la meva vida a les Holandes. Laura, moltíssimes gràcies per dissenyar la tapa de la meva tesi, ningú podria haver captat millor el que volia. Vull agrair a la Núria que sempre hagi tingut la porta oberta per mi quan ho he necessitat. Gràcies per ajudar-me a créixer. Finalment vull donar les gràcies al Dr. Joan-Antoni Farrera que, ara fa 8 anys, em va brindar la primera oportunitat d'anar a Holanda amb una beca Erasmus.

Erik, the end of our theses is just the beginning for us. Thank you for your patience, your help, your support, and your care. And above all: Thank you for making me laugh every morning! Lidy, Richard, Jeroen en Sanne, ook bedankt voor jullie liefde en steun.

Pare, mare, Antonio, Maribel, Laia, Andreu i David. GRÀCIES! Per tot el que he rebut de vosaltres aquests anys, per tot el que hi ha de vosaltres en aquest llibre, perquè malgrat la distància sempre us he sentit a prop, per confiar en mi sempre. És aquesta confiança la que em fa tirar endavant i encarar la vida amb entusiasme. Us estimo molt.

The last words I kept for my paranimfs: Joost and Henar, because somehow you have been, in two different ways, a big support for me during my thesis. Joost, your patience and guidance at the beginning of the Ph.D. really helped me to start and trust in what I was doing. Any questions I had about things in the lab or with the computer you were there. It has been a pleasure to have you as a neighbor and I still wish I was as organized as you are! Henar, tota la seguretat que m'ha donat el Joost a la universitat me l'has donat tu fora d'ella. Aquests anys a Holanda no haurien estat el mateix sense tu, per mil raons impossibles d'anomenar o resumir. Només puc donar-te les gràcies per tot el que hem pogut compartir, casa, viatges, festes... per tot el que m'has ensenyat, i per ser-hi sempre. És un plaer tenir-te de paranimf.

Moltes gràcies a tots.

List of Publications

Self-assembled nanoreactors
D. M. Vriezema, M. Comellas Aragonès, J. A. A. W. Elemans,
J. J. L. M. Cornelissen, A. E. Rowan, R. J. M. Nolte
Chemical Reviews **2005**, *105*, 1445–1489

Monodisperse polymer-virus hybrid nanoparticles
F. D. Sikkema, M. Comellas-Aragonès, R. G. Fokkink, B. J. Verduin,
J. J. L. M. Cornelissen, R. J. M. Nolte
Organic & Biomolecular Chemistry **2007**, *5*, 54–57

A virus-based single-enzyme nanoreactor
M. Comellas-Aragonès, H. Engelkamp, V. I. Claessen, N. A. Sommerdijk,
A. E. Rowan, P. C. Christianen, J. C. Maan, B. J. Verduin, J. J. L. M. Cornelissen,
R. J. M. Nolte
Nature Nanotechnology **2007**, *2*, 635–639

Viral capsids as templates for the production of monodisperse Prussian blue
nanoparticles
A. de la Escosura, M. Verwegen, F. D. Sikkema, M. Comellas-Aragonès,
A. Kirilyuk, T. Rasing, R. J. M. Nolte, J. J. L. M. Cornelissen
Chemical Communications **2008**, 1542–1544

Controlled integration of polymers into viral capsids
M. Comellas-Aragonès, A. de la Escosura, A. J. Dirks, A. van der Ham,
A. Fusté-Cuñé, J. J. L. M. Cornelissen, R. J. M. Nolte
Biomacromolecules **2009**, *10*, 3141–3147

Structural study of cowpea chlorotic mottle virus and capsid by Small-Angle
Neutron and Dynamic Light Scattering
M. Comellas-Aragonès, Guillaume Delaittre, F. D. Sikkema, A. Terry, S. M. King,
D. Visser, R. M. Heenan, R. J. M. Nolte, J. J. L. M. Cornelissen, M. C. Feiters
In preparation

194

Curriculum Vitae

Marta Comellas Aragonès was born on the 7th of February 1978 in Barcelona, Spain. After high school she studied chemistry at the University of Barcelona. At the end of her studies she was awarded an Erasmus fellowship for an internship of one year in the group of Prof. Roeland Nolte at the Radboud University in Nijmegen. During this year she worked on the construction of protein–polymer biohybrids using temperature responsive polymers. After obtaining her Master's degree in Barcelona, Marta decided to go back to Nijmegen and continue her career in The Netherlands. Starting in May 2003, she worked on a project under the supervision of Prof. Jan van Hest at the Radboud University Nijmegen and the University Medical Center St. Radboud (UMC) in Nijmegen involving peptidic blood substitutes. In November 2003, she started as a Ph.D. student on a new line of research in the group of Prof. Roeland Nolte under the supervision of Dr. Jeroen Cornelissen. Within these new research activities in the Supramolecular and Physical-Organic Chemistry group of Prof. Nolte, Marta has set up the required infrastructure to obtain and work with the cowpea chlorotic mottle virus (CCMV) and managed to construct a virus-based nanoreactor. In 2008, Marta took up a position as a postdoctoral fellow in the research team of Prof. Jeroen Cornelissen to extend the investigations in the field of "Chemical Virology", in particular those involving enzyme-based viral nanoreactors. In this position, she was also involved in the training of new students and postdoctoral fellows in this research area. Early 2010, Marta will move to San Diego (California, USA), where she has the opportunity to work in the group of Prof. M.G. Finn at the Scripps Research Institute.

Printed with Permission. "Piled Higher and Deeper" by Jorge Cham